This work is dedicated to the memory

of Norman Martyn Sosnow, 1944 - 1967.

Once, with the Author, a Scholar of

Christ's College,

Cambridge.

THE ELECTRICAL AND MAGNETIC PROPERTIES OF SOME RARE EARTH COMPOUNDS

A Thesis submitted by

Andrew Morven Stewart M.A., A.M., E.E.

for the Degree of

Doctor of Philosophy

of the University of London

Department of Electrical Engineering
Imperial College
London

1970

ABSTRACT

The magnetic susceptibilities of the following intermetallic compounds of the Rare Earths and Zinc have been measured in the temperature range $2^{o}K$ - $300^{o}K$:: R_2Zn_{17} for R = Gd, Tb, Dy, Ho, Er, Tm and RZn_{12} for R = Sm, Gd, Tb, Er, whose electrical resistivities have been measured as well. The susceptibilities of Yb_2Zn_{17} and $YbZn_{11}$ have been measured down to $77^{o}K$.

The Rare Earth ions in all the compounds were found to be in a trivalent state, except for Yb, which was divalent. Apart from the two Yb compounds and $SmZn_{12}$, the susceptibilities of the materials followed the Curie Weiss Law down to about $50^{o}K$, where deviations from the Law, due to crystal field effects, began to occur. Most of the compounds ordered in some type of coherent long-range antiferromagnetic mode, probably an incommensurate spiral, in the region of $50^{o}K$ or below. Four of the R_2Zn_{17} materials did not appear to order at temperatures down to $2^{o}K$. The two Gd compounds showed signs of an anomalous pseudo-ordering at temperatures well above their main ordering temperature, which has been observed before in other Gd compounds. A method of analysing the susceptibilities of Sm materials has been suggested, and using it, the properties of $SmZn_{12}$ were found to be consistent with those of the other compounds.

The RZn_{12} resistivities were found to obey well-defined temperature power laws in the magnetically ordered regime. The magnetic resistivities of the Gd, Tb (and possibly Er) compounds go as $T^{3/2}$, and of $SmZn_{12}$ as $T^{5.2}$. The s-f coupling constant has been estimated in several ways, using a free electron band-structure, to be a few tenths of an eV in these materials.

An experimental problem which has often afflicted users of the Faraday Magnetometer, is that when large magnetic moments are measured, it is found that lateral forces, which act on the magnetic specimen, cause the suspension to swing out of the vertical. The reasons for this have been analysed, and a particularly simple means of predicting when it will occur has been suggested.

ACKNOWLEDGMENTS

I am extremely grateful to my Supervisor, Professor J. C. Anderson, for his support and encouragement throughout the course of this work.

The project was undertaken in conjunction with the Metal Physics section. I am very grateful to Professor B. R. Coles for allowing me the full use of his section's facilities, for suggesting that the magnetic properties of the dilute Rare Earth-Zinc compounds would be interesting to investigate, and for his subsequent keen and continual interest in the work. I am also indebted to all members of the Metal Physics section for their help and co-operation, and in particular to Dr D. Griffiths for his wise guidance and advice on the writing of the paper on Lateral Instability, and to Mr J. B. Dunlop for close liaison on many problems of experimental technique, and also for measuring the magnetic susceptibility of $SmZn_{12}$ above $16^{\circ}K$.

I have had enlightening correspondences with Mr D. W. Parker on the Lateral Instability problem, and with Dr J. T. Mason on Rare Earth-Zinc metallurgy. Discussions with Dr N. Rivier on the subject matter of Appendix E have also been very illuminating.

Finally I should like to thank the Science Research Council and The Clothworkers Company for financial support.

CONTENTS

		Page No.
	ABSTRACT	2
	ACKNOWLEDGMENTS	4
	CONTENTS	5
	INTRODUCTION	9
CHAPTER 1	THEORY AND PAST WORK	11
1.1	The Free Rare Earth Ion	11
1.2	Crystal Field Effects	15
1.3	The Formation of Moments in Metals	28
1.4	The s-f Interaction in Metals	38
1.5	The Divergence of Perturbation Theory	54
1.6	Interactions between Moments	58
1.7	Magnetic Ordering	64
1.8	Ground State Singlet Ordering	68
1.9	Resistivity	72
CHAPTER 2	THE INTERMETALLIC COMPOUNDS	76
2.1	Metallurgical Properties	76
2.2	Crystal Structures	79
2.3	Symmetry Properties of the Structures	82
2.4	Preparation and Analysis of Materials	87

		Page No.
CHAPTER 3	EXPERIMENT	95
3.1	Susceptibility Measurement	95
3.2	General Modifications	102
3.3	Temperature Measurement	113
3.4	Helium Exchange Gas Pressure	116
3.5	Lateral Instability	123
3.5.1	Forces Caused by Small Deviations from the Position of Symmetry	123
3.5.2	Stability of the Faraday Magnetometer	130
3.5.3	Stability of the Gouy Magnetometer	134
3.5.4	On the Radial Variation of the Field Gradient Ratio G_x	136
3.6	Experimental Procedure	145
3.7	Suggestions for Future Improvements	147
3.8	Resistivity Measurement	150
CHAPTER 4	RESULTS AND THEIR INTERPRETATION	153
4.1	Introduction	153
4.2	R_2Zn_{17} Results	156
4.3	RZn_{12} Results	163
4.4	Summary	178
APPENDIX A		221
a)	Formalism of Static Linear Response Theory	221
b)	Two Band Molecular Field-Linear Response Model for a Transition Metal	223
APPENDIX B	Stability Condition for a Two Link Suspension	232

		Page No.
APPENDIX C	The Lateral Force due to an Infinite Series of Images	234
APPENDIX D	Magnetic Properties of Some Manganese-Silicon Compounds	237
APPENDIX E	Interactions in the Anderson Model	246
	REFERENCES	253
	CHAPTER 1	253
	CHAPTER 2	262
	CHAPTER 3	264

LIST OF FIGURES

Fig.	1.1	13
	1.2	14
	1.3	13
	1.4	24
	1.5	45
	2.1	77
	2.2	80
	2.3	80
	2.4	77
	3.1	97
	3.2	100
	3.3	101
	3.4	106
	3.5	97
	3.6	110

Page No.

LIST OF FIGURES (Contd)

Fig. 3.7	120
3.8	121
3.9	120
3.10	137
3.11	138
3.12	139
4.1.....	180
B.1	233
C.1	233
D.1.....	241

INTRODUCTION

The subject of Magnetism in Metals is one which offers both many theoretical problems of great subtlety, and also a prospect of developing magnetic materials of technological value (R 1.2).

The magnetic behaviour of the 3d transition metals, and even of the universally-used material Iron, is still not fully understood, such is the complexity of the interactions taking place within them (Herring R 1.2, Vol. 4). However, compounds which contain Rare Earths provide problems which are more tractable. This is because the unfilled 4f electron shell of the Rare Earth, which is responsible for its magnetism, lies deep inside the atom and is little influenced by its surroundings.

The effects of the environment may thus be treated as a perturbation upon the lowest lying states of the free ion, whose magnetic properties are well understood as a result of Van Vleck's distinguished theoretical work of forty years ago (R 1.133). When the ions are situated in a metal they are affected in two ways. First, the degeneracies of the lowest ionic states will be split by energies of the order of 100°K by internal electric fields in the metal, and also by covalent bonding. Second, a conduction electric travelling through the metal will be exchange scattered by the spin of one ion, procede on to the next, and be scattered by that, so producing a strong coupling between the ionic spins.

Materials in which only the first interaction is present, are

very dilute solid solutions of the Heavy Rare Earths in Silver and Gold. These have been investigated previously by workers at Imperial College (R 1.15, R 1.98, R. 1.99, R. 1.16), who have been able to interpret their results primarily in terms of the symmetry considerations involved, but have had rather less success in calculating the magnitudes of the observed effects. In the pure Heavy Rare Earth metals, although both interactions are present, exchange effects tend to predominate. Many papers, reviews (R 1.80, R 1.81, R 1.121, R 1.82) and Conference Proceedings (R 1.83a, R 1.84) have been published which discuss the exotic varieties of magnetic behaviour, and their influence upon other physical characteristics of the materials, which take place in the Rare Earth metals and in their compounds.

In the work described here, we have investigated the properties of some intermetallic compounds of the heavier Rare Earths with Zinc, which have the compositions R_2Zn_{17} and RZn_{12}, R being a Rare Earth. The Compounds are crystallographically ordered, so that the theories developed for the pure Rare Earth metals apply equally well to them, and are magnetically very dilute, so that their behaviour should be of a form intermediate between the two types which have been described.

It is hoped that this work will lead to a better understanding of the nature of the interactions taking place within these substances, and so contribute towards the development of magnetic materials with the high magnetisations and anisotropies which the Rare Earths can provide.

CHAPTER I

THEORY AND PAST WORK

1.1. The Free Rare Earth Ion

The free tripositive f^n Rare Earth ion consists of a Xenon core, which has all shells occupied up to and including the 5p, plus n 4f electrons. The unfilled 4f shell has an average radius of roughly 0.4 Å and lies well within the 5s and 5p shells which tend to isolate it from its environment.

The principal components in the free ion Hamiltonian consist of the interactions of the electrons with the nucleus, the electronic Coulomb repulsion, and the spin-orbit coupling. The Russell-Saunders coupling scheme applies well to the low lying levels (R 1.1, p46), and Hund's rules give the nature of the lowest term. This will consist of that set of states, characterised by the total spin S, and orbital L, quantum numbers respectively, which have S the maximum possible for a given f^n configuration, and L the largest possible, consistent with the maximum S. The spin orbit interaction will split the term into a multiplet whose lowest level will have a total angular momentum quantum number J given by $L \mp S$, where the + and - sign are for a more than or less than half filled shell, and L and S are the orbital and spin quantum numbers of the term.

The energy splittings between terms are typically about 10^5 °K, and those between multiplet levels 10^3 °K. The spin orbit interaction may mix higher lying terms into the ground level which may then be not purely that given by Hund's Rules. For instance (R 1.1, p204), the lowest level of $Gd^{3+}(^8S_{7/2})$ becomes:

$$Gd^{3+} = 0.9844 \left| {}^8S_{7/2} \right\rangle + 0.1736 \left| {}^6P_{7/2} \right\rangle - 0.014 \left| {}^6D_{7/2} \right\rangle \qquad 1.1$$

Hartree Fock calculations of the ionic wavefunctions have been made, and Freeman and Watson (R 2.2, vol. 2B) have tabulated radial expectation values. An important feature which arises from Unrestricted Hartree Fock calculations (allowing the wavefunctions of electrons of different spin in the same (lm) orbital to have different radial variations) is that the core electrons will become spin polarised. In Fig. 1.1 is shown the contributions to the spin density in the Gd^{3+} ion from the 4f shell and from the core electrons. The contribution from the core electrons must of course integrate to zero, but it can be seen that in the outer reaches of the ion it isnegative, and this is the region which may well interact most strongly with the ion's environment. The spin density at the nuclear site will then also be non-zero, and this becomes of great significance in the treatment of the hyperfine interaction.

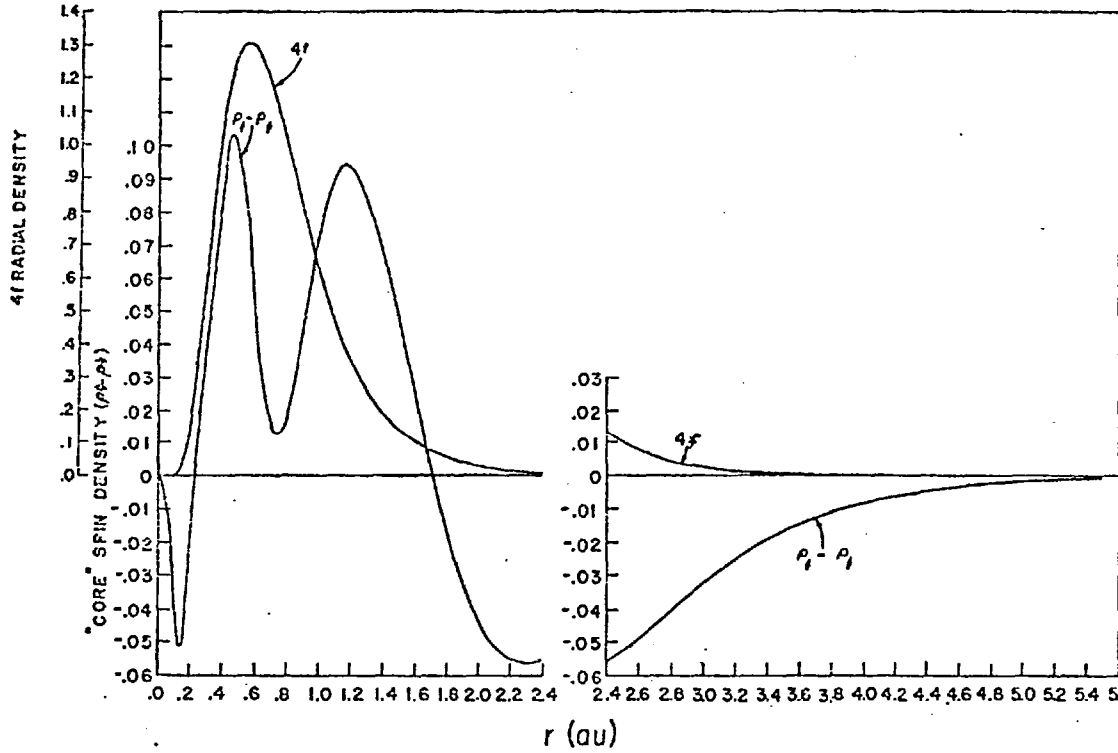


FIG. 1.1 The computed "core" electron spin density ($\rho_\uparrow - \rho_\downarrow$) for all the electrons other than the *4f* shell and, for comparison, the *4f* density as well. Note the change of scales at $r = 2.4$ au to a common scale for both ($\rho_\uparrow - \rho_\downarrow$) and the *4f* spin density.

Fig. 1.3	R	J	D_4
RZn_{12}	Sm	5/2	$\rightarrow \Gamma_6 + 2\Gamma_7$
($D_{4h} = D_4 \times J$)	Tb	6	$\rightarrow 2\Gamma_1 + \Gamma_2 + 2\Gamma_3 + 2\Gamma_4 + 3\Gamma_5$
	Er	15/2	$\rightarrow 4\Gamma_6 + 4\Gamma_7$

R_2Zn_{17}	R	J	C_{3v}
(C_{3v})	Tb	6	$\rightarrow 3\Gamma_1 + 2\Gamma_2 + 4\Gamma_3$
	Dy	15/2	$\rightarrow 5\Gamma_4 + 3\Gamma_5 + 3\Gamma_6$
	Ho	8	$\rightarrow 3\Gamma_1 + 2\Gamma_2 + 6\Gamma_3$
	Er	15/2	$\rightarrow 5\Gamma_4 + 3\Gamma_5 + 3\Gamma_6$
	Tm	6	$\rightarrow 3\Gamma_1 + 2\Gamma_2 + 4\Gamma_3$

Fig. 12

$D_{4h} = D_4 \times J$ Character Table and Basis Functions for the Group D_4

	D_4	E	$\bar{E}$	$2C_4$	$2\bar{C}_4$	C_2 / $\bar{C}_2$	$2C_2'$ / $2\bar{C}_2'$	$2C_2''$ / $2\bar{C}_2''$	Bases for D_4
	Γ_1	1	1	1	1	1	1	1	R
	Γ_2	1	1	1	1	1	−1	−1	z or S_z
	Γ_3	1	1	−1	−1	1	1	−1	(x^2-y^2)
	Γ_4	1	1	−1	−1	1	−1	1	xy
z	Γ_5	2	2	0	0	−2	0	0	S_x, S_y
x,y,z	Γ_6	2	−2	$\sqrt{2}$	$-\sqrt{2}$	0	0	0	$\phi(1/2,-1/2)$, $\phi(1/2,1/2)$
x,y,z	Γ_7	2	−2	$-\sqrt{2}$	$\sqrt{2}$	0	0	0	$\Gamma_6 \times \Gamma_3$

Character Table and Basis Functions for the Group C_{3v}

	C_{3v}	E	$\bar{E}$	$2C_3$	$2\bar{C}_3$	$3\sigma_v$	$3\bar{\sigma}_v$	Bases for C_{3v}
	Γ_1	1	1	1	1	1	1	R or z
	Γ_2	1	1	1	1	−1	−1	S_z
x,y,z	Γ_3	2	2	−1	−1	0	0	$(S_x - iS_y)$, $-(S_x + iS_y)$
x,y,z	Γ_4	2	−2	1	−1	0	0	$\phi(1/2,-1/2)$, $\phi(1/2,1/2)$
z	Γ_5	1	−1	−1	1	i	−i	$\phi(3/2,-3/2) - i\phi(3/2,3/2)$
z	Γ_6	1	−1	−1	1	−i	i	$-(\phi(3/2,3/2) - i\phi(3/2,-3/2))$

1.2. Crystal Field Effects

When a Rare Earth ion is situated in a diamagnetic insulator it is found that the $2J + 1$ degeneracy of the multiplet levels is removed, and they become split by typically, 100 ^{o}K (see for instance Bleaney and Stevens R 1.3). Because the next higher multiplet level is about 1000 ^{o}K above the ground state it is in many cases adequate to regard the influence of the solid as being a perturbation which acts only on the states of this lowest multiplet level.

The Hamiltonian of the free ion is invariant under the operations of the full rotation group R_3 and so (R 1.4) eigenfunctions of the Hamiltonian which belong to the same energy level will form the basis for an irreducible representation D^J of R_3. When the ion is in a solid, its Hamiltonian will be invariant under a point group G which is a subgroup of R_3, and the split levels will each form a basis for an irreducible representation of the finite group G.

Therefore to find the degeneracies and symmetries of the split levels it is necessary to perform the decomposition:

$$D^J \longrightarrow \sum_i n_i \Gamma_i$$

where the Γ_i are the irreducible representations of the finite

group G and n_i the number of times each of them occurs in the decomposition. n_i is given by:

$$n_i = \frac{1}{h} \sum_P \chi_i(P) \chi_J(P) \quad . \qquad 1.3$$

$\chi_i(P)$ is the character of the representation for one of the h operations P of the finite group. The character of the matrix of D^J corresponding to P is:

$$\chi_J(P) = \frac{\sin(2J + 1)\, \phi/2}{\sin \phi/2} \qquad 1.4$$

where ϕ is the angle of rotation (about any axis) of the symmetry operation P.

For states having half-integral J it can be seen from 1.4 that the character of an irreducible representation of R_3 corresponding to a rotation of 2π is minus $(2J+1)$. Thus D_J can not be decomposed into irreducible representations of G, as these possess the property that a rotation of 2π leaves their basis functions unchanged. This apparent paradox was resolved by Bethe (R 1.5) who introduced a new group operation $\bar{E}$ which represents a rotation of 2π and has the property that $\bar{E}^2 = I$, the identity operator. The resulting group has twice as many operations as the original one, although not necessarily twice as many irreducible representations. It is called the double group

and its character table is found by using the Grand Orthoganality Relation (R 1.4), as is that of the ordinary group.

The two point groups of relevance to this work are D_{4h} (4/mmm) and C_{3v} (3m). Their character tables are given in Fig. 1.2. If a small magnetic field is applied to the ion, some of the levels which are degenerate under the crystal field may be split, and in the first column an indication is made of which levels will be affected. A letter z in the column means that the levels will be split by a magnetic field applied in the z direction. The condition for the splitting of a level which transforms according to Γ_i by a perturbation which transforms according to Γ_j, is that the product representation:

$$\Gamma_i^* \times \Gamma_j \times \Gamma_i \qquad 1.5$$

contains the identity representation Γ_1. This is a consequence of the Wigner Eckart Theorem (R 2.26, R 1.6). The perturbation will be of the form $(\underline{L} + 2\underline{S}).\underline{H}$; $\underline{L}$ and $\underline{S}$, as do all axial vectors $\underline{J}$, transform according to the following scheme:

$$\begin{array}{llll} D_{4h} & J_z \sim \Gamma_2 & , (J_x, J_y) & \sim \Gamma_5 \\ C_{3v} & J_z \sim \Gamma_2 & , (J_x, J_y) & \sim \Gamma_3 \end{array} \qquad 1.6$$

The decompositions of D_J into the irreducible representations of

D_{4n} and C_{3v} by means of equation 1.3 are given in Fig. 1.3.

If, for an ion with an even number of electrons, the lowest lying level is degenerate, the degeneracy will in principle be removed by a lattice distortion, as was pointed out by Jahn and Teller (R 1.7). If the lattice distorts so as to split the level, the centre of gravity of the resulting levels will remain unchanged, and so one of the split levels will be below the original unsplit level. The electronic splitting will tend to be proportional to the lattice distortion, while the energy of the lattice distortion will be proportional to the square of the distortion, because the lattice was originally in a position of minimum energy. An equilibrium state with a non-vanishing distortion will then be reached. However, the coupling of the f shell of Rare Earth ions with the lattice is so weak, that splittings arising from this cause are considered to be unlikely to be of significance.

For an ion with an odd number of electrons there will always remain an, at least, two-fold degeneracy in the absence of a magnetic field, because of the invariance of the Hamiltonian under time reversal (Kramers. R 1.8).

In order to make quantitative calculations of the splittings, it is necessary to adopt a particular model of the perturbation which affects the ion. This is commonly considered

as being an electrostatic potential $V(\underline{r})$ which has the symmetry of the lattice site of the magnetic atom. It is expanded in spherical harmonics Y_{lm} as:

$$V(\underline{r}) = \sum_{l=0}^{\infty} + \sum_{m=-l}^{l} r^{l} \quad A_l^m \, Y_{lm} \qquad 1.6$$

Certain restrictions are placed on the allowed values of l by the Wigner Eckart Theorem. The matrix elements of $V(\underline{r})$ between the states of an f^n configuration will reduce to the forms:

$$\langle 3m' | \, Y_{lm} \, | 3n \rangle \qquad 1.7$$

where $|3m\rangle$ are the single particle 4f wavefunctions which transform according to D^3. The Y_{lm} term in $V(\underline{r})$ transforms according to D^l, and so 1.7 will only be non-zero for $l \leqslant 6$ because:

$$D^3 \times D^l = D^{l+3} + \ldots\ldots + D^{|l-3|} \qquad 1.8$$

Furthermore, operating on 1.7 with the inversion operator shows that only for l=2,4,6 will 1.7 be non-zero.. $V(\underline{r})$ is then reduced to its final form by requiring it to be invariant under the operations of the relevant point group. The derivations of $V(\underline{r})$ for the groups D_{4h} and C_{3v} are given in Chapter 2.

A convenient method of calculating the matrix elements of $V(\underline{r})$ within the manifold of the states of a given J was put forward by Stevens (R 1.9). He pointed out that the matrix elements of the potential would be proportional to the matrix elements of any other operator which transformed under rotation in the same way. In particular, combinations of the components of the angular momentum operator $\underline{J}$ may be used, due allowance being made for the non-commutivity of the components. These operator equivalents have been tabulated by Hutchings (R1.10). The constant of proportionality is obtained by expressing one state, usually $|J,J\rangle$, in $m_l m_s$ quantisation, and calculating the expectation value of the operator equivalent and the original potential.

The interaction with a magnetic field is taken into account by adding a term $-g\mu_B \underline{J}.\underline{H}$, where g is the Lande g factor. The matrix of the crystal potential plus the magnetic energy is diagonalised in a $|JM\rangle$ representation, and from the eigenfunctions, the thermal average of the magnetisation $g\mu_B\underline{J}$ may be obtained.

From evidence provided mainly by susceptibility and resonance studies on dilute Rare Earth Salt Crystals (R 1.3, R 1.11) it is deduced that the splittings of the lowest multiplet level by the crystal field are of the order of 100 ^{o}K. In metals the splittings are found experimentally to be in the same range,

although rather less evidence is available due to the difficulty of growing & making resonance and susceptibility measurements on, metallic single crystals. Also, the interpretation of results is complicated, except for very dilute samples, by long range exchange couplings.

White et al (R 1.12) were able to fit fairly well the susceptibility of Ce diluted in $LaAl_2$ to a model in which the ground state of Ce is split by the cubic field into a doublet and a quartet separated by 200 ^{o}K. The susceptibility has an apparent paramagnetic Curie temperature of 40 ^{o}K, and the Curie Wiess law is followed down to about 20 ^{o}K. However, Maple and Fisk (R 1.13), from resistivity and more accurate susceptibility measurements, deduced that the susceptibility may be interpreted partially in terms of a spin compensated state. Mader and Swift (R 1.14) have been able to fit the susceptibility of the concentrated hexagonal compound $CeAl_3$ with a model involving an overall splitting of the Ce ground level of about 300 ^{o}K, plus an exchange field with a characteristic energy of roughly 20 ^{o}K. Again, there may be more possible interpretations that the one given; different values of the exchange and crystal field parameters may give equally good agreement with experiment.

As will be discussed in the next section, Ce often behaves in an anomalous manner when in a metal, so that the work of

Williams and Hirst (R. 1.15) and Murani (R. 1.16) on dilute solid solutions of heavy Rare Earths in Gold and Silver provides evidence which isopen to less ambiguity in its interpretation. They found that level splitting schemes could be devised which would fit the susceptibilities throughout the range of measurement. The overall splittings varied between 50 ^{o}K and 200 ^{o}K. Murani also found that, for the AuDy and AuHo alloys, the same level scheme which fitted the susceptibility, also fitted the spin disorder scattering resistivity, when calculated according to the theory of Hirst (R. 1.17), assuming a reasonable value for the exchange parameter.

Two significant features of the results of the work of Murani, and Williams and Hirst are that first, apparent Curie-Weiss behaviour may persist down to 10 ^{o}K – 40 ^{o}K, in the absence of any substantial interactions, even though the overall splittings are as great as 200 ^{o}K. Secondly, crystal field effects may give pseudo-paramagnetic Curie Temperatures of magnitudes up to 10 ^{o}K. These results were obtained for cubic materials, and for crystals of lower symmetry, such as the Rare Earth-Zinc intermetallic compounds discussed in this work, the lower symmetry crystal field might be expected to produce greater splittings. However, for measurements on polycrystalline materials, Van Vleck and Penney (R 1.18) have showed that anisotropies of susceptibility tend to cancel out.

An illustration of how a pseudo-Paramagnetic Curie Temperature may arise is given by the model of the levels of a magnetic ion shown in Fig. 1.4(a) (R 1.19). The ground state is a singlet, and there is an excited triplet of spectroscopic splitting factor g, D ^{o}K above it; it is assumed that there is no matrix element of the magnetic moment operator between the two levels.

The partition function Z is given by:

$$Z = 1 + e^{-\frac{D}{T}} \left(1 + e^{\frac{g\mu_B H}{kT}} + e^{\frac{-g\mu_B H}{kT}}\right) \qquad 1.9$$

and the magnetic moment M is $M = -kT \frac{\partial}{\partial H} \ln Z$. For low fields, this gives a susceptibility χ of:

$$\chi = \frac{2g^2 \mu_B^2}{kT(3 + e^{D/T})} \qquad 1.10$$

which is drawn in Fig. 1.4(b). At high temperatures the Curie Weiss Law is obeyed:

$$\chi = \frac{2g^2 \mu_B^2}{k(4T + D)} \qquad 1.11$$

and at low temperatures χ will go to zero unless there is a small matrix element of the magnetic moment operator between the

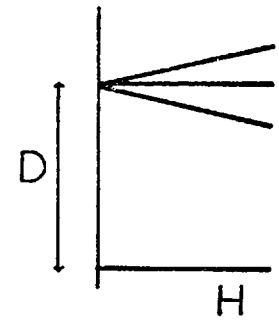


Fig. 1.4 a

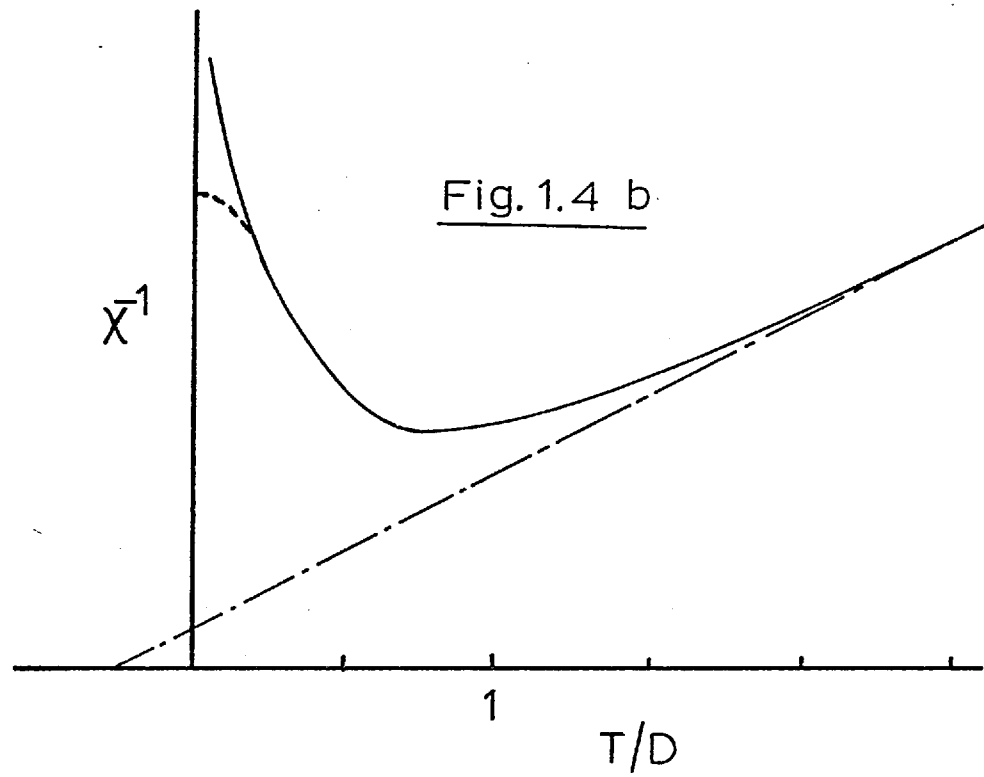


Fig. 1.4 b

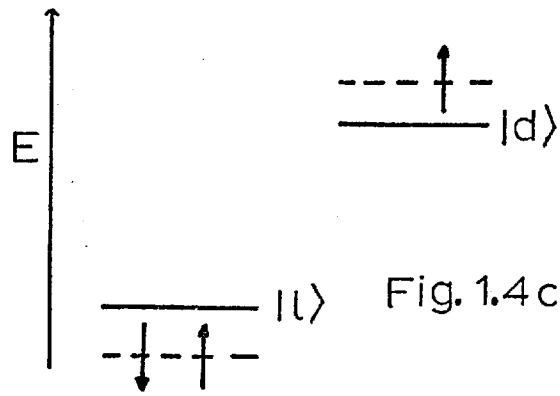


Fig. 1.4 c

two levels. If there is,a Van Vleck temperature independent term will be present and the behaviour will be given by the dotted line in Fig. 1.4(b).

The satisfactory fits obtained to susceptibility data by the authors quoted above are a consequence of the fact that they invoke only the symmetry properties of the solid. Attempts to calculate the magnitudes of the parameters of the crystal potential in metals have met with less success. The traditional approach has been to assume that the potential is caused by electric monopoles situated at the nuclei of the surrounding atoms. The applicability of this in a metal is dubious, and indeed the calculations of Williams and Hirst, made by placing a charge of one electronic charge at the surround atomic sites, gave values of the potential parameters which were about ten times smaller than the experimental values and one was of the wrong sign. An electric field will be shielded from the f shell by the outer and inner core states, but calculations of this effect, (R 1.20, R 1.21, R 1.22) which show that enhancements of the field may also occur, demonstrate that it is not sufficiently large enough to give a tenfold change. Williams and Hirst (R 1.15) attributed their large negative crystal field parameters to the Coulomb interaction with the screening change, part of which would lie in d-like virtual bound state, (to be discussed

in more detail in section 1.3), located on the Rare Earth site.

The point change model, even for insulators is, believed to be fundamentally inadequate, and a correct treatment must take the form of a multi-electron, multi-centre molecular orbital calculation. From the starting point of a linear combination of Atomic Orbitals scheme, the important principle is that the one electron Hamiltonian of the system will in general have non-zero matrix elements between the orbitals of the magnetic ion and those of its ligands. An insulator for which several calculations (for instance Sugano and Shulman R 1.23, Watson and Freeman R 1.24, Gladney and Veillard R 1.25) of this type have been made is $KNiF_3$.

In this compound the Ni ion is octohedrally co-ordinated by eight F^- ions. Let $|d\rangle$ and $|l\rangle$ be an orbital on the magnetic ion and one ligand ion respectively. h is the self-consistent Hamiltonian of the complex, which contains a kinetic energy term and potential contributions from both the metal ion and the ligands.

Applying first order perturbation theory the (unnormalised) states are:

$$|l\rangle \rightarrow |l\rangle - \frac{|d\rangle\langle d|h|l\rangle}{E(d) - E(l)}$$

$$|d\rangle \rightarrow |d\rangle + \frac{|l\rangle\langle l|h|d\rangle}{E(d) - E(l)} \qquad 1.12$$

with energies:

$$E(1) - \frac{|\langle d|h|1\rangle|^2}{E(d) - E(1)}$$

and

$$E(d) + \frac{|\langle d|h|1\rangle|^2}{E(d) - E(1)} \qquad 1.13$$

respectively, where $E(1)$ and $E(d)$ are the unperturbed energies of $|1\rangle$ and $|d\rangle$. (See Fig. 1.4C). Because there are two electrons in state $|1\rangle$ and only one in $|d\rangle$ the energy of the complex will be reduced by the Bonding Energy:

$$\frac{|\langle d|h|1\rangle|^2}{E(d) - E(1)} \qquad 1.14$$

Magnetic states having different symmetries will have different overlaps with the ligands and thus different energy splittings; the differences between their splittings will be the crystal field splittings discussed previously. Such calculations of the crystal field splitting in $KNiF_3$ agree with experiment to an accuracy of about 40% (R 1.25).

It can be seen that roughly a proportion:

$$\left| \frac{\langle d|h|1\rangle}{E(d) - E(1)} \right|^2$$

of an electron will be transferred out of the ligand orbital on to the magnetic ion, therefore leaving some unpaired spin on the ligand. This may be detected in the form of ligand hyperfine structure, (R 1.25, R 1.27) and provides direct evidence that the effects discussed above are taking place. The application of this type of calculation to Rare Earth ions is considerably more complicated (Watson and Freeman R 1.28) as the non-magnetic 5p shell of the ion plays an important part in the mixing process.

1.3. The Formation of Moments in Metals

When a magnetic atom is placed in a metal, two situations may occur. First, the energies of the occupied magnetic orbitals may lie well below the range of conduction band energies. In this case the magnetic state will mix with the conduction states to a small extent, as in equation 1.12, but will retain most of its free ion character. This will be called a Real Bound State.

In the other situation, the magnetic orbitals will lie within the range of conduction band energies; by equation 1.12 the mixing with band states will be very large and the concept of a local bound state breaks down. Friedel (R 1.29) considered the problem of electrons in a metal scattering from a potential which represented the effect of an impurity atom. By analysing the incident plane waves into spherical harmonics

and examining the phase shifts due to scattering, he found that a well defined entity, composed of scattered conduction states, termed a Virtual Bound State, existed localised in space and energy near the impurity. If this Virtual Bound State lies near the Fermi Level it will have a large scattering cross-section and make a large contribution to properties which depend on the density of states at the Fermi Surface. If, furthermore, the states of spin up do not occupy the same range of energies as those with spin down, one lying mostly above the Fermi level, the other below, then the state will be magnetised. Although, for reasons which will become apparent later, it is probable that the magnetic states of all the materials examined in this work are in the Real Bound State category, the Magnetised Virtual Bound State model is of such great value in understanding magnetism in metals that it will not be out of place to discuss it briefly.

Anderson (R 1.32) proposed a model consisting of an orbitally non-degenerate d impurity situated in a simple metal. The Hamiltonian, H, of the system consists of three terms:

$$H = H_k + H_d + H_{kd} \qquad \text{where}$$

$$H_k = \sum_{k,\sigma} E(k)\, n_{k,\sigma}$$

$$H_{kd} = \sum_{k,\sigma} V_{kd} \left(c^{+}_{k,\sigma} \, c_{d,\sigma} + c^{+}_{d,\sigma} \, c_{k,\sigma} \right)$$

$$H_{d} = \sum_{\sigma} E(d) \, n_{d,\sigma} + U n_{d\uparrow} n_{d\downarrow} \qquad 1.15$$

The c's are the usual Fermion Operators (see for instance Abrikosov et al R 1.33) and $n_a = c^{+}_{a} \, c_a$. H_k is the band energy, H_d consists of the single particle energies of the d states plus a Coulomb term between electrons on the impurity site, and H_{kd} is the mixing term, V_{kd} being the matrix element of the self-consistent one-electron Hamiltonian between the states $|k\rangle$ and $|d\rangle$.

A competition will result between the mixing term, which will attempt to transfer an electron, which has opposite spin to the one already on there, onto the impurity (by the Pauli principal it cannot transfer one of the same spin), and the correlation energy which tends to favour an electron of only one spin on the impurity at a time.

Anderson treated the Hamiltonian in the Hartree Fock approximation and found that a moment could exist if the following conditions were obeyed:

$$0 \leqslant \frac{-E(d)}{U} \leqslant 1$$

$$U/\Delta > \pi \qquad 1.16$$

where the energies are measured from the Fermi Energy, E(d) is the energy of unperturbed d state, and Δ is the half-width of the Virtual Bound State:

$$\Delta = \pi \langle V_{kd}^2 \rangle \rho(E) \qquad 1.17$$

and $\rho(E)$ is the density of conduction states of one spin direction. If $U/\Delta < \pi$ the state will be non-magnetic. Anderson also shows that for degenerate orbitals the criterion for the existence of orbital magnetism is even more severe. Wolff (R 1.34) has given a similar model in terms of Wannier functions.

The non-physical sharp boundary between the magnetic and non-magnetic states in the Anderson model is removed if one considers the time scale over which the moment exists (R 1.35, R 1.36). As a non-magnetic impurity atom approaches the transition point, excited states of finite moment become lower in energy and easier to attain, and the characteristic time over which a moment exists (the localised spin fluction time) increases until it is long enough to affect an experimental probe.

The essential feature that a localised state must possess for it to be described by the above Friedel-Anderson model, is that its unperturbed magnetic levels should lie within the range of conduction band energies. Band structure calculations for Gd (R 1.37) show that the 4f state is about 11 ev below the

conduction bands, thus suggesting that this situation does not obtain, and that Gd, at least, should behave as a real bound state. However, some of the Rare Earths, having unstable valence states near a full or half full shell, fall into the virtual bound state category. Ce is the element which most often gives this behaviour, for instant YCe alloys (R 1.38) show signs of a spin compensated state in the 3 ^{o}K region. Pr shows a Kondo-like resistivity when diluted in ZrB_{12} (R 1.39), Eu (in a nearly divalent state) has shown a giant thermopower in Au (R 1.40) and Yb shows Kondo effects in the resistivity when diluted in Au-Ag alloys (R 1.41).

Where a true bound state does exist, the form of its interaction with the conduction electrons in the metal may be obtained from the Coulomb energy (R 1.33).

$$\sum_{s,s'} \tfrac{1}{2} \Psi_s^{+}(\underline{r}) \Psi_{s'}^{+}(\underline{r}') V(\underline{r}-\underline{r}') \Psi_{s'}(\underline{r}') \Psi_s(\underline{r}) \, d\underline{r}' \, d\underline{r} \qquad 1.18$$

where $\Psi_s(r)$ is the Fermian Field Operator and $V(\underline{r} - \underline{r}')$ is the two body interaction between the particles.
Expressing the Field Operator in basis dependent form:

$$\Psi_s(\underline{r}) = \sum_j \phi_{j,s}(\underline{r}) \, c_{j,s} \quad , \qquad 1.19.1$$

where $c_{j,s}$ is an operator which destroys a particle in state j with spin s, having wavefunction $\phi_{j,s}(\underline{r})$, and using for this basis the conduction states plus bound states on the magnetic atom, the following expression is obtained (R 1.42, R 1.43)::

$$H_{sf} = -\frac{1}{N} \sum_{n} \sum_{\underline{k};\underline{k}} \sum_{s,s'} J(\underline{k},\underline{k}') e^{i(\underline{k}-\underline{k}').\underline{Rn}}$$

$$\underline{S}_n \cdot \underline{\sigma}_{ss'} \; c^{+}_{\underline{k}s} \; c_{\underline{k}'s'}$$

where

$$J(\underline{k},\underline{k}') = Ne^{-(\underline{k}-\underline{k}').\underline{Rn}} \int d\underline{r} d\underline{r}' \; V(\underline{r}-\underline{r}')$$

$$\phi^{*}_{\underline{k}'}(\underline{r})\phi^{*}_{f}(\underline{r}'-\underline{Rn})\phi_{k}(\underline{r}')\phi_{f}(\underline{r}-\underline{Rn}). \qquad 1.19.2$$

$\underline{\sigma}_{ss'}$ are the matrix elements of the Pauli Spin Operator, the metal is of volume V and has N atoms (including both magnetic and non-magnetic ones), and the magnetic atoms are situated at $\underline{R}_n$. The ϕ_R and ϕ_f are the wavefunctions of the conduction and magnetic states respectively. Equation 1.192contains only terms with two Fermion operators on the f site. Bailyn (R 1.43) has examined other terms, but finds the above to be most significant.

$J(\underline{k},\underline{k}')$ is often taken to depend only on $\underline{k} - \underline{k}'$ (R 1.42), however, this a poor approximation (Kaplan and Lyons R 1.48 , Freeman and Watson R 1.49), but even so, for the purposes of interpreting

experimental results it is usually necessary to go further and take $J(\underline{k},\underline{k}')$ equal to a constant $\bar{J}$. Doniach (R 1.50) has shown that this is equivalent to assuming that the impurity interacts only with that conduction electron Wannier function which is located on the impurity site.

In a Wannier representation the interaction will be of the form:

$$H_{sf} = -\bar{J} \sum_{\substack{n \\ ss'}} \underline{S}_n \cdot \underline{\sigma}_{ss'} \, a^{+}_{ns} a_{ns'} \qquad 1.20$$

where a_{ns} destroys a particle in the Wannier function based on the site at $\underline{R}_n$.

When the magnetic ion consists of several electrons Hund's rule coupled to give a resultant $\underline{S}$, $J(\underline{k},\underline{k}')$ will be an average over the various ϕ_f's. Equation 1.20 is equivalent to taking the interaction between a conduction electron at $\underline{r}_i$ with spin operator $\underline{s}_i$ as:

$$-2\bar{J} \frac{V}{N} \underline{S}_n \cdot \underline{s}_i \, \delta(\underline{R}_n - \underline{r}_i) \qquad 1.21.1$$

or a total interaction of:

$$H_{sf} = -2\bar{J} \frac{V}{N} \underline{S}_n \cdot \underline{s}(\underline{R}_n) \qquad 1.21.2$$

where the conduction electron spin density operator $\underline{s}(\underline{r})$ is given by:

$$\underline{s}(\underline{r}) = \sum_i \delta(\underline{r} - \underline{r}_i)\underline{s}_i$$

The notation for $\bar{J}$ which we use here is the same as the J used by Kasuya (R 1.51), Yosida (R 1.52), and Kondo (R 1.53, R 1.42). However, several European workers have used other notations. De Gennes (R 1.54) used $\Gamma = 2\bar{J}$, Rocher (R 1.55) used the same symbol with a different value $\Gamma = 2\bar{J}V/N$, V/N being the atomic volume, and Peter, Dupraz and Cottet (R 1.56) have used $J = 2\bar{J}$.

Any results of other workers which we quote here will be translated into our usage.

An estimation of the size of $\bar{J}$ may be obtained from equation 1.20 and the difference between the ^7S and ^9S states of the free Gd^{2+} ion. From this, the value $\bar{J} = +0.05$ eV is deduced.

When the moment falls into the Virtual Bound State category, Bailyn (R 1.43) and Schrieffer and Wolff (R 1.63) have shown, following Anderson (R 1.32) and Kondo (R 1.60), that in the limit of large U/Δ (equations 1.15 and 1.16) the Anderson Hamiltonian may be transformed into a form consisting of a potential scattering term plus a scalar spin term like equation

1.20 and $\bar{J}$ given approximately by:

$$\bar{J} = 2 |V_{kf}|^2 U / E_f(E_f + U) \quad , \qquad 1.21$$

where the energies are measured from the Fermi level. The arguments leading to equation 1.21 are analogous to those in Anderson's Theory of Superexchange in Insulators. There will, then, be two contributions to the coupling constant $\bar{J}$, a direct exchange part and an antiferromagnetic part, equation 1.21. Freeman et al (R 1.61) have examined the case of a Gd^{3+} ion interacting with an orthogonalised plane wave. They find that the antiferromagnetic part may be comparable in magnitude to the direct exchange part, but in view of the difficulty of estimating the equivalent of the mixing matrix element V_{kf} it is not clear how much relevance this has to real physical situations.

For Rare Earth ions, whose lowest lying levels are characterised by the quantum number J, the matrix elements of $\underline{S}$ will be proportional to those of $\underline{J}$, within a manifold of constant J, according to the Wigner-Eckart Theorem. The expression is, in fact,

$$\underline{S} = (g-1)\,\underline{J} \qquad (J \text{ constant}) \qquad 1.22$$

where g is the Lande g factor. This led De Gennes (R 1.68) to suggest that the correct expression for the spin coupling in Rare Earth materials would be obtained by replacing $\underline{S}$ in equation 1.20 by $(g-1)\underline{J}$. Liu (R 1.69) showed that this approximation was reasonable, provided that the conduction electrons were primarily s-like, and that the radius of the f shell was small compared with the inverse of the Fermi wave-vector - a condition which is not particularly well obeyed in typical metals.

1.4. The s-f Interaction in Metals

For one Rare Earth atom, situated at the origin of co-ordinates, in a metal, the first order change in energy is $\langle H_{sf} \rangle$ and from 1.19.2this is equal to, in the $J(\underline{k},\underline{k}') = J(\underline{k} - \underline{k}')$ approximation:

$$- \frac{J(0)}{N} (g - 1)J^z(n_+ - n_-) \qquad 1.23$$

where n_s is the number of conduction electrons of spin s in the metal. To a first approximation:

$$n_+ - n_- = \chi HV/\mu_B = 2\rho N \mu_B H \qquad 1.24$$

where χ is the volume uniform spin susceptibility of the conduction electron gas, and ρ is defined by equation 1.24. For a simple metal, ρ will be equal to the density of conduction states in energy, per atom, for <u>one</u> spin direction. This notation follows that of Kondo 1969 (R 1.42).

Thus the total energy, including that of the bare moment in the field $- g\mu_B J^z H$, becomes:

$$- g\mu_B H J^z \left(1 + \frac{2(g - 1)}{g} J(0)\rho\right) \qquad 1.24.1$$

neglecting a small term due to the Pauli susceptibility. Therefore the system of (ION plus CONDUCTION ELECTRONS) will behave as if it were a spin of multiplicity 2J + 1 and spectroscopic splitting factor g' where:

$$g' = g\left(1 + \frac{2(g-1)}{g} J(0)\rho\right)$$

$$= g\left(1 + \frac{\Delta g}{g}\right) \qquad 1.25$$

and Δg is defined by the equation..

The magnetic moment$\langle m \rangle$will be given by:

$$\langle m \rangle = g' \mu_B J B_J(Jg' \mu_B H/kT) \qquad 1.26$$

$B_J(x)$ being the Brillouin function; and the paramagnetic moment ρ and the ferromagnetic moment n will both be enhanced by a factor of $(1 + \Delta g/g)$. The electron spin resonance g factor will also be enhanced by a similar amount, as shown by Yosida (R 1.52), but the presence of dynamical effects (Hasegawa R 1.70, Peter et al R 1.56) complicates the interpretation of the resonance spectra considerably.

The simple first order model given above, which is valid as $J(0) \rightarrow 0$, is based on the assumption that the crystal field splittings in non S-state ions are zero. However, within a

manifold of constant J, the crystal field split states will be linear combinations of the $|J,M\rangle$ and so the enhancement factors remain valid. In particular, the crystal field susceptibility will be enhanced by a factor of $(1 + \Delta g/g)^2$.

The sf interaction will also enhance the Van Vleck temperature independent susceptibility in non S-state Rare Earths. Replacing $(g - 1)J^z$ by S^z in equation 1.23, an interaction of $-\mu_B H\, S^z 2\rho J(0)$ is obtained, in addition to the Hamiltonian $-\mu_B H(L^z + 2S^z)$ which is the normal cause of Van Vleck paramagnetism in Rare Earths. Now, between states of $|J\rangle$ and $|J \pm 1\rangle$, the matrix elements of $\underline{S}$ and $(\underline{L} + 2\underline{S})$ are exactly the same, because $\underline{J}$ is diagonal in J, by definition. Therefore, both the matrix elements and the susceptibility are enhanced by factors of $(1 + 2\rho J(0))$. Thus, if in the absence of the s-f interaction, the susceptibility of a Rare Earth ion is:

$$\chi(T) + V \qquad 1.27$$

where $\chi(T)$ is the temperature (T) dependent part of the susceptibility, which arises from matrix elements of the magnetic moment operator withinthe lowest J level, and V arises from Transitions between $|J\rangle$ and $|J \pm 1\rangle$, then in the presence of the s-f interaction the susceptibility will become:

$$\chi(T)\left(1+\frac{2(g-1)}{g}J(0)\rho\right)^2+V(1+2\rho J(0))^2 \qquad 1.28$$

The extra Van Vleck term is, in fact, too small to be detected in the results described in this work, and will be ignored from now on..

The above way of treating the first order sf interaction is similar to the means used to calculate the Knight shift - the change in nuclear resonant frequency due to the Contact Interaction with the conduction electrons - in a metal. Another approach to the static s-f interaction uses Linear Response Theory (for instance Doniach R 1.50), and this possesses the convenience of separating the effects due to the band structure of the conduction electrons from those due to the wavevector dependent properties of $J(\underline{k}-\underline{k}')$.. The formalisms of Linear Response Theory are set down in Appendix Aa.

From comparing the form of the sf interaction of equation 1.21.2with equation A.1, it can be seen that the $\underline{q}$th Fourier component of the effective field acting on the conduction electron system is:.

$$H'(\underline{q}) = J(\underline{q})\frac{V(g-1)}{N\mu_B}\langle J^z\rangle \qquad 1.29$$

and so the magnetisation $M(\underline{r})$ induced by the spin is:

$$M(\underline{r}) = \frac{(g-1)\langle J^z\rangle}{N\mu_B} \frac{V}{(2\pi)^3} \int J(\underline{q}) \chi(\underline{q}) e^{i\,\underline{q}\cdot\underline{r}}\, d\underline{q} \qquad 1.30$$

Now, for a non interacting free electron gas:

$$\chi(\underline{q}) = \chi^o(\underline{q}) = \chi f\frac{(\underline{q})}{2k_f}/2 \qquad 1.31$$

where χ is the uniform Pauli susceptibility and:

$$f(q) = 1 + \frac{1-q^2}{2q} \ln\left|\frac{1+q}{1-q}\right| \qquad 1.32.1$$

Putting 1.32.1 into 1.30, assuming that $J(\underline{q}) = \overline{J}$, and integrating, one obtains:

$$M(\underline{r}) = -9\pi Z^2 \mu_B \frac{\overline{J}}{E_F} \frac{N}{V} (g-1)\langle J^z\rangle F^4(2k_f r) \qquad 1.32.2$$

where Z is the number of conduction electrons per atom, k_f is the Fermi wavevector, and E_f the Fermi Energy, and:

$$F^4(x) = (x\cos x - \sin x)/x^4 \qquad 1.33$$

This expression was first derived by Yosida R 1.52 who also considered the case of:

$$J(\underline{q})f(\underline{q}) = 2\bar{J} \quad , \quad q < 2kf$$
$$J(\underline{q})f(\underline{q}) = 0 \quad , \quad q > 2kf \qquad 1.34$$

and obtained an expression similar to equation 1. 32.2 but with $F^3(2k_f r)$ replacing $F^4(2k_f r)$ where:

$$F^3(x) = \frac{2x}{\pi} F^4(x) \qquad 1.35$$

The total magnetic moment $m = \int M(\underline{r})d\underline{r}$ induced in the electron gas may be obtained from Equations A.6 and 1.29. It is found to be:

$$m = 2(g - 1)J(0)\rho\langle J^z\rangle \qquad 1.36.1$$

thus, recovering equation 1.24.1. Equation 1.36.1may also be obtained by directly integrating over real space equations 1.33 and 1.35. The answer must, of course, be the same in both cases if equation A6 is to be valid.

A consequence of equation 1.30 is that moments situated at different places in the metal will be coupled indirectly by the conduction electrons, as one moment will interact with the polarisation caused by another. By second order perturbation theory the expression for the total interaction energy H_I is:

$$H_I = -\frac{V}{2N\mu_B^2} \sum_{i,j} (g_i - 1)(g_j - 1)\underline{J}_i \cdot \underline{J}_j$$

$$\sum_{\underline{q}} J_i(\underline{q}) J_j(q) \quad \chi(\underline{q}) e^{i\,\underline{q}\cdot(\underline{R}_i - \underline{R}_j)} \qquad 1.36.2$$

When the magnetic atoms are all of the same species, $J(\underline{q})$ is approximated by $\bar{J}$, and the conduction electrons are free, with their wavevector dependent susceptibility given by equation 1.31, then the above expression reduces to:

$$H_I = \frac{1}{2} \sum_{\substack{i,j \\ i \neq j}} \frac{9\pi Z^2 \bar{J}^2 (g-1)^2}{E_F}$$

$$F^4(2k_f|\underline{r}_i - \underline{r}_j|)\underline{J}_i \cdot \underline{J}_j \qquad 1.37$$

This indirect coupling between moments, and the oscillatory conduction electron polarisation which results from the sf interaction are associated with the names of Ruderman and Kittel (R 1.58), Kasuya (R 1.51) and Yosida (R 1.52), (RKKY).

If the susceptibility of the metallic matrix in which the moment is situated is not free-electron like, then the resulting spin polarisation may be substantially different from that given by equation 1.31. Wolf (R 1.71) has shown that

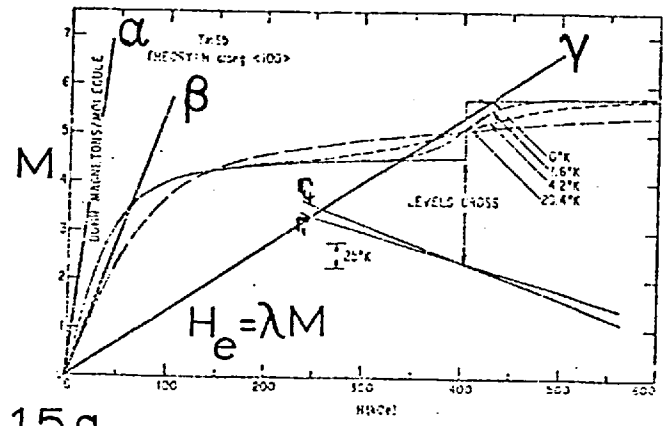


Fig.1.5 a Predicted magnetization of TmSb for H along ⟨100⟩ hard axis. Variation of Γ_1 and lowest Γ_4 levels with field is shown with separation in °K as indicated. Theory is for $x = -1$, $W = 0.939$°K.

see p70

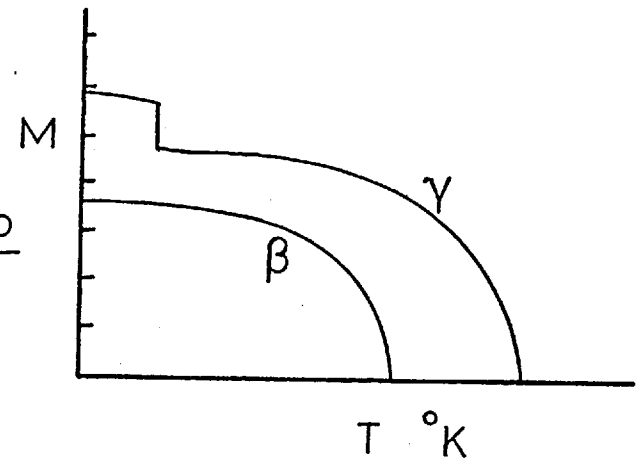


Fig.1.5 b

when interactions within the electron gas are taken into account, the wavevector dependent susceptibility $\chi(\underline{q})$ becomes, in the Random Phase Approximation:

$$\chi(\underline{q}) = \chi^{o}(\underline{q}) \quad (1 - \chi^{o}(\underline{q}) I/2\mu_B^2)^{-1} \qquad 1.38$$

where I is the strength of a Delta Function interaction between the particles. If the second term in the denominator approaches unity at any particular $\underline{q}$, the susceptibility will diverge, and a magnetically polarised state of characteristic wavevector $\underline{q}$ will result. For a free electron gas, I $\chi^{o}(\underline{q})$, of course, has its potential instability at $\underline{q} = 0$, but for a general matrix it may well not as $\chi^{o}(\underline{q})$ is given (for one band), by (R 1.71):

$$\chi^{o}(\underline{q}) = -2\mu_B^2 \sum_{\underline{k}} \frac{f(\underline{k}+\underline{q}) - f(\underline{k})}{E(\underline{k}+\underline{q}) - E(\underline{k})} \qquad 1.39$$

where $f(\underline{k})$ and $E(\underline{k})$ are the occupation number and band energy respectively of the state $\underline{k}$. There is, in general, no necessity why this should have its maximum value at $\underline{q} = 0$.

Because the range of the conduction electron polarisation induced by a localised spin depends mainly on $\chi(\underline{q})$ at low $\underline{q}$, and the total moment induced is proportional to $\chi(0)$, any enhancement of a free electron gas according to equation 1.38 will, as its effects are largest at low $\underline{q}$, have its greatest influence on the above two properties. This was pointed out by Giovannini et al (R 1.77).

It can be seen then, that there are three characteristic types of metallic matrix which may be encountered. The first is the simple metal with bands constructed primarily from s functions lying well above any d-like states, Au, Ag, Zn are examples. The second is the unenhanced transition metal which has a large density of states at the Fermi level, caused by several degenerate d bands. This will have a correspondingly large static susceptibility and electronic specific heat, and a tendency towards superconductivity. Typical examples ar La, Y, Nb, Mo and the intermetallic compound $LaAl_2$. The last group consists of transition metals whose d bands have susceptibility enhanced according to equation 1.38. Pd is the best known of these, its enhancement factor $\chi(0)/\chi^{o}(0)$ being in the range 6 to 10 (R 1.31, R 1.78) and some others are Pt and the intermetallic compounds $LaRu_2$ (R 1.62) and Ni_3Ga (R 1.79).

The results of measurements of the susceptibilities of Rare Earths dissolved in simple metals have been mentioned in section 1.2. The workers found that the paramagnetic moments were in good agreement with free ion values, but because the solute concentrations were not known very accurately, it was not possible to detect small deviations from these ionic values. Maple (R 1.72) found the effective moment of Gd dissolved

in $LaAl_2$ to be 5% higher than the free ion value. According to Lowin (R 1.86) this leads to J(0) = +.05 eV, but Coles et al (R 1.87) from g shift measurements, obtained a smaller value J(0) = +.017. Finnemore et al (R 1.88) found that Gd in La possessed a paramagnetic moment 5% higher than the free ion value for Gd concentrations greater than about 1%. but claimed that for smaller concentrations there was no increase in moment.

The difficulty of accurately estimating the concentration of dilute alloys, which casts doubt on the interpretation of their effective moment results is less in the case of intermetallic compounds, as the composition of their magnetic components, in general being larger, can be estimated more accurately.

Wallace (R 1.83) has compiled data on the magnetic properties of several binary intermetallic compounds consisting of a Rare Earth in conjunction with a non-transition metal or a 3d or 4d transition metal. Many of the compounds are ferromagnetic, so that an estimation of the effective moment per Rare Earth atom may be obtained, and interpreted by means of equations 1.25 and 1.26. It has to be assumed that the ferromagnetic state is truly ferromagnetic and saturated. Where the ordered state is not ferromagnetic, the paramagnetic moment is taken. To avoid complications due to crystal field effects

only Gd compounds are considered, and of course, only those Gd compounds are taken account of whose partner is clearly not contributing any moment.

Examining these data in this fashion, a simple rule is found to hold in most cases. When the partner of the Rare Earth is non-transition like the moment per Rare Earth atom will tend to be increased, and when the partner is a transition metal the moment will be reduced.

Compounds which obey the first half of this rule are GdCu, GdIn, GdSb, GdBi, $GdSn_3$, $GdZn_{12}$ (this work), and $GdIn_3$ (R 1.91). Exceptions are GdAu, which is 0.2% below the free ion value, $GdSi_2$ which is 1.5% below, Gd_2Zn_{17} (this work) 1% below, and GdZn (R 1.89) and $GdZn_2$ (R 1.90) whose ferromagnetic moments are 4% and 1.5% respectively below, although the paramagnetic moment of $GdZn_2$ is 7% above the free ion value. However, as the workers who obtained the results for $GdZn_2$ announced a few years earlier (R 1.93) that its paramagnetic moment was 13% greater than the free ion value, perhaps the results need not be taken too seriously.

Compounds obeying the second half of the rule are $GdRu_2$ $GdRh_2$, $GdOs_2$, $GdIr_2$, $GdPt_2$. Gd dissolved in Pd (R 1.46, R 1.47) and in $LaRu_2$ (R 1.62) also shows a reduction in moment.

The only 3d partner which is non-magnetic, Ni, shows variable behaviour. As the Ni concentration increases, the Gd moment is reduced. Gd in GdNi has a moment increased by +6%, $GdNi_2$ by 1%, but $GdNi_5$ has a moment which is 3% less than the free ion value. $LaAl_2$ is a material which is harder to categorise. It has a positive transition metal-like Pauli susceptibility (R 1.72) and is a superconductor. As we have noted before, Gd dissolved in it has an enhanced effective moment (R 1.72) and a positive g shift (R 1.87). However, the intermetallic compound $GdAl_2$ has a ferromagnetic moment of 6.9 μ_B, 1.5% down on the free ion value, and a negative g shift with $\Delta g/g = -5\%$ (R 1.94) in the paramagnetic region.

Materials in which the enhancement of the Gd moment is particularly large are, Gd metal +8% (R 1.95), $GdRu_2$ - 10%, and Gd dissolved in Pd. Shaltiel et al (R 1.47) found after correcting the Pd matrix susceptibility for the change caused by the addition of Gd, that the Gd paramagnetic moment was reduced by 26%. Crangle (R 1.46) found that the ferromagnetic moment of Gd (in the dilute limit) was reduced by 27%, in good agreement. Cottet and Peter (R 1.76) found that in the dilute limit the g shift of Gd in Pd tended to $\Delta g/g = -0.11$.

Hitherto, the explanation offered for these reductions of the moment has been than for Gd, the antiferromagnetic

contribution to J(0) from kf mixing (Bailyn R 1.43, Shrieffer and Wolff R 1.63) outweighs the direct exchange contribution. B. R. Coles and others (R 1.87) have put forward an alternative suggestion. They argue that because the $4f^7$ configuration is expected to be extremely stable, and the energy denominators in the perturbation theory treatment of the antiferromagnetic contribution to J(0) are expected to be of the order of 10 eV, J(0) will always be positive. They suggest that in the transition like materials which we have been discussing, it is meaningful to divide the conduction electron states at the Fermi surface into s and d bands. The s band will be coupled parallel to the f electrons by the positive J(0) direct exchange constant, but the spin densities of the s and d bands will be coupled antiparallel by s-d hybridisation. This will be the analogue, in a band, of the antiferromagnetic coupling between an s band an a d-like virtual bound state which was envisaged by Anderson (R 1.32), Kondo (R 1.60), De Gennes (R 1.54) Bailyn (R 1.43) and Schrieffer and Wolff (R 1.63). This anti-parallel polarisation is observable in the pure transition metals Fe (R 1.96), Co (R 1.105), Ni (R 1.104), in which neutron diffraction experiments show areas of negative magnetisation inbetween the Fe atoms.

In Appendix A(b) of this thesis we make some suggestions for an approach to a phenomenological mathematical model of Coles' idea. A molecular field model, using static linear response theory, is used to calculate the total magnetic moment induced in a conduction electron system consisting of an s and a d band, by one local spin. The spin is allowed to couple into both bands, and the s-d hybridisation energy is taken to be of the form:

$$H_{sd} = A \int M_s(\underline{r})\, M_d(\underline{r})\, d\underline{r} \qquad 1.40$$

where $M_s(\underline{r})$ and $M_d(\underline{r})$ are the z components of the s and d band magnetisations. Applications of thismodel to the GdPd and FePd systems are discussed briefly.

Peter et al (R 1.56) have compiled the g shift results of Gd in several metallic matrices. These data do not fit our simple rule so well, for although the g shifts of Gd in simple metals are positive, and those in transition matrices are mainly negative, 5% Gd in $LaPt_5$, for instance, has a g shift of +.03, and this material might be expected to be substantially transition-like. Dynamical effects (R 1.70, R 1.56) are known to be important in these alloys, and at the high Gd concentrations used (mostly around 5% in these results),

may be significant.

Resonances of non S-state ions have been reported by Griffiths and Coles (R 1.98) for ErAg and by Hirst et al, (R 1.99, R 1.15) for ErAu, AuYb. These workers were not able to discern a g shift, but from line-width measurements estimated $|\bar{J}|$ to be roughly 0.1 eV. Burr and Orbach (R 1.100) found a resonance of Er in single crystal Mg. They were able to fit an anisotropic temperature dependent line-width to an isotropic $|\bar{J}| = .06$ eV.

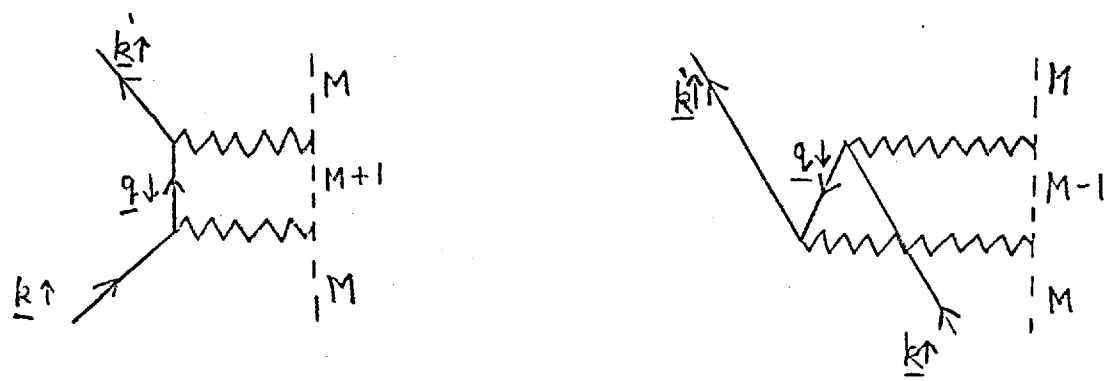
Another manifestation of the sf interaction is the reduction of the transition temperature Tc of a superconductor by local moments. When diluting Gd in the intermetallic compound $LaAl_2$, Maple (R 1.72) found excellent agreement with the theory of Abrikosov and Gorkov (R 1.73). Maple and Fisk (R 1.13) also found that the reduction of T_c of $LaAl_2$ by different Rare Earths was roughly proportional to the projected spin $(g-1)J(J+1)$, with the exception of Ce, which gave an anomalously large reduction indicative of virtual bound state behaviour. Similar results were found for Rare Earths dissolved in La (Matthias et al R 1.74) and in YB_6 (Fisk et al R 1.75). The value of the modulus of the sf coupling constant $\bar{J}$ deduced from the reduction of T_c by Gd for these materials was in La: .025 eV (R 1.31), YB_6: .023 eV (R 1.31) $LaAl_2$: .042 eV

The latter result is decreased by a factor of 3 from the result obtained from assuming a free electron density of states, in order to take account of the increased density of states, which was (arbitrarily) assumed to have been enhanced by the same factor as was that of the heavy Rare Earth metals (R 1.54). The other two results assume that the band structure is free-electron like.

1.5. The Divergence of Perturbation Theory

When the s-f Hamiltonian is treated in the first Born approximation (Kasuya, R. 1.51), it is found that in the dilute limit the resulting resistivity is independent of temperature. This does not explain the phenomenon of the resistance minimum which is often observed when magnetic atoms are dissolved in metals (reviewed by Van den Berg R 1.106), and this was not understood until the publication of Kondo's famous paper in 1964 (R 1.53).

Kondo showed that when the scattering process was taken to second order, an interference occurs between the two scattering modes shown below.



More generally, any scattering Hamiltonian will be of the form:

$$\sum_{ij} T_{ij}\, c_i^{+}\, c_j \qquad 1.41$$

and in the calculation of scattering probability in second order, certain commutators $[T_{ij}, T_{ji}]$ arise. When the T's are c numbers, as in potential scattering, these commutators and several of the scattering terms will vanish, but when they are quantum mechanical operators, such as spin operators, they may not. For instance $(S^{+}, S^{-}) = 2S^{z}$, and including terms arising from non-zero commutators of this sort, Kondo found a scattering cross-section which diverged as the energy of the scattered electron approached the Fermi Energy. At finite temperatures the magnetic resistivity ρ_M was found to be given by:

$$\rho_M = \rho_o(1 + 4\bar{J}\rho \ln kT/D) \qquad 1.42$$

where D is of the order of the Fermi Energy and:

$$\rho_o = (2\pi\rho\, m\, c/ZNe^2\hbar)\bar{J}^2\, S(S+1) \qquad 1.43$$

c is the fractional concentration of magnetic atoms, and the expression is derived for the spin-only case. For negative $\bar{J}$, ρ_M will increase as the temperature is lowered and this, in conjunction with the phonon resistivity which increases as the temperature is raised, provides the resistance minimum.

The resistance minima which are observed when moment bearing 3d transition metal atoms are dissolved in simple metals (R 1.106) are interpreted as being due to the admixture antiferromagnetic exchange of the d virtual bound state with the conduction electrons.

Kondo behaviour indicative of both positive and negative $\bar{J}$ has been observed for Rare Earths diluted in metals. Gd dissolved in Y gives a resistivity which decreases with decreasing temperature. (Sugawara R 1.107), and from equation 1.42 a value of $\bar{J}$ of +0.08 eV is deduced. Tb in Y shows possibly similar behaviour, but because of the presence of crystal field effects, the interpretation of the results is less certain. On the other hand, Ce often forms a virtual bound state in metals with a consequent negative exchange coupling; for intance, Ce in Y (R 1.107) in La(R 1.112) and in $LaAl_2$(R 1.13) gives a resistance minimum. It would appear from equation 1.42 that if the s-f Hamiltonian is taken, in the spirit of De Gennes' (R 1.68) proposal as $-2\bar{J}$ V/N (g-1) $\underline{J}.\underline{s}$, then a positive $\bar{J}$ would be needed to give a resistance minimum, as for Ce (g-1) is negative. However, Coqublin and Schrieffer (R 1.66), starting from the Anderson model for Ce, suggested that the Kondo effect in Ce alloys was caused by a negative $\bar{J}$ due entirely to antiferromagnetic admixture exchange.

Logarithmic terms appear in other quantities when the s-f perturbation is taken to higher order. The susceptibility (Yosida and Okiji R 1.108) and g shift (Spenser and Doniach R 1.109) are increased by the factor$(1 + 4(\bar{J}\rho)^2 \ln kT/D + \ldots\ldots)$. The RKKY spin polarisation

around the impurity $\rho(\underline{r})$ becomes:

$$\rho(\underline{r}) = \rho^{o}(\underline{r})\,(1 - 2\bar{J}\rho \ln(2k_f r) + \ldots) \qquad 1.44$$

where $\rho^{o}(\underline{r})$ is the first order RKKY polarisation (Fullenbaum and Falk R 1.110).

Perturbation calculations of these and other quantities to infinite order (R 1.42) show that for $\underline{J}$ negative, the calculations diverge at a temperature T_K given by:

$$kT_K = E_F \exp(-1/2\,|\bar{J}|\rho) \qquad 1.45$$

Nagaoka (R 1.64) suggested that below this temperature a singlet state would occur with the local spin being compensated by a cloud of anti-parallel spin conduction electrons which would condense around it. Ce$\underline{Y}$ in the $1^{o}K$ range appears to be an example of this situation, and many 3d solutes show this behaviour. The relation of this state to the Friedel-Anderson unmagnetised virtual bound state is not clear, and the two may be connected by the spin fluctuation concept. Theoretical and experimental work in this field has been reviewed by Kondo (R 1.42) and Heeger (R 1.111).

Kondo phenomena are not expected to be important in the concentrated magnetic materials dealt with in this thesis, first because from equation 1.45, for $\bar{J}$ = .05 eV and the density of states equal

to the free electron value $\rho(E_F) = 0.165$ states/eV atom for one spin direction and $E_F = 9.5$ eV, then T_K turns out to be much lower than experimental temperatures. Secondly, the large exchange fields in the magnetically ordered state will quench the internal degrees of freedom of the spins, and inhibit Kondo scattering. In the present work we therefore only consider phenomena which arise from the first order s-f interaction.

1.6. Interactions Between Moments

We have seen, in the previous section, that the interaction between Rare Earth moments in a metal may be expressed in Heisenberg form as (equation 1.37):

$$\mathcal{H} = \sum_{\substack{i,j \\ i \neq j}} J_{ij}\, \underline{S}_i \cdot \underline{S}_j \qquad 1.46$$

For virtual bound states Caroli (R 1.67) has also derived a similar expression, but the coefficients J_{ij} are typically much larger than those for bound states.

From molecular field theory, in the free electron approximation (R 1.54), the Paramagnetic Curie Temperature θ is predicted to be given by:

$$k\theta = -(3\pi Z^2 \bar{J}^2/E_F)(g-1)^2 J(J+1) \sum_{j \neq 1} F^4(2k_f R_{ij}) \qquad 1.47.1$$

where R_{ij} is the distance between two magnetic ions and the summation is made by taking one magnetic atom as the origin and summing the function F^4 (equation 1.33) over all the others. Several of these calculations have been made for various materials, but many give the wrong sign for θ .. Calculations for the heavy Rare Earth metals (R 1.54) and CuMn (R 1.50) give the correct sign, but in calculations for the following materials the sign of θ turns out to be incorrect: $GdAl_2$ (R 1.57), GdCu (R 1.113), GdAl (R 1.114), $GdZn_2$ and $GdCu_2$ (R 1.90) and $GdZn_{12}$ (this work).

The discrepancies are clearly due to the fact that the band structures of these materials are very far from being free-electron like. De Wijn et al (R 1.113) have argued that because the crystallographic unit cells of these compounds tend to be large, Brillouin Zone effects are expected to be weak, However, starting from the same premise we come to exactly the opposite conclusion. Because the crystal cell is large, the Brillouin Zone is small, and therefore the free Fermi Sphere will be cut by many Zone boundaries and have its spherical shape severely distorted. In addition, a portion of the band states will be built up from functions originating from 5d like states localised on the Rare Earths, and this again will produce a very non-free-electron like Structure. Because of this, the range of the conduction electron spin polarisation produced by a moment and hence the spin coupling, will be altered, flat areas of the Fermi Surface giving rise to strong long range interactions in the direction perpendicular to them. At high temperatures the effect of the finite

electron mean free path might also invalidate the free electron RKKY result (R 1.54). This effect could be included phenomenologically by multiplying each term in the sum of equation 1.47 by $\exp(-R_{ij}/\lambda)$.

Another consequence of the spin polarisation induced by the local moments is that an extra Knight shift of the nuclei of the non-magnetic atoms will occur. This may be calculated on a free electron model in a manner similar to that used to obtain θ, except that $\bar{J}$ appears to the first power, and the summation is taken over all magnetic atoms with a non-magnetic one at the origin. Bushow and co-workers (R 1.92, R 1.113, R 1.114) have measured the Knight shifts and Paramagnetic Curie Temperatures of several Rare Earth-Aluminium and Copper compounds, and from them obtained the two parameters $\bar{J}$ and k_f by allowing k_f to vary by a small amount about its free electron value. They find (R 1.113) that as the bandwidth increases $\bar{J}$ tends to become negative, as might be expected on the basis of the work of Watson et al (R 1.61). However, there is little theoretical justification for the scheme of approximation used by Bushow et al, and we do not believe that their results provide unambiguous evidence for the existence of negative $\bar{J}$'s.

For non-cubic materials, such as the ones dealt with in this work, the susceptibility will in general be anisotropic (equation 2.7) because of the low symmetry crystal field terms in the Hamiltonian. Cooper (R 1.115), taking only the A_2^o (equations 2.4 and 2.5) terms of it into account, has calculated that the slope of the inverse

Paramagnetic Susceptibility - Temperature curve is still given by the square of the ionic moment, but that different Paramagnetic Curie Temperatures are obtained for different directions. For measurements on polycrystalline specimens, however, the anisotropies cancel out, and θ is indeed given by equation 1.47.1.

The calculation of the susceptibility of Samarium compounds needs a more complicated approach, because the contribution to the magnetic moment from states of the J = 7/2 multiplet level, which have been mixed into the ground state by the applied fields, may be comparable to the moment arising from the states of the J = 5/2 ground multiplet level itself. It is also essential to take into account the fact that the magnetic moment of the spin will be changed by the s-f interaction according to equation 1.25. For Sm, $(g-1)/g = -5/2$ for the ground multiplet. This quantity is far larger in magnitude than that for any of the other Rare Earths, the next largest being Gd with $(g-1)/g = +1/2$, and consequently the change in moment of Sm will be greatest.

From equation 1.46, the exchange field $\underline{H}_e$ acting on an ion i is given by:

$$2\mu_B \underline{H}_e \cdot \underline{S}_i = -2 \sum_{j \neq i} J_{ij} \underline{S}_i \cdot \underline{S}_j \qquad 1.47.2$$

whence

$$\mu_B H_e = -\langle S^z \rangle \sum_j J_{ij}$$

$$= -\langle S^z \rangle J_{ff} \qquad 1.48$$

where the molecular field approximation is adopted.

If there is no exchange field, then the expectation values of the magnetic moment and spin are given by:

$$-\langle L^z + 2S^z \rangle = (a/T + b)H$$

$$-\langle S^z \rangle = \left(\frac{g-1}{g}\frac{a}{T} + b\right)H \qquad 1.49$$

where H is the applied field, $a = \mu_B g^2 J(J+1)/3k$, and b is the temperature independent Van Vleck contribution to the susceptibility which arises from transitions between the J = 5/2 and 7/2 levels (R 1.133). The latter equation is valid because, as we previously noted, the matrix elements of $\underline{S}$ and $(\underline{L} + 2\underline{S})$ are exactly the same between states of different J.

When exchange fields are present, White and Van Vleck (R 1.116) have pointed out that equations 1.49 should be replaced by:

$$-\langle L^z + 2S^z \rangle = \frac{a}{T}\left(H + 2\frac{(g-1)}{g}H_e\right) + b(H + 2H_e)$$

$$-\langle S^z \rangle = \frac{g-1}{g}\frac{a}{T}\left(H + \frac{2(g-1)}{g}H_e\right) + b(H + 2H_e) \qquad 1.50$$

because, again, the matrix elements of the additional Hamiltonian $2\ S^z \mu_B$ are equal to those of $\mu_B(L^z + 2S^z)2(g-1)/g$ within the ground multiplet, and $2(L^z + 2S^z)\ \mu_B$ between the J and $J \pm 1$ multiplets.

Equations 1.50 may be solved to give:

$$-\langle S^z \rangle / H = b\frac{T_\infty}{T_\theta}\left(\frac{T - T_o}{T - T_\infty}\right) \qquad 1.51$$

$$-\langle L^z + 2S^z \rangle / H = \frac{a}{T} + b + \frac{a}{T} \frac{(T - T_o)^2 T_\infty}{(T - T_\infty) T_o^2} \qquad 1.52$$

where

$$T_o = \frac{-(g-1)}{g} \frac{a}{b} \qquad 1.53$$

$$T_\theta = 2 J_{ff} a(g-1)^2/g^2 \mu_B \qquad 1.54$$

and

$$T_\theta/T_\infty = 1 + gT_\theta / T_o(g-1) \qquad 1.55$$

Equations 1.51 and 1.52 hold when only the ground multiplet is thermally populated. De Wijn et al (R 1.117) have derived more general expressions valid, at arbitrary temperatures, within a term, and have attempted to fit the susceptibility of $SmAl_3$ with them. They did not, however, make any allowance for the change in effective moment.

Equation 1.52 may be manipulated into the more convenient pseudo-Curie Weiss form:

$$-\langle L_z + 2S_z \rangle / H = b + aT_\infty / T_o^2 + a(1 - T_\infty / T_o)^2/(T-T_\infty) \qquad 1.56$$

which may be easily fitted to experiment data by a computer program which used, for instance, the method of least squares. As $b \rightarrow 0$, corresponding to an infinite distance between the ground and excited multiplet levels, equation 1.56 becomes:

$$-\langle L^z + 2S^z \rangle / H = a/(T-T_\theta) \qquad 1.57$$

and we see that $T_\theta = \theta$ of equation 1.47 and that the quantity (a) corresponds to the square of the magneton number of the lowest multiplet level. The first order s-f interaction will change both the temperature dependent and independent parts of the susceptibility, but because the temperature independent contributions to the susceptibility from the metallic matrices of the compounds examined in this work are not known well, only the change in (a) due to the s-f interaction will be taken account of, and this is given by equation 1.25. In order to analyse the data it is necessary to know the temperature T_o. This is substantially a property of the single ion. From Knight shift measurements on $SmAl_3$ De Wijn et al (R 1.117) estimate it to be 310°K, and we use this value for our analysis of the susceptibility of $SmZn_{12}$ in Chapter 4.

1.7. Magnetic Ordering

As the temperature is lowered, the Rare Earth compound will be in general (exceptions to this are discussed in the next section) become magnetically ordered.

Immediately below the ordering temperature T_N, the expectation value of the spin at site i will be given by (for the spin only case);

$$\langle \underline{S}_i \rangle = \frac{2S(S+1)}{3kT} \sum_{j \neq i} J_{ij} \langle \underline{S}_j \rangle \qquad 1.58$$

We take the ordered state to be characterised by a wavevector $\underline{q}$ such that:

$$\langle \underline{S}_k \rangle = \langle \underline{S}_1 \rangle \exp(i\underline{q}.(\underline{R}_k - \underline{R}_1)) \qquad 1.59$$

So that the magnitude of each moment is the same but the direction rotates in a spiral as one advances from one moment to the next (real and imaginary parts of equation 1.59). Kaplan and Lyons (R 1.85) have shown that this type of periodic structure will be the classical ground state for a Bravais Lattice, and their arguments may be extended to the R_2Zn_{17} Lattice as well. Therefore, more complex arrangements, such as the Yafet-Kittel type (R 1.65) need not be considered. There are, however, spiral orderings found in the Rare Earth metals in which there is a constant or oscillatory moment in the direction perpendicular to the plane of the spiral. These are dealt with in an analogous manner.

Substituting 1.59 into 1.58 an ordering temperature T_N is obtained which is given by:

$$T_N = 2S(S+1)\, J^*(\underline{q})/3k \qquad 1.60$$

where

$$J^*(\underline{q}) = \sum_{j \neq i} J_{ij} \exp(i\underline{q}.(\underline{R}_j - \underline{R}_i)) \qquad 1.61$$

and the ordering which occurs is at that $\underline{q}$ for which $J^*(\underline{q})$ is maximum (R 1.118, R 1.122, R 1.185). We note that θ is given by the same equation incorporating $J^*(0)$ instead of $J^*(\underline{q})$.

Smart (R 1.119) has calculated $J^*(\underline{q})$, and so obtained the modes of ordering, for a body-centred tetragonal lattice in which each atom

is allowed to interact with three sets of nearest neighbours. He finds a ferromagnetic mode, three collinear antiferromagnetic ones, and an incommensurate spiral in which the ordering vector $\underline{q}$ has no integral relation to the reciprocal lattice vectors. Mattis and Donath (R 1.124) have calculated $J^*(\underline{q})$ for a simple cubic lattice using the free electron RKKY result, equation 1.32, and a delta function s-f interaction. They find that as the electron concentration in increased, ferromagnetism and antiferromagnetism appear alternately. Fedro and Arai, (R 1.123) though, have found that the $\underline{q}$ dependence of the s-f interaction may markedly affect the type of ordering which occurs.

For non S-state Rare Earths two modifications are made to the theory. First $J^*(\underline{q})$ is multiplied by the De Gennes factor $(g-1)^2J(J+1)$ instead of $S(S+1)$, and second the Crystal Field Hamiltonian is considered to act as a perturbation upon the exchange ordered states and so produce anisotropy terms which are functions of $(\langle J_x\rangle,\langle J_y\rangle,\langle J_z\rangle)$. Using a Hamiltonian of this type, consisting of an exchange term plus an anisotropy term, much understanding has been gained of the rich varieties of magnetic ordering found in the Rare Earth metals. This work has been reviewed by Elliot (R 1.80), Kasuya (R 1.81) and Cooper (R 1.121).

Below the ordering temperature T_N Nagamiya (R 1.120) has shown that the low field susceptibility perpendicular to the plane of the spiral is constant and proportional to $(J^*(\underline{q}) - J^*(0))^{-1}$. At T_N the susceptibility in the plane of the spiral is equal to that perpendicular to it, but at lower temperatures it drops to reach a value at T=0

proportional to $(2J^*(\underline{q}) - 2J^*(2\underline{q}) - J^*(0))^{-1}$. If the characteristic energies associated with the applied field are smaller than anisotropy energies, then the observed susceptibility of a polycrystalline specimen will be the appropriate combination of the susceptibilities in each direction, but if the field energies are greater, then the spins will flop over so that they are all perpendicular to the field, and only the perpendicular susceptibility will be observed.

$J^*(\underline{q})$ is determined by the conduction electron band structure, whose details therefore decide the nature of the ordered state. For instance, Jackson and Doniach (R 1.127) have suggested that the ordering waveve ctor of Tb is directly associated with width of the webbing on the feet of the Tb hole Fermi Surface.

In the nearly free electron approximation $J^*(\underline{q})$ is given by (Yosida R 1.126):

$$J^*(\underline{q}) = (2\mu_B^2 N)^{-1} \left(\sum_{\underline{G}} |J(\underline{q} + \underline{G})|^2 \chi^o(\underline{q} + \underline{G}) - N^{-1} \sum_{\underline{Q}} |J(\underline{Q})|^2 \chi^o(\underline{Q}) \right) \qquad 1.62$$

where $\underline{G}$ is a reciprocal lattice vector. The omission of the second term in this equation would appear to be the reason for Doniach's (R 1.50) statement that θ is always positive. His theory applies equally well to Rare Earth compounds, and for many of these, for instance the ones described in this work, θ is found to be negative.

When the metal is magnetically ordered, a conduction electron travelling through the crystal will be subject to, as well as the crystalline Coulomb potential, an exchange potential having the periodicity of the magnetic order. This coupling, via the first order s-f interaction, creates gaps in the Fermi distribution which are proportional to the magnetisation, and so leads to a new Brillouin Zone structure. This will alter $\chi(\underline{q})$ and $J^*(\underline{q})$ and so one expects to have, in the ordered state, exchange parameters which are magnetisation dependent and which may even change the nature of the ordering. Elliot and Wedgewood (R 1.123) have used this idea, with a free electron model, to calculate the changes in the ordering wavevector, and of the resistivity of some of the heavy Rare Earth metals.

1.8. Ground State Singlet Ordering

In the previous section, the crystal field Hamiltonian was taken account of by assuming that it acted as a perturbation upon the ordered states which were determined by the exchange interaction. The opposite procedure is followed when dealing with the weak long-range couplings between Rare Earth ions in dilute insulating crystals (for instance Baker R 1.127). In these, the ions are taken to be in their lowest crystal field state, and the interactions between them are treated as the perturbation, usually using a Spin Hamiltonian formalism.

However, there remains a class of materials for which exchange and crystal field energies are comparable, and for these, both Hamiltonians must be diagonalised simultaneously within the lowest multiplet level. For compounds which incorporate Rare Earths other than Sm and Eu, the molecular field, as we showed in section 1.6., will be proportional to the magnetisation. If $\chi^{o}(T)$ is the susceptibility of the non-interacting ion due to crystal field effects, λ is the molecular field constant, and $\chi(T)$ the resulting susceptibility in the paramagnetic phase then:

$$\chi^{-1}(T) = \chi^{o^{-1}}(T) - \lambda \qquad 1.63$$

and the effect of exchange, as pointed out by Bleaney (R 1.128), is to shift the inverse susceptibility curve vertically.

To obtain the behaviour in the ordered state it is necessary to self-consistently determine the magnetisation which will give a molecular field which will in turn produce that magnetisation. The procedureis similar to that used in standard molecular field theory, except that now the energy levels of the magnetic ion are initially split by the crystal field. The most interesting effects occur when the lowest crystal field level is a non-magnetic singlet or doublet. An illustration of this is the singlet-triplet model of Fig. 1.4(p 24) If, at $0^{o}K$, the exchange field H_e satisfies the condition $g\mu_B H_e > D$ then the magnetisation will be $g\mu_B$. If this condition is not obeyed

then the magnetisation will be zero. As the molecular field is given by λ M, the condition $g^2\mu_B^2\lambda > D$ must be satisfied if the material is to order at all at 0°K. The existence of such conditions was first shown by Trammel (R 1.129).

A more realistic example is shown in Fig. 1.5a (p 45) (R 1.131). Here the magnetisation of the cubic compound TmSb caused by a magnetic field applied in the <100> direction has been calculated, for a crystal field scheme having a singlet lowest, by diagonalising the crystal field Hamiltonian together with a magnetic field term $-g\mu_B J_z H$. The thermal average of the magnetic moment operator over the eigenstates can then be computed. If the assumption is made that the material is potentially ferromagnetic, with ordering occurring along the <100> direction, then the spontaneous magnetisation may be obtained from the intersection of the M-H curve with the line $H_e = \lambda M$. The lines corresponding to three different strengths of λ are shown in Fig. 1.5a and the resulting magnetisations in Fig. 1.5b For α, no spontaneous magnetisation will occur at 0°K: for β and γ the M-T curves will be schematically as shown in Fig. 1.5b. It can be seen in the γ curve that a discontinuous charge of magnetisation with temperature is possible, and that for both the β and γ exchange fields the magnetisation will be less than gJ. Bleaney (R 1.128) has used arguments similar to these to explain why the ferromagnetic compounds RNi_2 (R = Rare Earth) bear less than the free ion moment in the ordered state.

In this qualitative discussion of singlet ground state ordering in TmSb we have assumed that when several ordered states are given by the graphical solution, as in Fig. 1.5a, then the stable state is that with the highest magnetisation. This would have to be confirmed by a full calculation of the free energy, such as that done by Blume (R 1.19). Secondly, free energy calculations would have to be made for situations in which the magnetisation lay along the other axes, to determine the true easy axis. Furthermore, the easy axis might be found to change with temperature.

In practice the exchange field in TmSb is not strong enough to cause spontaneous magnetisation at $0^{\circ}K$, but in TbSb a material with a similar crystal field structure, it is. Cooper and Vogt (R 1.132), by varying the parameter x in the compound $Tb_xY_{1-x}Sb$, have been able to sweep the compound across the ordering threshold so that at low x it is a Van Vleck Paramagnet at $0^{\circ}K$, and at high x an antiferromagnet. However, they have had to include a term proportional to M^3 in the molecular field to interpret their high field magnetisation measurements.

For a system consisting of singlet states, Wang and Cooper (R 1.130) have developed more sophisticated statistical techniques which go beyond the molecular field approximation, and have investigated the nature of the collective excitations of the system.

1.9. Resistivity

There are three main scattering mechanisms which contribute to the resistivity of crystallographically ordered Rare Earth compounds. The first is the scattering from lattice defects such as vacancies, impurities and dislocations; this will give a residual resistivity at $0^{\circ}K$. The second is scattering from lattice vibrations (phonons). At high temperatures the resistivity arising from this cause will be proportional to the temperature T, and at low temperatures to T^5 (R 3.34, R 3.35, R 3.36). At intermediate temperatures, an extrapolation between the two dependencies was suggested by Gruneisen (discussed for instance by Meaden R 3.36) on the assumption of a Debye phonon spectrum, a free electron gas, and the inclusion of no scattering processes which involved a reciprocal lattice vector. The semi-empirical formula for the lattice resistivity ρ_L is:

$$\rho_L = C\,T^5 \int_0^{\theta'/T} \frac{z^5\,dz}{(e^z-1)(1-e^{-z})} \qquad 1.64$$

where θ' is the Debye temperature in the theoretical model, but in practice an adjustable parameter. These two contributions to the resistivity, together with that from magnetic scattering (the manifestations of this in the Rare Earths and other magnetic materials have been reviewed by Coles (R 1.140)), which we will discuss next, will be additive according to Matthiessen's rule.

As we noted in section 1.5, the spin scattering in the magnetically disordered regime is independent of temperature. When the non S-state ions condense into their lower crystal field states with decreasing temperature, it might be expected that the scattering will decrease. A preliminary calculation by Elliot showed this effect (R 1.136) and Hirst (R 1.137) made a later calculation which used the first order s-f interaction and included both elastic and inelastic scattering. Murani (R 1.16), using Hirst's theory, was able to fit the resistivity of HoAu and DyAu alloys with the same crystal field schemes as fitted their susceptibilities, and found the s-f parameter $|\bar{J}|$ to have a value of about 0.06 eV.

When magnetic ordering occurs, the resistivity will be affected in two ways. First, the scattering probability will be reduced because that component of the spins which has ordered will not be available for scattering. If each spin is regarded as being an individual scattering centre then the spin relaxation time τ_s will go as (R 1.51).

$$\tau_s^{-1} \propto |\bar{J}|^2 (1 - \langle \underline{J} \rangle^2 / J(J+1)) \qquad 1.65$$

Secondly, when magnetic ordering does occur at a given wave vector, energy gaps will appear at corresponding planes in reciprocal space, will distort the Fermi Surface and may even increase the resistivity below the ordering temperature. Such increases, first noted and qualitatively

interpreted in this way in α Mn, are found also in the resistivities of Ho and Dy and have been explained in some detail by Elliot and Wedgewood (R 1.123) in this manner. In addition, there may be a small increase in resistivity above the ordering temperature due to critical scattering (De Gennes and Friedel R 1.138).

Equation 1.65 will be incorrect at low temperatures, as in that region the spin system will be more suitably described by its collective excitations, the spin waves. For a ferromagnet, Mannari (R 1.134) has calculated that a spin wave energy proportional to $\underline{q}^2$ ($\underline{q}$ being the spin wave vector) will lead to a resistivity proportional to T^2.

Mackintosh (R 1.139) has generalised this result to the case where the ferromagnet has a gap Δ in the spin wave spectrum at q=0 due to anisotropy. He suggested that the resistivity would be modified to $T^2\exp(-\Delta/T)$, and fitted the low temperature resistivities of the aniosotropic ferromagnets Dy and Ho to this expression with reasonable success. Mackintosh has also suggested that the magnetic resistivity of an antiferromagnet having a spin wave energy rising linearly from $\underline{q}$=0, which goes as T^4, may be modified by a similar exponential factor to take anisotropy into account. The spin wave energy of an incommensurate spiral, even with anisotropy, will vary linearly with $\underline{q}$, at low $\underline{q}$ and have no gap (R 1.121) but what form the temperature dependence of the resulting resistivity will take, in not clear apart from the fact that the exponential factor will be absent.

Liu (R 1.135) has pointed out that the s-f interaction which gives the magnetic resistivity should not be treated as a small perturbation upon the magnetically ordered states, which are after all determined by the s-f interaction itself. In a higher order calculation of the resistivity of a ferromagnet he finds a term in $T^{3/2}$ in addition to the T^2 term, and claims that the former may predominate at temperatures below one tenth of the ordering temperature.

Resistivity measurements have been made by Van Daal and Buschow (R 1.141) on the ferromagnetic intermetallic compounds RAl_2. With the exception of $CeAl_2$, which has a resistance minimum, all the compounds show a monotonically decreasing resistivity with decreasing temperature. The resistivity slope was found to increase in the ordered regime, but because of difficulty in separating the phonon and magnon contributions, it was not possible to discover which power law was obeyed by the magnetic scattering.

CHAPTER 2

THE INTERMETALLIC COMPOUNDS

2.1. Metallurgical Properties

The Rare Earth-Zinc systems are prolific formers of intermetallic line compounds, and most systems contain half a dozen or more of them (R 2.1-4, R 2.6, R 2.17). The only phase diagrams at present known are those of the systems of Zinc with La (R 2.5, R 2.8), Ce (R 2.9), Pr (R 2.10), Sm (R 2.11), Yb (R 2.12) and Y (R2.13). Work on the phase diagram of the Nd-Zn system has been started (R 2.22).

The phase diagrams of the Sm-Zn and Ce-Zn systems are shown in Fig. 2.1. The Zinc rich portions of the two diagrams are of similar form to those of the others, with the exception of the Yb-Zn system, which is slightly different. This is because Yb and Eu tend to be divalent in these compounds whereas the rest of the Rare Earths are trivalent.

The second most Zinc-rich compound is of the composition R_2Zn_{17}, and forms congruently at around 950 °C. Iandelli and Palenzona (R 2.14) have reported that two structural forms with this composition exist. Compounds formed from the melt possess the rhombohedral Th_2Zn_{17} (R 2.20) type structure, but compounds formed by prolonged heating at low temperatures (420 °C-600 °C)

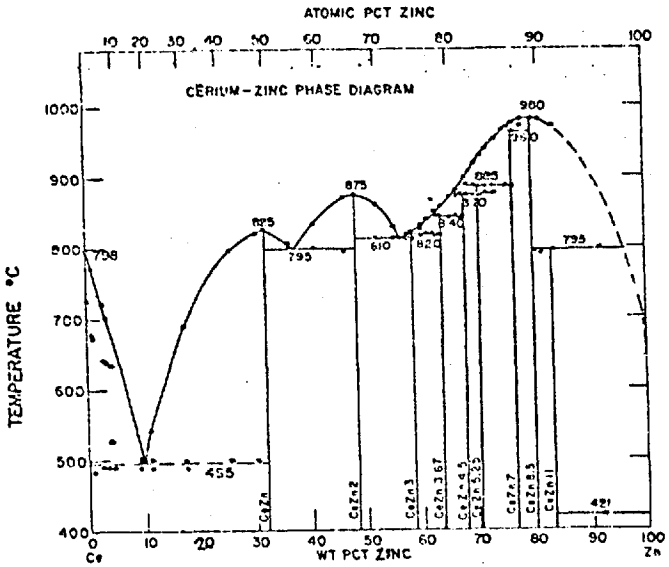
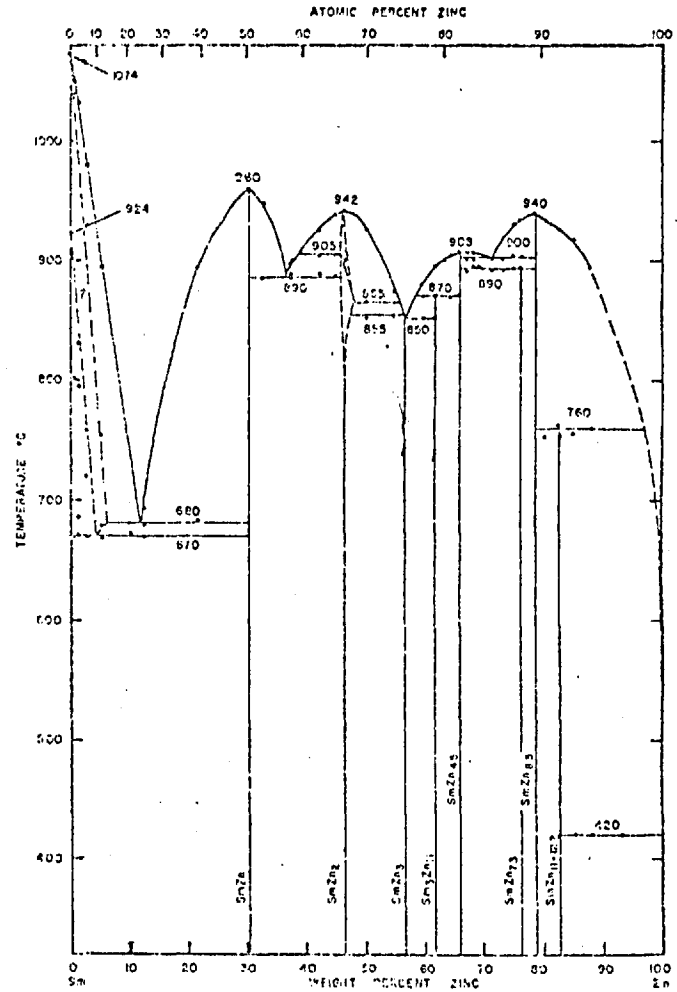


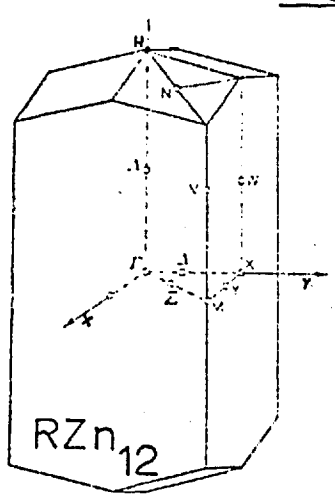
Fig. 2.1

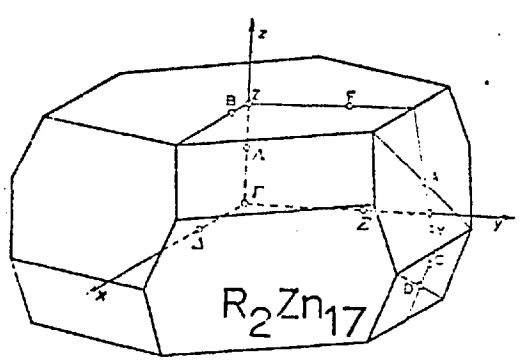
Phase diagram for the Ce-Zn system under constrained vapor conditions.



Phase diagram for the Sn-Zn system.

Fig. 2.4





have the hexagonal Th_2Ni_{17} (R 2.21) structure. This latter result had been previously reported by Kuzma et al (R 2.18, R 2.19). All of the Rare Earths, apart from Eu, form the Th_2Zn_{17} type compound, and all of them, except Eu and La, form that of the Th_2Ni_{17} type.

The compounds most rich in Zinc are formed peritectically at around 750 °C from the Zinc rich melt and the R_2Zn_{17} compounds. They are of the composition RZn_x, where x = 11, 12 or 13. All the compoundsexamined in the present work were of the composition RZn_{12}, which isof the $ThMn_{12}$ type (R 2.16), apart from $YbZn_{11}$ ($BaCd_{11}$ type, R 2.23). Not shown on the Sm-Zn phase diagram is a structural transformation of the low temperature compound $SmZn_{12}$ (stoichiometry and structure found by Kuzma et al R 2.18, R 2.19, and Iandelli and Palenzona R 2.14) into a disordered hexagonal compound of composition $SmZn_{10.9}$, which was discovered by Mason et al (R 2.10). The transformation is reported to take place at between 500 °C and 600 °C. It is not known whether similar transformations occur in the other dilute compounds.

Iandelli and Palenzona (R 2.14) reported that all these Zinc rich phases showed a very restricted homogeneity range, and this was confirmed by observations made in the course of the work described here. Preparations of the compounds

which contained a little excess Zinc were found to give X-ray powder diffraction patterns which consisted of the lines of the exactly stoichiometric compound, plus the lines of pure Zinc. This shows that the solubility of Zinc in the compounds is negligibly small, as if it were not, the lattice constants of the compounds might be expected to change as the dissolved zinc distorted the lattice.

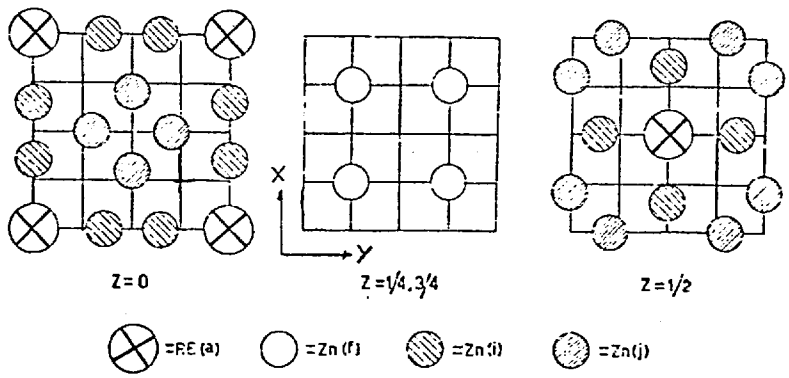
2.2. Crystal Structures

The RZn_{12} compounds have the body centred tetragonal $ThMn_{12}$ type (R 1.16) lattice, space group I 4/mmm - D^{17}_{4h} (R 2.24). A diagram of the tetragonal cell is shown in Fig. 2.2, together with the lattice constants of the compounds which were made. Each Rare Earth atom is surrounded by 4 Zn(i) at 3.13 Å, 8 Zn (j) at 3.18 Å, and 8 Zn(f) at 3.39 Å. These parameters do not vary by more than 1% throughout the series. The Rare Earth atoms are not nearest neighbours, and the shortest distance between them is roughly 5 Å. The crystallographic point symmetry at the Rare Earth site is 4/mmm-D_{4h}.

For reasons which will be discussed later in this Chapter only the R_2Zn_{17} compounds which had the Th_2Zn_{17} structures

The figure shows three sections of the unit cell, at heights of $z=0$, $z=\frac{1}{2}$, $z=\frac{1}{4}$; $\frac{3}{4}$. Each RE atom is surrounded by 4 Zn (i) at 3.13 Å, 8 Zn (j) at 3.18 Å and 8 Zn (f) at 3.39 Å. The Zn atoms have inter-atomic distances varying from 2.60 to 2.90 Å. Taking the values of the atomic radii of Tm and Zn with co-ordination numbers 8 and 12, the calculated distances are 3.05–3.12 Å (Tm–Zn) and 2.68–2.74 Å (Zn–Zn).

Fig. 2.2



ThMn$_{12}$ type; sections of the unit cell.

LATTICE CONSTANTS (Å) OF $REZn_{12}$ PHASES

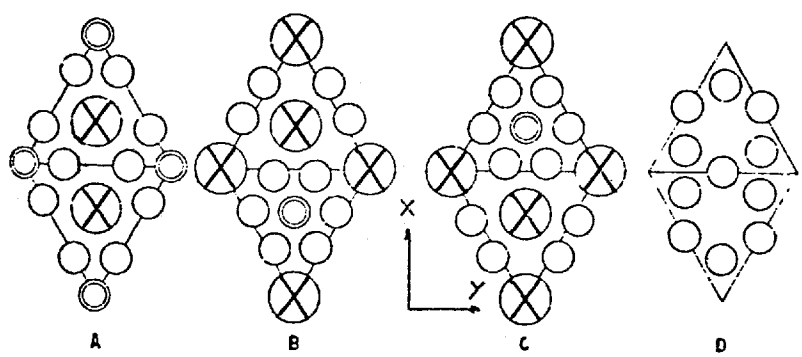
Compound	*a*	*c*
	±0.003	±0.002
$SmZn_{12}$	8.927	5.215
$GdZn_{12}$	8.898	5.210
$TbZn_{12}$	8.884	5.200
$DyZn_{12}$	8.877	5.193
$HoZn_{12}$	8.868	5.195
$ErZn_{12}$	8.863	5.193
$TmZn_{12}$	8.852	5.190
$LuZn_{12}$	8.848	5.186

LATTICE CONSTANTS (Å) OF RE_2Zn_{17} PHASES (Th_2Zn_{17} TYPE)

Compound	*hexagonal axes*	
	a	*c*
	±0.004	± 0.005
La_2Zn_{17}	9.131	13.334
Ce_2Zn_{17}	9.088	13.290
Pr_2Zn_{17}	9.066	13.274
Nd_2Zn_{17}	9.052	13.236
Sm_2Zn_{17}	9.017	13.211
Gd_2Zn_{17}	8.994	13.169
Tb_2Zn_{17}	8.977	13.161
Dy_2Zn_{17}	8.967	13.139
Ho_2Zn_{17}	8.956	13.133
Er_2Zn_{17}	8.942	13.118
Tm_2Zn_{17}	8.937	13.110
Yb_2Zn_{17}	9.040	13.216
Lu_2Zn_{17}	8.920	13.096
Th_2Zn_{17}	9.060	13.234
U_2Zn_{17}	8.983	13.161

Fig. 2.3





Atomic layers in the M_2Zn_{17} structures. Large circles are M atoms, small circles zinc atoms. Double circles represent pairs of zinc atoms above and below the plane of the others.

were made. This has the space group $R\bar{3}m - D^5_{3d}$, and a diagram of the crystal structure is shown in Fig. 2.3. The rhombohedral structure is referred to hexagonal axes and is stacked in the order ADBDCDA .... along the z axis. The crystal structure is more clearly conceived when it is referred to rhombohedral axes and this cell is also shown in Fig. 2.3. There are two magnetic atoms in each rhombohedral primitive cell, and they are in crystallographically equivalent sites of point symmetry $3m - C_{3v}$, 1/3 and 2/3 of the way along the $\langle 111 \rangle$ axis. Each magnetic atom is co-ordinated by 6 + 12 Zn atoms, the two values corresponding to increased R-Zn distances. No magnetic atoms are nearest neighbours and the distances between them are, again, about 5 Å.

The factors determining the composition of Intermetallic Compounds (Reviewed by Laves, R 2.25) are considered to be:

a) Geometrical considerations.

b) Electron concentration (through the filling of the Brillouin Zones).

c) Electronegativity.

The variation of structure for a given stoichiometry is unlikely to be greatly influenced by the latter two factors, except for the anomalous Rare Earths at the ends and in the middle of the series, as they may be expected to vary little throughout the Rare Earth series, and metallurgists who have examined these

compounds previously (R 2.18, R 2.19, R 2.14) are of the opinion that the size effect is of primary importance. To quote Iandelli and Palenzona (R 2.14):

"The five structure types found for the compounds richest in Zinc are characterised by the formation of a network of Zinc atoms, containing a certain number of nearly spherical holes in which the RE, or other atoms, may be arranged. The diameter and the number of holes vary according to the structure, and the whole is stabilised through the introduction of M* atoms in the corresponding positions. Hence the structure and the formula change if the dimensions of the M atoms become too large or too small"

This argument indicates why the large Yb^{2+} ion form the $BaCd_{11}$ structure whereas all the small R^{3+} ions, from Sm onwards form that of the $ThMn_{12}$ type.

* By M is meant Rare Earth.

2.3. Symmetry Properties of the Structures

As was discussed in the previous chapter, one theory of how the Rare Earth ion is affected by the crystalline environment assumes that the ion is subject to the influence of an electrostatic field having the symmetry of the magnetic site. This crystalline potential may be expanded in spherical harmonics

as it is a solution of Laplace's equation. It may be written as:

$$V(\underline{r}) = \sum_{l} \sum_{m=-l}^{+l} A_l^m r^l Y_{l,m}(\theta, \phi)$$

where A_l^m are constants and the summation over l is for l = 2, 4, 6. The spherical harmonic $Y_{l,m}$ is defined (following Edmonds, R 2.26) as:

$$Y_{l,m}(\theta, \phi) = (-1)^m \left[\frac{(2l+1)(l-m)!}{4\pi(l+m)!}\right]^{\frac{1}{2}} \cdot P_l^m(\cos\theta) e^{im\phi} \qquad 2.1$$

the $P_l^m(x)$ being the Associated Legendre functions (op.cit).

The number of components in the crystalline potential is reduced by requiring it to be invariant under the symmetry operations of the relevant point group.

For the RZn_{12} compounds, the point symmetry group of the magnetic site is 4/mmm - D_{4h}. We take the axes describing the potential to lie along the crystallographic axes. The z axis is parallel to the crystal c axis, ϕ is measured from x, and θ from z.

One symmetry operation of 4/mmm is $C(\frac{\pi}{2}, z)$, signifying a rotation of $\frac{\pi}{2}$ about the z axis. By inspection of 2.1:

$$C(\alpha, z)\, Y_{l,m} = e^{-im\alpha}\, Y_{l,m} \qquad 2.2$$

using the convention that $C(\alpha, z)$ rotates the function about the Z axis in the direction of ϕ. If $V(\underline{r})$ is then required to be invariant under $C(\alpha, z)$, the result is obtained that m may only equal an integer multiple of 4.

The next symmetry operation to use is m(xz), which denotes a reflection in the xz mirror plane. This leaves θ unaltered but changes ϕ to $-\phi$, and it can be seen from inspection of 2.1 that:

$$m(xz)\, Y_{l,m} = (-1)^{-m}\, Y_{l,-m} \qquad 2.3$$

When this applied to the potential the result is:

$$V(\underline{r}) = A_2^0 r^2 Y_{2,0} + A_4^0 r^4 Y_{4,0} + A_4^4 r^4 (Y_{4,4} + Y_{4,-4}) + A_6^0 r^6 Y_{6,0} + A_6^4 r^6 (Y_{6,4} + Y_{6,-4}) \qquad 2.4$$

No further reduction is made by applying the other symmetry operations.

In the R_2Zn_{17} ($\bar{R}3m$) compounds there are two magnetic atoms per unit cell which are in crystallographically equivalent sites. However, the two sites are transformed into each other by the inversion operator acting at a lattice point in Fig. 2.3 , and because the crystalline potential is invariant under inversion (it contains only l = even terms) the potential is exactly the same at both sites when described by parallel oriented co-ordinate axes. The sites are magnetically equivalent. The form of the crystalline potential may be obtained in a manner similar to that used for the tetragonal compound by making use of the operators $C(\frac{2\pi}{3}, z)$ and $m(xz)$ to obtain the $3m$-C_{3v} potential:

$$V(\underline{r}) = A_2^0 r^2 Y_{2,0} + A_4^0 r^4 Y_{4,0} + A_4^3 r^4 (Y_{4,3} - Y_{4,3})$$

$$+ A_6^0 r^6 Y_{6,0} + A_6^3 r^6 (Y_{6,3} - Y_{6,-3})$$

$$+ A_6^6 r^6 (Y_{6,6} - Y_{6,-6}) \qquad 2.5$$

An attempt to estimate the magnitudes of the crystal field parameters A_l^m is sometimes made by considering the potential to be due to electric monopoles situated at the nuclear sites of the co-ordinating atoms. For instance, we might put charges of twice the electronic charge at the Zn^{2+}

sites surrounding the Rare Earth atoms and calculate $V(\underline{r})$ from these. However, in the structures examined here, the point symmetry groups of the majority of the co-ordinating Zinc atoms do not contain the inversion operator. Thus electric dipole contributions to the potential are allowed. Because there is no simple method of calculating these, and because there isno possibility of fitting 5 and 6 (equations 2.4 and 2.5) parameters to one measurement of polycrystalline susceptibility, we make no attempt to calculate the magnitudes of the parameters.

The reciprocal lattice of the RZn_{12} body centred tetragonal direct lattice is face centred tetragonal, and the reciprocal lattice of the R_2Zn_{17} rhombohedral lattice is also rhombohedral. The first Brillouin Zones of each lattice are shown in Fig. 2.4. The ratio of the volume of the free electron Fermi sphere V_F to that of the first Brillouin Zone V^* is given by:

$$V_F/V^* = n'/2 \qquad 2.6$$

where n' is the number of conduction electrons per primitive cell. This ratio is 13.5 for the RZn_{12} structure and 20 for the R_2Zn_{17} structure and indicates that in the extended zone scheme, the Fermi sphere is cut by many zone boundaries.

The physical properties which have been measured in this work, are magnetic susceptibility and resistivity. Both may be represented as second rank Cartesian Polar Tensors. For the point groups, $4/mmm$ and $\bar{3}m$, of the paramagnetic states of the structures discussed here, it may be shown (see for instance Birss R 2.28) that both tensors are of the form:

$$\begin{bmatrix} a_{11} & & \\ & a_{11} & \\ & & a_{33} \end{bmatrix} \qquad 2.7$$

referred to the axes of Fig. 2.2 and Fig. 2.3. For a polycrystalline specimen the quantity measured will be a scalar, a, given by:

$$a = \tfrac{2}{3} a_{11} + \tfrac{1}{3} a_{33} \qquad 2.8$$

2.4. Preparation and Analysis of Materials

The Russian workers, Kuźma et al. (R 2.18, R 2.19), prepared specimens of the RZn_{12} compounds by pressing mixtures of powders of the Rare Earth metals and Zinc, wrapping the pressings in molybdenum foil, and sintering them in an evacuated

glass ampule for five days at 500 °C. Iandelli and Palenzona (R 2.14) mixed turning of the Rare Earth metals with filings of Zinc and heated them for several days at 450 °C - 500 °C in an evacuated glass tube. However, the writer was told by a member of Iandelli's group at Genoa, (1968 private communication) that small quantities of unreacted Rare Earth metal remained in the compounds, making magnetic measurements difficult. Iandelli and Palenzona prepared the R_2Zn_{17} compounds (with rhombohedral structure) by melting the component metals in tantalum containers under argon. This method was also adopted by Chiotti and Mason in their phase diag ram determinations (R 2.9, R 2.11, R 2.12, R 2.13).

The materials used to make the compounds described in the present work consisted of Rare Earth Metals, obtained from Koch Light Laboratories Limited, of nominal purity 99.9% by weight, with the exception of Sm and Tm, which were of 99.7% purity. The Zinc was obtained from Johnson Matthey Chemicals Limited and was claimed, from spectroscopic observations, to contain only a few p.p.m. of impurities.

Most of the RZn_{12} compounds were prepared by heating the components for a long time below the (unknown) peritectic temperature. The metals were cut into ingots of a few grams with a hacksaw, and the ingots were filed smooth with a hard steel

file which was used only for that purpose. The surface of the ingot was rubbed with emery paper to remove any contamination and cleaned with an organic solvent. The pieces of metal, in stoichiometric proportions, were then placed in a Pyrex glass tube, which had been previously cleaned with Aqua Regia and distilled water, and the tube was evacuated to a pressure of 10^{-5} Torr. The tube and specimen were heated at 200 ^{o}C for several hours, whilst at this pressure, in order to drive off any surface contamination. After the tube was sealed off, it was placed in a horizontal furnace and heated at 500 ^{o}C for three weeks.

The products of the reaction were examined by the following means:

a) Metallographic Examination

The compounds were polished, etched and examined under a microscope at magnifications up to several X100 in order to find the grain size and to see whether the compounds were single phase. The etch used for all the specimens was 3% conc.. HCl in Alcohol Absolute. This revealed many features which were not shown up by the Nital etch (HNO_3 in Alcohol) used by Mason and Chiotti.

b) X-Ray Powder Diffraction

TheX-ray powder patterns of all the compounds were

obtained by the Debye-Scherrer method, and the positions of the lines and their intensity were compared with the data published by Kuźma et al (R 2.18 , R 2.19) and Iandelli and Palenzona (R 2.14).

c) Electron Microprobe Analysis

In this method an electron beam is allowed to impinge on the surface of the specimen. This produces X-rays, characteristic of the elements contained in the specimen, and these are detected and analysed. The area which is examined is very small, a few microns in diameter, and the composition of intermetallic compounds may be determined to an accuracy of a a few percent in areas of size.

All the compounds formed were brittle silvery metallic substances whose surfaces did not dull significantly when exposed to air, apart from two Cerium compounds which corroded rapidly and had to be kept under Benzene. Their Vickers Hardness was in the region of 200, as compared to about 40 for pure zinc.

Of the RZn_{12} compounds only those with R = Sm, Gd, Tb, Er gave satisfactory X-ray, metallographic and Microprobe results. The grain size varied throughout each of the specimens, ranging from 30 microns to 150 microns, and they appeared visually to be single phase. The $TbZn_{12}$ specimen, although satisfactory under X-ray and metallographic examination was found from

microprobe examination to have very small amounts of second phase in it, and this ingot was used for resistivity measurements only. The remaining compounds, with R = Ho, Dy, Tm gave satisfactory X-ray results, showed small amounts of second phase under microscopic examination, but gave very uneven probe scans.

An attempt was made to form the compounds with R = Tb, Ho, Dy, Tm in another way by sealing them in a silica tube, heating them at 1000°C for two hours above their melting points, furnace cooling to 700°C and annealing at that temperature for one week. Only the Tb compound, made in this way, was successful. It had a grain size of about 150 microns and contained many voids, which meant that it could only be used for susceptibility measurements. In view of the two structural forms of the most Zinc rich Sm compound, found by Mason et al (R 2.15), it is possible that compounds of a given stoichiometry, which are formed in different ways, will not have the same structure. However, in the case of the two $TbZn_{12}$ compounds, both specimens gave similar X-ray powder patterns whereas the powder photographs of the high and low temperature forms of the $SmZn_{12}$ compound were distinctly different.

Because only a few of the RZn_{12} compounds had been prepared successfully, it was decided to make compounds of the next most Zinc rich composition R_2Zn_{17}. Preliminary attempts to form at low temperature the compounds with the Th_2Ni_{17} structure were unsuccessful and produced multiphase materials. Attempts to make compounds with

the rhombohedral Th_2Zn_{17} type structure, which are formed at high temperatures, were more successful and compounds with this structure, having R = Gd, Tb, Dy, Ho, Er, Tm, Yb were prepared. It is fortunate that the Th_2Zn_{17} type compounds are easy to make as they have several advantages over the Th_2Ni_{17} compounds. Their unit cell is simpler, their space group is symmorphic, and furthermore a certain amount of doubt has been cast on the nominal stoichiometries of the Th_2Ni_{17} type structure compounds by Johnson and Smith (R 2.29).

The R_2Zn_{17} compounds were prepared by sealing the metals, in ingot form, in evacu ated silica tubes, heating them above their (congruent) melting points for about 10 hours at 1070°C, and then quenching in air to retain their rhombohedral form and to achieve a small grain size. An automatic mechanism was constructed to agitate the molten metal by giving it a sharp jolt once a minute. This agitation was found necessary to ensure satisfactory alloying even when the melt was heated at temperatures as high as 1000°C.

When the R_2Zn_{17} compounds were removed from their tubes after quenching, they were found to have solidified in a hollow cylinder around the sides of the tube. Their irregular shape, together with the fact that they contained many voids, made them unsuitable for resistivity measurements. The RZn_{12} compounds which were prepared at low temperatures, on the other hand, were void-less, and resistivity specimens could easily be cut from them.

The R_2Zn_{17} compounds with R = Gd - Tm gave satisfactory results under examination, although their electron probe scans were a little less even than those of the RZn_{12} compounds, and the grain boundaries (grain size about 100 microns) were rather richer in Zinc that the grains. The Vickers hardness, was again around 200.

Although the melt was found to have reacted with the sides of the silica tube, the products of the reaction remained atta ched to the glass and did not appear to dissolve substantially in the melt. Electron probe scans showed the concentration of Si in the compounds to be less than several hundred parts per million. This absence of dissolved Si has also been noted by Wang (R 2.30) who found none after heating Gd and Zn at 800 °C. in quartz, in order to form the intermetallic compound $Gd_{13}Zn_{58}$. The iron content of the compounds was below the range of detectability, also a few hundred parts per million.

Yb_2Zn_{17} and $YbZn_{11}$ are reported by Mason and Chiotti (R 2.12) to form congruently at arcund 760 °. Accordingly, a Yb-Zn charge of intermediate composition was heated at 800 °C and quenched. The result was a two phase mixture of Yb_2Zn_{17} and a Yb_2Zn_{17} – $YbZn_{11}$ eutectic. The susceptibility of this material was found to be less than 2×10^{-6} emu/gram down to 77 °K, in agreement with the measurements of Iandelli and Palenzona. This, and the fact that the lattice parameter of the Yb_2Zn_{17}

compound corresponds to the Yb^{2+} ion indicates that Yb is divalent in these two compounds.

Finally, some comments about unsuccessful attempts to prepare compounds. Although Sm_2Zn_{17} is reported (R 2.11) to form congruently at 940°C, several samples quenched from 1050°C were found to be grossly multiphase containing a matrix of pure Zn, blobs of $SmZn_{12}$ and streaks of SmZn. A nominal Ce_2Zn_{17} compound was also multiphase, and contained a Zinc matrix, needles of Ce_2Zn (a compound not reported on the phase diagram of R 2.9) and blobs of $CeZn_{11}$. An attempt to make the compound $CeZn_{11}$ was also unsuccessful. Mason (1969, private communication) is of the opinion that an impurity stabilisation mechanism may be involved in the formation of some of the compounds. Whether it is due to the Tantalum containers used in his preparation of the Rare Earth Zinc compounds, or the silica ones used here, is not clear. One does, however, note the comment made previously that the amount of Silicon found dissolved in the R_2Zn_{17} compounds which were quenched from the melt, was extremely small.

An attempt was made to prepare a solid solution of .03% ErZn. The conditions for the formation of this solution are, from a Darken-Gurry map, extremely unfavourable, and no Er was detected to an accuracy of 20 parts per million. This is comparable with the solubilities of Pr and Nd in Zinc at 450°C, reported by Johnson and Anderson (R 2.7) as 14 and 26 parts per million respectively.

CHAPTER 3

EXPERIMENT

3.1. Susceptibility Measurement

The force $\underline{F}$ acting on a magnetic moment $\underline{m}$ in a magnetic field is given (R 3.1) by the expression:

$$\underline{F} = (\underline{m} \cdot \nabla)\underline{H} \qquad 3.1$$

where $\underline{H}$ is that part of the field not caused by the moment.

The field produced by the magnet used in the experiments described in this thesis is of cylindrical shape, as shown in Fig. 3.1a, so it is desirable to express $\underline{F}$ in cylindrical co-ordinates (r, θ, x) in order to take advantage of this symmetry. This is easily done by using the expression for the differential vector operator:

$$\nabla = \hat{r}\frac{\partial}{\partial r} + \hat{\theta}\frac{1}{r}\frac{\partial}{\partial \theta} + \hat{x}\frac{\partial}{\partial x}$$

where $\hat{r}$, for example, indicates a unit vector in the radial direction. $\underline{F}$ may then be worked out from equation 3.1 but in doing so it must be remembered that although $\partial \hat{i}/\partial j = 0$ in Cartesian co-ordinates for all i,j, this is not so in cylindrical co-ordinates; $\partial \hat{r}/\partial \theta = \hat{\theta}$ and $\partial \hat{\theta} / \partial \theta = -\hat{r}$,

the rest are zero.

The expression for $\underline{F}$ is given in full by, for instance, Boast (R 3.2), but it can be considerably simplified by invoking the physical symmetry of the situation and putting:

$$\frac{\partial}{\partial \theta} \underline{H} = 0$$

Because there is no facility for keeping specimens properly aligned on the apparatus used for the work described here, accurate measurements can only be made on magnetically isotropic materials (including polycrystalline specimens of aniosotropic ones) and for these $m_\theta = 0$.

With these two conditions the only non-vanishing force components are:

$$F_r = m_x \frac{\partial H_x}{\partial r} + m_r \frac{\partial H_r}{\partial r}$$

$$F_x = m_x \frac{\partial H_x}{\partial x} + m_r \frac{\partial H_x}{\partial r} \qquad 3.2$$

making use also of the fact that curl $\underline{H} = 0$. If the moment is placed in the $x = 0$ plane, in which the magnetic field has reflection symmetry, the only non-zero moment component is m_x and the only non-zero force component is $F_r = m_x \partial H_x / \partial r$. The moment is also positioned on the z axis (Fig. 3.1a) so that

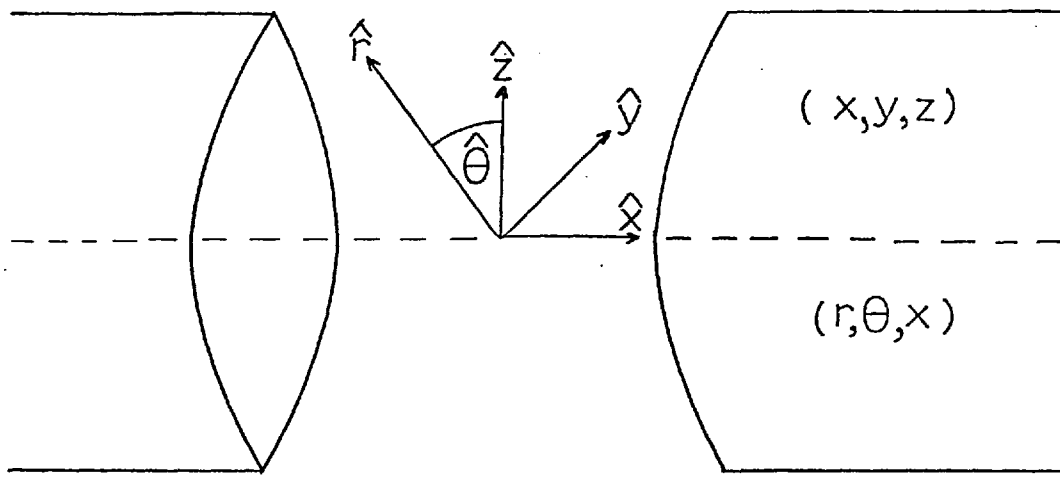

r̂
ẑ
θ̂
ŷ
x̂
(x,y,z)
(r,θ,x)

Fig. 3.1

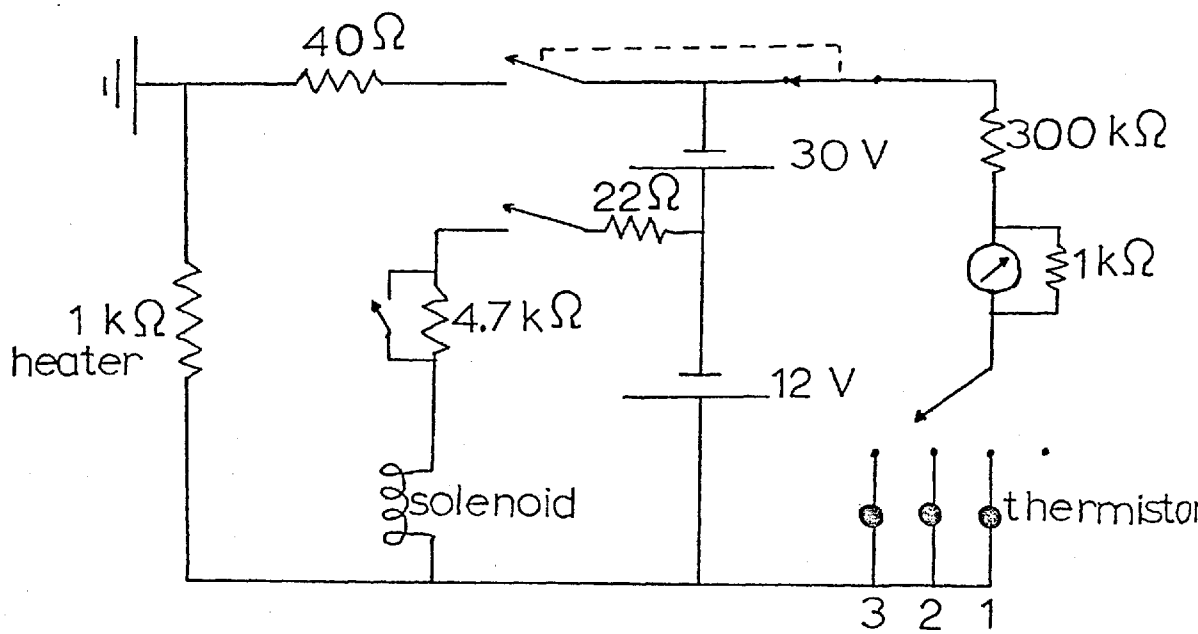

40 Ω
30 V
300 kΩ
22Ω
1kΩ
1 kΩ
heater
4.7 kΩ
12 V
solenoid
thermistor
3 2 1

Fig. 3.5

the radial force is directed vertically, and thus the magnetic moment of the specimen may be determined by measuring the vertical component of the force acting on it, and from a knowledge of $\partial H_x / \partial r$ at the specimen position. This is known as the Faraday method of magnetic measurement ; we will show later in this chapter what effects occur when using it if the magnetic specimen is not constrained to stay at the previously described position of symmetry.

If the specimen has a shape consistent with a demagnetising factor D and is of field independent mass susceptibility χ , as are all the Rare Earth compounds discussed in this thesis, then the vertical force F_z acting on the specimen is:

$$F_z = \frac{m\chi}{(1 + 4\pi D \chi \rho)} H_x \frac{\partial H_x}{\partial r} \qquad 3.3$$

where m is the mass of the specimen and ρ its density (all in c.g.s. units). The specimens used in this work were of roughly spherical shape and a factor of D = 1/3, suitable for a true sphere, was taken for all of them. As the largest demagnetising correction ever needed was 7% this was felt to be unlikely to introduce any substantial error.

The experiment thus consists of measuring the force

acting on a specimen in a known field at a known temperature, and to do this the force balance previously constructed by Dey (R 3.3) was used. A diagram of this in the form it had before the modifications to be described later were made to it, is reproduced in Fig. 3.2.

The magnetic specimen was suspended between the poles of an electromagnet having pole faces of the shape of truncated cylinders 7 inches in diameter with a 2 inch gap between them, and was connected by a two piece quartz suspension about 90 cm long to the lower end of a Sucksmith Ring (R 3.4). The small deflection of the ring was detected by observing the movement of a light spot, reflected by mirrors M1 and M2 on a split photocell. The photocell could be moved vertically on a rack by a micrometer screw and the differences in the positions at which it gave zero output with electromagnet current on and off gave a measurement which was proportional to the magnetic force acting on the suspension. The proportionality constant was found by dropping a calibrating weight onto the bottom of the Sucksmith Ring by means of a small electromagnet which could be energised from without a vacuum-tight glass enclosure which surrounds the ring. Damping of the ring vibrations was provided by four aluminium discs moving in the fields of small permanent magnets..

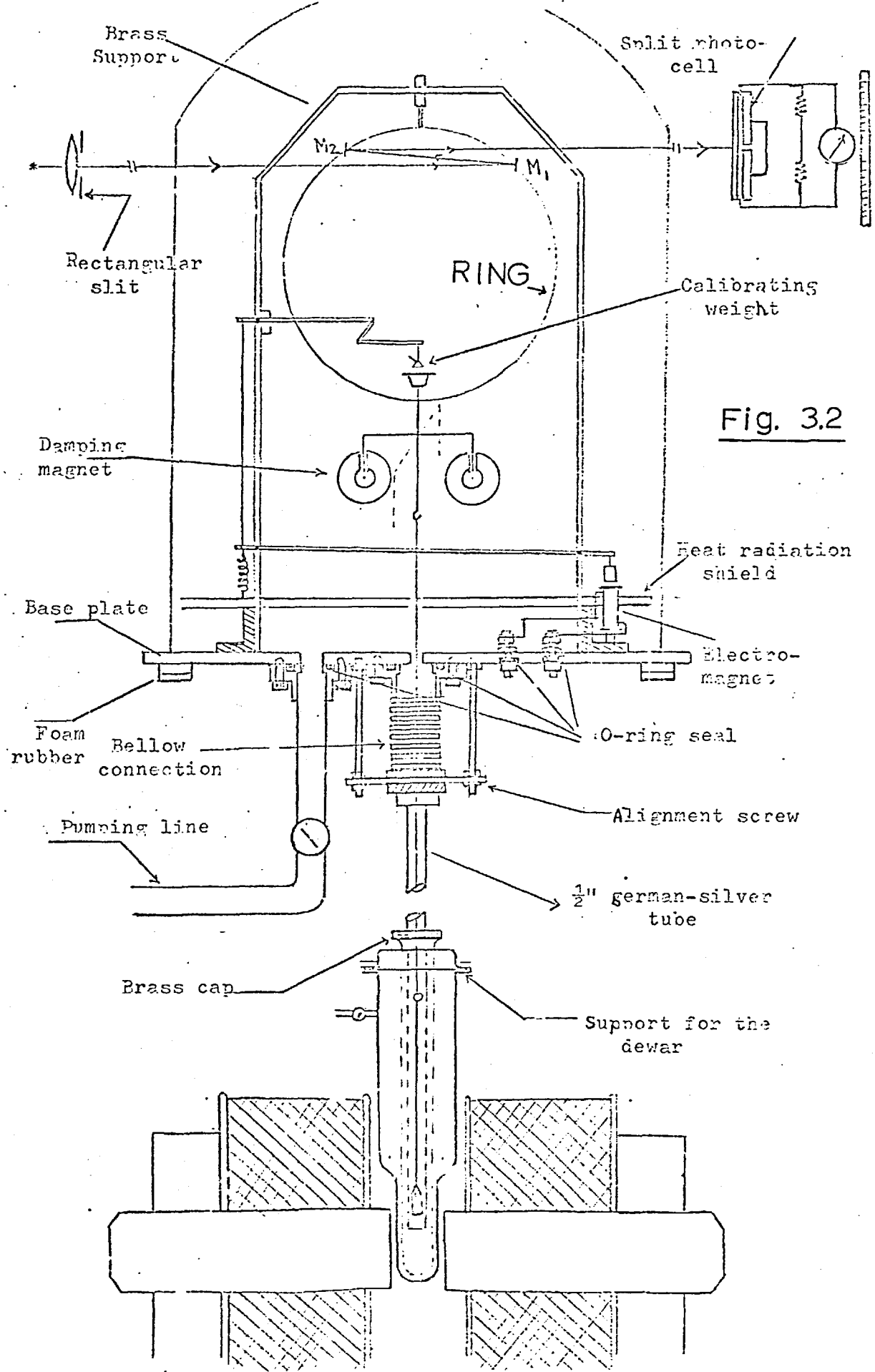

Brass Support
Split photo-cell
M_{12}
M_1
Rectangular slit
RING
Calibrating weight
Damping magnet
Heat radiation shield
Base plate
Electro-magnet
Foam rubber
Bellow connection
O-ring seal
Alignment screw
Pumping line
½" german-silver tube
Brass cap
Support for the dewar

Fig. 3.2

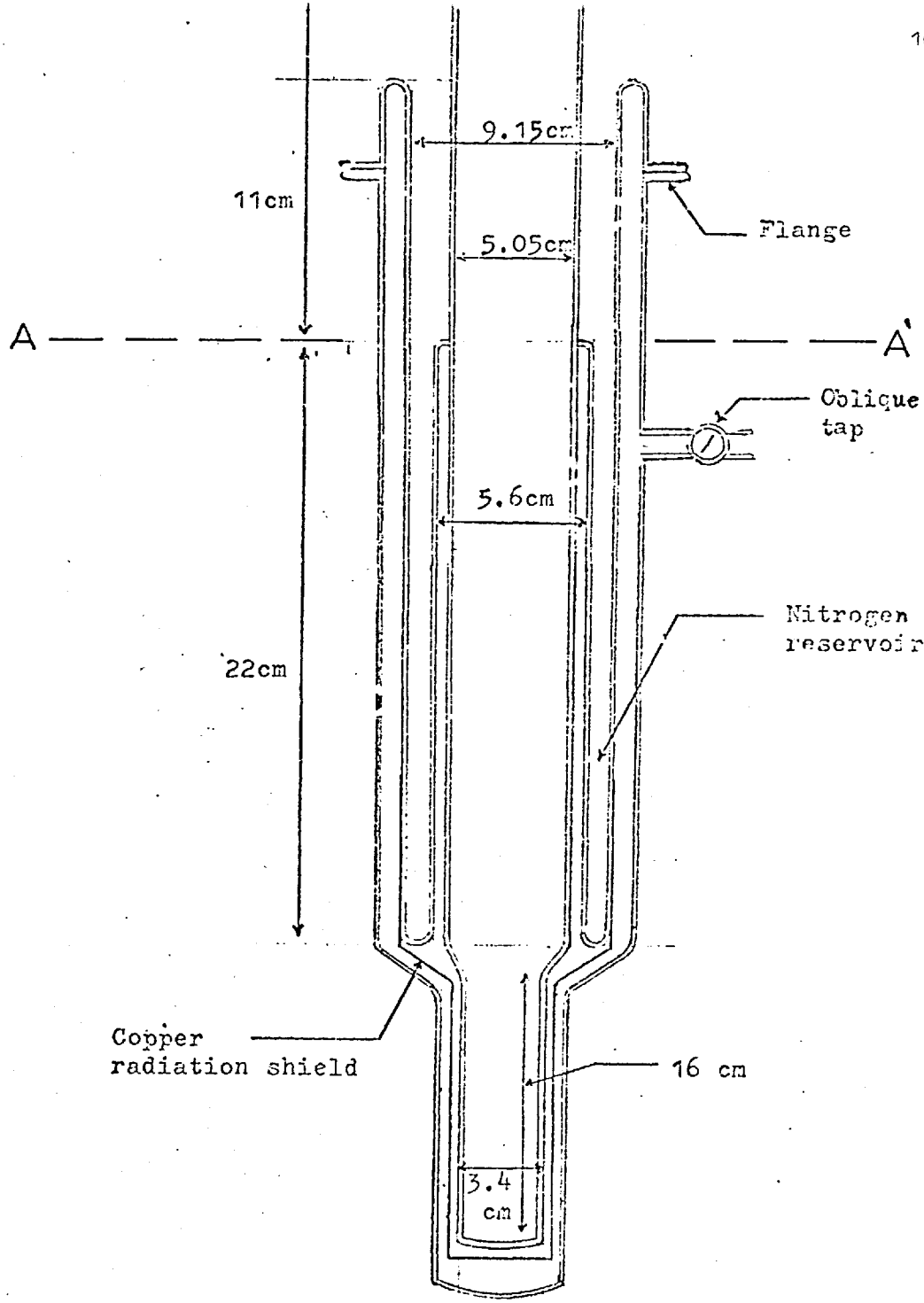


Fig.3.3 The glass dewar for liquid helium

The quartz suspension hung inside a German-silver down-tube which extended from room temperature at the top, to cryogenic temperature. The lower end of the down-tube was soldered to a copper end cap which consisted of two pieces fitted together by a cone joint (Fig. 3.6). The lower piece could be removed to give access to the suspension for the purpose of changing specimens.

For low temperature measurements the down-tube could be placed in the Pyrex glass cryostat shown in Fig. 3.3. This contains only one vacuum space. The Helium container is shielded from the outer wall of the cryostat, which is at room temperature, by a copper cylinder which is attached to, and cooled by, the liquid nitrogen reservoir. The procedure when operating with liquid helium and other liquid gases followed standard cryogenic usage (R 3.6, R 3.7).

3.2. General Modifications

In this section we discuss some modifications which were made to the susceptibility apparatus in order to increase its accuracy and the ease and rapidity of taking readings.

A large improvement to the sensitivity was made by changing the system of damping from electromagnetic to viscous.

The previous damping mechanism consisted of four aluminium discs which were attached to the bottom of the Sucksmith ring and which vibrated in the fields of four small magnets. The eddy currents induced in the discs provided the damping. From observations of the response to a step input the system was found to have a resonant frequency of about 5 cps and a damping coefficient of about 0.01. Due to this serious under-damping, building vibrations were picked up by the apparatus and produced random oscillations of large size in the photocell output which caused a serious reduction in the sensitivity.

The new viscous damping system improved the situation considerably. The aluminium discs were removed and replaced by two paddles which were allowed to move freely in pots of high viscosity vacuum oil. The paddles were of such a shape as to give damping against translations and rotations in all three dimensions, and were attached to the ring by two thin rigid wires passing through the surface of the oil. The buoyancy of the wire was estimated to increase the spring constant of the ring by only 1 part in 10^3, and using a reasonable estimate of the surface tension of the oil, the force acting on the ring due to this cause was found to be about 20 dynes. This is required to remain constant to 0.05 dynes during the few seconds it takes to obtain a reading, but in practice no errors were found which could be attributed to the variation of

surface tension force.

When the bell jar was evacuated, after having put fresh oil into the damping pots, it was found that considerable disturbance of the oil occurred due to dissolved air bubbling out under reduced pressure. However, this completely subsided after the oil had been left in a vacuum overnight, and so long as the oil was not exposed to the atmosphere for periods longer than a few hours, the trouble did not happen again. No difficulties were encountered either, due to oil creeping onto the balance, as it was sufficiently isolated from the damping pots for this not to occur.

The damping parameters obtained with this new arrangement were approximately: response time 0.5 seconds, damping coefficient 0.5, and an increase in usable sensitivity of about a factor of five. This revealed inaccuracies due to backlash in the photocell traversing rack, so a new all-metal one was constructed, and provided that thephotocell micrometer readings were always taken by rotating the micrometer downwards to eliminate the remaining backlash, and given a suitable means of detecting the photocell output, which will be discussed next, the smallest force detectable became 0.05 dynes. This was rather larger on windy days when low frequency building vibrations increased significantly.

The position of the light spot which has been reflected from the mirrors M1 and M2 on the ring, is found by letting it fall upon a split photocell and measuring the photocell output. The output is zero when the two halves of the photocell are equally illuminated. The circuit which was used (R 3.3) to do this when the writer first had access to the apparatus is shown in Fig. 3.4a. The two cells were connected in series opposition, the impedance of the galvanometer was 830 ohm and its sensitivity 4500 mm/μA. This is, however, an incorrect way of using a photocell which is a current operated device; the currents generated by the equal illumination of both cells will be forced tc flow through the high internal impedance of the cell thus upsetting its bias conditions. A much better circuit which is used by, for instance, Tinsley, in their galvanometer amplifer (type 5214) was adopted and is shown in Fig. 3.4b. The current due to the steady illumination flows around the photocell circuit and the output consists of only the difference between the currents due to the two halves. The output is detected by a Pye "Scalamp" galvanometer of rather more convenient size and slightly smaller sensitivity and higher impedance than the one used in circuit 3.4a. A switch is used to give two sensitivity ranges, and following Griffiths (R 3.5), the circuit is arranged so that the photocell sees the same impedance at both positions. A capacitor is connected across

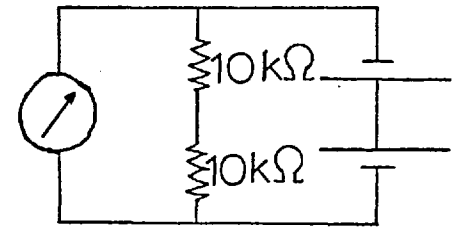


Fig.3.4a

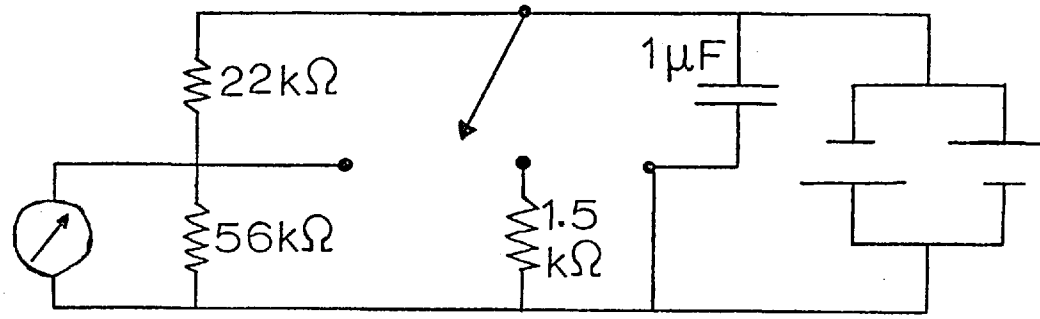


Fig. 3.4 b

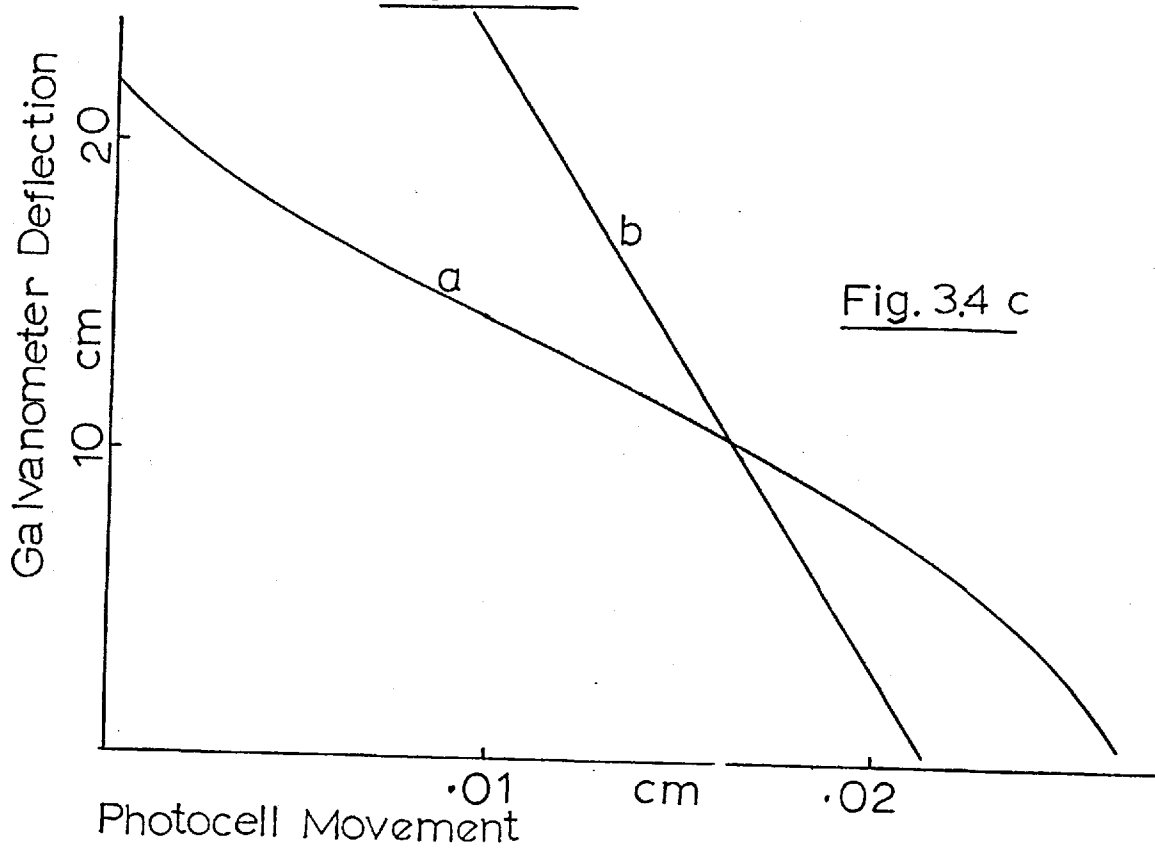


Fig. 3.4 c

the photocell to remove high frequency components in the output, and a damping resistor is placed across the terminals of the galvanometer.

The increase in sensitivity of the new circuit over that of the old is demonstrated in Fig. 3.4c in which the output galvanometer deflection is plotted against the movement of the light spot relative to the photocell. The extreme linearity of the new circuit suggested that readings of the force on the suspension might be taken very easily by feeding the photocell output into a resistor and measuring the resulting voltage with a digital voltmeter; this would avoid the nuisance of carefully adjusting the micrometer head for every reading. Unfortunately, attempts to make this system work were unsuccessful. An inadmissable amount of scatter in the readings was found which could not be reduced sufficiently by a resistor capacitor network, while at the same time preserving a reasonable response time. The point is that the dynamical properties of the galvanometer suspension play an essential part in damping out high frequency components of the input.

In magnetometers of this type it is necessary to measure the spring constant of the Sucksmith Ring during each experiment and the usual method of doing this is to lower a known weight onto the base of the ring and note the resulting deflection of the light spot. When the balance was originally

built, a relay electromagnet was used to operate a lever which lowered the weight, but this system had since been dismantled. A miniature solenoid has been fitted instead and this has the advantage over the relay magnet that when it is turned on, its magnetic circuit is closed, thus reducing the stray field which might interact with any magnetic impurities in the Sucksmith Ring and give a false reading. Furthermore, the current required to hold the solenoid in position is twenty times smaller than the current required to actuate it, and this too gives a further reduction in stray field and also an increase in battery life. A check was made to see if the operation of the solenoid would give any false reading and none was detected.

Because the dewar contained a copper nitrogen shield, the level of liquid helium inside it could not be determined visually by looking through a slit in the dewar which had been left unsilvered (R 3.6), and so instead three thermistor level gauges (R 3.8) spaced along the length of the down-tube were used to detect the helium level. The thermistors (type L094-3, MEG-HE-T2, obtained from the Keystone Carbon Company) had a voltage of 30 V applied to them. While they were immersed in liquid helium, the heat generated (0.3 mW) could be removed by the good thermal contact with the helium bath but when they were left above the level of the helium liquid the smaller thermal

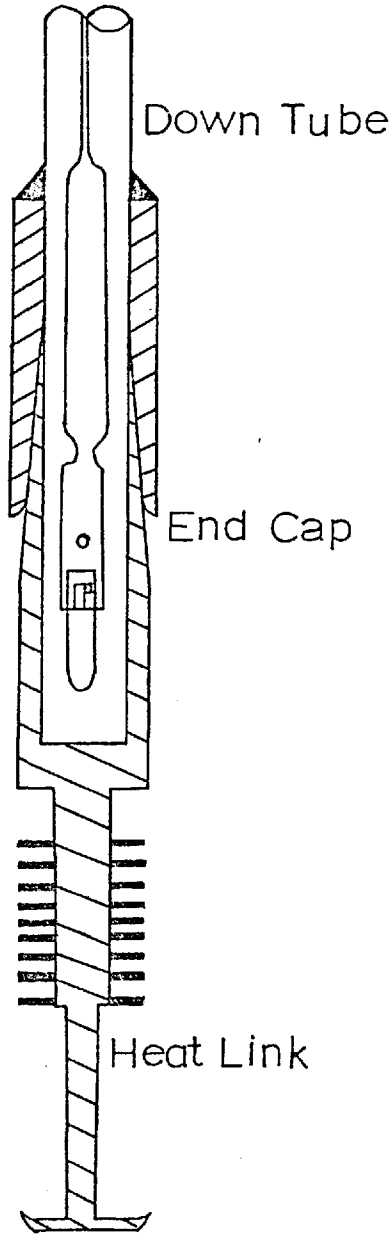
contact, together with the high temperature coefficient of resistivity produced a large change in resistance which could be easily detected.

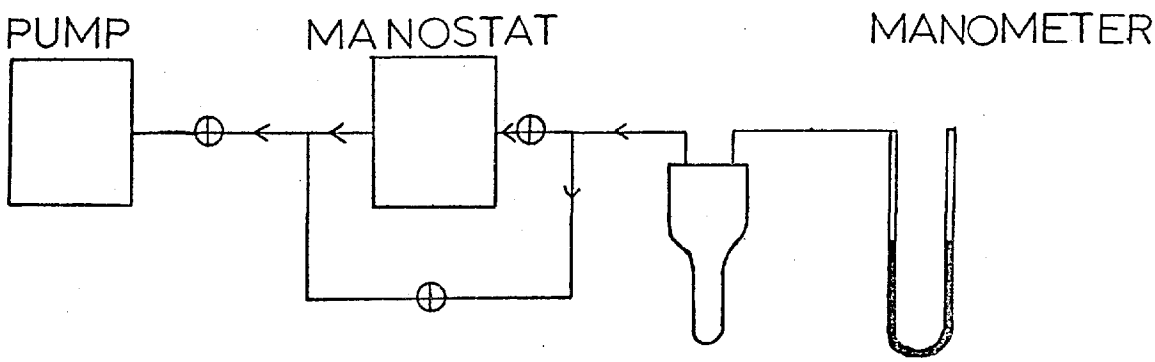
Sometimes after measurements had been made at helium temperature, some helium was left in the dewar, and in order to avoid having to wait a long time for it to evaporate a 1 kohm wire-wound resistor was placed near the bottom of the dewar to boil the remaining liquid off. The diagrams of the solenoid, thermistor and heater circuits are shown in Fig. 3.5.

The system of glass pipes and taps which originally connected the diffusion pump to the specimen chamber and dewar vacuum space was found to be very unreliable, as the taps often started to leak while an experimental run was under way. The glass assemblage has now been replaced by an entirely metal one, including the diffusion pump, using Edwards rubber diaphragm vacuum taps, and this system has been found to be completely satisfactory.

A diagram of the bottom of the down-tube and the end cap is shown in Fig. 3.6. The fillet joint between the tube and the end cap was originally made with lead-tin solder (R 3.3) but it is known (R 3.9) that these solders become superconducting at around $7^{\circ}K$ and have a critical field of the order of 1 kG at $4.2\ ^{\circ}K$. Accordingly all traces of lead-tin solder were

Fig. 3.6





removed and the joint was remade with an eutectic Cadmium-Zinc alloy of melting point 265 ^{o}C, which is non-superconducting in the helium range.

The cone joint between the two parts of the end cap was previously sealed with Wood's metal (R 3.3) but this also becomes superconducting at around 7 ^{o}K (R 3.6) so that at low temperatures the specimen was surrounded by a cylinder of superconducting metal (this may be clearly seen in Plate 3 p229 of R 3.3). In addition to this it was found that several blobs of Wood's metal had dropped into the bottom part of the end cap and were situated within a few mm. of the specimen. The presence of this superconducting metal is likely to give large field distortions at low fields and temperatures, so the surfaces of the cone joint were machined down to a smooth copper surface and the joint was made with silicone grease. This was found to be completely satisfactory at low temperatures, and unimportant minute leaks below the λ point were only detected once or twice in a dozen runs.

In order to improve the control and range of temperature in which measurements could be made, a facility for pumping on liquid gases was added. A diagram of this is shown in Fig. 3.6. It consists of a 150 litre/min pump, a Cartesian manostat (Gilmont R 3.38) for controlling the pressure, and a

mercury manometer for measuring it. By this means temperatures of down to 1.6 ^{o}K could be reached by pumping on liquid helium and precise temperature control in the range 77 ^{o}K - 53 ^{o}K could be achieved by pumping on liquid and solid Nitrogen, and if necessary, temperatures in the range 90 ^{o}K - 77 ^{o}K with liquid oxygen. With the more powerful pump on the resistivity apparatus in the Physics Department temperatures of 48 ^{o}K were attained with nitrogen.

Readings in the range 4 ^{o}K - 55 ^{o}K were taken as the end cap warmed up from liquid helium temperature. As the helium level fell below the bottom of the end cap, the cap started to warm up at a rate which was determined by the dimensions of the heat link (shown in Fig. 3.6) which connected it to the helium. This happened until all the helium in the bottom of the dewar had evaporated when the temperature rose rapidly. The dimensions of the heat link, including a variable cross section for it, were chosen by trial and error so that the temperature rose at a uniform rate until 55 ^{o}K when the last of the helium would just have evaporated. The warm up rate for the link which was finally used was about 0.3 ^{o}K per minute, but there is still room for improving the uniformity of warm up by making adjustments to the shape of the link.

3.3. Temperature Measurement

The method originally used for the measurement of low temperatures was as follows. Temperatures from 300°K to 77°K were measured with a copper constantan thermocouple having its reference junction in ice, from 77°K to 4°K a cobalt-gold versus gold-silver thermocouple with its reference junction in liquid oxygen was used, which was supplemented in the range 10°K - 4°K by a thermistor. This method of using three different thermomenters and two liquid reference baths is cumbersome, and because of this, and also because of the fact that the cobalt-gold thermocouple had been found to be damaged, it was decided to use only one thermocouple which would cover the whole temperature range.

The thermocouple which was adopted consists of one arm of 0.03% Atomic Fe Au and the other arm of Chromel (R 3.10-13). At 1°K the thermoelectric power is 10 μV/°K and at 4°K the total thermocouple voltage is about 4.5 mV when the reference junction is at 0°C. As well as its high sensitivity this thermocouple has the advantage that the FeAu system is a stable solid solution in the range where it is used, in contrast to the CoAu system which is supersaturated (R 3.14) and whose properties tend to change with time as the cobalt comes out of the solution.

The thermocouple wire, obtained from Johnson Matthey Limited, was of 0.08 mm diameter and was supplied in an annealed condition. The junctions were made by tinning the ends of the wires with soft solder and joining them together with a small blob. It was necessary to use a very cool soldering iron when tinning the gold wire as it tended to dissolve in the liquid solder if the temperature was too high. One junction was soldered to the end cap which had been previously tinned with non-superconducting solder (it was calculated that the tiny amount of superconducting solder which remained on the wires would have a negligible effect on the magnet field) and the two wires were wound round the end cap several times and led up the down-tube, through a vacuum seal, and into a small dewar flask which contained the reference junction fluid. The thermocouple wires were then soldered to screened copper leads which lead off to a potentiometer.

A liquid oxygen bath was originally (R 3.3) used for the reference junction but this was abandoned for several reasons. The first is that the use of it causes the thermocouple wires to be subjected to <u>two</u> thermal gradients, once in coming up from helium temperature to room temperature and then again in going down to the temperature of the oxygen bath. An even more serious objection is that it has been reported by Berry

(R 3.15), that the oxygen at the bottom of a dewar, where the junctions were originally situated, may superheat by up to 1.5 °K, and as the thermoelectric power of CoAu is much larger at 90 ° K that at 10 °K serious errors may have been introduced by this effect. This may explain, incidently, why Murani (R 3.16) found difficulty in fitting the resistivity-temperature characteristic of a copper resistor at 90 °K.

Dey (R 3.3) claimed that he was able to stabilise the temperature of the boiling oxygen bath to within 0.01 °K by using a Cartesian manostat to control the pressure over the liquid. The writer finds it difficult to understand how he achieved this precision, as in his own experience the manostat is ineffective in controlling pressures of below 1 cm Hg, which corresponds to 0.1 °K.

To avoid these problems it was decided to use an ice bath to give a reference temperature. Distilled water and ice made from distilled water were always used, and the thermocouple wires were carefully bent down to the bottom of the bath and then upwards, so that the junctions were surrounded by the melting ice at the top of the bath. The thermocouple was calibrated against a table of EMF versus temperature, which Dr R. Berman had kindly given to the writer, by measuring the thermocouple voltages at the boiling points of helium and

nitrogen and the triple point of nitrogen. Only a very small interpolation of the calibration table was needed.

This thermocouple has retained its calibration to 0.5 ^{o}K over a two year period, but the user of an FeAu chromel thermocouple made from the thicker wire of 0.3 mm diameter hasreported (R 3.17) that its reproducibility is even better - 0.1 ^{o}K. Presumably, this is due to the thinner wire being more susceptible to strains received while handling, which anneal out at room temperature, or strains received in thermal cycling.

This thermocouple provides an excellent method of measuring the temperature of the end cap to an accuracy of 0.2 ^{o}K in the range 4 ^{o}K - 300 ^{o}K, and below 4 ^{o}K the temperature may be found to an accuracy of 0.01 ^{o}K from the helium vapour pressure. However, it can not by any means be assumed that the temperature of the specimen is the same as that of the end cap; the relation between these two temperatures will be discussed in the next section.

3.4. Helium Exchange Gas Pressure

In order to ensure that the temperature of the specimen is close to that of the end cap (Fig. 3.6) it is standard practice (R 3.18, R 3.5, R 3.6, R 3.7) to admit a few Torr of

helium gas into the down-tube. However, in this pressure range, where the mean free path of the gas (1/6 mm at 1 Torr and 300 ^{o}K) is beginning to become comparable with the size of the apparatus, it is well known (R 3.19, R 3.20, R 3.21, R 3.22) that large vertical forces may be exerted on a suspension in a temperature gradient by thermomolecular pressures and flows. Gerritsen et al (R 3.19) found for a typical magnetometer suspension that the force could be as great as 1 dyne at a gas pressure of 0.1 Torr, with the top of the suspension at room temperature and the bottom at the temperature of liquid air, and Krupp et al (R 3.20) showed that above the pressure of maximum force the thermomolecular force was approximately inversely proportional to pressure. This adverse effect of the exchange gas is overcome by subtracting the measurement of the force with the field off from that with it on, but care must be taken (R 3.19) to see that the thermomolecular forces do not cause any lateral deflections of the suspension and move it into a part of the magnetic field where the vertical force is changed in the manner which will be discussed in section 3.5.

Gerritsen et al (R 3.19) also observed that there was a small variation of the specimen temperature with exchange gas pressure when the end cap was at helium temperature. They found the specimen temperature to be 0.1 ^{o}K high at a pressure of 0.1 Torr falling to .01 ^{o}K at 10 Torr.

Experiments were carried out on the susceptibility balance described here in order to find out whether any such temperature variation took place. The force acting on a specimen which was known to obey the Curie Law was measured as a function of exchange gas pressure. No variation of temperature, to an accuracy of 1%, was found at 77 °K in the range of exchange gas pressure from .01 Torr to 760 Torr and at 4 °K from .1 Torr to 20 Torr. There was, however, a steady temperature error, which will be mentioned at the end of this section, and a correction was always made for this when calculating the specimen temperature.

Magnetic measurements in the range 4 °K - 55 °K and 77 °K - 300 °K were always made while the temperature was changing. Therefore, the exchange gas must also carry out the function of ensuring that the temperature of the specimen rapidly follows any temperature changes of the end cap, as well as seeing that it reaches the correct temperature eventually.

The simplest assumption to make about the time dependent behaviour is that the equation:

$$\frac{\partial T}{\partial t} = -\frac{(T - T_o)}{\gamma} \qquad 3.4$$

is obeyed. T is the temperature of the specimen, T_o that of the

end cap, t the time co-ordinate and τ a time constant which will be a function of the temperature and pressure of the exchange gas and the properties of the magnetic specimen.

This first order differential equation may be solved in two simple cases. First if T_o is suddenly changed to a new constant value, T will rise to meet it exponentially with a time constant τ, secondly, if T_o is changed at a steady rate, then after a few τ when transients have died away, T will change at the same rate as T_o but lag behind it by a time τ. The second situation is just what is happening when readings are taken with the temperature drifting slowly, and implies that the temperature reading should be taken a time τ before the susceptibility reading; the first situation provides a means of measuring τ.

Experiments to measure τ in this way were carried out by pouring liquid nitrogen into the dewar and recording the force on a specimen, which obeyed the Curie law, as its temperature went down from 300 ^{o}K to 77 ^{o}K.

A typical example of the force against time curves obtained is shown in Fig. 3.7a. At t = 0 the nitrogen is put in, during AB the nitrogen percolates down to the end cap and cools it, BC is the exponential rise, and CD the steady state at the new temperature. τ may be estimated from the duration

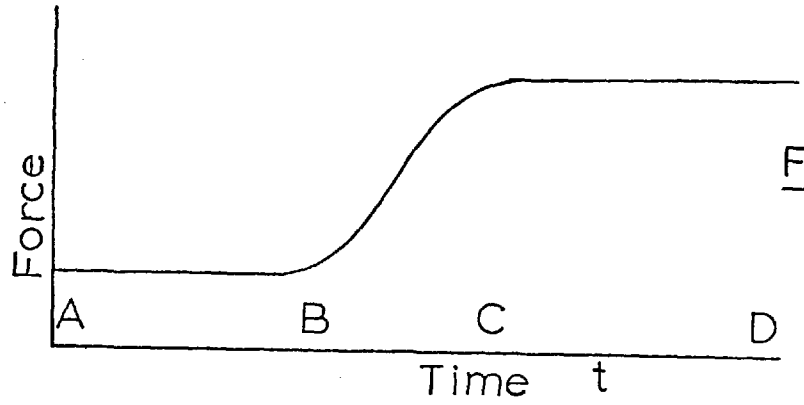


Fig. 3.7 a

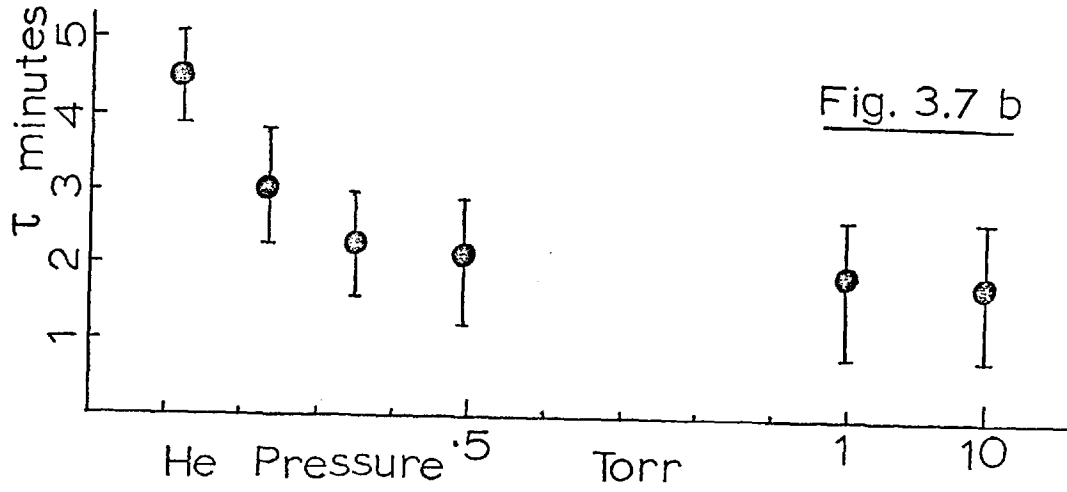


Fig. 3.7 b

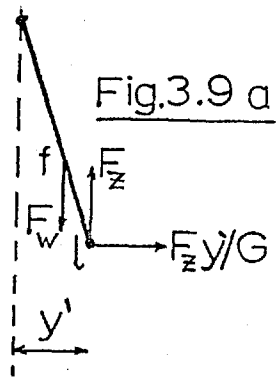


Fig.3.9 a

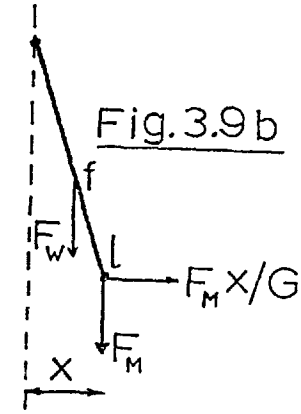


Fig.3.9 b

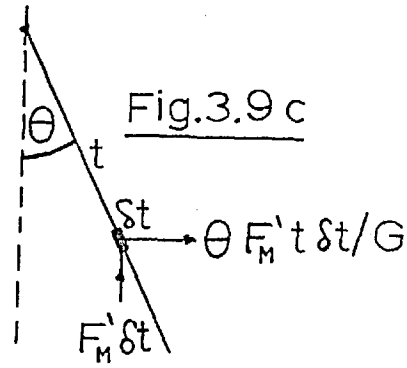


Fig.3.9 c

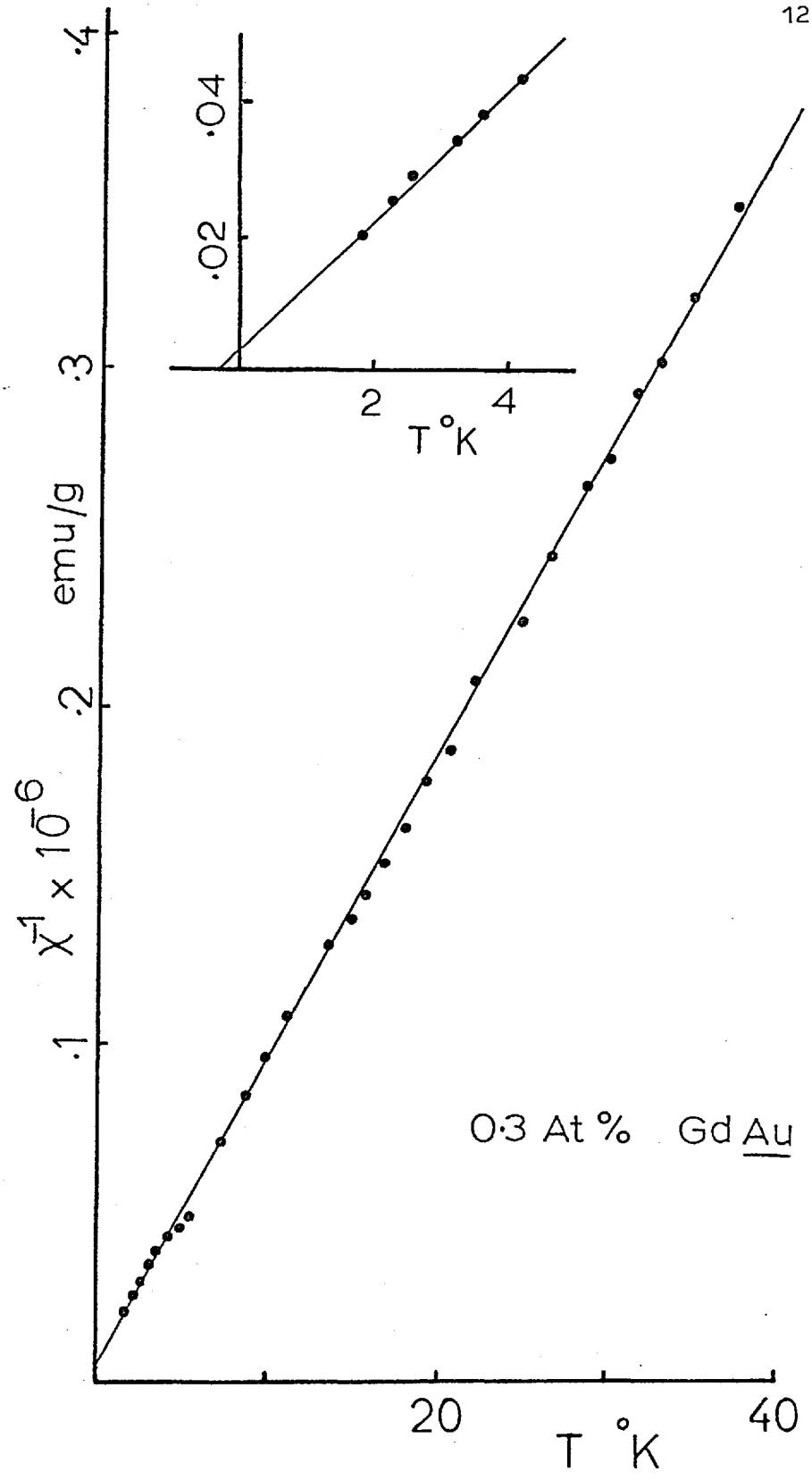


Fig. 3.8

of BC and in Fig. 3.7b τ is plotted as a function of exchange gas pressure. It can be seen that the exchange gas pressure of .01 Torr previously used by Dey (R 3.3, p240) is in this respect too small, and for all experiments done subsequently, a pressure of 5 Torr was used which gave a time constant in the 1-2 minute range.

The mechanism of heat transfer between the walls of the down tube and the specimen is clearly complicated. It involves the heat conducted through the gas, which will be independent of pressure and vary as roughly $T^{0.6-0.9}$ (R 3.6 p204) and heat transferred across the various solid-gas interfaces. This should be proportional to the number of collisions per unit time and area with the solid surface, which should go roughly as $p/T^{0.5}$. It is not, then, apparent that the measurement of a time constant over a large temperature range in which the constant may itself vary substantially will give an adequate indication of the behaviour to be expected at a temperature (4 ^{o}K) twenty times smaller than the lowest temperature at which the transient behaviour was investigated.

There is only one way to ensure that accurate readings are being obtained and that is to measure the apparent susceptibility of a specimen whose real susceptibility is known throughout the range of temperatures used. Accordingly, the

the susceptibility of a specimen of 0.3 % at. GdAu, (kindly given to the writer by A. P. Murani) which was known to obey the Curie law (R 3.16) to 0.05 ^{o}K was measured from 2 ^{o}K upwards with the results shown in Fig. 3.8. The slope of the $\chi^{-1} \sim T$ curve is consistent with the known concentration of Gd in the alloy but a temperature displacement of 0.3 ^{o}K was found, which was allowed when calculating the true specimen temperature. This steady error was not due to Brillouin curvature of the Gadolinium magnetisation, as a small field was used so that the magnetisation was well within the linear region. Higher temperature ranges were checked with specimens of Ferrous Ammonium Sulphate which was also used to calibrate the value of $H_x \partial H_x / \partial r$ at room temperature. The overall accuracy of measurement was estimated to be $\pm$ 1 ^{o}K in temperature, and $\pm$ 2.5% in susceptibility, provided that an adequate amount of the specimen was available so that the magnetic force was greater than about 5 dynes.

3.5. Lateral Instability

3.5.1. Forces Caused by Small Deviations from the Position of Symmetry

In section 3.1 it was shown that the vertical force F_z acting on a moment positioned on the line of symmetry in the

magnetic field is given by:

$$F_z = F_r = m_x \frac{\partial H_x}{\partial r} \qquad 3.5.$$

It is of great interest to know how this force varies, and what new forces are introduced, if the moment is moved a small distance away from the symmetry point. Differences in vertical force will cause measurement errors and any lateral forces, as we shall show, may lead to instability of the suspension.

First consider small deflections in the y direction (Fig. 3.1). The radial force will no longer act vertically and will have a small lateral component F_y in the y direction given by:

$$F_y = F_r \frac{y}{r} = y F_z/G_y \qquad 3.6$$

where we call G_y (= r) the Field Gradient Ratio for the y direction.

Because of the y displacement, the vertical force will be changed for two reasons. First, the resultant force will be at an angle y/r to the vertical and second, the radial distance will have increased by y^2/r. The new vertical force F_z' on a specimen of mass m' and paramagnetic susceptibility χ will be:

$$F_z = m' \chi \left(H_x + \frac{\partial H_x}{\partial r} \frac{y^2}{r} + \ldots\right)$$

$$\left(\frac{\partial H_x}{\partial r} + \frac{\partial^2 H_x}{\partial r^2} \frac{y^2}{r} + \ldots\right)\left(1 - \frac{y^2}{2r^2} + \ldots\right)$$

from which we obtain the change in vertical force ΔF_z in terms of the original vertical force F_z as:

$$\frac{\Delta F_z}{F_z} = y^2\left(\frac{1}{rH_x} \frac{\partial H_x}{\partial r} + \frac{1}{r} \frac{\partial^2 H_x}{\partial r^2} \Big/ \frac{\partial H_x}{\partial r} - \frac{1}{2r^2}\right) + \ldots \quad 3.7.$$

If the specimen is deflected a small distance x in the x direction a lateral force in the x direction will appear which is given by:

$$F_x = m_r \frac{\partial H_x}{\partial r} + m_x \frac{\partial H_x}{\partial x}$$

This expression may be simplified first by expanding H_x, following Henry and Rogers (R 3.23), as:

$$H_x(x) = H_x(0) + \tfrac{1}{2} \frac{\partial^2 H_x}{\partial x^2} x^2 + \ldots$$

hence

$$\frac{\partial H_x}{\partial x} = \frac{\partial^2 H_x}{\partial x^2} x + \ldots$$

and secondly by noting that the resultant moment of any magnetically isotropic specimen will lie along the resultant magnetic field so that::

$$\frac{m_r}{m_x} = \frac{H_r}{H_x}$$

Now by symmetry

$$H_r(x) = \frac{\partial H_r}{\partial x} x + ... \doteq \frac{\partial H_x}{\partial r} x$$

using curl $\underline{H} = 0$ so that:

$$F_x = x\, m_x \left(\frac{\partial^2 H_x}{\partial x^2} + \frac{1}{H_x}\left(\frac{\partial H_x}{\partial r}\right)^2\right)$$

$$\frac{F_x}{F_z} = \frac{x}{G_x} \qquad 3.8$$

where the Field Gradient Ratio for the x direction G_x is given by::

$$G_x^{-1} = \frac{\partial^2 H_x}{\partial x^2} \Big/ \frac{\partial H_x}{\partial r} + \frac{1}{H_x}\frac{\partial H_x}{\partial r} \qquad 3.9$$

It has been pointed out to the writer by Parker (R 3.29) that a simplification may be made to equation 3.9 in the special case when the magnetic specimen lies at the position of maximum

$H_x \partial H_x / \partial r$ as:

$$\frac{\partial}{\partial r}\left(H_x \frac{\partial H_x}{\partial r}\right) = H_x \frac{\partial^2 H_x}{\partial r^2} + \left(\frac{\partial H_x}{\partial r}\right)^2 = 0$$

However, we will not use this expression in the analysis here as it is an approximation which applies to only one position.

An expression for the change in vertical force ΔF_z when a paramagnetic specimen is deflected by a small amount x may also be obtained:

$$\frac{F_z}{m\chi} = H_r \frac{\partial H_r}{\partial r} + H_x \frac{\partial H_x}{\partial r} \qquad 3.10$$

First we treat the first term of this equation:

$$\text{From div } \underline{H} = \frac{\partial H_r}{\partial r} + \frac{H_r}{r} + \frac{\partial H_x}{\partial x} = 0,$$

$$H_r = \frac{\partial H_x}{\partial r} x \quad \text{and} \quad \frac{\partial H_x}{\partial x} = \frac{\partial^2 H_x}{\partial x^2} x$$

$$\text{we get } \left(\frac{\Delta F_z}{F_z}\right)_1 = -x^2\left(\frac{1}{rH_x}\frac{\partial H_x}{\partial r} + \frac{1}{H_x}\frac{\partial^2 H_x}{\partial x^2}\right)$$

$$\text{and using } (\nabla^2 \underline{H})_x = \frac{\partial^2 H_x}{\partial r^2} + \frac{1}{r}\frac{\partial H_x}{\partial r} + \frac{\partial^2 H_x}{\partial x^2} = 0$$

(R 3.2), we obtain:-

$$\left(\frac{\Delta F_z}{F_z}\right)_1 = x^2 \frac{1}{H_x} \frac{\partial^2 H_x}{\partial r^2}$$

The force deviation arising from the second term in equation 3.10 is calculated from:

$$(\Delta F_z)_2 = \frac{x^2}{2} m \chi \frac{\partial^2}{\partial x^2} \left(H_x \frac{\partial H_x}{\partial r}\right)$$

Now

$$\frac{\partial}{\partial x^2} \left(H_x \frac{\partial H_x}{\partial r}\right) = \frac{\partial^2 H_x}{\partial x^2} \frac{\partial H_x}{\partial r} + 2 \frac{\partial H_x}{\partial x} \frac{\partial^2 H_x}{\partial x \partial r} + H_x \frac{\partial^3 H_x}{\partial x^2 \partial r}$$

the middle term is zero because the differentials are evaluated at x = 0 and one finds:

$$\frac{\partial}{\partial x^2} \left(H_x \frac{\partial H_x}{\partial r}\right) = \frac{\partial}{\partial r} \left(H_x \frac{\partial^2 H_x}{\partial x^2}\right),$$

an expression which is rather more easy to evaluate. Again using $(\nabla^2 \underline{H})_x = 0$ one obtains for the deviation due to the second term in equation 3.10:

$$\left(\frac{\Delta F_z}{F_z}\right)_2 = \frac{x^2}{2} \left(\frac{\partial^3 H_x}{\partial r^3} \Big/ \frac{\partial H_x}{\partial r} + \frac{1}{r} \frac{\partial^2 H_x}{\partial r^2} \Big/ \frac{\partial H_x}{\partial r} + \frac{1}{H_x} \frac{\partial^2 H_x}{\partial r^2} + \frac{1}{r H_x} \frac{\partial H_x}{\partial r} - \frac{1}{r^2}\right).$$

Adding together the two components:

$$\frac{\Delta F_z}{F_z} = \left(\frac{\Delta F_z}{F_z}\right)_1 + \left(\frac{\Delta F_z}{F_z}\right)_2$$

we get

$$\frac{\Delta F_z}{F_z} = + \frac{x^2}{t^2} \qquad 3.11$$

where

$$-2t^{-2} = \frac{\partial^3 H_x}{\partial r^3} / \frac{\partial H_x}{\partial r} - \frac{1}{H_x}\frac{\partial^2 H_x}{\partial r^2} + \frac{1}{r}\frac{\partial^2 H_x}{\partial r^2} / \frac{\partial H_x}{\partial r}$$

$$+ \frac{1}{rH_x}\frac{\partial H_x}{\partial r} - \frac{1}{r^2}$$

The value of t was determined experimentally by direct measurement of the force, for the magnet described in this work, and was found to be 1.1 cm.. This means that a positioning error of 1 mm in the x direction will give an error in F_z of less than 1%; this positional accuracy is easily attainable.

Equations 3.8 and 3.11 have been derived in an equivalent form by Garber et al (R 3.24) for the simpler situation in which the magnetic field has zero variation in the y direction. Our equations reduce to theirs, after some manipulation, as

$r \rightarrow \infty$. It should be noted that equations 3.7 and 3.11, which give the alteration in vertical force, apply only to paramagnetic specimens, while equations 3.6 and 3.8 which give the lateral force apply to any isotropic magnetic material. The variations of force with deflection, in the first case quadratic, in the second linear, are simply a consequence of the symmetry of the situation, and one does not need the exact analysis which we have given here to obtain them. The analysis of the change in vertical force contains also the assumption that the specimen is deflected horizontally, which is only true if the length of the suspension to which the magnetic specimen is attached obeys the condition $l/r \gg 1$. If it does not, then extra terms will be introduced into the equations. However, the condition is well satisfied by the apparatus described here as $l/r \doteq 10$.

3.5.2. Stability of the Faraday Magnetometer

During the early stages of the experimental work with the magnetometer it was found that gross errors, typically $\pm$ 10% – $\pm$ 30% occurred in the measurement of large magnetic forces. These errors were found to be due to the suspension rubbing against the inside of the down tube, and an investigation of the reason for this lead to the discovery, described in references R 3.25 and R 3.26 which are bound into this thesis

and should be read in conjunction with this section, that large deflections of the suspension will take place when the magnetic force exceeds a critical value.

Lateral instability was first mentioned in 1929 by Sucksmith (R 3.27) who suggested that it was due to forces arising from the field term $H_x \partial H_x / \partial x$, that this quantity would be zero at the centre of the field and rise to positive values going in either direction towards the poles, and that the suspension would lie in a position of metastable equilibrium between the pole pieces. He did not take the analysis any further but solved the problem experimentally by putting constraints on the suspension so that it could move freely in the vertical direction, but not horizontally. The next significant development was when Garber et al (R 3.24) showed that the lateral magnetic force was proportional to the lateral deflection, deriving equation 3.8 for the case of magnetic field of zero variation in the y direction. They did not, however, realise that for a simple suspension the restoring force was also proportional to the lateral deflection. This was understood by Hill (R 3.28) who did not, on the other hand, recall Garber et al.'s point. Hill also neglected forces arising from the second term of equation 3.9 as did Stewart (R 3.26), until corrected (R 3.27) by Parker (R 3.29). A further clue was provided by Morris and Wold

(R 3.30) who observed that lateral instability tended to occur at the same value of magnetic force for different specimens.

The stability condition for a cylindrical magnetic field may be obtained by reference to Fig. 3.9a. The suspension is assumed to be a simple pendulum of length l, weight (in dynes) Fw, with its centre of gravity f from the top. y' is the small deflection in a general direction. Taking moments about the suspension point, the suspension will be stable if:

$$Fw \frac{f}{l} y' > F_z y' + y' \frac{lF_z}{G}$$

or

$$\frac{Fw}{F_M} \frac{f}{l} > 1 + \frac{l}{G} \qquad 3.12$$

where F_M is the modulus of F_Z.

For the y direction, G = r so the stability condition is:

$$\frac{Fw}{F_M} \frac{f}{l} > 1 + \frac{l}{r} \qquad 3.13$$

This is consistent with the remark made by Stewart R(3.25) at the end of section 2.5 of that paper, because if one compares

the expression for $(\nabla^2 \underline{H})_x$ (R 3.2) in Cartesian and Cylindrical co-ordinates one finds that:

$$\frac{\partial^2 H_x}{\partial y^2} \Big/ \frac{\partial H_x}{\partial r} = \frac{1}{r} = G_y^{-1} \quad .$$

The stability condition for the x direction is obtained by taking F_M to be the modulus of the magnetic force and G the modulus of G_x. The stability condition then becomes (Fig. 3.9b):

$$1 + \frac{Fw}{F_M} \frac{f}{l} > 1/G \qquad 3.14$$

where

$$G_x^{-1} = \frac{\partial^2 H_x}{\partial x^2} \Big/ \frac{\partial H_x}{\partial r} + \frac{1}{H_x} \frac{\partial H_x}{\partial r} \qquad 3.15$$

The stability condition for a suspension consisting of two rigid links was quoted but not proved in R 3.25, and we give a derivation of it in Appendix B.

The quasi-dynamical behaviour of the suspension system, when subjected to misalignment and non-linear forces, has been discussed in detail before (R 3.25) and will not be mentioned again here.

There is, however, one aspect of the image force calculation which needs further examination. It was shown in R 3.25 that although the image forces were of the correct

symmetry to give instability behaviour, they were far too small in magnitude to be significant. It was pointed out to the writer by Parker (R 3.29), after the publication of R 3.25, that the calculation, if it is to be done properly, should involve a whole series of images extending to infinity along the positive and negative x direction. We give this improved calculation in Appendix C, not that we believe that it is in any way more accurate, the initial assumptions are far too crude for that, but merely to show that no awkward divergences arise when the infinite series is considered. The result of the calculation is that the image forces are still negligible.

3.5.3. Stability of the Gouy Magnetometer

A criterion for lateral stability may be obtained for the Gouy magnetometer as well as for the Faraday magnetometer. We assume that the suspension, shown in Fig. 3.9c, is a single freely hinged rigid link, and that the magnetic material is distributed along it so that the vertical magnetic force on a length δt is $F'_M \delta t$, t is the distance from the suspension point, and θ the angular deflection. By the arguments which lead to equations 3.6 and 3.8 the lateral force will be $\theta F'_M t \delta t/G$ and the stability criterion is:

$$Fwf > \int F'_M t dt + \int \frac{F'_M}{G} t^2 dt \qquad 3.16$$

This expression is simplified if one considers only materials with field independent susceptibility so that:

$$F'_M = \chi' H_x \frac{\partial H_x}{\partial r}$$

where χ' is the susceptibility per unit length, and makes the assumption that the field is of constant "shape",

$$\underline{H}(\underline{r},I) = \underline{A}(\underline{r})\, B(I) \qquad 3.17$$

where $\underline{H}$ is the magnetic field vector, $\underline{r}$ the position vector, and I is the electromagnet current:

Thus $$F_M = \chi' B^2(I) \int A_x(t) \frac{\partial A_x(t)}{\partial t}\, dt$$

and the stability condition becomes:

$$\frac{Fw}{F_M} f \rangle \left(\pm \int A_x \frac{\partial A_x}{\partial t} t\, dt + \int \frac{A_x}{G} \frac{\partial A_x}{\partial t} t^2 dt\right) \Big/ \int A_x \frac{\partial A_x}{\partial t} dt \qquad 3.18$$

The + sign is for diamagnetic specimens for which the instability will be in the y direction; the - sign is for paramagnetic specimens. We keep to the same convention, as before, that the moduli of the magnetic force and the Field Gradient Ratio are used in the stability conditions.

The stability behaviour of the Gouy magnetometer is then similar to that of the Faraday magnetometer: if the magnetic force exceeds a certain value, independent of the type of specimen, instability will result.

3.5.4. On the Radial Variation of the Field Gradient Ratio G_x

In order to investigate the stability properties of the magnetic field further, measurements were made of the variation of several field quantities with r, the radial distance from the cylindrical axis of symmetry. The magnet used, as mentioned in R 3.25, was a Newport Instruments type E Electromagnet (7 inch diameter plane pole faces and a 5 cm gap). In Fig. 3.10 the quantities H_x, $H_x \partial H_x/\partial r$, and $\partial H_x/\partial r$ are plotted against r. $H_x \partial H_x/\partial r$ was found from measuring the force exterted on a paramagnetic specimen, H_x was measured with a Hall-probe fluxmeter (probe dimension 3mm x 7 mm) and $\partial H_x/\partial r$ was found from the quotient of the two. The edge of the pole faces is at r = 8.9 cm and the dotted line on the diagram is a Gaussian fit to $\partial H_x/\partial r$; this will be discussed later. All the measurements were made at a magnet current of 20A; at this current the field at r=0 is 7.3 kOe, which indicates that the magnet is far from saturation. Even at the full current of 40A, ($H_x(0)$ = 10 kOe), saturation does not occur at the centre of the magnet but may do so at the pole

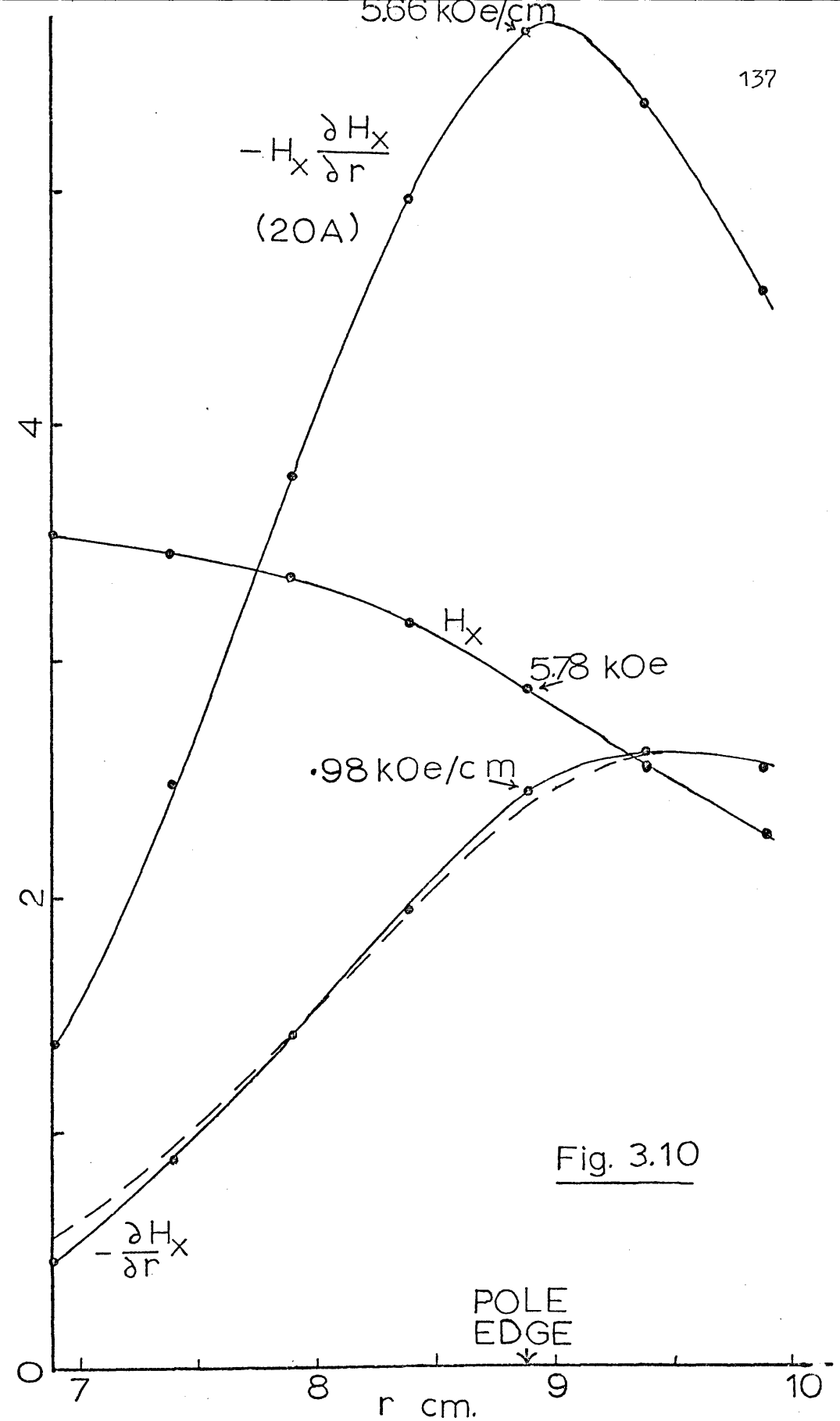

5.66 kOe/cm
$-H_x \frac{\partial H_x}{\partial r}$
(20A)
H_x
5.78 kOe
·98 kOe/cm
$-\frac{\partial H_x}{\partial r}$
POLE
EDGE
0
2
4
7
8
9
10
r cm.

Fig. 3.10

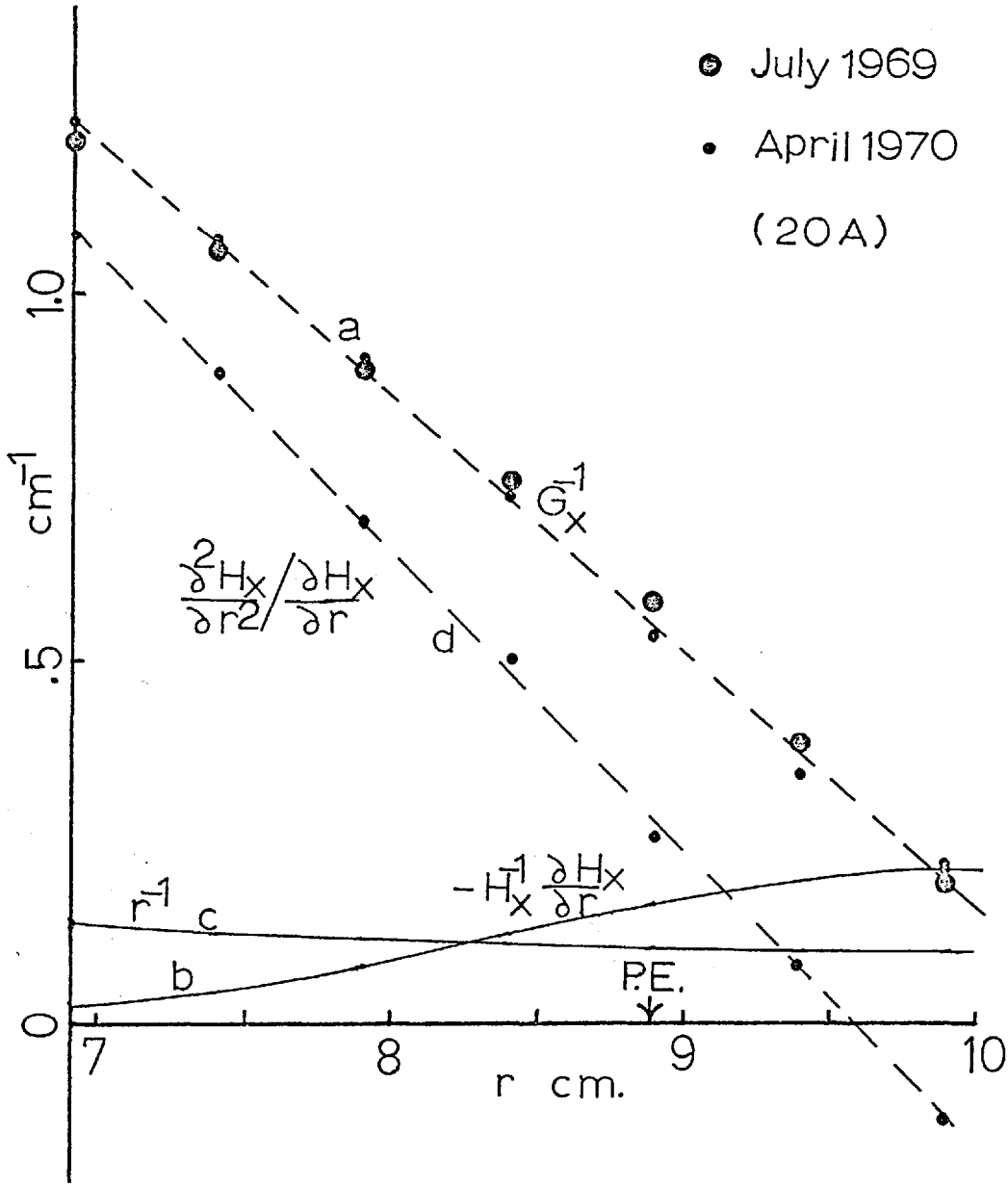

July 1969
April 1970
(20 A)
1.0
.5
0
cm⁻¹
a
d
G_x^{-1}
$\frac{\partial^2 H_x}{\partial r^2} / \frac{\partial H_x}{\partial r}$
r^{-1}
c
$-H_x^{-1}\frac{\partial H_x}{\partial r}$
b
P.E.
7
8
9
10
r cm.

Fig. 3.11

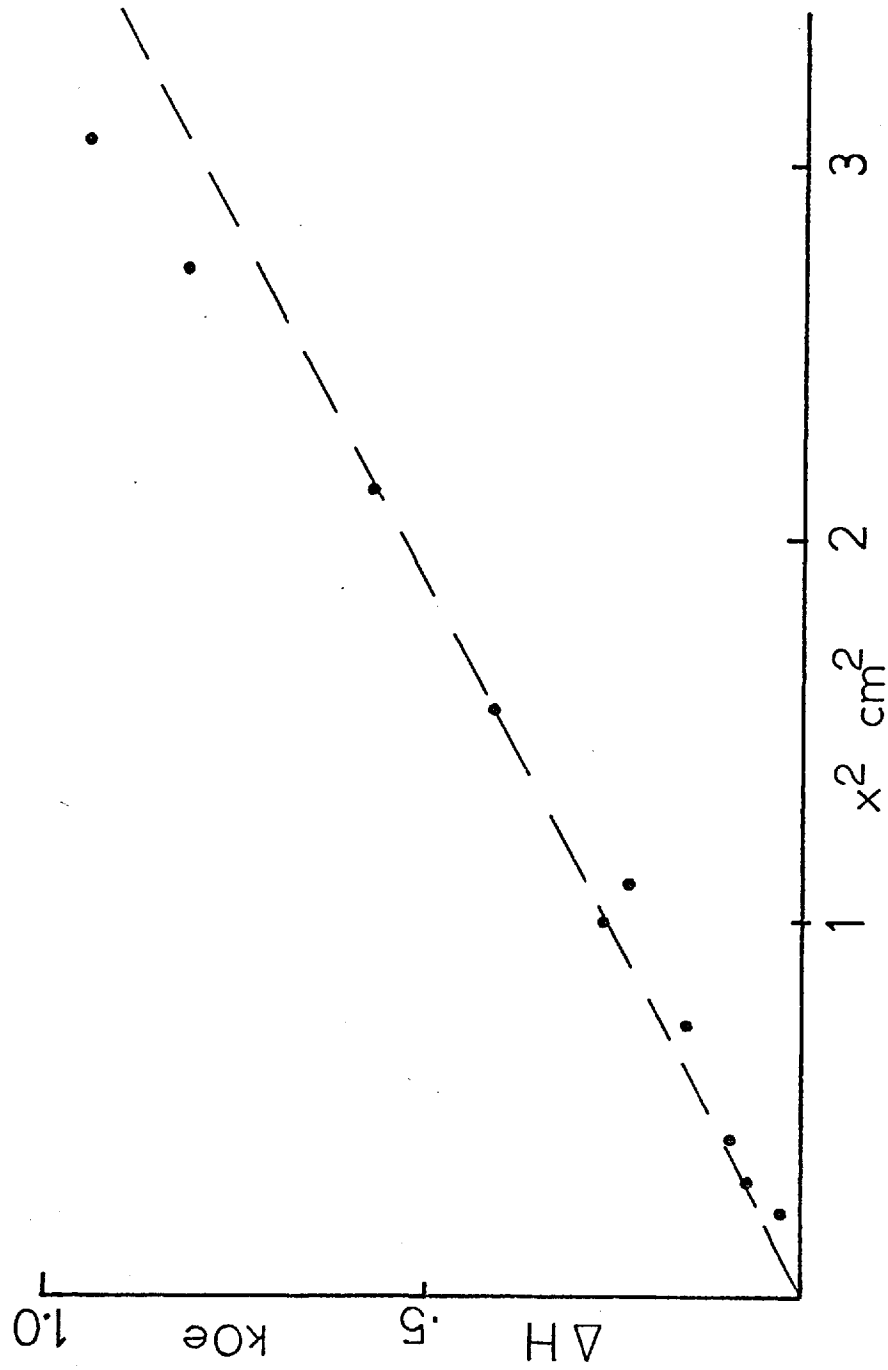


Fig. 3.12

tips. It was also found that the shape of the $H_x(r)$ profile, in the region shown, at a magnet current of 37A, agreed with that at 20A to 1%, and that the value of $H_x^{-1} \partial H_x / \partial r$ at r=9 cm was constant to 3% for a range of magnet current from 10A to 40A.

All these observations, and also the fact that F_M^c is found to be substantially independent of magnet current, lead one to suppose that the approximation of constant "shape" is a good one for the magnet considered here. However, it must be realised that this assumption is most likely to apply to a magnet with flat poles, as with this shape, the poles are least likely to become saturated. Therefore arguments used with regard to the magnetic effects considered here should not be uncritically extended to deal with magnets of a different shape.

The results shown in Fig. 3.10 are in disagreement with the statement of Dey (R 3.3, p11) that the maximum value of $H_x \partial H_x / \partial r$ is roughly 1 cm from the pole edge. A specimen of length 2 mm placed so that its centre was at the position of the maximum value of $H_x \partial H_x / \partial r$ would be subject, over its length, to a variation of $\pm$ 0.5% in that quantity, whereas a specimen placed at a position 1 cm out from the edge of the poles would be subject to a variation of $\pm$ 4%. When

susceptibility measurements were made the specimen was always placed at the position of maximum $H_x \partial H_x / \partial r$ to minimise this error.

If F_M^c is measured, G_x may be deduced from it by means of equation 3c of R 3.25 (G_x was called G in that reference). In Fig. 3.11 we show (curve a) a plot of $-G_x^{-1}$ against r. All the measurements of F_M^c were made with paramagnetic Gadolinium specimens at electromagnet currents of between 10A and 30A. Great care needed to be taken in adjusting the lateral position of the magnet, in order to record the true value of F_M^c. This is because, as discussed in R 3.25, B in equation 2 of that reference was found to be positive. This means that as F_M approaches F_M^c, the region of x in which there is stability approaches zero, and vanishes when $F_M = F_M^c$. Thus the full value of F_M^c can only be obtained when the magnet is positioned laterally to a fraction of a mm. and there is a complete absence of suspension oscillations due to draughts and vibrations.

The approximately linear variation of G_x^{-1} with r in Fig. 3.11 is remarkable, and we can give only a plausible but incomplete explanation for it. G_x^{-1} is defined in equation 3.9, and when the expression $(\nabla^2 \underline{H})_x = 0$ is substituted in it we obtain:

$$\frac{\partial^2 H_x}{\partial r^2} \Big/ \frac{\partial H_x}{\partial r} = -G_x^{-1} + \frac{1}{H_x} \frac{\partial H_x}{\partial r} - \frac{1}{r} \qquad 3.19$$

$H_x^{-1} \partial H_x / \partial r$ and r^{-1} are plotted as curves b and c in Fig. 3.11 and from them we may deduce the quantity, on the left hand side of equation 3.19: it is plotted in Fig. 3.11 as curve d.

Now let us make the arbitrary assumption that the variation of $\partial H_x / \partial r$ is Gaussian:

$$\frac{\partial H_x}{\partial r} = C e^{\frac{-(r-b)^2}{s^2}} \qquad 3.20$$

where b is the position of the maximum value of the Gaussian and s is a parameter characteristic of its width. Therefore:

$$\frac{\partial^2 H_x}{\partial r^2} \Big/ \frac{\partial H_x}{\partial r} = \frac{-2(r-b)}{s^2} \qquad 3.21$$

It is linear with r, in excellent agreement with Fig. 3.9d, and from its slope and intercept on the r axis we can determine s = 2.21 cm, and b = 9.6 cm. With these two parameters we have plotted equation 3.20 on Fig. 3.10 as a dotted line, taking C to be the measured value of $\partial H_x / \partial r$ at r = 9.6 cm. We emphasise that what is being fitted is the spread of the Gaussian curve, and the position of its maximum value. The remarkably good agreement of the dotted fitted curve with the experimental continuous curve on Fig. 3.10 is gratifying but raises further queries which have to be answered. First, it is not clear why $\partial H_x / \partial r$ should be so nearly Gaussian.

Secondly, can curves a or d of Fig. 3.11, which to within experimental error are straight lines, be proved by analytical means to be so, or are they only approximately straight ? One direction which further work on these questions might take might be accurate analytical or numerical calculations of $H_x(r)$, as from this, via equation 3.19, the other quantities may be derived. The calculation would have to be based on the assumption that the pole pieces were uniformly magnetised. However, measurements of B_x on the pole face show that B_x on the edge of the pole is about 30% greater that at the centre, and this would case some doubt on the validity of the starting point of the calculation.

It was pointed out by the writer (R 3.26) that the value of:

$$- \frac{\partial^2 H_x}{\partial x^2} / \frac{\partial H_x}{\partial r}$$

measured directly with a fluxmeter, as reported in R 3.25, was in disagreement with the new theoretical calculation of that quantity from F_M^c. The values are:

Means of Prediction	Value (cm^{-1})
Fluxmeter	0.54
Old Theory (R 3.25)	0.59
New Theory (R 3.26)	0.41

The discrepancy between the numerical values is considered to be due to errors in the fluxmeter measurements, which were made with a Hall probe of 3 mm width.

In Fig. 3.12 we show a plot of x^2 against:

$$\Delta H = H_x(1 \text{ cm}) - H_x(0)$$

with the centre of the fluxmeter probe aligned with the pole edges, (i.e. at r = 8.9 cm, where magnetic specimens are situated). There is some scatter in the readings but it is unlikely that all the error could have come from that source. A more likely cause is misalignment of the probe along the radial direction. Using $(\nabla^2 \underline{H})_x = 0$ and Fig. 3.11 it is found that a 3 mm misalignment would be sufficient to give the error. An error of this size is perhaps possible, as for those measurements the probe was aligned by eye, whereas for the measurements of H_x in Fig. 3.10 it was aligned with a travelling microscope.

3.6. Experimental Procedure

The experimental technique used with the magnetometer has been discussed in some detail by Dey (R 3.3), and here we only mention some of the new procedures which were made necessary by modifications to the balance.

The magnet must first of all be aligned. This is done with a spirit level which checks the orientation of the magnet, and a travelling telescope, which ensures that the magnet is at the right height by allowing the top edge of the poles to be aligned with the bottom of the inside of the specimen container. The lateral misalignment h, (R 3.25) is reduced to zero by the means described in that paper. It must be stressed that to attain the necessary accuracy of measurement the alignment is required to be precise to a fraction of a mm.

The silica suspension and specimen bucket are cleaned with Trichloroethylene and Aqua Regia and then the lower suspension link is hooked onto the upper one. A small amount of Silicon grease is put on the lower part of the end cap which is inserted into the upper part and then the bell jar is evacuated with the diffusion pump. If the system is found to be leak free, 5 Torr pressure of helium exchange gas is admitted into the bell jar. It is best to admit more than is needed and pump the remainder out with the rotary pump. The helium is

extracted from a cylinder of pure gas, obtained from the British Oxygen Company or else gas from a liquid helium dewar is used. It is important not to use helium which has been recompressed after an experiment as it may be contaminated with oxygen. The cryostat is then lifted up into position, centred, and a copper shim is placed under its supporting ring so that its upper lip mates evenly with the vacuum seal on the down tube. It is evacuated to below a pressure of 10^{-3} Torr with the diffusion pump and its vacuum tap is closed.

Susceptibility measurements between 300 ^{o}K and 77 ^{o}K are made with the temperature slowly drifting downwards, and to do this the outside reservoir of the cryostat is filled with liquid nitrogen upto the level AA' in Fig. 3.3. The end-cap cools down evenly to 77 ^{o}K in the course of a few hours, and if necessary the cool down rate may be increased by putting more nitrogen into the outer reservoir.

As was mentioned in section 3.2, temperatures between 77 ^{o}K and 53 ^{o}K are attained by pumping on liquid and solid nitrogen. About 300 cc of liquid nitrogen is poured into the inner reservoir of the dewar which is initially at room temperature, (there is no necessity to put any coolant in the outer reservoir) and the liquid is pumped, using the manostat to control the pressure, according to standard procedures.

(R 3.6, R 3.7). Although the temperature is measured with the thermocouple, the mercury manometer is always used to give further information about transient pressure variations in the cryostat. Considerable delicacy is needed, when operating the system, to avoid sudden large pressure changes which could damage the manostat or the manometer. Liquid helium is pumped in a similar manner except that the temperature is obtained from the vapour pressure of the helium. Readings in the range 4 ^{o}K - 53 ^{o}K are made in the manner discussed in section 3.2.

The value of $H_x \partial H_x / \partial r$ was obtained by a calibration at room temperature with ammonium ferrous sulphate. A correction was of course made for the force on the empty bucket; this was measured throughout the range of temperature 2 ^{o}K-300 ^{o}K.

3.7. Suggestions for Future Improvements

The main disadvantage of the susceptibility balance, in its present form, is that the magnetic force can only be measured over rather a narrow range. For adequate accuracy it must be greater than 5 dynes, but if it exceeds 50 dynes instability problems occur. By modern standards the sensitivity (.05 dyne) of the balance is very low. Commercial instruments are available, (Sartorius and Cahn) which measure to .0001 dyne,

and simple instruments of good sensitivity, for instance Griffiths (R 3.33) 0.002 dynes, Gerritsen et al (R 3.19) .0002 dynes, have been built by several experimenters.

The reason for the poor sensitivity is that the balance is directly susceptible to vertical building vibrations. This is a basic defect of the Sucksmith device and it can not be eliminated by improved damping. If greater sensitivity is needed another means of force measurement, such as the beam balance, which is intrinsically less easily affected by vibration, must be used.

However, the purpose for which the magnetometer was orignally built was to measure the properties of highly magnetic materials, and in view of this it may be more desirable to consider means of increasing the greatest magnetic force which may be measured, rather than increasing the sensitivity. F_M^c is a function of three quantities, the length of the suspension, its weight, and the Field Gradient Ratio G. The length can not be altered without substantially modifying the construction of the balance; the weight has been increased once already and any further increase would be likely to distort severely the shape of the Sucksmith Ring. It is possible, though, that an alternative choice of magnet pole pieces might enlarge G and F_M^c. A set of conical poles is available but

it is not clear whether their use would decrease or increase the critical force. If conical poles were used, the spread s of the $\partial H_x/\partial r$ pseudo-Gaussian would be increased, and from equation 3.21 this is likely to be favourable. On the other hand, the distance between the positions of the maximum values of $\partial H_x/\partial r$ and $H_x \partial H_x/\partial r$ would increase, and from Fig. 3.11 this can be seen to be unfavourable. It is not, then, clear whether any overall improvement would result, but it would be valuable to try out the conical pole pieces and also find out how their $F_M^c(r)$ characteristic compares with the results in Fig. 3.11 for plane poles.

A simple improvement of the means used to control the specimen temperature would be to wind a heater coil of fine manganin wire round the end cap. A few watts dissipated in the coil would be sufficient to keep the temperature steady in the range 300 ^{o}K to 77 ^{o}K. The power could be adjusted manually, or a simple automatic control system could be constructed to keep the temperature steady.

The thermocouple potentiometer has a null indicator consisting of a mirror galvanometer which reflects a light spot onto a frosted glass screen. The light spot could be arranged to fall on a photocell which would switch a transistor, in series with the heater, on or off. If the dynamical problems associated

with the control system could be solved, the specimen temperature would be determined simply by setting the potentiometer dials to the value desired.

Another improvement which might be made is a reduction of the exchange gas time constant. If the specimen bucket were made of much thinner silica than at present, the heat transfer rate between the specimen and its surroundings might be increased. Also, experiments might be carried out to see whether a gas pressure of much greater than 5 Torr is effective in reducing the time constant. Care would have to be taken to see that no trouble arose from the gas liquifying inside the end cap when the pressure over the pumped helium was lower than the pressureof the exchange gas.

3.8. Resistivity Measurement

Resistivity specimens were cut from the ingots of the intermetallic compounds with a Servomet Spark Machine. The specimens were in the form of rectangular prisms of approximate dimensions 10 mm x 1 mm x 3 mm. As their resistance was low, a four probe terminal connection was used. Current leads of copper wire were soldered onto the ends of the specimen and platinum potential leads, placed well away from the ends, were spot-welded onto the sides. It was only found possible to make

resistivity specimens from the RZn_{12} compounds, the R_2Zn_{17} materials were too brittle and porous.

The resistances were measured by standard potentiometric techniques (R 3.34, R 3.35, R 3.36). A five dial Tinsley Potentiometer of the Diesselhorst pattern, with a null detector consisting of a Photocell Galvanometer Amplifier with a secondary galvanometer, was used to compare the voltage developed across the specimen with that across a standard resistor in series with the specimen. A reversing switch was used to reverse the potentiometer and specimen currents simultaneously. The current in the specimen was such (about 0.3A) that the power dissipated in the specimen did not exceed 0.1 mW. The relative resistance, at its smallest values could be measured to $\pm$ 1%, but the absolute error, due to the difficulty in measuring the dimensions of the specimen, was $\pm$ 30%. There were possibilities of further errors from cracks and voids in the specimen.

The low temperature readings were taken in a cryostat constructed by Wipf (R 3.37). The specimens were fixed to a holder, which was surrounded by a metallic enclosure, and placed in the cryostat. Temperatures down to 30 ^{o}K were measured with a copper-constantan thermocouple, and below that with a Gold/Iron-

-Chromel thermocouple. This had its upper junction near the specimen and the lower one immersed in the liquid Helium which remained at the the bottom of the cryostat during warm-up. The resistance specimen was in direct contact with the liquid Helium during the pump-down, and so very accurate temperature readings could be obtained in this region.

CHAPTER 4

RESULTS AND THEIR INTERPRETATION

4.1. Introduction

In this chapter, after reviewing the results of the magnetic measurements which have been previously made on other Rare Earth Zinc compounds, we present and analyse the susceptibility measurements we have made on the compounds R_2Zn_{17} for R = Gd, Tb, Dy, Ho, Er, Tm and the susceptibility and resistivity measurements made on $SmZn_{12}$, $GdZn_{12}$, $TbZn_{12}$ and $ErZn_{12}$. A brief report on this work was given at the 1970 Solid State Physics Conference at Manchester.

Kanematsu et al (R 1.89) found that ,of the RZn series of compounds with the CsCl structure ,those with R heavier than Gd were ferromagnetic, and those lighter antiferromagnetic, with the exception of SmZn which was a ferromagnet of saturation moment 0.07 μ_B per ion. The paramagnetic Curie temperatures of all the compounds except CeZn were positive, and their moments close to the free ion values.

Debray et al (R 1.93) published data on the paramagnetic susceptibilities of the RZn_2 ($CeCu_2$ type structure) compounds, and later Debray and others (R 1.90) reported on their low temperature magnetic behaviour. Although there are some unexplained minor discrepancies between the two sets of results, both agree that the paramagnetic moments are close to the free ion values, and the paramagnetic Curie temperatures are positive,

$NdZn_2$ orders ferromagnetically with about half the free ion value, and $GdZn_2$ is a ferromagnet, or possibly a metamagnet, with rather less than the full $7\mu_B$. The only compound on which resistivity measurements were made was $CeZn_2$ (Debray 1970, unpublished) but no anomalous Kondo-like behaviour was observed. Debray and Ryba also made ESR measurements on $GdZn_2$ in the paramagnetic regime. In a preprint (1969) they reported a negative g shift, but in an abstract of a paper given at the 1970 Grenoble Conference on Magnetism they reported a small positive one.

Iandelli and Palenzona (R 2.14) found that the Zinc rich Yb compounds bore no magnetic moment, and this has been confirmed in our work. Yb_2Zn_{17} and $YbZn_{11}$ have no strongly temperature dependent magnetic susceptibility down to 77^oK. It would appear that Yb is divalent when compounded with Zinc.

In the present work, no anomalies in the susceptibilites of $GdZn_{12}$ and Gd_2Zn_{17} were found at the Curie temperatures of Gd, GdZn, and $GdZn_2$, and the M-H curves of the two compounds were linear at 4.5^oK. This confirms, in practice, the high metallurgical homogeneity which was found by the methods of analysis described in Chapter 2. Also, the fact that the ratios of the resistivity at 300^oK to that at 0^oK for the RZn_{12} compounds were in the region of 100, a very high value for intermetallic compounds (the electron mean free path at 0^oK being about 5000 $\mathring{A}$), indicates their metallurgical excellence.

At the end of this chapter we have set down the results of the measurements of susceptibility χ and resistivity ρ which have been made

on the compounds. The graphs of the experimental results are given for each compound in order of atomic number, summarising tables coming first, followed by the R_2Zn_{17} results and then the RZn_{12} results.

All the compounds, with the exception of the two Yb ones obey the Curie Weiss law down to 100°K. The paramagnetic moments p, the paramagnetic Curie temperatures θ, and the Neel temperatures T_N are given in Fig. 4.1. T_N is defined to be that temperature at which the susceptibility is maximum. Readings of magnetisation versus applied field (M-H curves) were taken, for all compounds, at 300°K and 77°K up to 7.5 kOe, and at 4.5°K up to the field H_{max} (4.5) tabulated in Fig. 4.1. No deviations of the M-H curves from straight lines were found, indicating that Brillouin saturation and spin flops did not occur. Accordingly, only the M-H curves of one typical compound $GdZn_{12}$, are reproduced here, in Fig. 4.7. Susceptibility readings at intermediate temperatures were made while the temperature of the specimen was changing slowly. Above 77°K, they were made at 7.5 kOe; below, they were made at a field of H_{max} (4.5) or smaller. In some cases it was necessary to restrict the field to avoid approaching the lateral instability regime, and also for this reason, small polycrystalline specimens of about 15 mg wt. were used. Demagnetising corrections were made when necessary, using a demagnetising factor of 1/3. This is accurate only for a sphere, but as the correction was at most a few percent, large errors are not likely to have been introduced.

The susceptibility graphs contain the actual readings which were

taken. No correction has been made for the temperature independent component of the susceptibility, whether caused by the Van Vleck mechanism (R 1.133) or the metallic properties of the matrix. The correction needed is smaller than the experimental accuracy. The only exception to this is $SmZn_{12}$ whose susceptibility has been analysed in detail using the method of section 1.6. The resistivity graphs are also as measured; the residual resistivity has been subtracted only from the readings in the logarithmic plots.

4.2. R_2Zn_{17} Results

Gd_2Zn_{17}

The compound follows the Curie Weiss Law (CWL) down to 30°K where a deviation from it (the extrapolated CWL is given by the dotted line) occurs which grows larger until 10°K. Here the susceptibility has a maximum and then decreases to a finite value as the temperature approaches zero. A deviation from the CWL in the same region is also observed in $GdZn_{12}$. In these two compounds it is not due to crystal field effects, as the splittings of Gd, which is an S-state ion, tend to be very small, less than 1°K.

We will discuss these deviations more fully when we come to $GdZn_{12}$. The maximum in the susceptibility (the minimum in the inverse susceptibility) is interpreted as indicating a transition into some type of antiferromagnetic ordered state. We note that the Singlet Triplet model (Fig. 1.4(a), R 1.19) would also give a susceptibility curve which had the same qualitative features,

but this mechanism may be ruled out in the case of Gd. The splittings are too small, and being an ion containing an odd number of electrons in the magnetic shell, its lowest level will be magnetic, and so the susceptibility would diverge as the temperature approached $0^{\circ}K$.

The susceptibility of the magnetically ordered compound does not remain constant below T_N, as it should according to the straightforward Nagamia theory (R 1.120), if the applied field is larger than the anisotropy fields. This condition should be satisfied in Gd compounds, because the Zeeman energy of a Gd ion in a field of 5 kOe is $2.5^{\circ}K$, which is much larger than the $0.1^{\circ}K$ expected for the crystal field splittings. However, this temperature variation of the ordered susceptibility is common in Gd antiferromagnets; $GdAl_3$ (R 1.144) and $GdIn_3$ (R 1.143) for instance exhibit it. It may be due to the breakdown of the $J(\underline{k},\underline{k}') = J(\underline{k} - \underline{k}')$ approximation.

Tb_2Zn_{17}

In this compound, deviations from the CWL occur at an unusually high temperature, $90^{\circ}K$. The inverse susceptibility has a broad minimum in the region of $28^{\circ}K$ and then increases to a finite value as T approaches $0^{\circ}K$. It might be possible to explain this behaviour using a model of non-interacting ions, crystal-field split to give a non-magnetic ground state, analogous to the Singlet-Triplet model discussed previously. However, we reject this interpretation because the behaviour of Tb_2Zn_{17} is qualitatively similar to that of Gd_2Zn_{17}, a compound to which we know the explanation can not apply. The maximum in the susceptibility at $28^{\circ}K$ is interpreted as being caused by a transition to an aniferromagnetically

ordered state, but a non-magnetic crystal field ground state could well be responsible for the deviations from the CWL which start at 90°K. In this case the exchange field is large enough compared with the crystal field splittings to produce a magnetically ordered state at low temperature. In Fig. 4.4, where we have plotted θ and T_N against the De Gennes factor $(g-1)^2J(J+1)$, it can be seen that θ and T_N for Gd_2Zn_{17} and Tb_2Zn_{17} are not on the straight lines on which they might be expected to lie if crystal field effects were negligible and the band structures of the two materials were the same. We have seen in Chapter 1 that crystal field effects are unlikely to give pseudo-paramagnetic Curie temperatures of more than 10°K or so, and thus the most likely reason for the difference between the θ's of Gd_2Zn_{17} and $TbZn_{17}$ (allowing for the De Gennes factor), is the change in band structure due to the difference between the Gd and Tb atomic potentials. Anisotropic exchange may also play a part.

As θ/T_N for Tb_2Zn_{17} is -.6 compared with -5.3 for Gd_2Zn_{17}, it is probable that the modes of magnetic ordering in the two compounds are different. Furthermore, some fine structure can be seen in the susceptibility of Tb_2Zn_{17} below T_N, and this suggests that one mode of ordering is being replaced by others at lower temperatures. This might be due to temperature dependent exchange couplings caused by magnetic superzone effects in the band structure.

$\underline{Dy_2Zn_{17}}$

The susceptibility of this compound starts to deviate from the CWL in the region of 40°K and these deviations are attributed to crystal

field splittings. The most notable characteristic of the magnetic behaviour is that there does not appear to be any sign of magnetic ordering down to 2°K. From Fig. 4.4 it can be seen that θ is consistent with the θ of Tb_2Zn_{17}. If T_N is also consistent, then T_N would be expected to be in the region of 20°K. If, however, the magnetic behaviour is analogous to that of Gd_2Zn_{17}, then T_N might be expected to be around 5°K. Neither is observed, but because the ratio θ/T_N changes so violently from Gd_2Zn_{17} to Tb_2Zn_{17}, it is not to be expected that Dy_2Zn_{17} will fit in with either. Such behaviour is not unprece dented; for instance, Buschow et al (R 1.143) have reported that $TmIn_3$ obeys the CWL down to 2.5°K, and Buschow and Fast (R 1.144) found no sign of ordering of the compound $NdAl_3$ down to 4.2°K. This latter compound, and also Dy_2Zn_{17} must, of course, order eventually, as they both have an odd number of electrons in their f shells. Their failure to do so down to 2°K is attributed to an accidental feature of the bandstructure which permits the Fourier Transformed exchange coupling $J^*(\underline{q})$ (equation 1.61) to have a maximum value which is only just greater than zero. It seems that $|J^*(\underline{q}_{max})| \ll |J^*(0)|$ for these compounds.

Ho_2Zn_{17}

After this compound had been quenched from the melt its grain size was found to be large, in the region of 0.5 mm. Because of this, magnetic specimens had a tendency to have an anisotropic susceptibility as they had a volume of about a cubic mm. The susceptibility graphs

show the readings which were obtained on one specimen; an indication of the readings on another is given by the dotted line. The specimens were freely orientable in the applied magnetic field, and so the measured susceptibility was always that along the easy axis of the specimen. When the field was slowly increased from zero, the specimen suddenly jumped round and aligned its easy axis parallel to the field. The existence of anisotropy could be detected by observing whether a jump occurred, and this was the basis for the choice of the readings shown.

The CWL is seen to be obeyed well down to 2°K, and there again appears to be no sign of ordering, despite the fact that θ is -11°K, a fairly large value. However, as we noted before, $TmIn_3$ (R 1.143) which has a θ of -6°K has also been reported to obey the CWL exactly down to 2.5°K.

Er_2Zn_{17}

The CWL is obeyed down to 20°K where deviations occur which are attributed to crystal field splittings. No sign of ordering is seen at 2°K, and the same considerations as those which applied to the previous two compounds are relevant here. If the type of ordering which occurs at low temperature is the same as that in Gd_2Zn_{17}, then from the ratios of the De Gennes factors (Fig. 4.4) ordering would be expected at about 1.5°K, which is beneath the lowest temperature at which measurements were made.

Tm_2Zn_{17}

This compound obeys the CWL to 40°K where crystal field deviations begin to occur, and no ordering is seen at temperatures down to 2°K. From the shape of the susceptibility curve it seems possible that the lowest crystal field state is non-magnetic, and that the susceptibility is beginning to flatten out into a Van Vleck temperature independent paramagnetic regime. Because the susceptibility curve appears to intersect the susceptibility axis at a positive value, the exchange field will not be strong enough to cause a transition to an ordered state even at 0°K.

From equation 1.28 it follows that the change Δp in the effective paramagnetic moment p of the Rare Earth ions due to the first order s-f interaction is given by:

$$\Delta p/p = 2(g-1)g^{-1} J(0)\rho$$

In Fig. 4.3 the fractional changes in the moments of the R_2Zn_{17} compounds have been plotted against $(g-1)/g$. All the compounds except Gd_2Zn_{17} show an increased moment, and hence a positive J(0). It is not clear why Gd_2Zn_{17} should behave exceptionally. The accuracy of measurement of the relative change is about $\pm$ .013, which could take J(0) into the positive region, but a more probable explanation is metallurgical imperfection of

the specimen. An excess Gd concentration of one or two% is unlikely to have been detected by the means of metallurgical analysis which were used.

If the density of conduction electron states can be estimated, J(0) may be deduced. On a free electron model, taking each Rare Earth ion to contribute three and each Zinc atom two electrons to the conduction band, a Fermi Energy of 9.5 eV and a density of states ρ = 0.165/eV atom for one spin direction is obtained for the compound $DyZn_{12}$. The values for the other RZn_{12} compounds will be negligibly different, and to within reasonable accuracy, this value may also be taken for the R_2Zn_{17} compounds. The values of J(0) worked out in this way are given in Fig. 4.1 and are seen to be of the order of a few tenths of an eV. However, this is likely to be an overestimate, because the free electron model will tend to underestimate the density of conduction states. This is because the true band-structure is built up from bands originating from orthoganal Wannier functions, for instance 5d and 6s-like functions on the Rare Earth sites, and there may be a substantial overlap in energy between the different bands which will lead to an increase of the density of states. above the value deduced from the free electron model in which, of course, the bands are non-degenerate.

However, despite the fact that the magnitude of J(0) is difficult to estimate from the change in effective moment, the method has the advantage that it can determine the sign. It is essential though, that the accuracy of measurement and stoichiometry should be high. One set of materials in which stoichiometry is no problem is the Rare Earth metals

themselves. The effective moments of the metals from Gd to Tb are greater than the free ion values (R 1.82) and those of Ce, Pr, Nd smaller (R 2.4), but the (g-1)/g variation is not followed well. Kasuya (R 1.81) attributes this to the fact that the temperature dependence of the density of states changes the paramagnetic Curie Temperature.

In Fig. 4.4 θ and T_N of the R_2Zn_{17} compounds are plotted against the De Gennes factor. As mentioned before, the marked deviations of θ from a straight line are attributed primarily to changes in bandstructure from compound to compound and secondarily to crystal field splittings. Both will be important in determining T_N and the mode of magnetic ordering, but from susceptibility measurements alone, it is not possible to acquire more precise knowledge.

4.3. RZn_{12} Results

The resistivities of these compounds have been measured as well as the susceptibilities, and other workers have done ESR experiments on $GdZn_{12}$ and Neutron Diffraction experiments on $TbZn_{12}$. This extra information has been very useful in interpreting the susceptibility results.

$SmZn_{12}$

Because the effective moment of the ground state J = 5/2 multiplet level of the Sm^{3+} ion is so low, and the next highest level, the J = 7/2, lies only about 1500°K above it, the magnetic properties of Sm compounds are anomalous. We will postpone discussion of $SmZn_{12}$ until after we have examined the properties of the other three RZn_{12} compounds.

$GdZn_{12}$

The compound followed the CWL down to about 50°K where small deviations from it began to occur. These continued until 16°K, at which temperature some type of antiferromagnetic ordering took place. The susceptibility then flattened out to a finite value as the temperature approached zero. The characteristic form of the resistivity behaviour of $GdZn_{12}$ and the other compounds can be seen from a glance at the resistivity of $ErZn_{12}$. There are seen to be four regions. At high temperatures the resistivity varies approximately linearly with temperature and as the temperature is reduced the slope of the resistivity gradually decreases, until in the third region it is zero. At a lower temperature still, ordering occurs, and the resistivity decreases further as the spin disorder component quenches out.

The form of the resistivity of $GdZn_{12}$ is similar to that of $ErZn_{12}$, except that the ordering occurs within the region in which the slope of the phonon resistivity is changing. By extrapolating the phonon resistivity back to 0°K, the spin disorder resistivity ρ_s (equation 1.43) may be estimated. The values of this for all the RZn_{12} compounds, together with the values of the residual resistivities ρ_0, the resistivity ratios ρ_{300}/ρ_0, the high temperature slopes $\partial\rho/\partial T_p$ and the transition temperatures $T_N(S)$ deduced from the resistivity curves, are given in Fig. 4.2.

In Fig. 4.30 the logarithm of the difference between the resistivity at a given temperature and the residual resistivity (which was obtained by extrapolating to 0°K) is plotted against the logarithm of the temperature.

No correction has been made for the phonon contribution to the resistivity; at the ordering temperature it is at most 0.2 $\mu\Omega$cm, much less than the spin disorder component.

It can be seen that the magnetic resistivity obeys a power law of $\rho - \rho_o = AT^n$ almost right up to the ordering temperature. A value of $n = 1.44$ gives the best fit, but a value of $n = 3/2$ would not be inconsistent with the experimental accuracy. Two conclusions may be drawn from the resistivity result. First, from the fact that there is a sharp change in the slope of the resistivity curve at the ordering temperature it can be deduced that the order which occurs is of a coherent long-range type. Second, because there is no sign of an exponential term in the resistivity it is apparent that there is no energy gap in the spin wave spectrum of the material. For a Gd compound this is not surprising, as the crystal field splittings will not be large enough to give substantial anisotropy fields.

It is not clear why a $T^{3/2}$ law is obeyed. A T^2 variation of resistivity is expected for a ferromagnet, and T^4 for a conventional antiferromagnet. It is possible that the $T^{3/2}$ law is directly derivable from the spin wave spectrum of whatever mode of ordering the compound takes up, but on the other hand it may be caused by the considerations which Liu (R 1.135, discussed in section 1.9) took account of in his theory and which produced both a T^2 and $T^{3/2}$ term. A $T^{3/2}$ law has also been observed by Dunlop (R 1.146) in the dilute transition metal-Zinc compound $MnZn_{13}$, in which the Mn bears a local moment.

It is remarkable that the power law holds so well right up to the ordering temperature, as the spin-wave approximation might be expected to break down or at least need renormalisation in this region, and that no effects in the resistivity caused by superzone boundaries are apparent. Further progress in understanding these details of the resistivity curves will not be able to be made until the precise form of the ordering is known.

A notable feature of the $GdZn_{12}$ and Gd_2Zn_{17} susceptibility results is that deviations from the CWL are seen at temperatures two or three times greater than T_N. This has also been observed in GdB_6 (R 1.142) whose resistivity is found to be reduced below the phonon value in the region where these susceptibility deviations are taking place, indicating that some of the spin disorder is being quenched out above T_N. GdB_4 shows similar behaviour (Z. Fisk 1970, private communication). The Curie temperatures of the two ferromagnets GdZn (R 1.89) and $GdZn_2$ (R 1.90) are too high for the effect to be apparent from the measurements on them. $GdIn_3$ (R 1.143) shows no sign of the effect, nor does $GdAl_3$ (R 1.144), but GdCu (R 1.113) may possibly do so.

There is evidence that the resistivity of $GdZn_{12}$ is reduced below the phonon value in the temperature region above T_N. If the linear portion of the resistivity of $ErZn_{12}$ is extrapolated, it intersects at $24^{\circ}K$ the resistivity horizontal (which is at about $0.42 \mu\Omega$ cm) at which the phonon contribution has dropped to zero. The phonon contribution

to the resistivity of $ErZn_{12}$ at 24°K is then seen from Fig. 4.39 to be 0.25 $\mu\Omega$cm, and this should be much the same for all the compounds. For $TbZn_{12}$ it is 0.22 $\mu\Omega$ cm, for $GdZn_{12}$ 0.17 $\mu\Omega$cm, and for $SmZn_{12}$ 0.4 $\mu\Omega$ cm. Ignoring the anomalous Sm compound, it is seen that the apparent phonon resistivity of $GdZn_{12}$ at 24°K is about .07 $\mu\Omega$cm less than that of the others. It appears to have lost this amount of its spin disorder resistivity by this temperature, although as the errors in the measurements of the absolute resistivities are so large, these differences are only just on the verge of significance.

E.S.R. measurements have been made on $GdZn_{12}$, in the Imperial College Physics Department, by R. H. Taylor. He found that the g factor was, to within experimental accuracy, equal to the free ion value until just above 20°K. Below that temperature, the resonance went to lower fields and had disappeared completely by T_N(16°K). The linewidth varied linearly with temperature down to 60°K, and a rough calculation of $|\bar{J}\rho|$ assuming a Korringa relaxation mechanism via the s-f interaction, gave a value which is about thirty times smaller than that obtained from the increase in paramagnetic moment; this suggests severe bottlenecking. Below 60°K the linewidth increased anomalously to become twice as large at 24°K as it was at 77°K. Taylor has found (1970, private communication) similar anomalous increases in the linewidths of GdB_6 and GdB_4.

It seems clear that some sort of ordering is occurring in these Gd compounds well above T_N. Fisk (R 1.39) noted that for the Gd borides

$|\theta|$ was substantially greater than T_N. For instance, the pairs of values (θ ,T_N) were (-55,14) for GdB_6, (-60,42) for GdB_4 and (-58,16) $GdZn_{12}$, (-53,10) Gd_2Zn_{17}. Fisk suggested that in the borides, ordering was attempting to take place at a temperature comparable with $|\theta|$, but as soon as it started, it produced superzone band gaps which altered the band-structure in a way which prevented the ordering from going to completion. Ordering would finally take place in a different mode at a lower temperature. In more detail, the Fourier transformed exchange integral $J^*(\underline{q})$ will have its maximum at a value $\underline{q}_o$ in the paramagnetic state. When ordering first occurs, the resulting band gaps shift the magnitude of the maximum continuously to lower values at the same or at a different wavevector, until the shifted maximum lies below another maximum at another wavevector, at which ordering can take place without interruption. A continuous variation of the $\underline{q}$ at which $J^*(\underline{q})$ has its maximum value is less likely to take place with non S-state ions, as crystal field anisotropies will tend to clamp the ordering into one mode. A continuous variation of the magnitude of $J^*(\underline{q}_o)$ at a given wavevector $\underline{q}_o$ is still possible, but its manifestations in the susceptibility are likely to be swamped by the effects of crystal fields. We note, however, that there seems to be no decrease in the resistivity of $ErZn_{12}$ above T_N, so that the effect does not seem to be happening in that compound, and apparently occurs only with S-state ions.

These high temperature pseudo-ordering phenomena are not yet understood. It is not even clear if the order is of short or long range

and this question is unlikely to be resolved except by Neutron Diffraction experiments. Unfortunately, these are difficult to make on Gd compounds because the most common isotope of Gd has a very high Neutron Absorption cross-section.

$TbZn_{12}$

The compound follows the CWL to $60^{o}K$ where deviations due to crystal field effects start to occur. Ordering takes place at $14^{o}K$ with a sharp discontinuity in inverse susceptibility, which indicates that the ordering is of a coherent long range form. The susceptibility extrapolated to $0^{o}K$ is 0.7 of that at T_N, which is close to the value of 2/3 expected for a simple antisotropic antiferromagnet (the spins at the corners of the bc tetragonal lattic up, the spin in the centre down).

Neutron Diffraction experiments have been done on this compound by J. B. Forsyth at Harwell. Magnetic superlattice scattering has been observed at $4.2^{o}K$, but the results have not yet been fully analysed, except in that it is found that the scattering is not that which would be expected from the simple antiferromagnet model.

The resistivity is similar to that of $GdZn_{12}$. No critical scattering is found near T_N, and a $T^{3/2}$ power law is obeyed in much of the region below T_N, indicating no gap in the spin wave spectrum. The absence of a gap, in the presence of strong crystal field anisotropies, suggests that the ordering is in the form of an incommensurate spiral.

$ErZn_{12}$

In contrast to the other RZn_{12} compounds, the θ of this one is positive, an effect probably due mainly to changes in band structure. The compound orders antiferromagnetically at a temperature slightly below θ ; a result which is not expected on the basis of the simple molecular field theory discussed in section 1.7. The difference is only $0.1^{o}K$, and as the accuracy in estimating θ is about $1^{o}K$, it may not be significant. If it is, then crystal field effects are responsible; their presence is indicated by the large deviations from the CWL below $30^{o}K$.

The resistivity results are interesting, as ordering does not occur until well into the regime where phonon scattering is negligible. There appears to be no sign of critical scattering above T_N, and the results in Figs. 4.39 and 4.40 give a justification (to the relative experimental accuracy of 5% in this region), of thosetheories which claim that the resistivity contribution from spin disorder scattering is constant above the ordering temperature. Below T_N it is difficult to determine which power law is obeyed, because only a few experimental points are available. However, the results are not inconsistent with a $T^{3/2}$ variation.

Above T_N, the additional resistivity is expected to be mainly due to phonon scattering. From inspection of the Gruneisen curve (in for instance, R 2.36), equation 1.64, it is seen that the extrapolated linear portion of the phonon resistivity curve intersects the zero resistance line at 0.145 of θ , the Debye temperature. In $ErZn_{12}$ the intersection

is at 24°K (Fig. 4.39) which gives θ' = 168°K, compared with 175°K (R 3.36) for pure Zn. With the parameter θ' known, equation 1.64 may be compared with the experimental results. This is done in Fig. 4.39 in which equation 1.64 is drawn as the continuous curve. It is not surprising that the fit is poor. The electron and phonon spectra of the compound will be far from having the simple form which is used in the calculation of equation 1.64. In addition, there may be changes in the elastic and inelastic scattering of the crystal field levels, such as those which were found in the same temperature region by Murani (R 1.16) in HoAu and DyAu. Deviations from Matthiessen's Rule may also occur.

In Fig. 4.41 the logarithm of the increase in resistivity above that at 4.2°K is plotted against the logarithm of the temperature. A $T^{3.9}$ power law is found. To within experimental accuracy this could be T^4, which may be compared with the T^5 law expected for a pure metal. We note, though, that here the metallic lattice is not periodic because of the presence of the disordered spins. There is need for a rigorous theoretical treatment of this problem.

$SmZn_{12}$

Because the lowest multiplet level of the Sm^{3+} ion has a low effective moment, it was necessary to use a more sensitive magnetic balance (Griffiths R 3.33) to measure the susceptibility of $SmZn_{12}$ at temperatures above T_N. I am very grateful to J. B. Dunlop for making

these measurements. The measurements below T_N were made with the Sucksmith balance by myself. The high temperature susceptibility results are plotted in Fig. 4.20, together with a theoretically fitted curve whose derivation we will now discuss.

In section 1.6 we showed that the susceptibility χ of a Rare Earth compound would, if only the lowest J level was thermally occupied, be given by the pseudo-Curie Weiss Law (equations 1.50 - 1.56):

$$\chi / N^* \mu_B = b\left(1 - \frac{g}{(g-1)} \frac{T_\infty}{T_o}\right) + a(1 - T_\infty/T_o)^2/(T - T_\infty) \qquad 4.1$$

where the susceptibility of the non-interacting ion is given by $N^* \mu_B (b+a/T)$, $T_o = -(g-1)a/gb$, and T_∞ is related to T_θ, which is the Paramagnetic Curie Temperature which the material would have in the absence of the Van Vleck paramagnetic contribution by equation 1.55. N^* is the number of Sm atoms in a gram of the compound.

The experimental susceptibility results at temperatures above $77^\circ K$ have been fitted to a curve of the form $\chi = \chi_o + C/(T - \theta^*)$ by the method of least squares (A. P. Murani is thanked for providing a computer program which does this). The best fit was given by the parameters $\theta^* = -34.5^\circ K$, $\chi_o = 0.61 \times 10^{-6}$ emu/g, $C = 75.7 \times 10^{-6}$ emu $^\circ K$/g. The quality of the fit is shown in Fig. 4.21, in which $(\chi - \chi_o)^{-1}$ is plotted against T, and also in Fig. 4.20. In each figure the continuous curve is the least squares fit. Deviations from the fitted curve are evident below $70^\circ K$ and are attributed to crystal field effects.

An analysis of the fitted results can now be made using the equations of section 1.6. Identifying θ^* of the fitted curve with T_∞ of equation 1.55, we obtain $T_\infty = -36.3^\circ K$ using $g = 2/7$ and $T_o = 310^\circ K$, as discussed in section 1.6. T_θ, the Paramagnetic Curie Temperature the compound would have if Van Vleck transitions were absent, is therefore placed in the θ column of the table in Fig. 4.1, and in the De Gennes plot of Fig. 4.4. Both T_θ (or θ) and T_N are larger proportionally in $SmZn_{12}$ than in the other RZn_{12} compounds. This may be because the s-f exchange integral $J(\underline{k}', \underline{k})$ is bigger, as the wavefunction of the 4f shell of this lighter Rare Earth ion is more widely spread out in real space.

We may now analyse the effective moment of the Sm ion in this compound. The pseudo effective p_{eff} is obtained from the value of C by the equation $C = N^* p_{eff}^2/3k$ and is found to be $p_{eff} = 0.75$ Bohr Magnetons. From equation 4.1 we see that the number of Magnetons p corresponding to the ground multiplet level of the ion is given by:

$$p_{eff} = p(1 - T_\infty/T_o) \qquad 4.2$$

and as we know both T_∞ and T_o, we obtain the value of $p = 0.673\ \mu_B$ which is accordinly entered in the table in Fig. 4.1. This is smaller than the free ion value $g\sqrt{J(J+1)} = 0.847$, in contrast to the other RZn_{12} compounds, but on the other hand $(g-1)g = -2.5$, a negative number, whereas the same quantity for the heavy Rare Earth ions is positive. In Fig. 4.3 the

dotted line goes through the point corresponding to Sm ($\Delta p/p = -0.204$, $(g-1)/g = -2.5$) and is seen to be consistent with results for the other three compounds for which $(g-1)/g$ is positive. These changes of paramagnetic moment are attributed to the conduction electron polarisation induced by the ion, and we see that the same value of J(0) as that which gives a positive polarisation for the heavy Rare Earths, gives a negative polarisation for Sm.

The last aspect of the high temperature susceptibility results of $SmZn_{12}$ which needs to be discussed, is the temperature independent contribution $\chi_o = 0.61 \times 10^{-6}$ emu/g. This will be composed of two parts. The first is the susceptibility of the metallic matrix, the second is the contribution from Van Vleck transitions.

The quantity b in equation 4.1 may be calculated by Van Vleck's theory (R 1.133) to give a susceptibility contribution of 0.742 emu/gram$\times 10^{-6}$. In deriving this result we have taken a screening number σ of 33 (R 1.133) to calculate the spin orbit constant, and this gives a splitting of 1548°K between the J = 5/2 and J = 7/2 multiplet levels. N* is 6.44×10^{20}/gram.

From the first term of equation 4.1 the temperature independent contribution to the susceptibility from Van Vleck transitions is 0.733×10^{-6} emu/gram, using the previously deduced values of T_o, T_∞ and $g = 2/7$. This indicates that the metallic matrix must have a diamagnetic susceptibility of $(0.61 - 0.73) \times 10^{-6} = -0.12 \times 10^{-6}$ emu/gram. Zinc itself has a susceptibility of -0.16×10^{-6}, so this result is not unreasonable.

This technique of expressing the susceptibility of Sm compounds in a pseudo-Curie Weiss form, and so making the analysis of their magnetic properties as easy as those of conventional Rare Earth compounds, does not appear to have been used before. In future work it will be applied to other Sm materials, in particular to Sm metal. White and Van Vleck (R 1.116) have suggested how the method may be extended to take account of crystal field effects, and another improvement which is needed is a rigorous treatment of conduction electron polarisation. A calculation is in progress using a two sub-lattice molecular field model, such as that used by Owen et al (R 1.59) and Cottet et al (R 1.62, R 1.56) in which the magnetic ions form one sub-lattice and the conduction electrons the other.

$SmZn_{12}$ orders antiferromagnetically at 16°K, and the susceptibility decreases rather steeply below that temperature to its value at 0°K. The fact that $(\chi(T_N) - \chi_o)/(\chi(0°K) - \chi_o) = 0.67$ is close to the value of 2/3 expected for a conventional antiferromagnet again suggests that this may be the mode of ordering which occurs. However, the spin disorder resistivity follows a simple power law of $T^{5.2}$, and no exponential term, characteristic of the anisotropic antiferromagnet, is present. The spin disorder resistivity above T_N will be caused by scattering from ions which (in the absence of a magnetic field) will be mainly in their $J = 5/2$ state. The spin disorder resistivity should therefore be that characterised by this lowest J level, as inelastic scattering to a level 1500°K higher may be expected to be small at around 20°K. In Fig. 4.5 the resistivity is

seen to be rather larger than that which would be expected. This may also be due to an increase of $J(\underline{k}',\underline{k})$ in the lighter Sm ion, or to the crystal field mixing the $J = 7/2$ level into the ground state. Below T_N the situation is more complicated as the exchange field will mix a temperature dependent amount of the $J = 7/2$ level into the $J = 5/2$ ground state.

The elementary excitations of the ordered state have yet to be treated theoretically. They will be a combination of ordinary spin waves, and the Wang and Cooper (R 1.130) excitations. The simple molecular field theory of spiral ordering which was discussed in Section 1.7 is also clearly inadequate for Sm compounds. There is much theoretical work to be done in this field.

In Section 1.6 it was shown how the Paramagnetic Curie temperature could be calculated using the free electron form of the RKKY interaction (equation 1.47.1). We have computed the lattice sum for the RZn_{12} lattice and the result has been plotted as a function of the Fermi wavevector K_f (a is the lattice constant) in Fig. 4.6. The sum is only slowly convergent and it was necessary to sum over 14,000 neighbours to obtain convergence to a few per cent. The sum is the same for all the RZn_{12} lattices, because any expansion in the lattice constant 'a' results in a corresponding contraction in k_f so that the product $k_f a$ remains the same. The alterations introduced by the slightly differing c/a ratios are negligible.

The sum can be seen in Fig. 4.6 to be a strongly oscillatory function of k_f. At the k_f corresponding to the free electron value (given by FE in Fig. 4.6) the sum is negative, therefore from equation 1.47.1 θ is expected to be positive. But for the majority of the RZn_{12} compounds θ is found to be negative, and this provides another example of the inadequacy of the free electron model. If, however, we attempt to estimate the sf coupling constant $|\bar{J}|$ by using the modulus of the sum in equation 1.47.1, then a value of about 0.4 eV is obtained for $GdZn_{12}$ and $TbZn_{12}$, and slightly different values for the others. In Fig. 4.2 all the calculations of $\bar{J}$ for the RZn_{12} compounds are collected together. Only the calculation of the value $\bar{J}$ from the change in the paramagnetic moment gives the sign, the calculations from spin disorder resistivity and from θ give only the modulus. All the values are in the range of a few tenths of an eV. However, because, as we argued previously, the true density of conduction electron states is likely to be larger than that calculated from a free electron model, these values of $\bar{J}$ are probably overestimated.

For all four RZn_{12} compounds, it is notable that the discontinuity in the slope of the resistivity occurs below the temperature of the peak in the susceptibility. The difference between the two is within experimental error, but may be a real result. Fisher (R 1.145), using an antiferromagnetic Heisenberg model, has found this effect theoretically.

4.4. Summary

We have found that in all of the Rare Earth Compounds examined in this work, the Rare Earth ions (with the exception of Yb, which is divalent) are in a tripositive state with a well defined magnetic moment, and obey the Curie Weiss Law down to low temperatures. Deviations from the Curie Weiss Law due to crystal fields are observed, and at temperatures in the region of 15°K most of the compounds are found to order magnetically in some sort of coherent long-range antiferromagnetic mode, probably in the form of an incommensurate spiral. However, some of the R_2Zn_{17} compounds are not observed to order down to 2°K and this may be a consequence of strong crystal field anisotropies not allowing ordering to occur in the mode most favoured by exchange forces. In these magnetically very dilute materials, crystal field effects can not be treated as a perturbation upon exchange determined states, as they can in the Rare Earth metals, and both must be considered simultaneously.

The resistivities of the RZn_{12} compounds have been found to follow well defined power laws in the ordered state. Theoretical explanations for these are required, and also an elucidation of the nature of the collective magnetic excitations in Sm materials.

It has been found that some type of anomalous pseudo-ordering is taking place in the Gd compounds at temperatures well above the Neel point, and the reason for this is also not yet fully clear.

The value of the s-f coupling constant $\bar{J}$ has been determined from

several independent sources, to be of the order of a few tenths of an eV, and, from the increase of the effective paramagnetic moment, positive in sign.

Fig. 4.1 SUSCEPTIBILITY RESULTS FOR R_2Zn_{17} COMPOUNDS

	p_o	p	$\Delta p/p_o$	θ	T_N	$H_{max}(4.5)$	J(0)
UNIT	μ_B	μ_B	%	^oK	^cK	kOe	eV
Gd	7.94	7.84	- .7	- 53.	+ 10.0	7.5	- .04
Tb	9.72	9.84	+ 1.5	- 17.	+ 28.0	7.5	+ .14
Dy	10.63	11.01	+ 3.5	- 14.	-	7.5	+ .42
Ho	10.60	10.08	+ 2.0	- 11.5	-	6.8	+ .30
Er	9.59	9.63	+ 0.5	- 4.0	-	5.4	+ .09
Tm	7.57	7.64	+ 1.0	+ 7.0	-	7.5	+ .22

Susceptibility Results for RZn_{12} Compounds

	p_o	p	$\Delta p/p_o$	θ	T_N	$H_{max}(4.5)$	θ/T_N
UNIT	μ_B	μ_B	%	^oK	^oK	kOe	
Sm	.847	.673	- 20.4	- 36.3	+ 16.0	7.5	- 2.3
Gd	7.94	8.40	+ 6.0	- 58.	+ 16.0	7.5	- 3.6
Tb	9.72	10.14	+ 4.5	- 38.	+ 14.0	7.5	- 2.7
Er	9.59	9.67	+ 0.75	+ 3.0	+ 2.9	5.4	1.0

$YbZn_{11}$ and Yb_2Zn_{17} bear no moment down to 77^oK

$p_o = g\sqrt{J(J+1)}\,\mu_B$, p is the paramagnetic moment which is obtained from the slope of the $\chi^{-1} \sim T$ curve

$\Delta p = p - p_o$, J(0) is the exchange integral estimated from Δp_o

$H_{max}(4.5)$ is the maximum field at which susceptibility measurements were made at $4.5\ ^oK$

Fig. 4.2 RESISTIVITY RESULTS FOR RZn_{12} COMPOUNDS

	ρ_{300}/ρ_o	ρ_o	$\partial\rho/\partial T_p$	$T_N(s)$	ρ_s
UNIT	1	$\mu\Omega$ cm	$\mu\Omega$cm/°K	°K	$\mu\Omega$ cm
Sm	120	.157	.064	14.0	.71
Gd	100	.18	.055	15.25	1.7
Tb	120	.10	.041	13.0	.55
Er	84	.18	.054	2.8	.24

Values of $\bar{J}$ for RZn_{12} estimated by various means

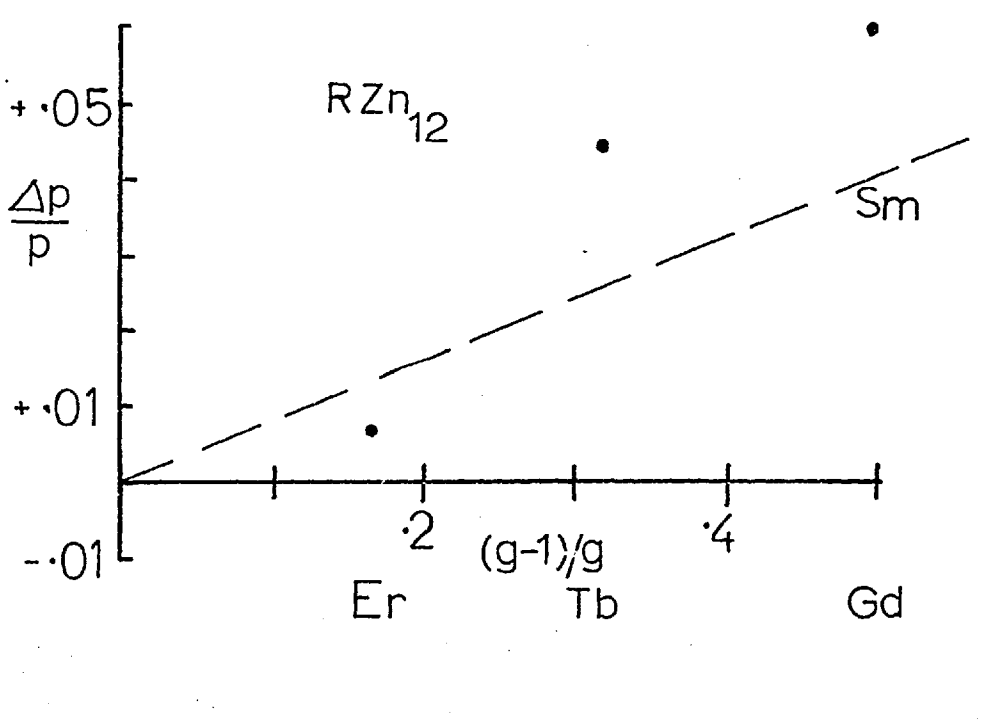
	Δ p	θ	ρ_s
UNIT	eV	eV	eV
Sm	+ .25	.56	.22
Gd	+ .36	.38	.18
Tb	+ .41	.38	.13
Er	+ .16	.22	.17

ρ_x = Resistivity at temperature x

ρ_s = Estimated resistivity due to spin disorder

$\partial\rho/\partial T_p$ = Resistivity slope in paramagnetic state

$T_N(s)$ = Magnetic transition temperature from discontinuity in slope of resistivity


+·05
Δp/p
+·01
-·01
RZn12
Sm
·2
(g-1)/g
·4
Er
Tb
Gd

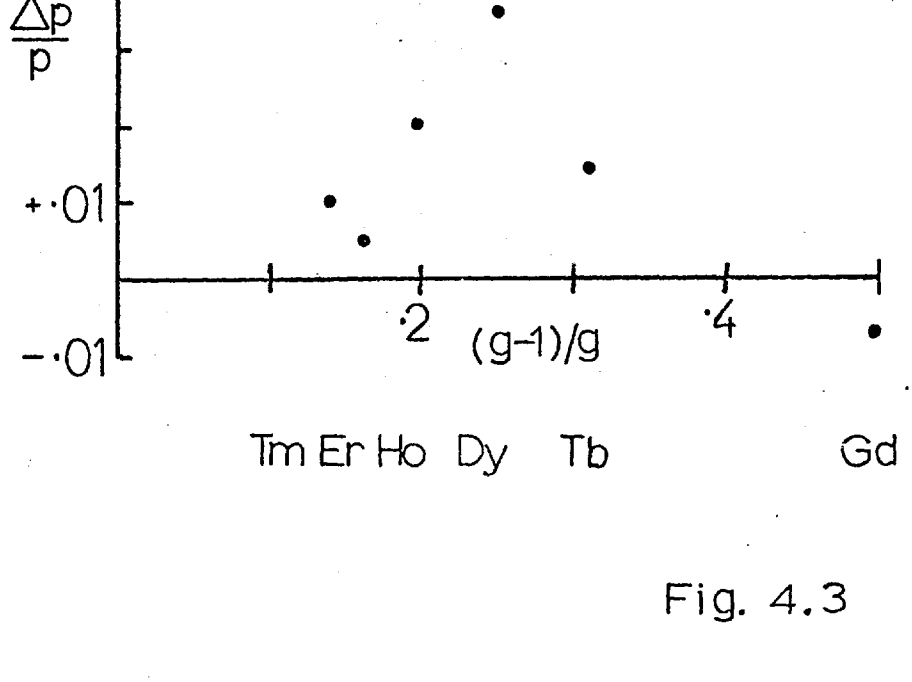

+·05
Δp/p
+·01
-·01
R2Zn17
·2
(g-1)/g
·4
Tm Er Ho Dy Tb
Gd

Fig. 4.3

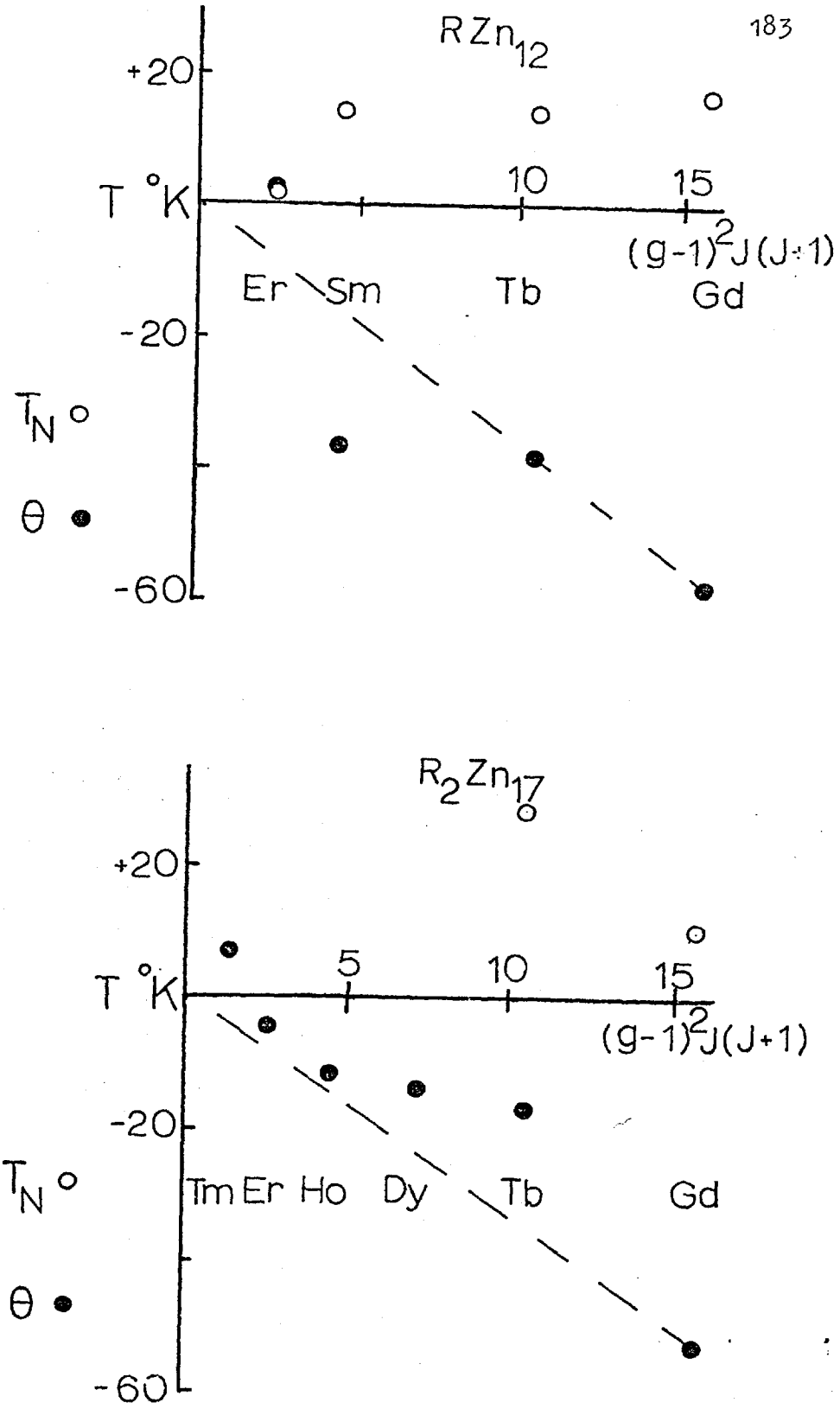

RZn12
+20
T °K
10
15
(g-1)²J(J+1)
Er
Sm
Tb
Gd
-20
TN °
θ
-60
R2Zn17
+20
5
10
15
T °K
(g-1)²J(J+1)
-20
TN °
Tm
Er
Ho
Dy
Tb
Gd
θ
-60

Fig. 4.4

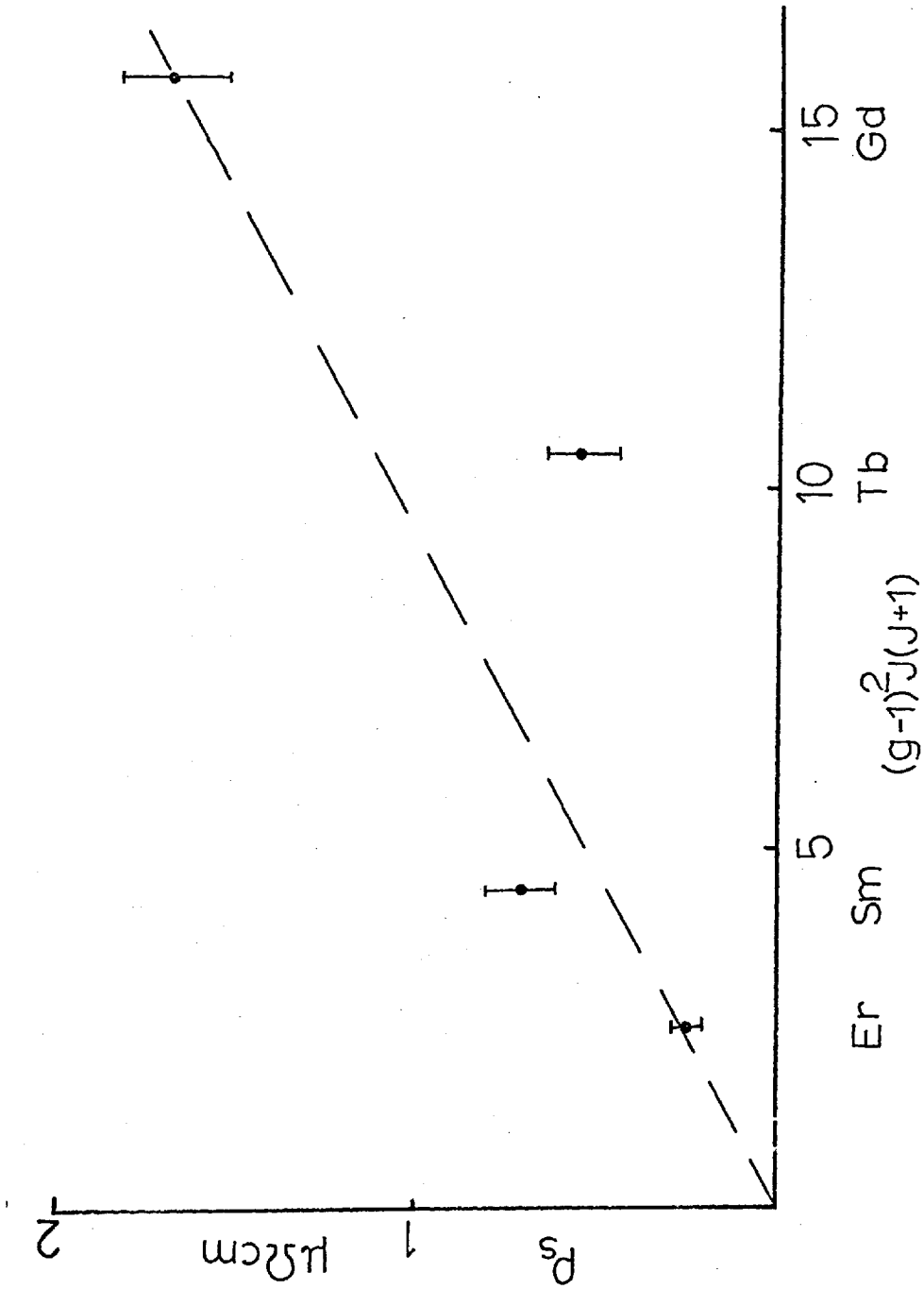


Fig. 4.5

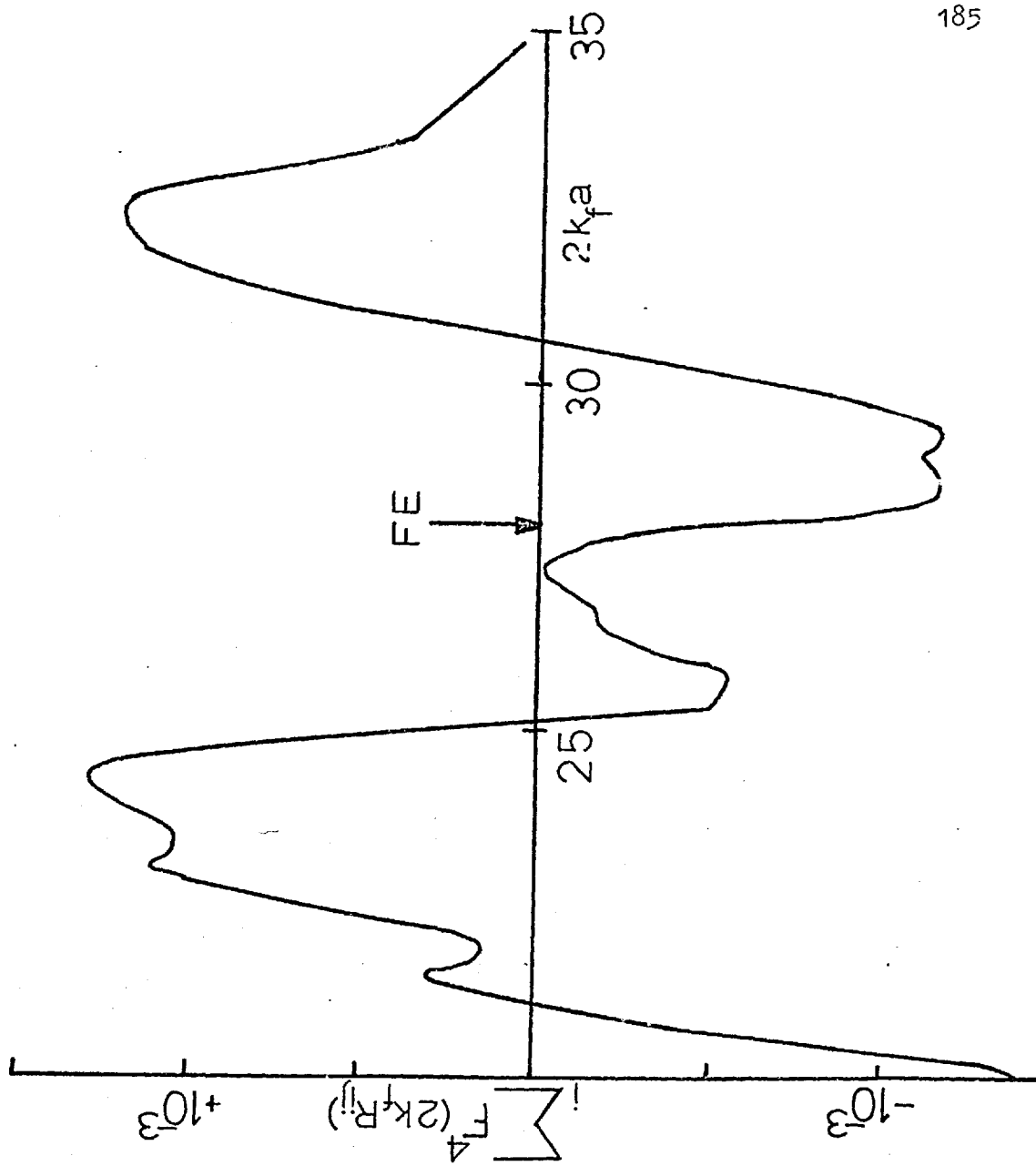


Fig. 4.6

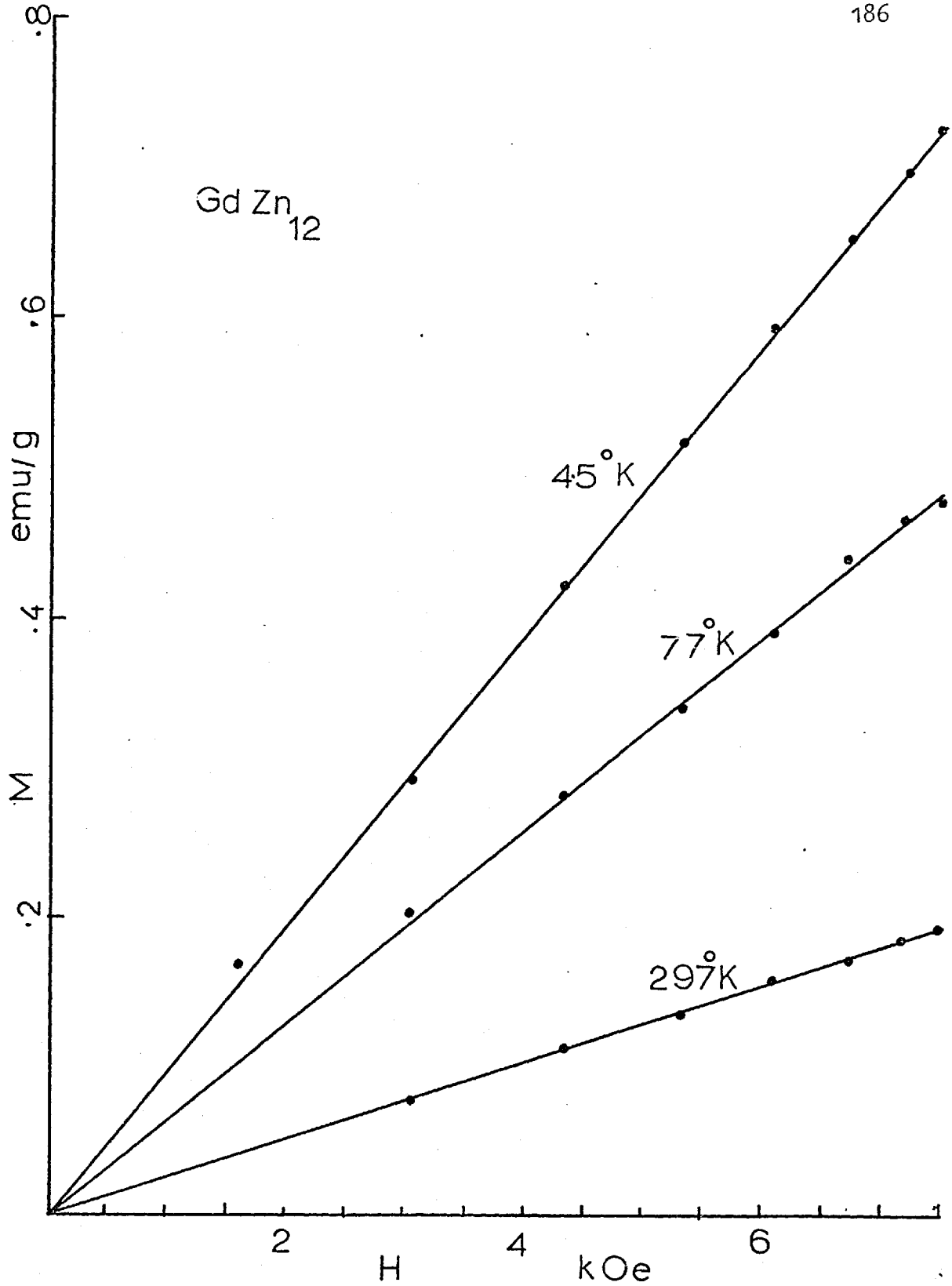


Fig.4.7

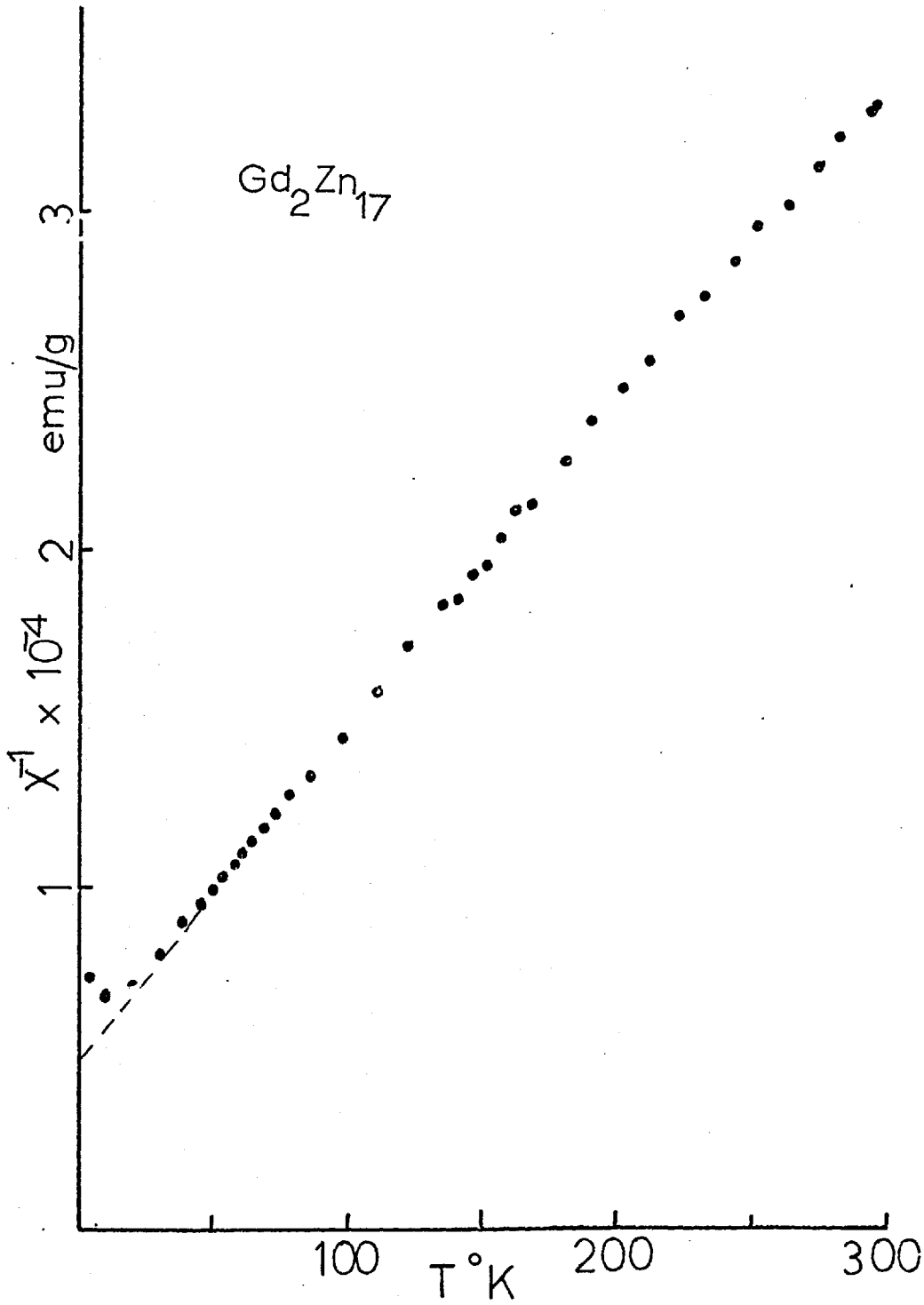


Fig.4.8

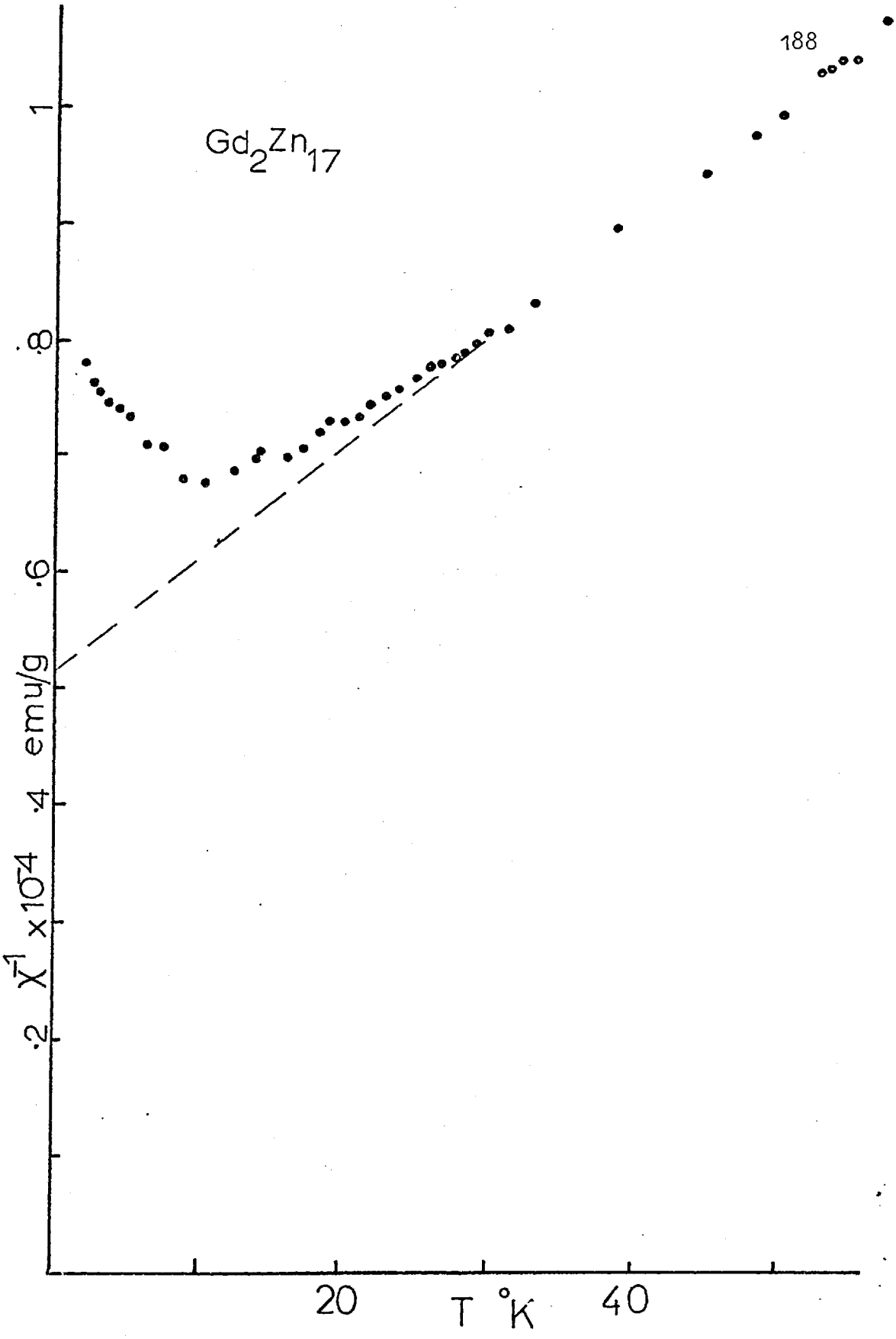


Fig. 4.9

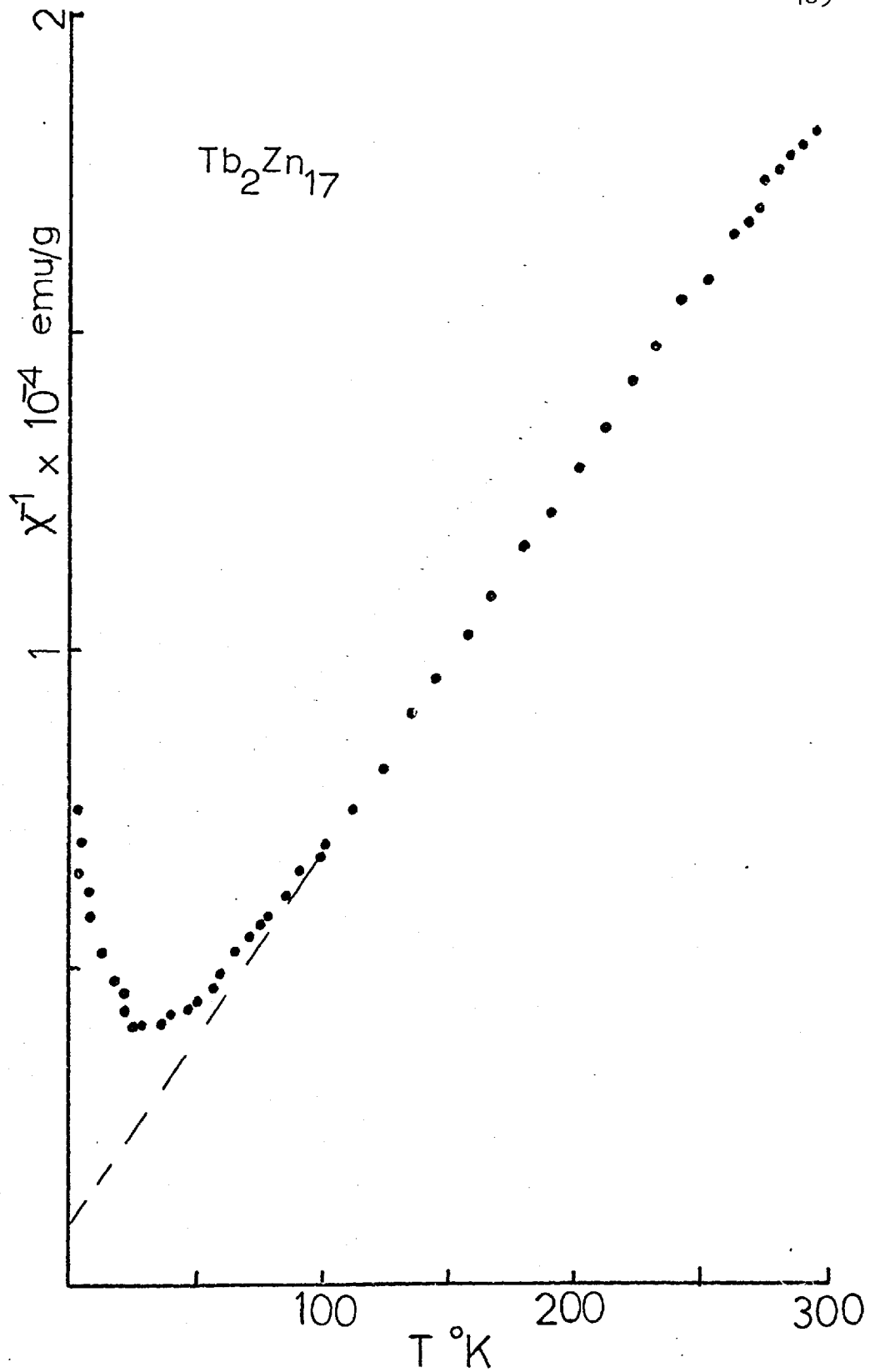


Fig. 4.10

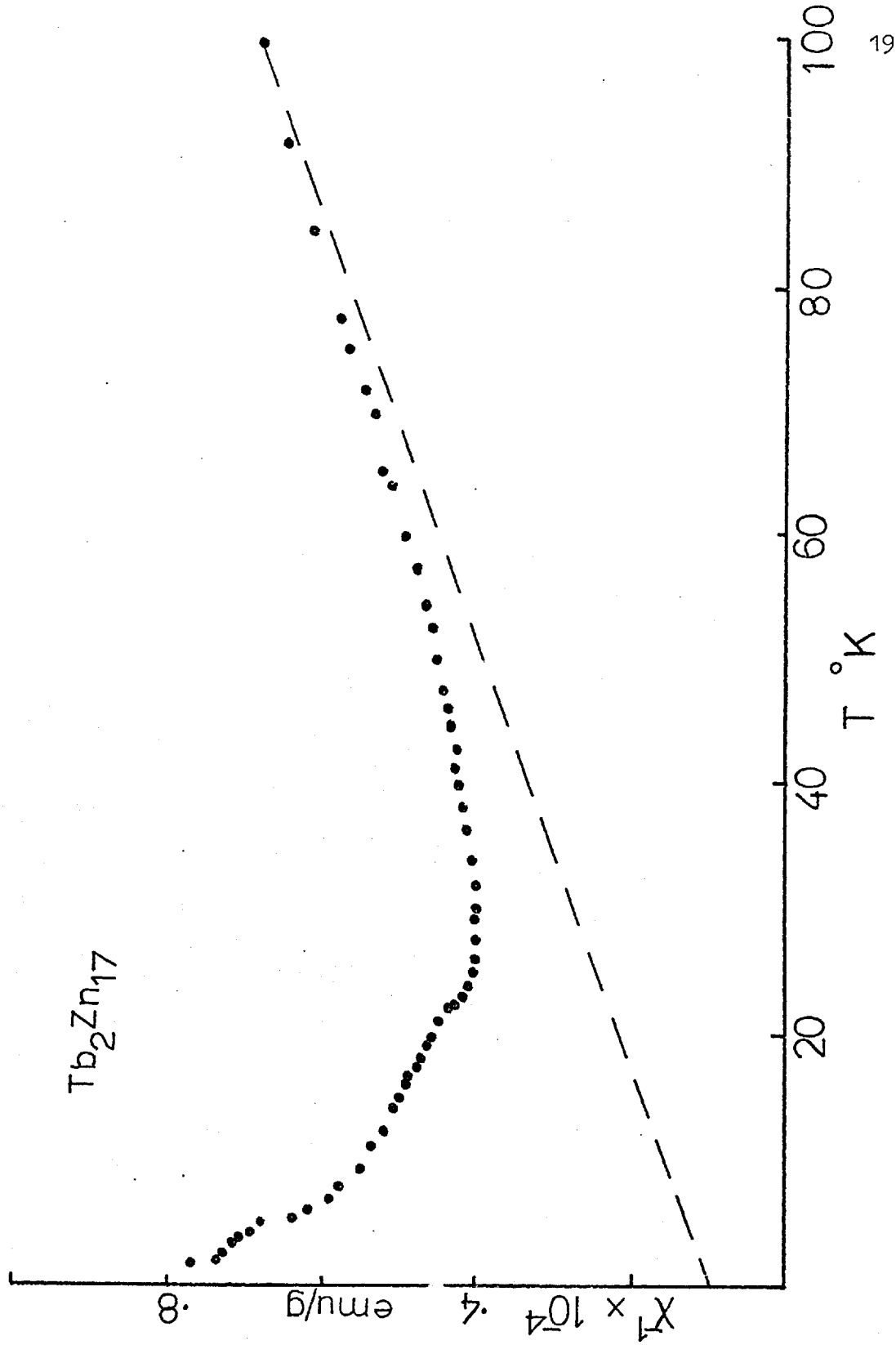


Fig. 4.11

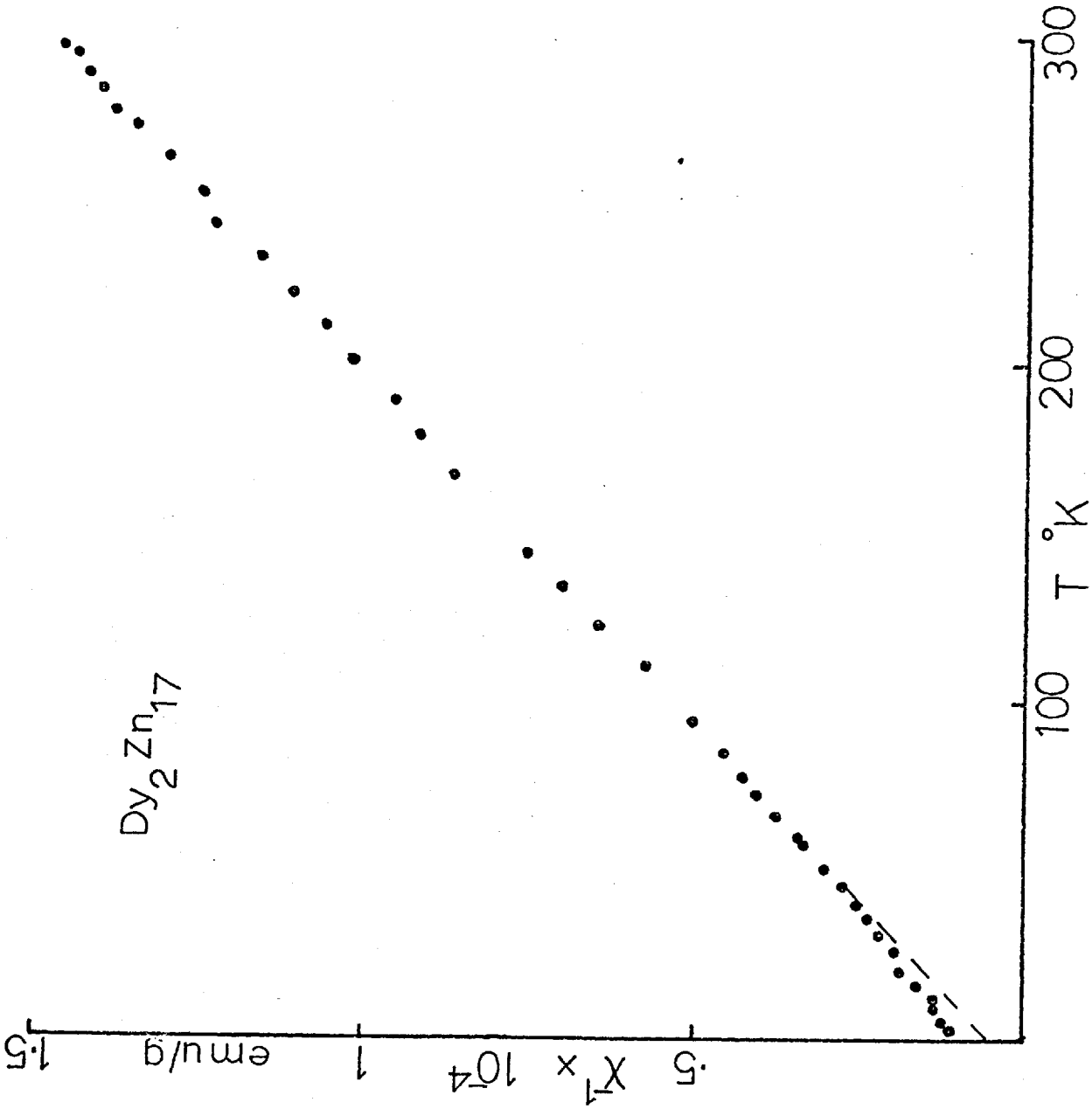


Fig. 4.12

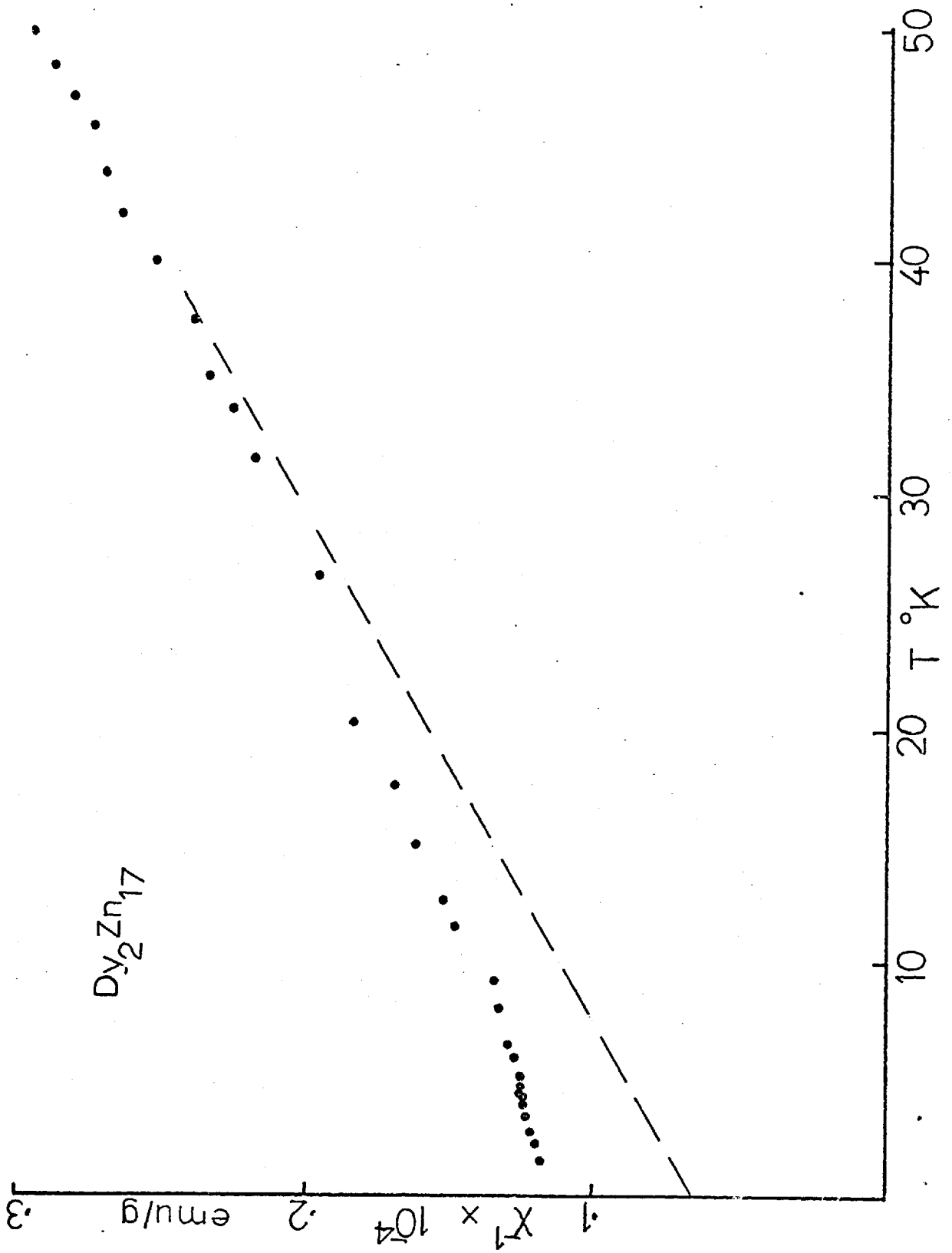


Fig. 4.13

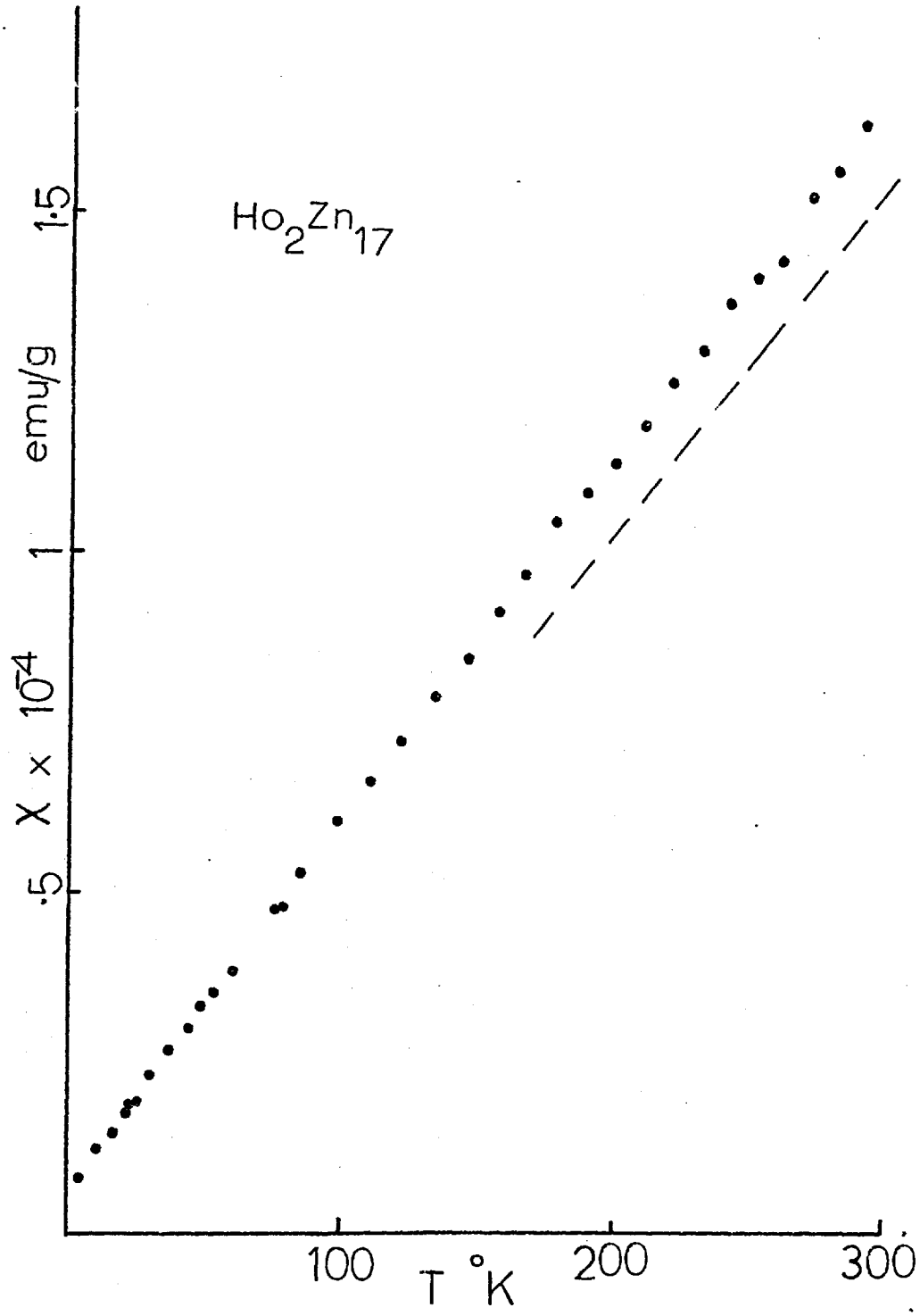


Fig.4.14

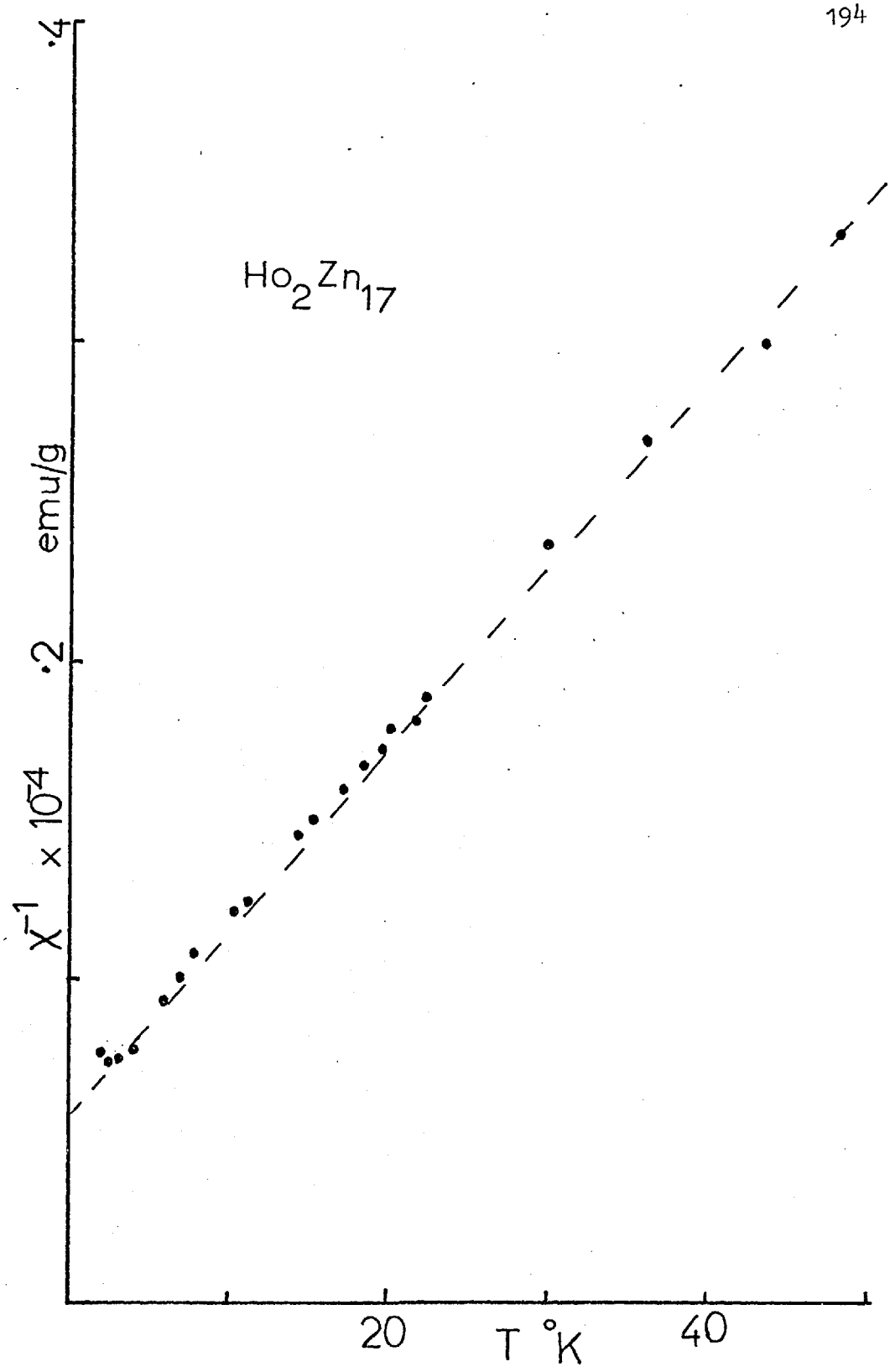


Fig. 4.15

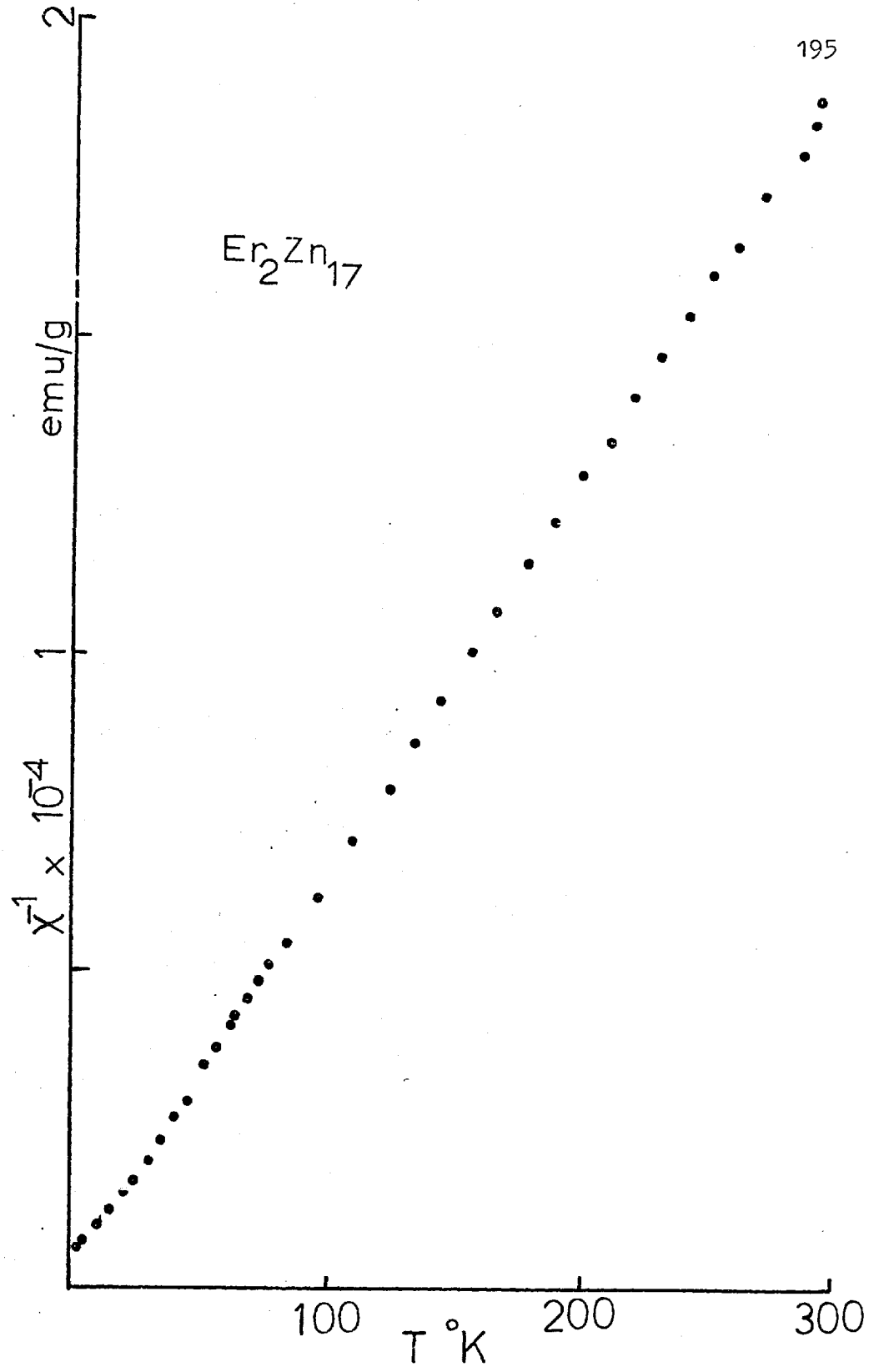


Fig. 4.16

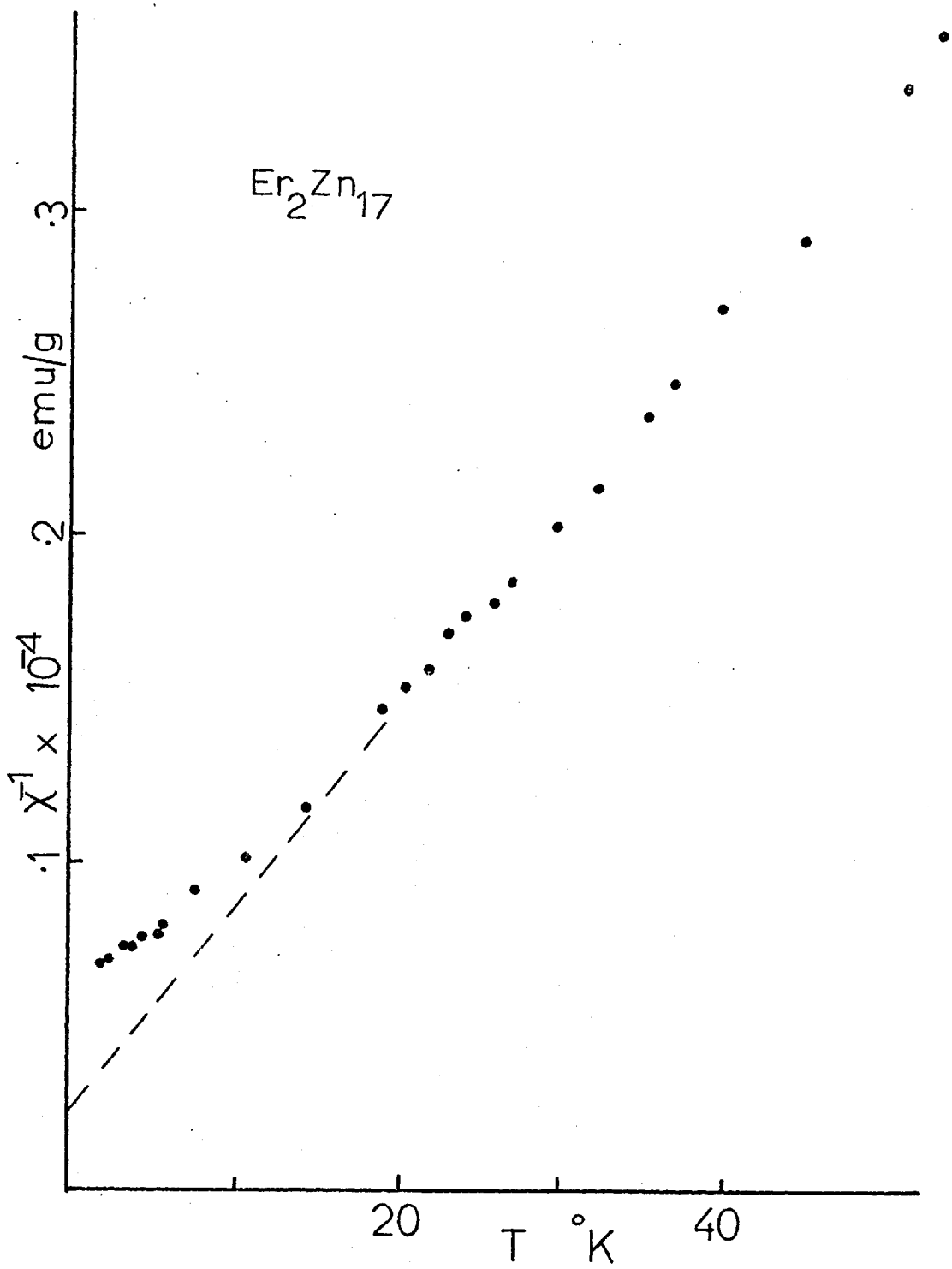


Fig.4.17

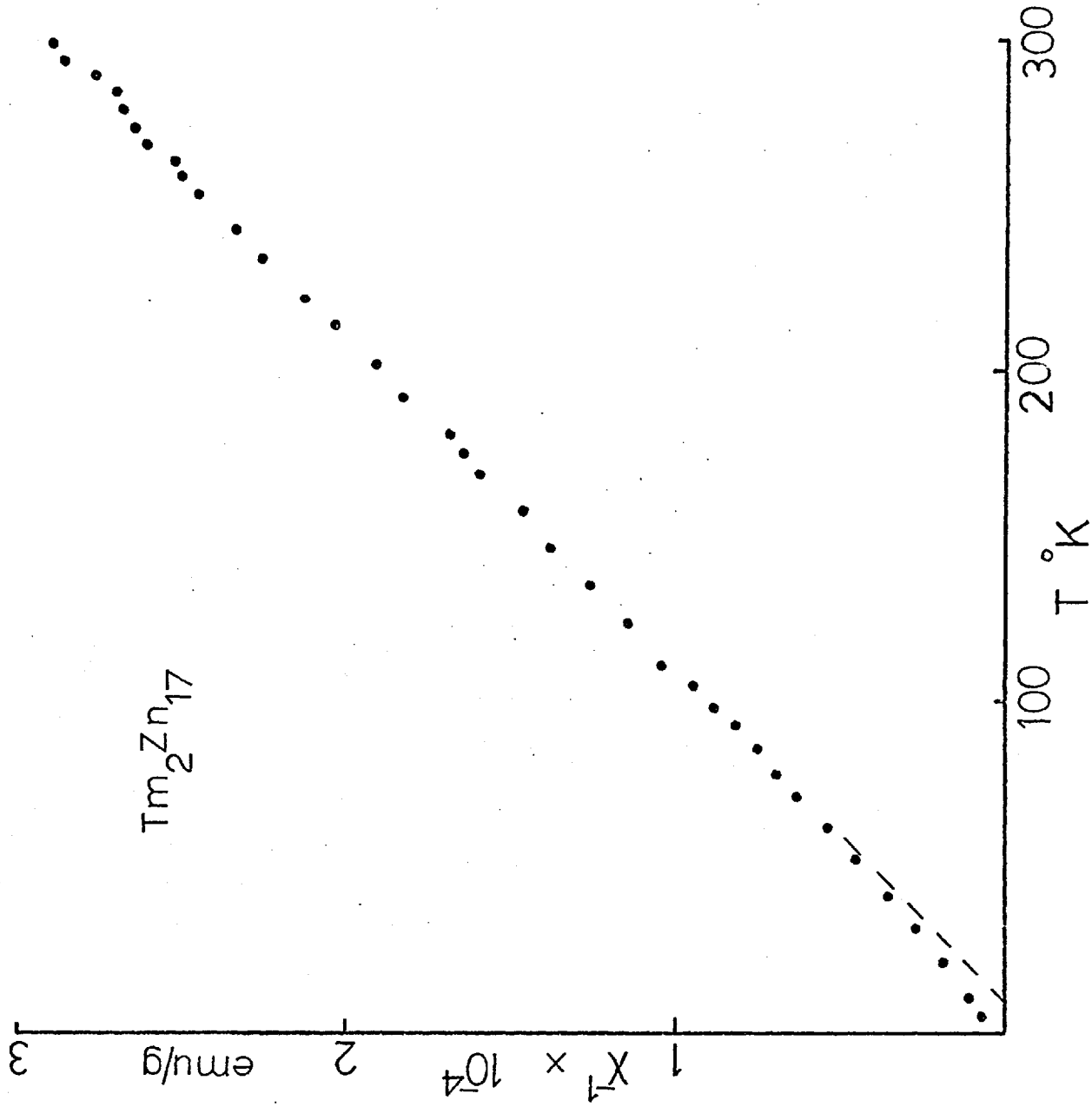


Fig.4.18

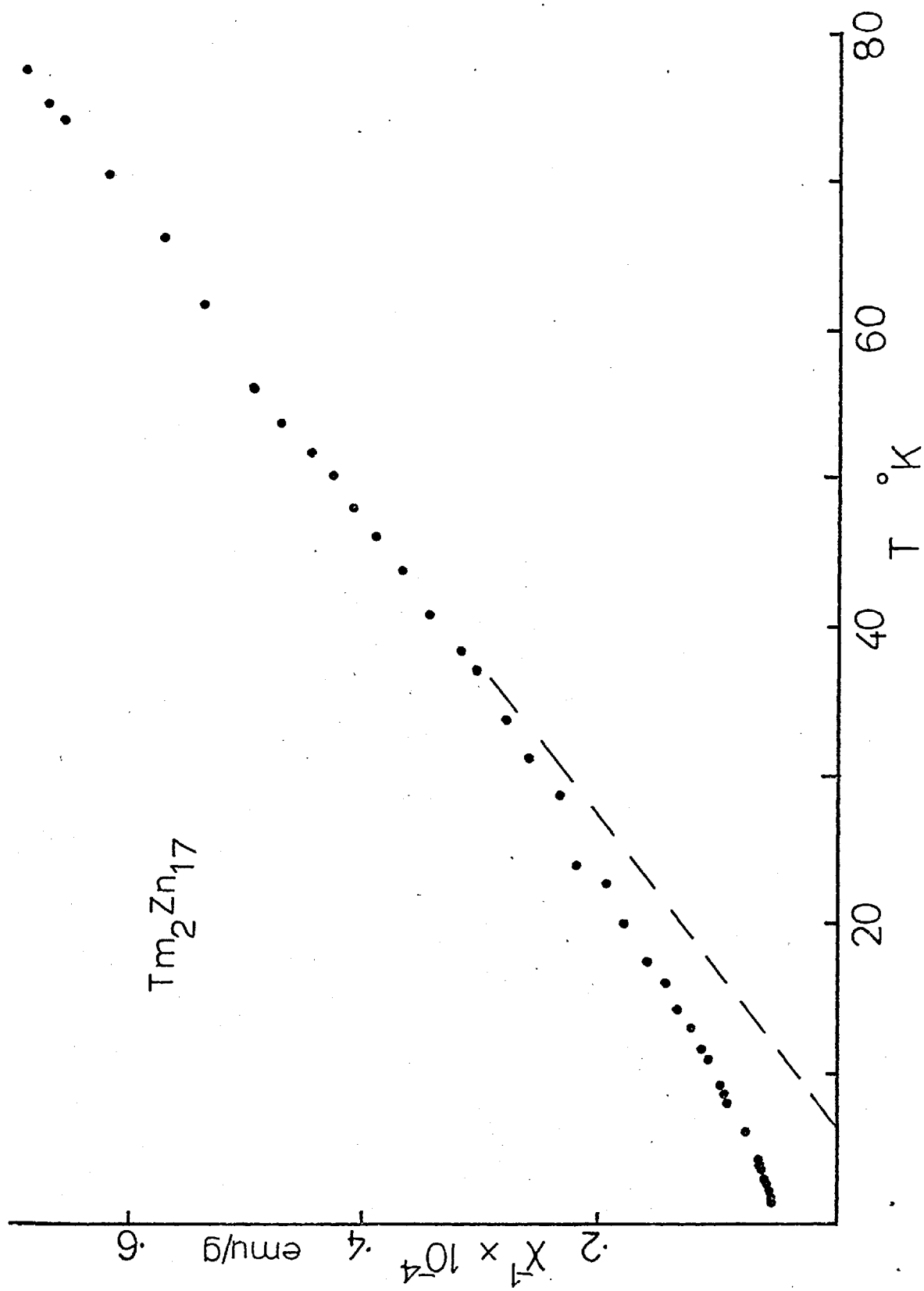


Fig. 4.19

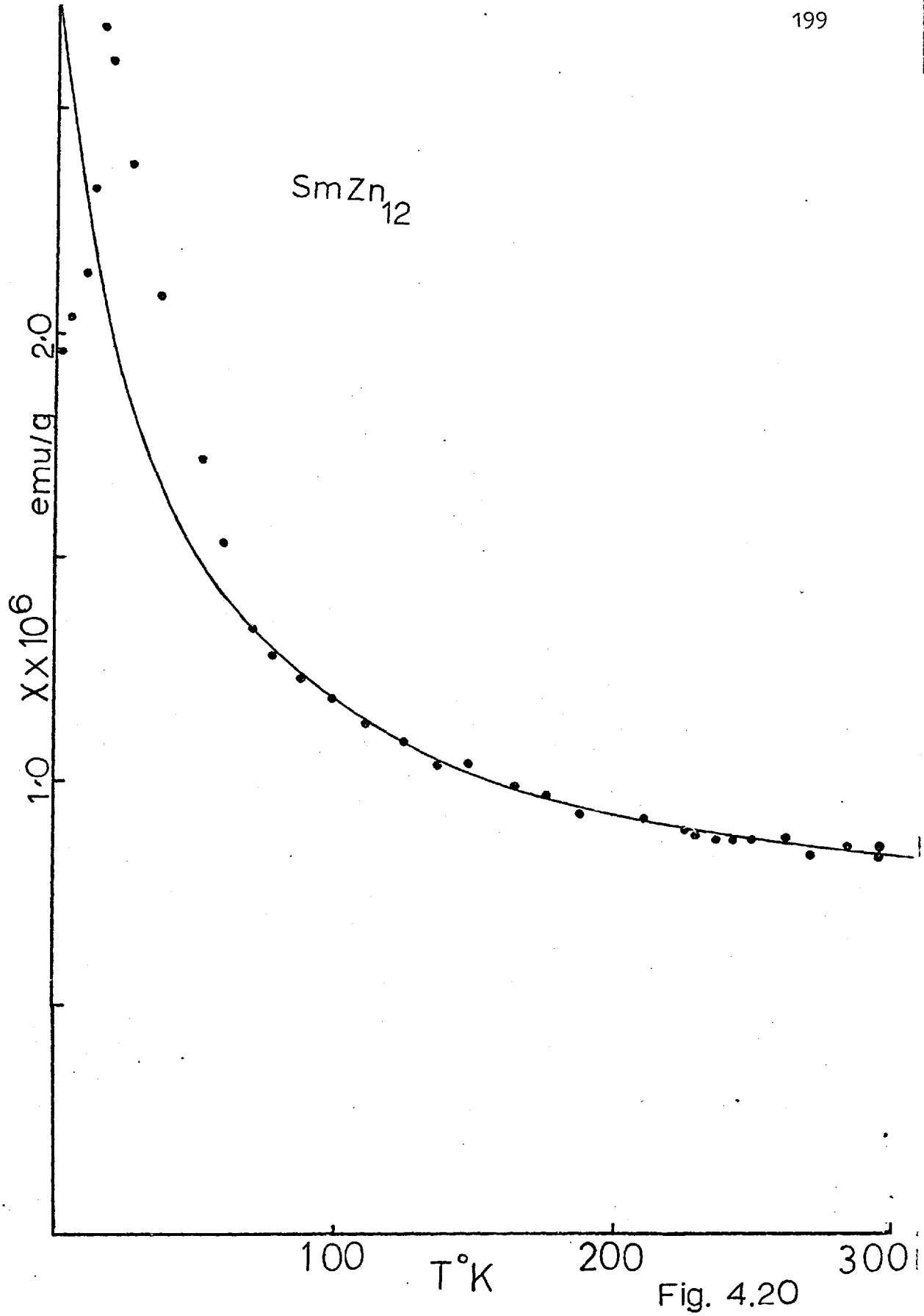


Fig. 4.20

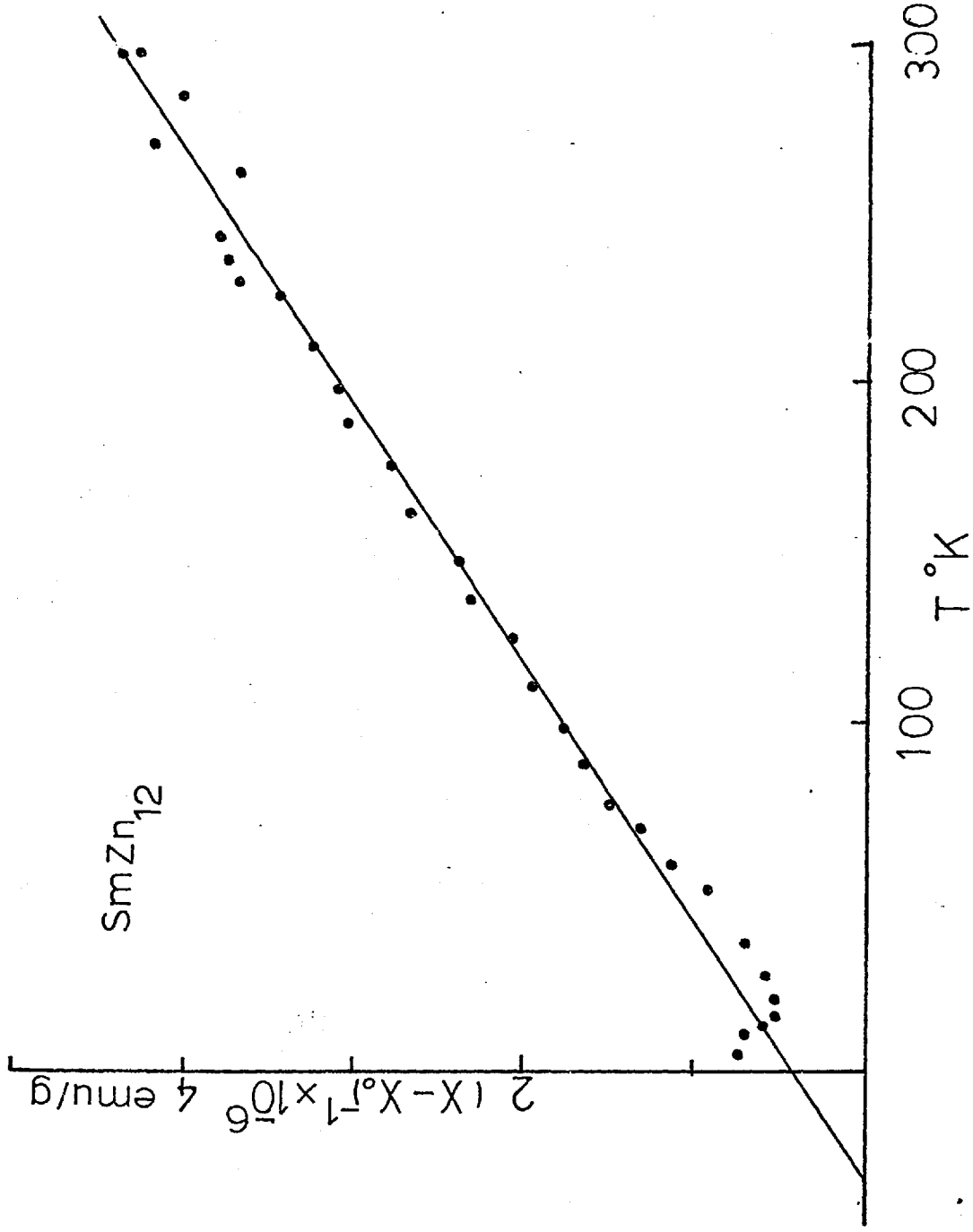


Fig.4.21

Fig. 4.22

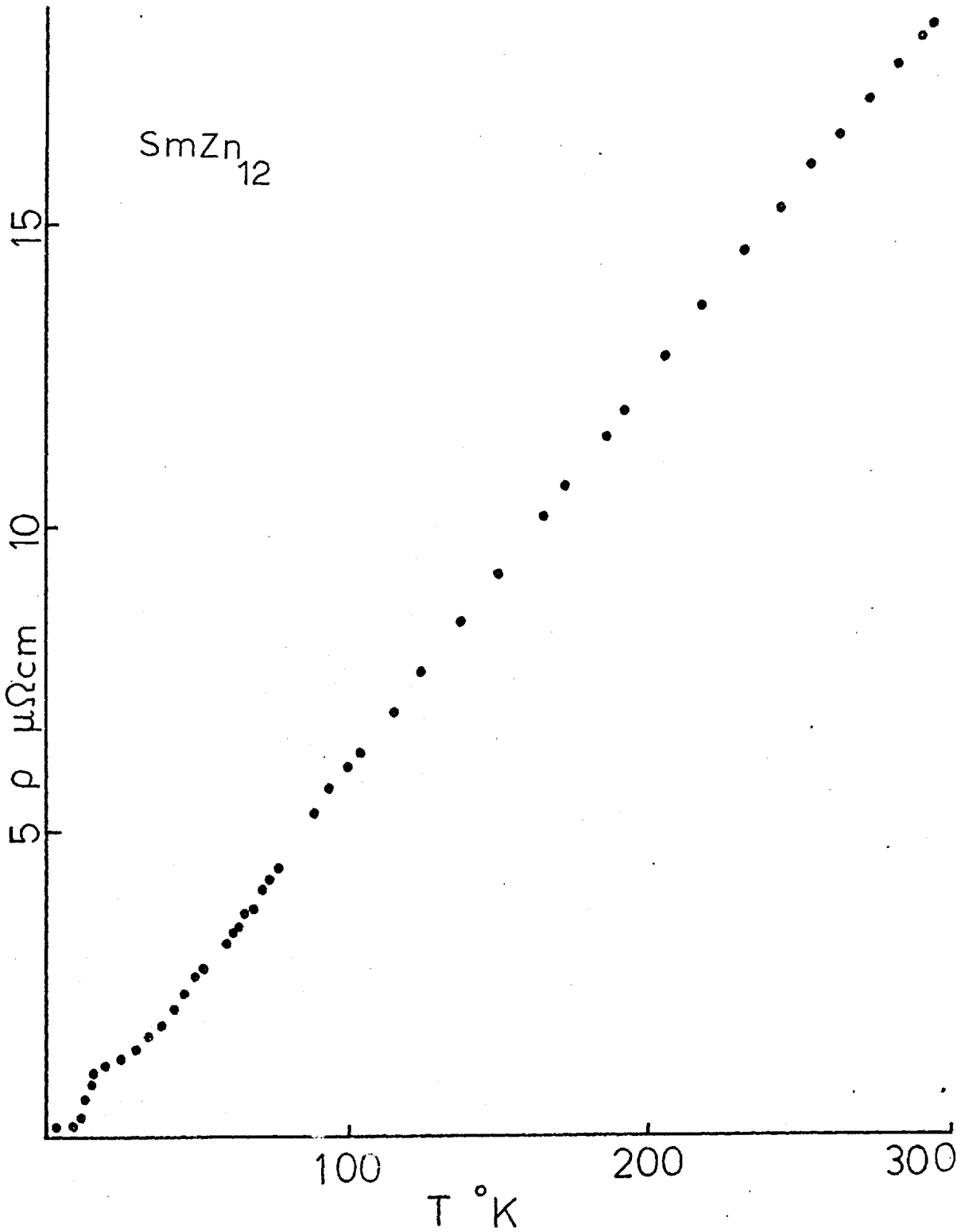


Fig. 4.23

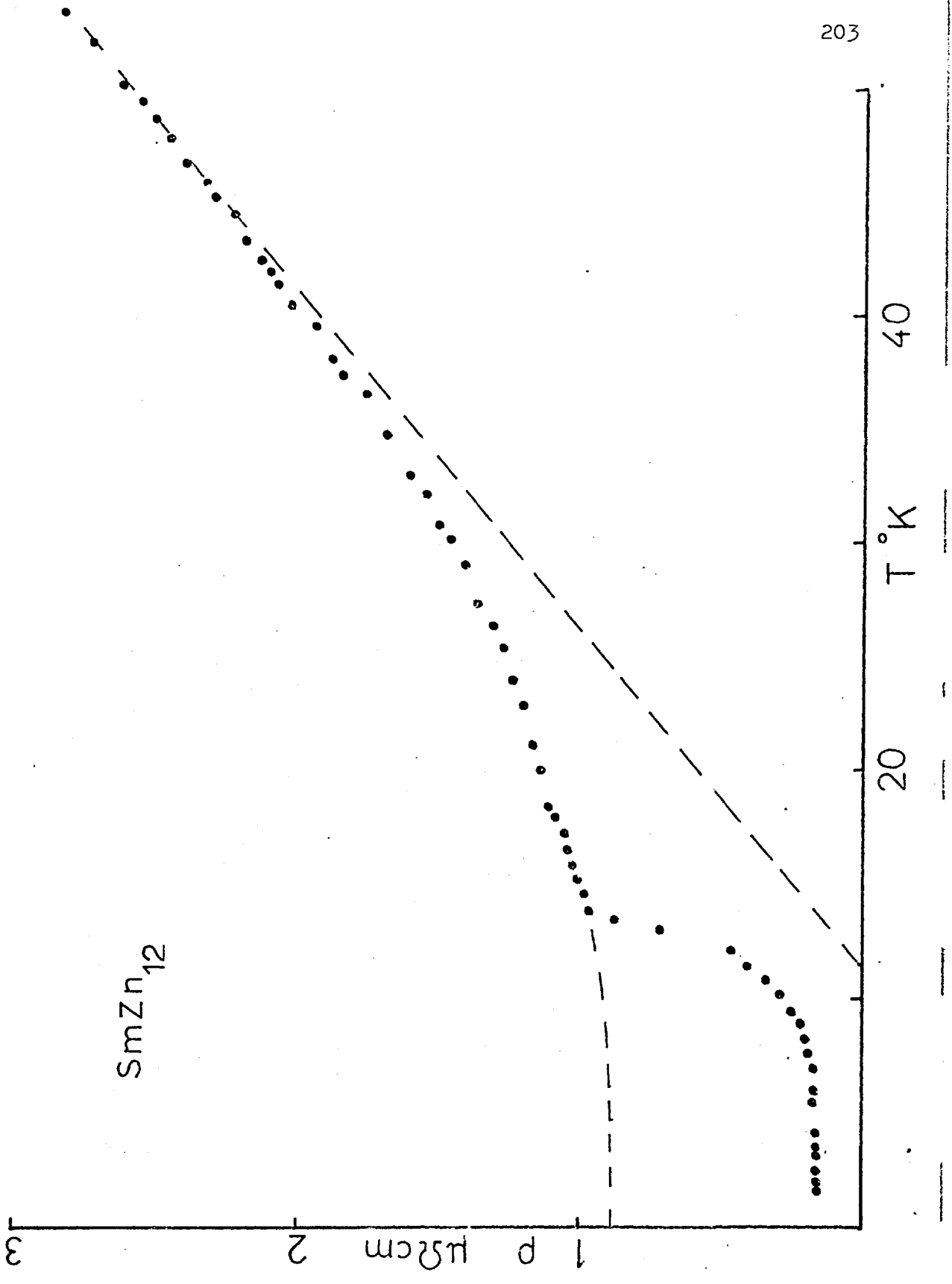


Fig. 4.24

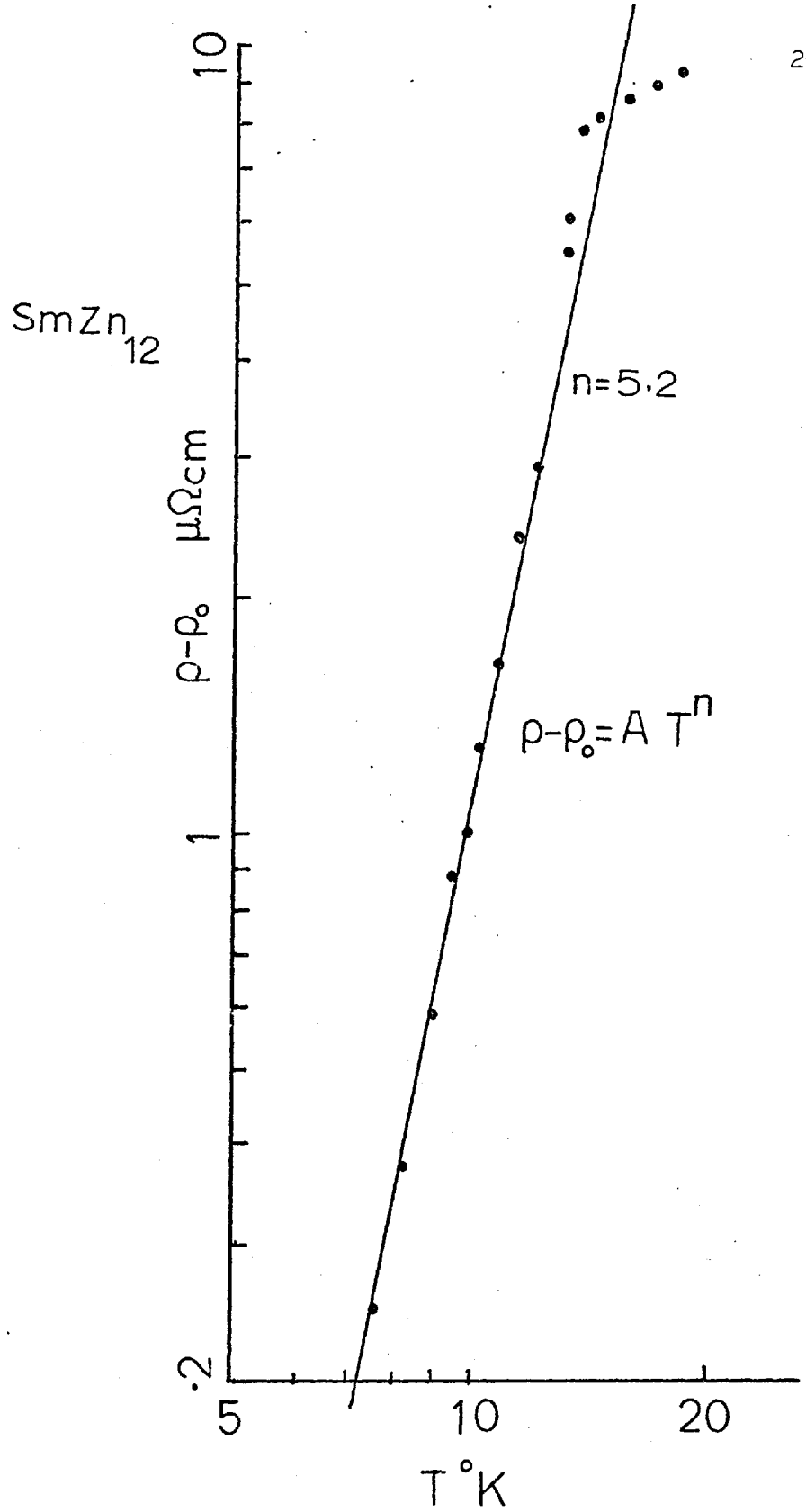


Fig. 4.25

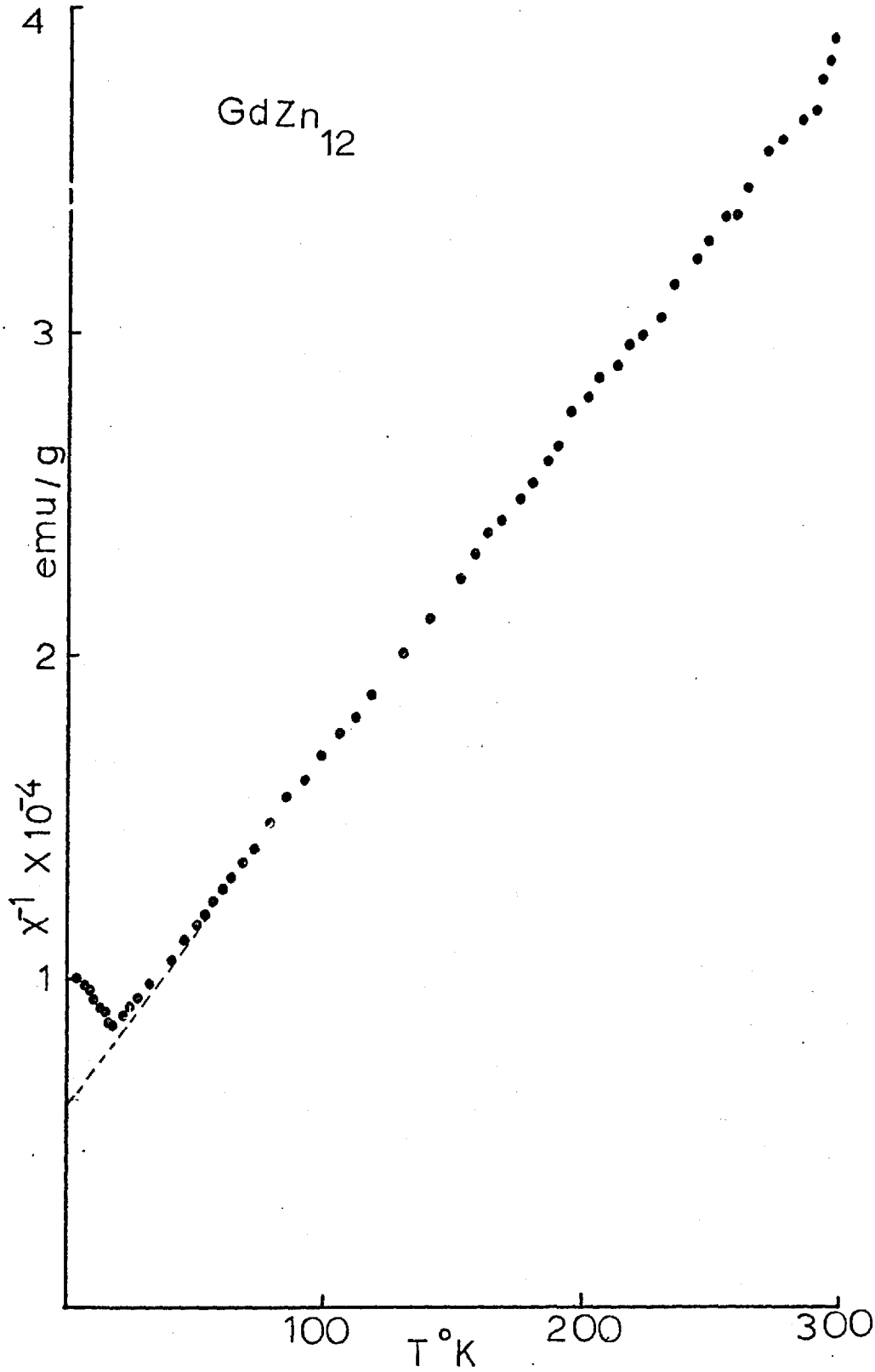


Fig. 4.26

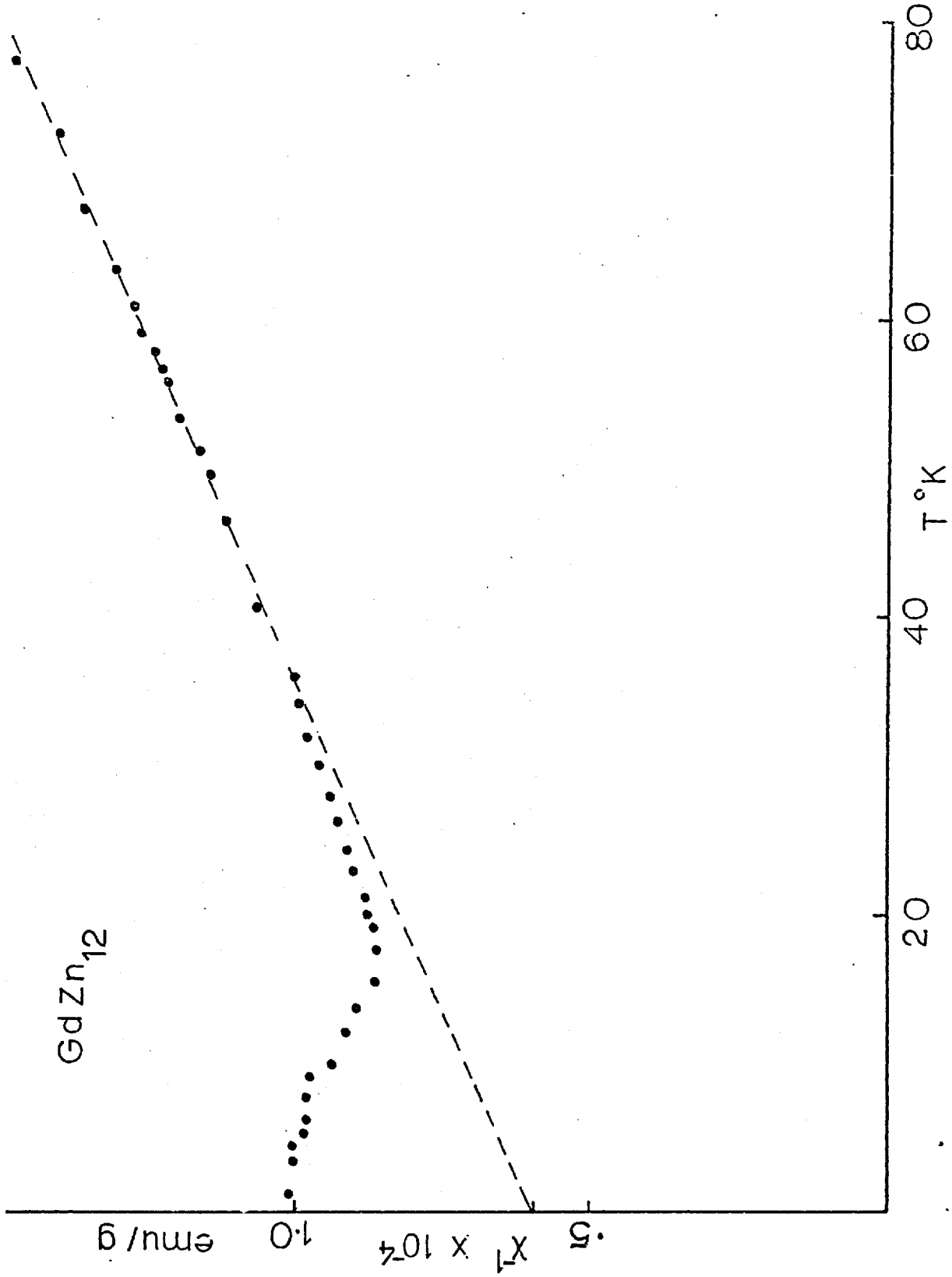


Fig. 4.27

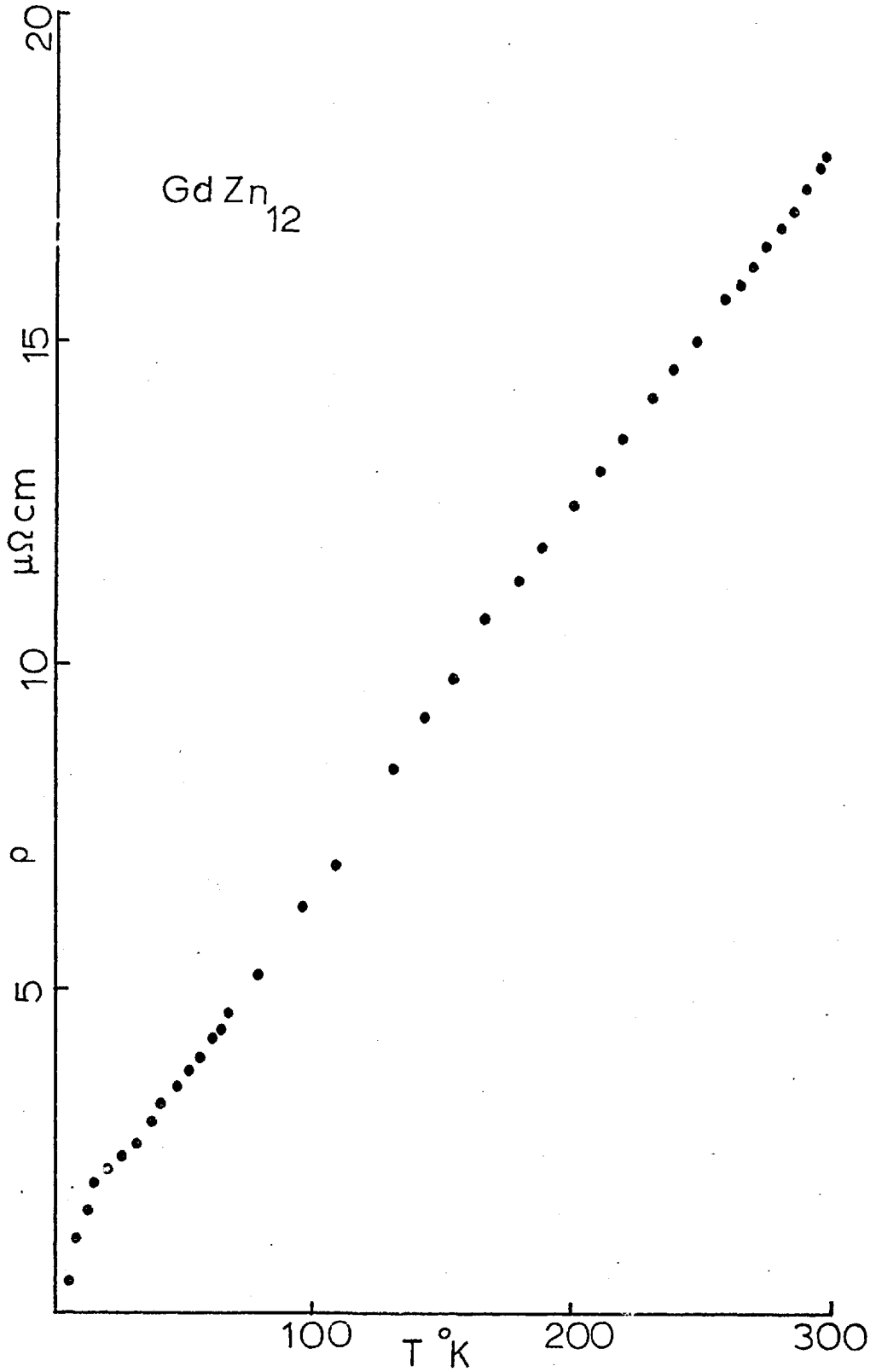


Fig. 4.28

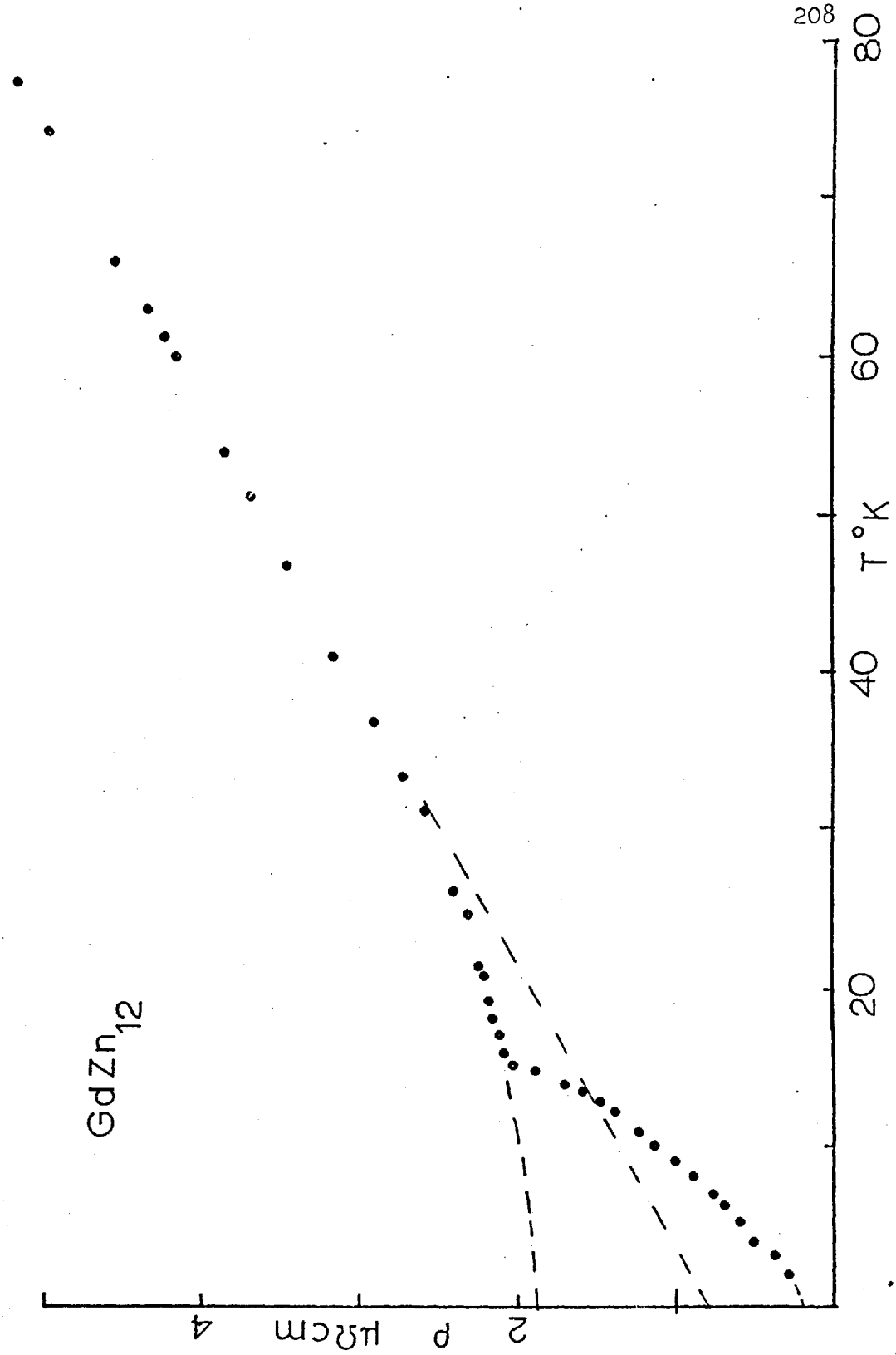


Fig. 4.29

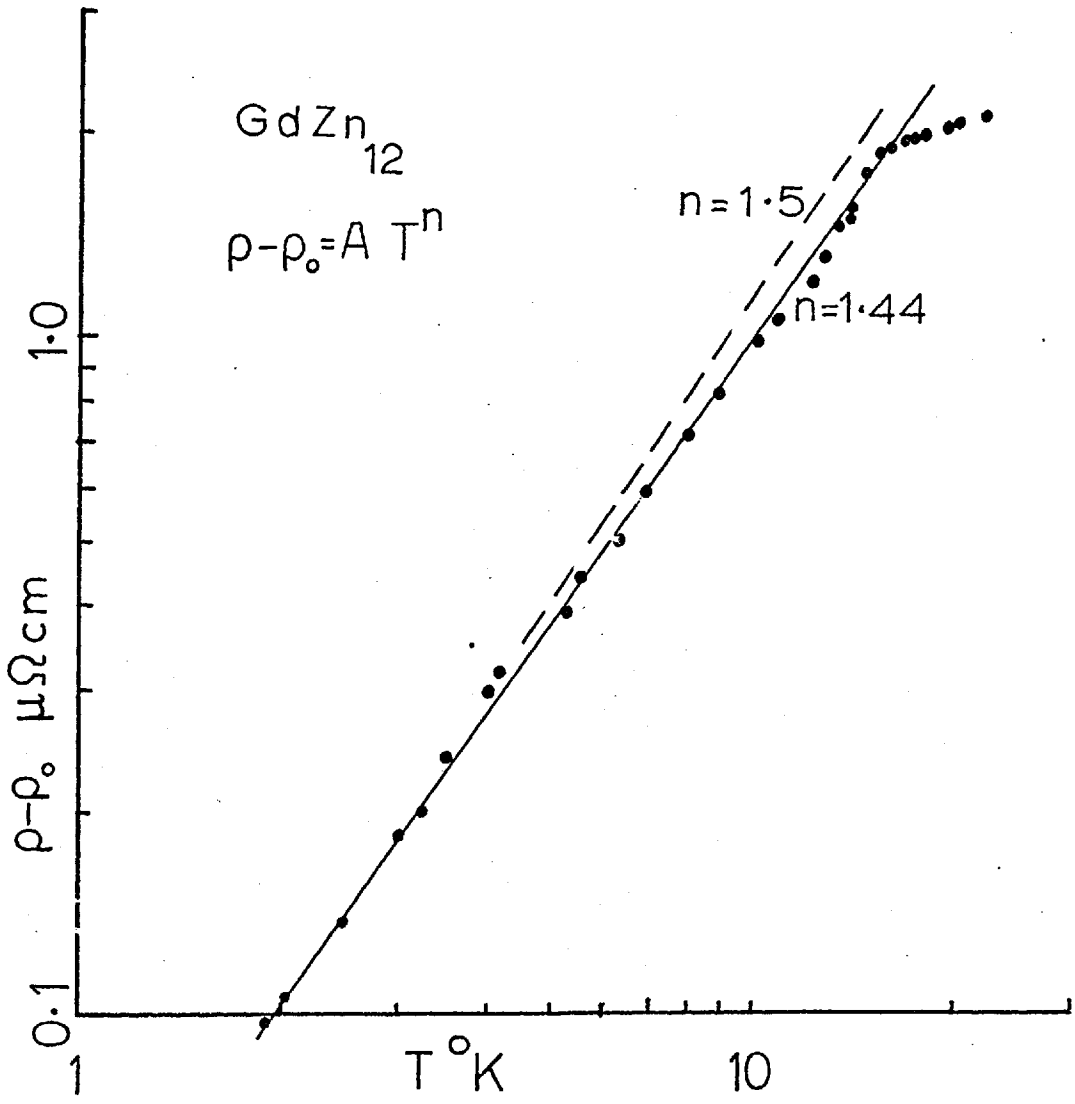


Fig. 4.30

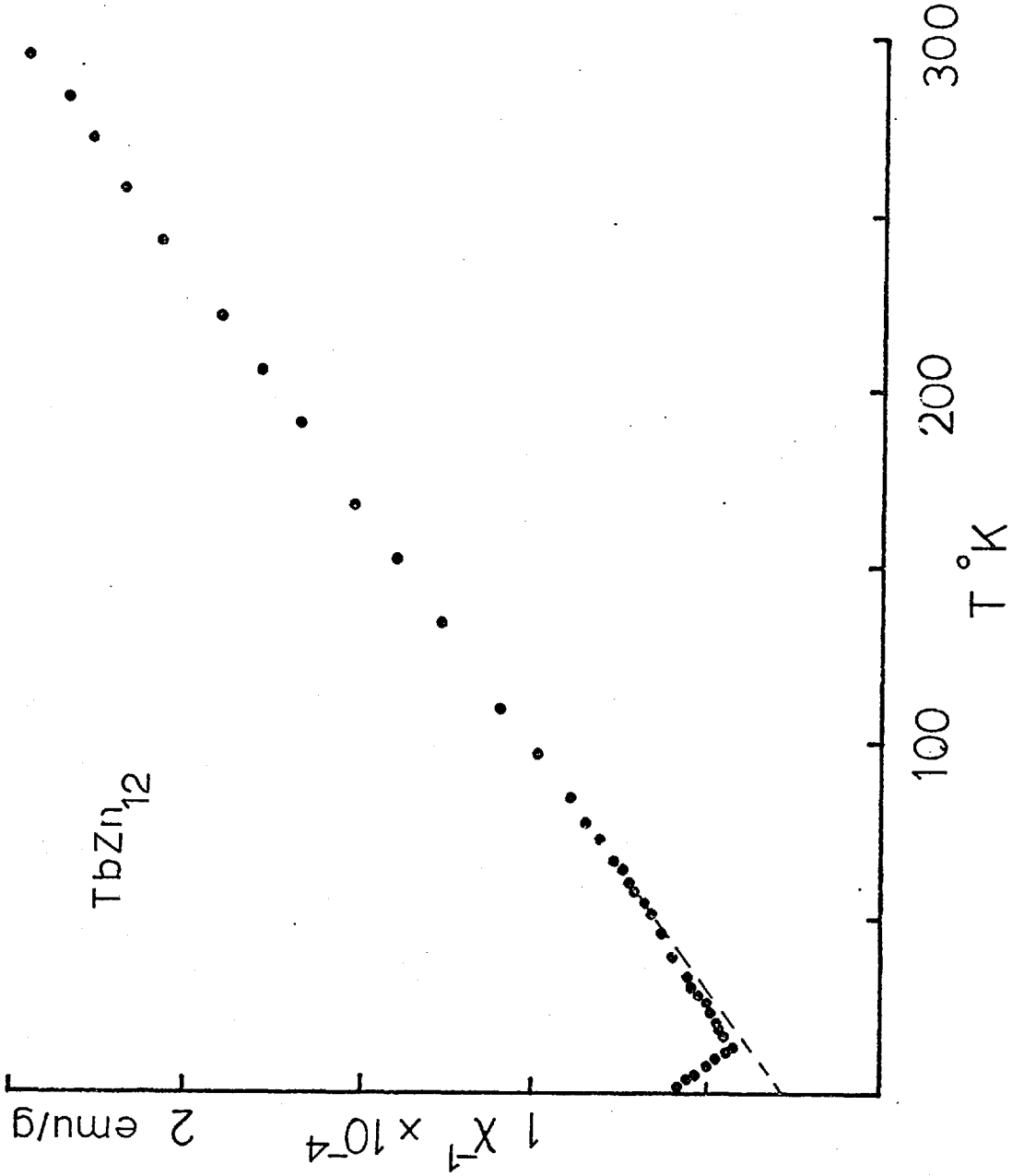


Fig. 4.31

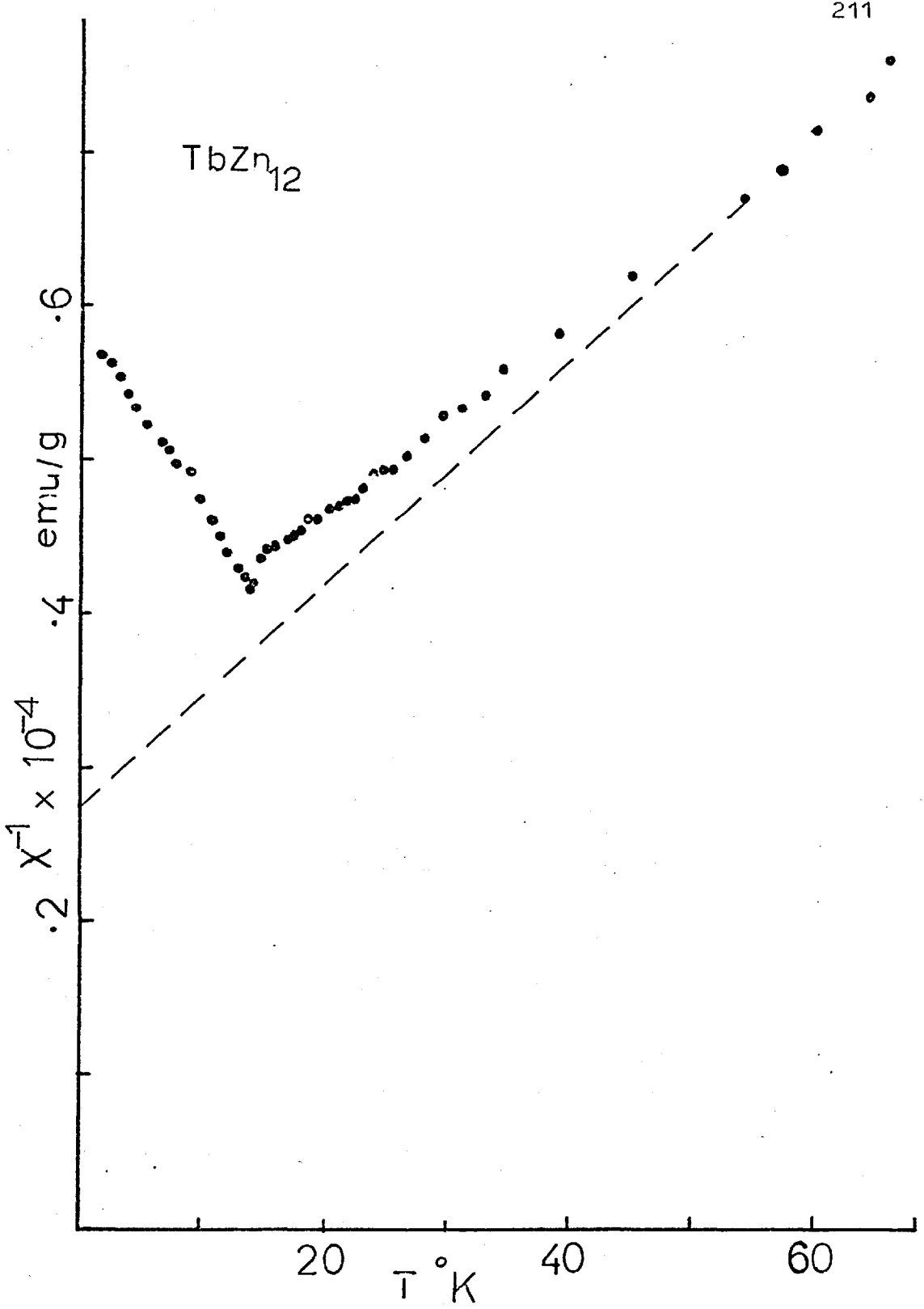


Fig. 4.32

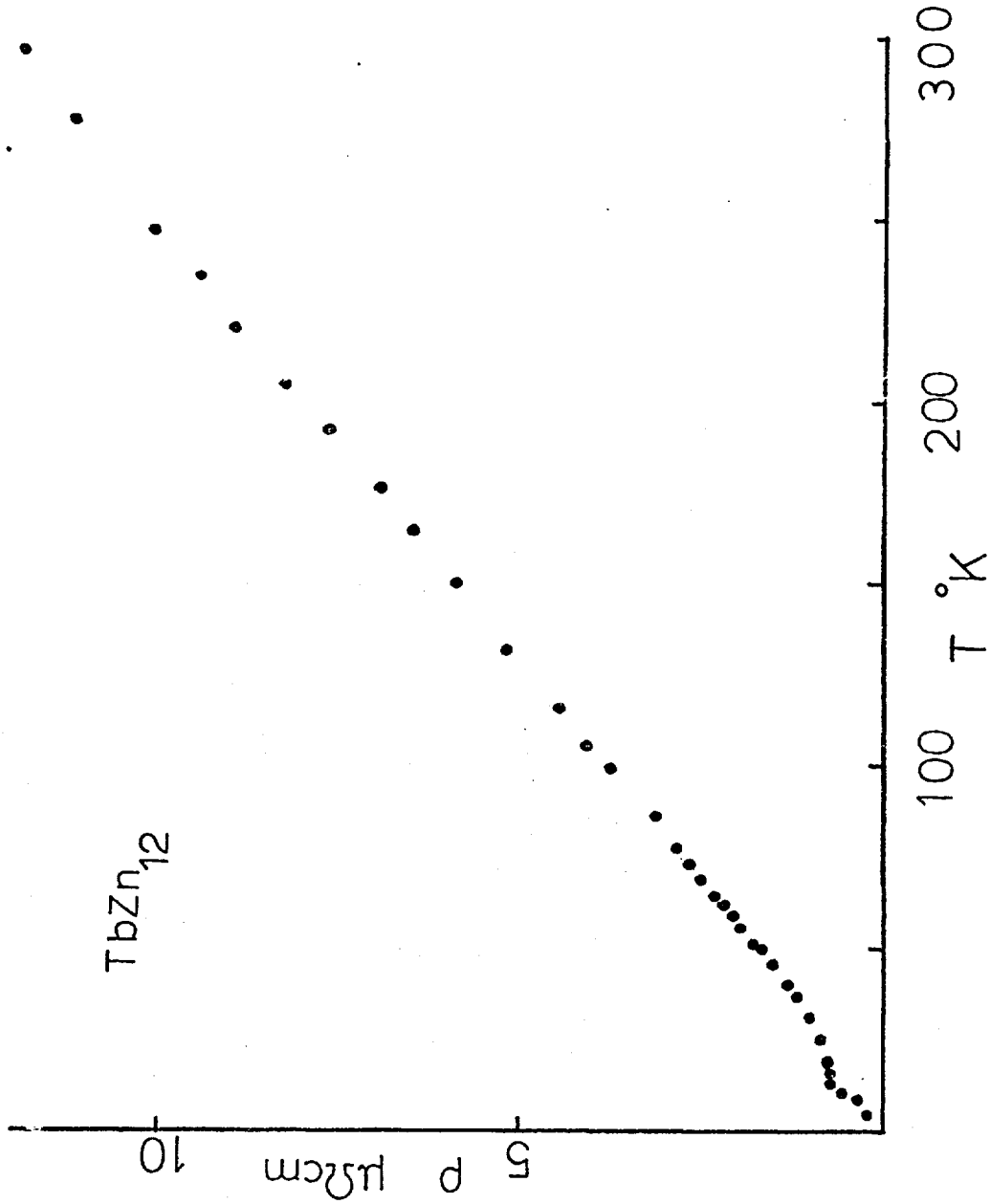


Fig. 4.33

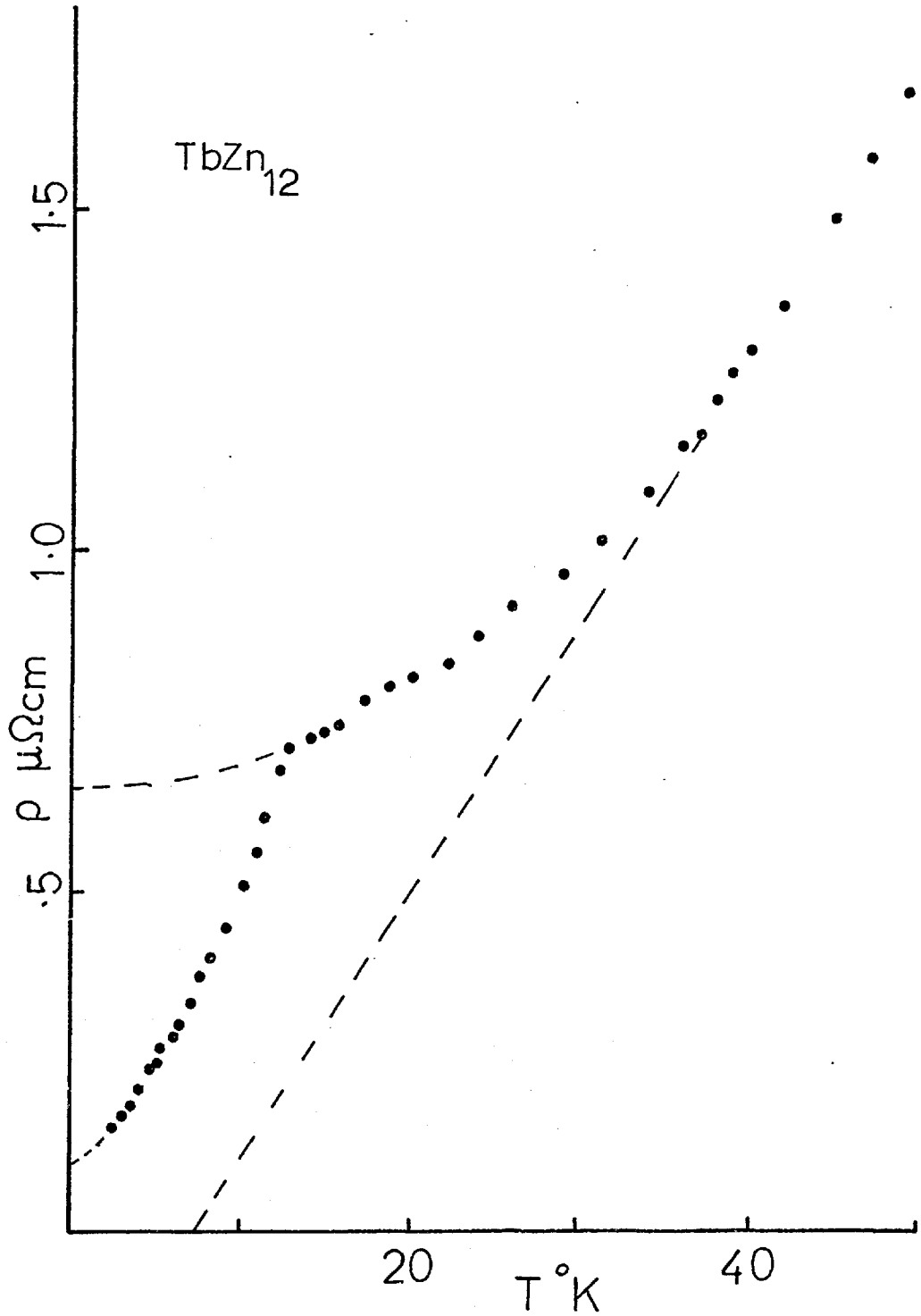


Fig. 4.34

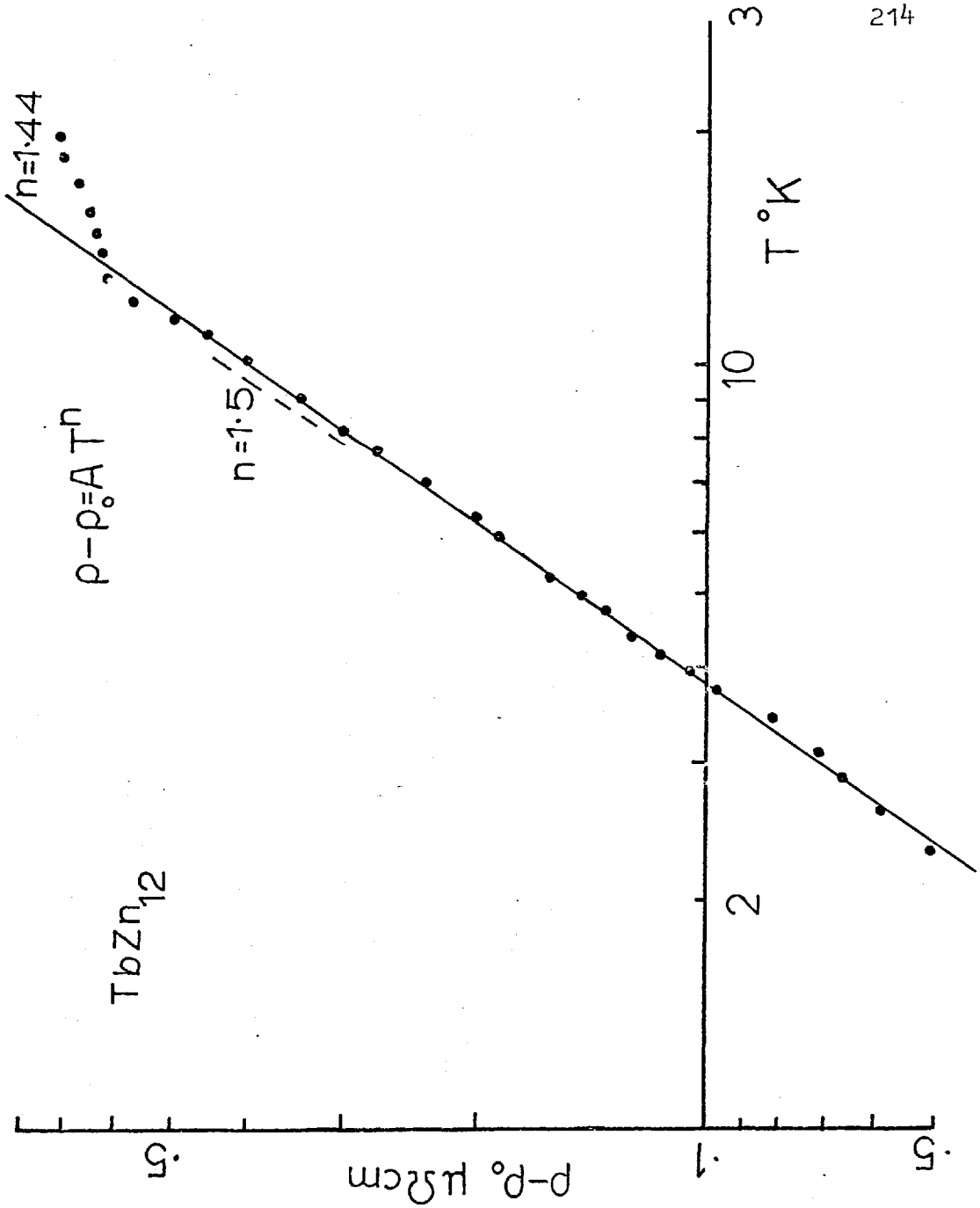


Fig. 4.35

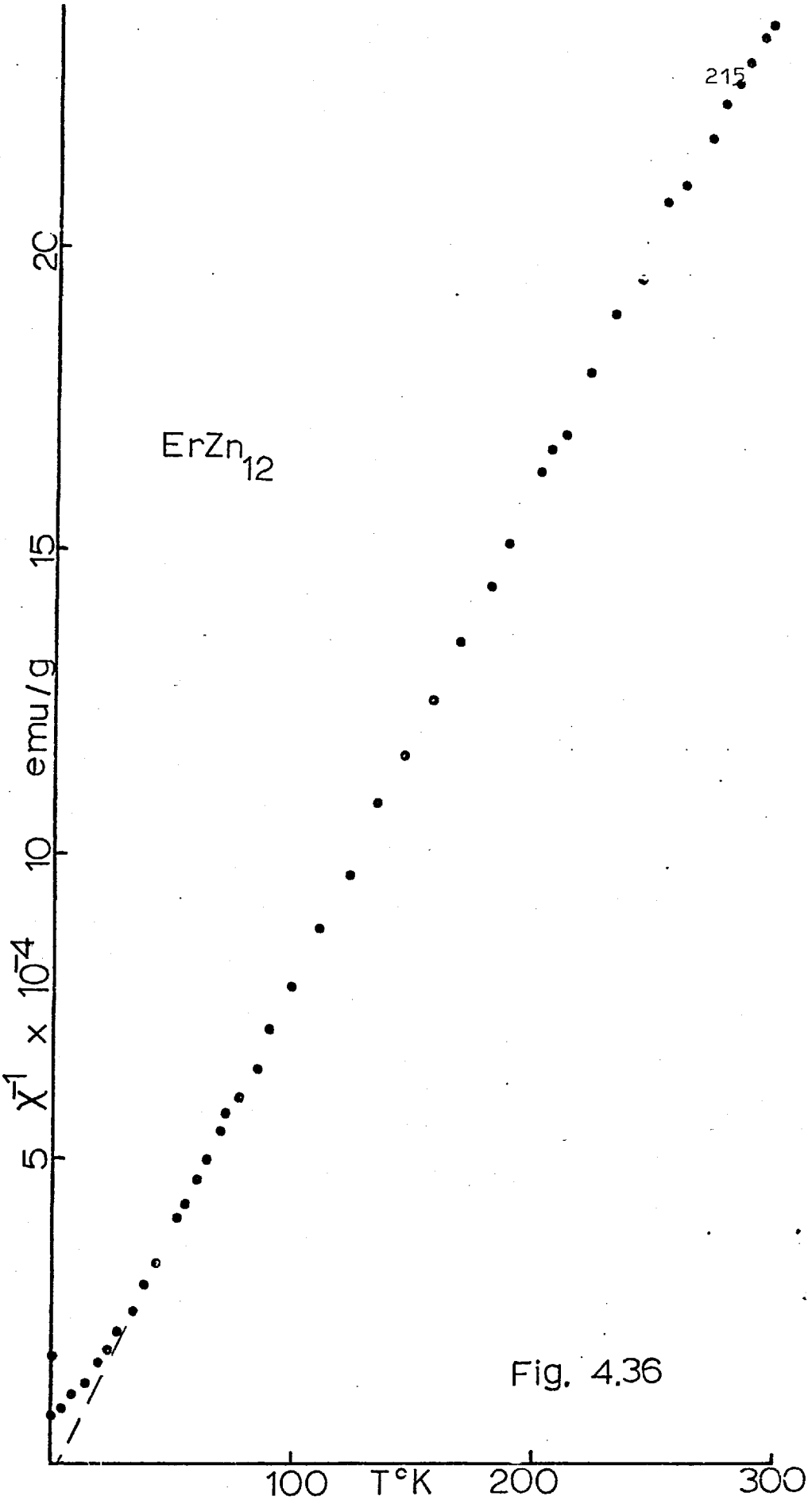


Fig. 4.36

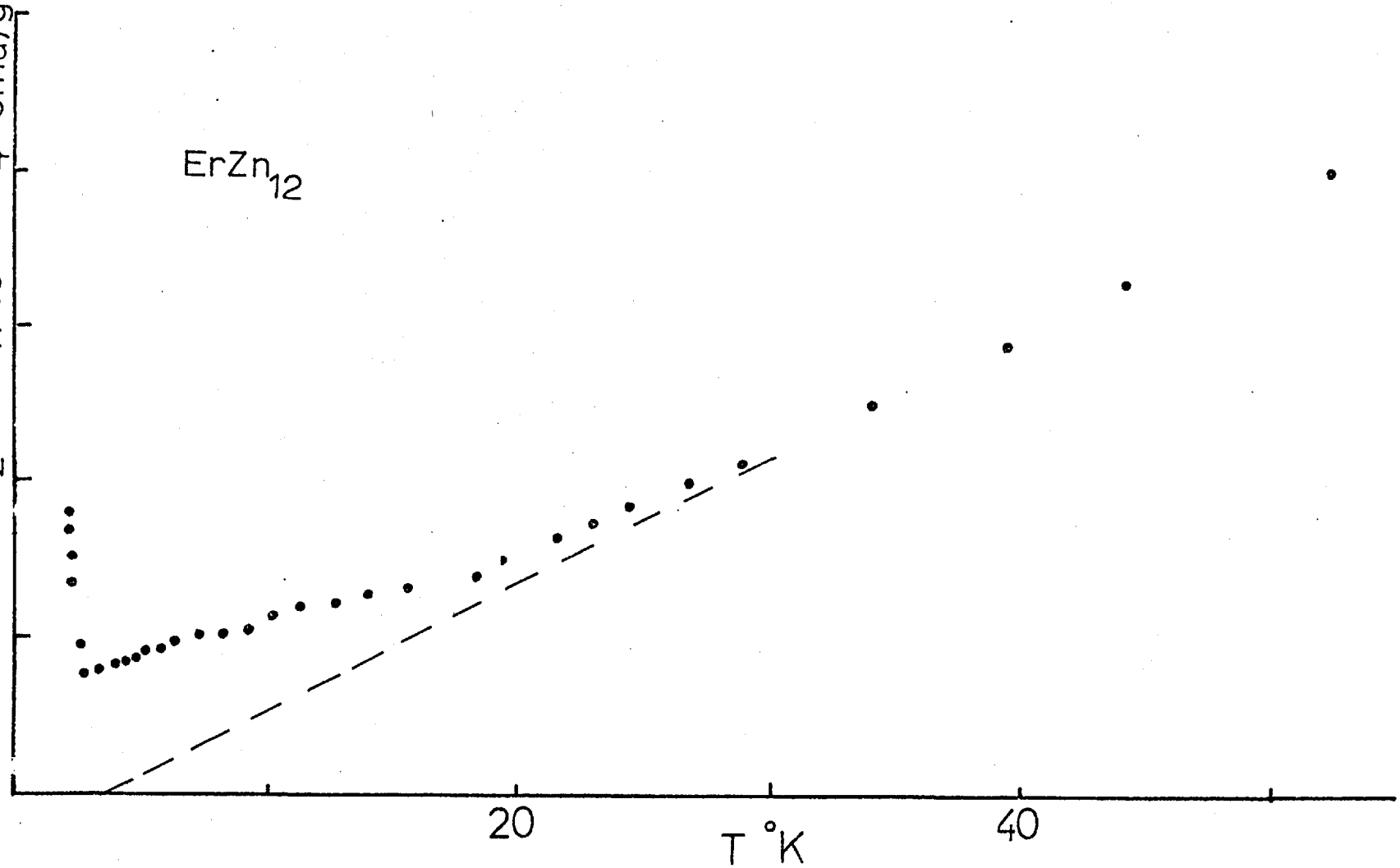


Fig. 4.37

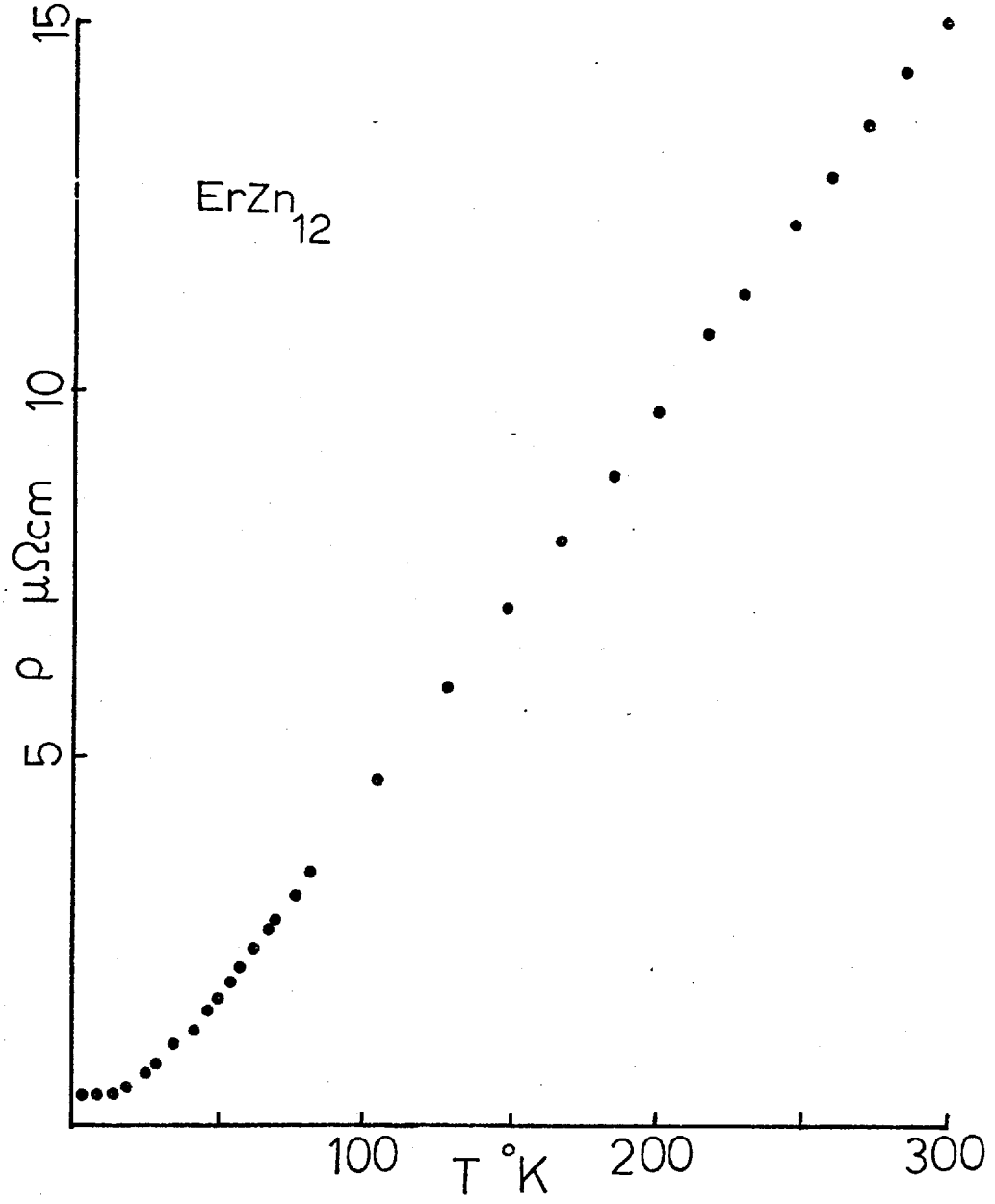


Fig. 4.38

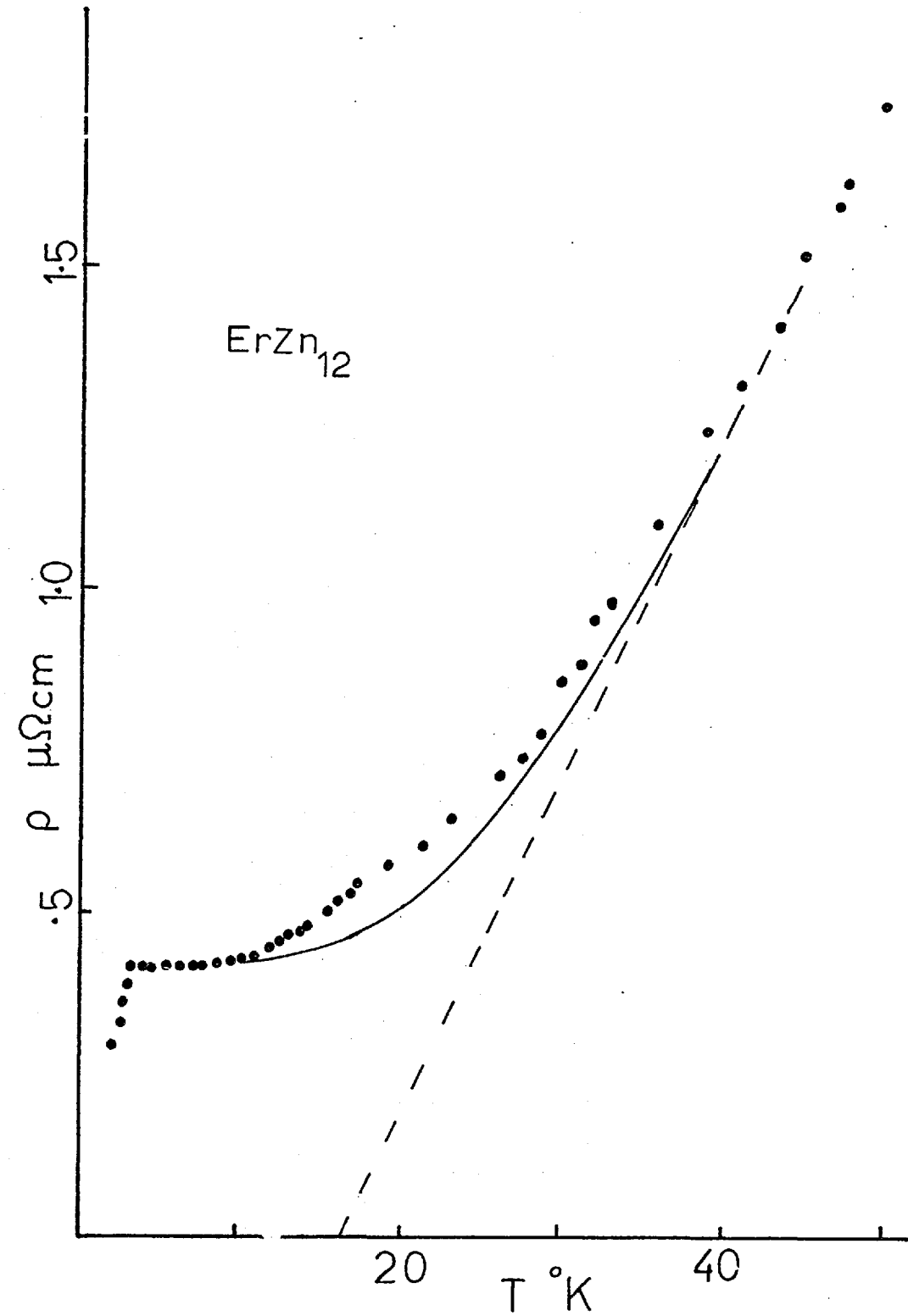


Fig. 4.39

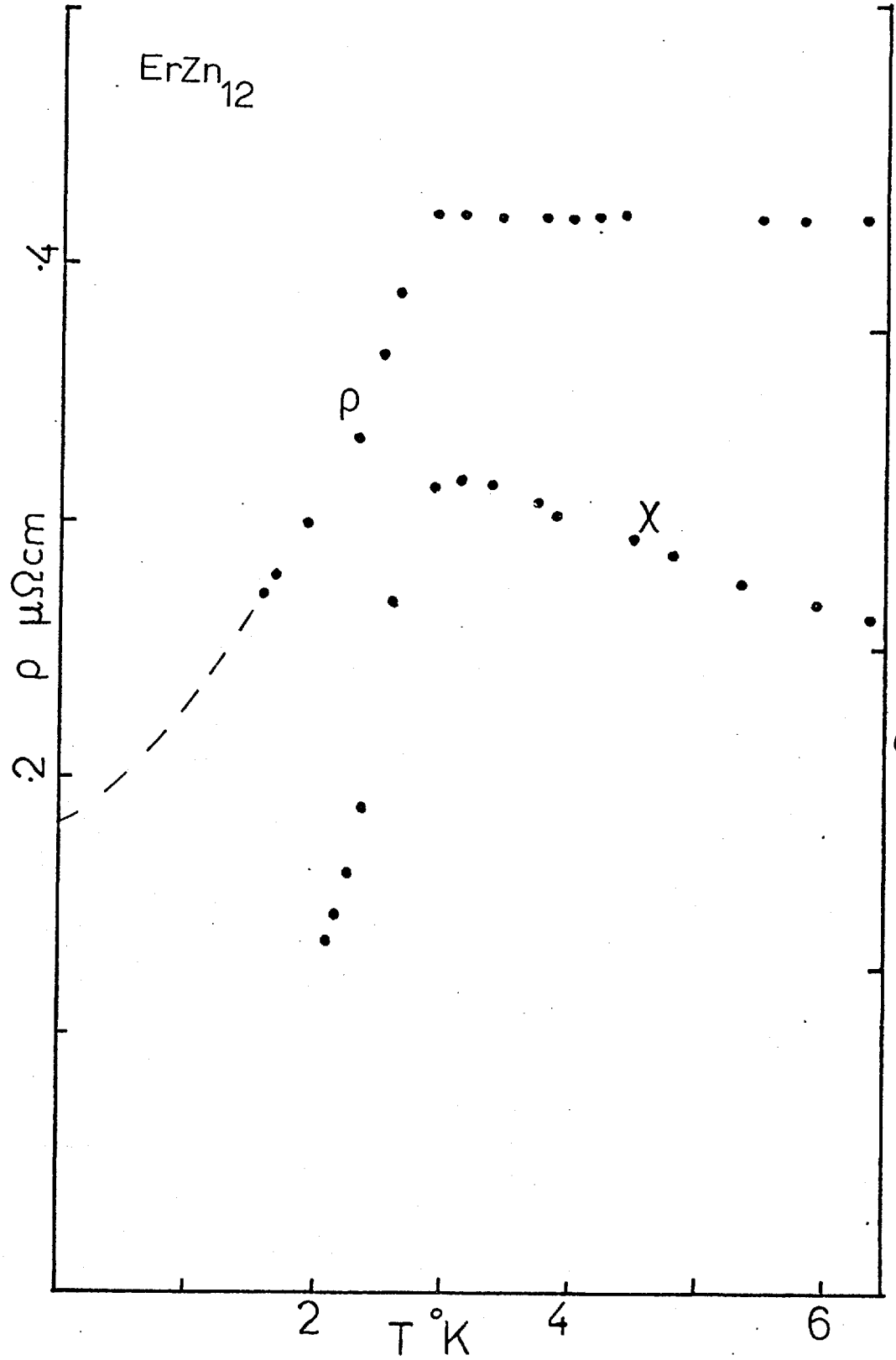


Fig. 4.40

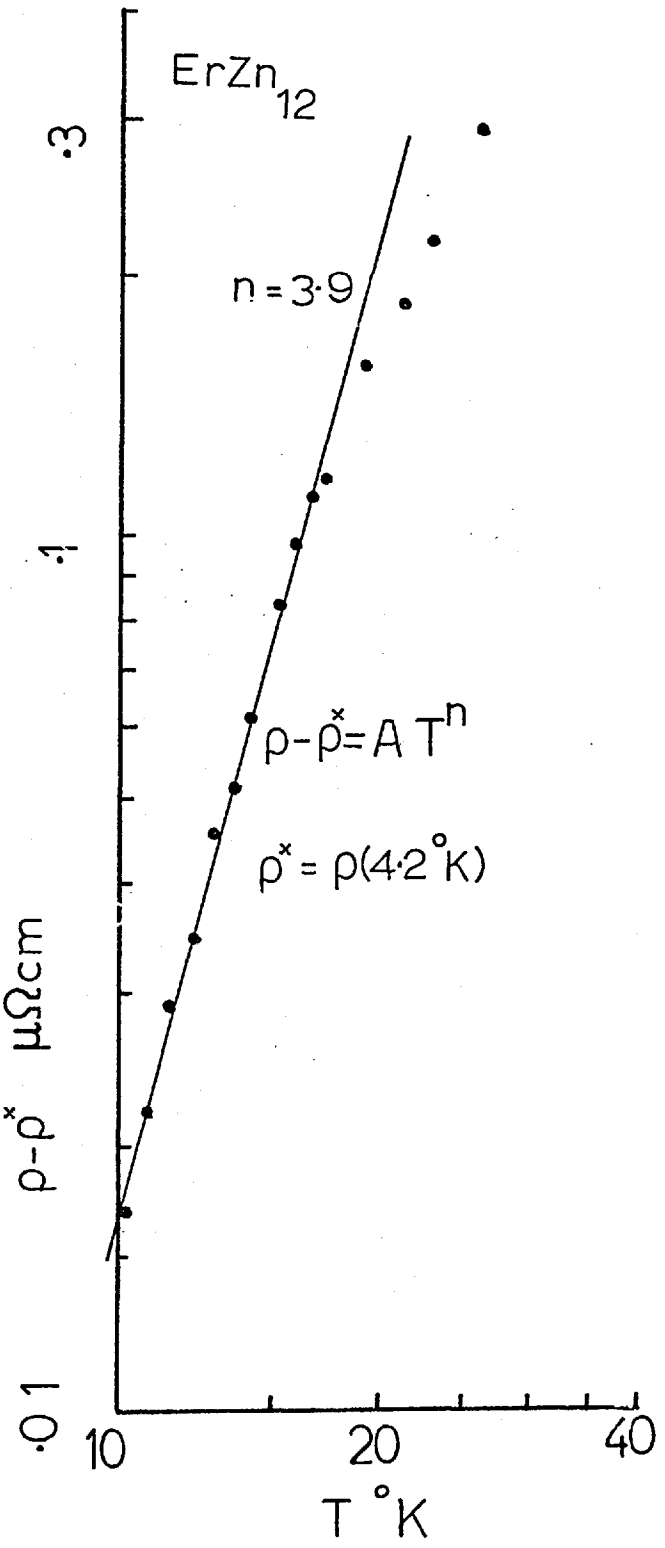


Fig. 4.41

APPENDIX A

a) Formalism of Static Linear Response Theory

Consider the magnetisation $M(\underline{r})$ induced in an isotropic body by a magnetic field of z component $H(\underline{r})$. The associated energy will be:

$$\mathcal{H} = -\int M(\underline{r})\, H(\underline{r})\, d\underline{r} \quad , \qquad \text{A.1}$$

and we define a generalised susceptibility $\chi'(\underline{r})$ such that:

$$M(\underline{r}) = \int \chi'(\underline{r} - \underline{r}')\, H(\underline{r}')\, d\underline{r}' \qquad \text{A.2}$$

$\chi'(\underline{r})$ is related to its Fourier Transform $\chi(\underline{q})$ by:

$$\chi'(\underline{r}) = 1/(2\pi)^3 \int \chi(\underline{q}) e^{i\underline{q}\cdot\underline{r}}\, d\underline{q}$$

and

$$\chi(\underline{q}) = \int \chi'(\underline{r}) e^{-i\underline{q}\cdot\underline{r}} d\underline{r} \qquad \text{A.3}$$

and the pairs $(M(\underline{r}), M'(\underline{q}))$ and $(H(\underline{r}), H'(\underline{q}))$ are connected by similar equations.

From the property of the Delta function $\delta(\underline{q})$:

$$\delta(\underline{q}) = 1/(2\pi)^3 \int e^{-i\underline{q}\cdot\underline{r}}\, d\underline{r} \qquad \text{A.4}$$

it follows that:

$$M'(\underline{q}) = \chi(\underline{q})H'(\underline{q}) \qquad A.5$$

For a uniform field $H(\underline{r}) = H$, $H'(\underline{q}) = (2\pi)^3 H\, \delta(\underline{q})$ so:

$$M(\underline{r}) = H \int \chi(\underline{q})\, \delta(\underline{q}) e^{i\underline{q}\cdot\underline{r}}\, d\underline{q}$$
$$= H\, \chi(0)$$

$\chi(\underline{q})$ for $\underline{q} = 0$ is therefore identified as the uniform static susceptibility χ of the system.

The total magnetic moment m induced by a magnetic influence is:

$$m = \int M(\underline{r})d\underline{r} = 1/(2\pi)^3 \iint M'(\underline{q}) e^{i\underline{q}\cdot\underline{r}} d\underline{q}\, d\underline{r}$$
$$m = M'(0) = \chi H'(0) \qquad A.6$$

from the Delta function property. This useful theorem, that the total moment induced is equal to the uniform static susceptibility multiplied by the zeroth Fourier component of the applied field, was proved by Doniach and Wohlfarth (R 1.31) for the special case where $H(\underline{r}) = H\, \delta(\underline{r})$, so that $H'(\underline{q}) = H$, but it can be seen to be more general.

b) Two Band Molecular Field-Linear Response Model for a Transition Metal

We consider a metal consisting of two bands, an s and a d band. External fields $H_s(\underline{r})$ and $H_d(\underline{r})$ respectively are applied to the bands and we make the assumption that they interact with each other to give an energy of:

$$H_{sd} = A \int M_s(\underline{r})\, M_d(\underline{r})\, d\underline{r} \qquad \text{A.7}$$

where the M's are the magnetisations of the bands. The effective fields $H^+(\underline{r})$ acting on the bands are now:

$$\begin{aligned} H_s^+(\underline{r}) &= H_s(\underline{r}) - A\, M_d(\underline{r}) \\ H_d^+(\underline{r}) &= H_d(\underline{r}) - A\, M_s(\underline{r}) \end{aligned} \qquad \text{A.8}$$

By Fourier transforming these equations according to equation A.3, the $\underline{q}$th Fourier components of the magnetisation $M'(\underline{q})$ are given by:

$$\begin{aligned} M_s'(\underline{q}) &= \chi_s(\underline{q})(H_s'(\underline{q}) - A\, M_d'(\underline{q})) \\ M_d'(\underline{q}) &= \chi_d(\underline{q})(H_d'(\underline{q}) - A\, M_s'(\underline{q})) \end{aligned} \qquad \text{A.9}$$

where $\chi_s(\underline{q})$ and $\chi_d(\underline{q})$ are the susceptibilities of the two bands.

The total magnetic moments m_s and m_d induced in each band are now obtained from equation A.6 as:

$$\begin{aligned} m_s &= \chi_s(H_s'(0) - A\, m_d) \\ m_d &= \chi_d(H_d'(0) - A\, m_s) \end{aligned} \qquad \text{A.10}$$

These two equations are solved simultaneously to give:

$$\begin{aligned} m_d(1 - \chi_s\, \chi_d A^2) &= \chi_d(H_d'(0) - A\, \chi_s H_s'(0)) \\ m_s(1 - \chi_s\, \chi_d A^2) &= \chi_s(H_s'(0) - A\, \chi_d H_d'(0)) \end{aligned} \qquad \text{A.11}$$

which gives a total magnetic moment $m = m_s + m_d$ of:

$$\begin{aligned} m(1 - \chi_s\, \chi_d A^2) = {} & H_s'(0)\, \chi_s(1 - A\, \chi_d) \\ & + H_d'(0)\, \chi_d(1 - A\, \chi_s) \end{aligned} \qquad \text{A.12}$$

We now particularise the form of the applied fields as:

$$H_{\substack{s \\ d}}(\underline{r}) = H + H^*_{\substack{s \\ d}}\, \delta(\underline{r}) \qquad \text{A.13}$$

so that the Fourier transforms of the fields are:

$$H'_{\substack{s \\ d}}(\underline{q}) = (2\pi)^3 H\, \delta(\underline{q}) + H^*_{\substack{s \\ d}} \qquad \text{A.14}$$

Substituting this into equation A.12 the resulting magnetic moment induced in a specimen of volume V is:

$$m = \left(\chi_s + \frac{\chi_d (1 - \chi_s A)^2}{1 - \chi_s \chi_d A^2} \right) VH$$

$$+ \frac{H_s^* \chi_s (1 - A \chi_d)}{1 - \chi_s \chi_d A^2} + \frac{H_d^* \chi_d (1 - A \chi_s)}{1 - \chi_s \chi_d A^2} \qquad \text{A.15}$$

where we have taken $\underset{\underline{q} \to 0}{\text{Limit}} \quad \delta(\underline{q}) = V(2\pi)^{-3}$

From the form of the interaction between a local moment and conduction electrons, equation 1.21.2

$$\frac{-2JV}{N} \underline{S} \cdot \underline{s}(0) = -\frac{JV}{N \mu_B} \langle S_z \rangle \int M(\underline{r}) \delta(\underline{r}) \, d\underline{r} \qquad \text{A.16}$$

where $M(\underline{r}) = 2 \mu_B s(\underline{r})$ and N is the number of atoms in the solid, one can see, from comparison with equation A.1, that:

$$H_{\substack{s \\ d}}^* = J_{\substack{s \\ d}} \frac{V}{N \mu_B} \langle S_z \rangle \qquad \text{A.17}$$

where J_s and J_d indicate the strength of the interaction of the moment at $\underline{r} = 0$ with the s and d bands.

The coupling constant A may be estimated in a similar

manner by taking the interaction between an s band and a set of local d moments at $\underline{R}_n$ to be of the form of equation A.16 and then smearing the local d moments out into a d band. If J_{sd} is the Schrieffer-Wolff coupling constant then the interaction energy is:

$$H_{sd} = -\frac{J_{sd}\, V}{\mu_B N} \sum_n \langle S_z^n \rangle \int M_s(\underline{r})\, \delta(\underline{r} - \underline{R}_n)\, d\underline{r} \qquad A.18$$

and because:

$$M_d(\underline{r}) = 2\mu_B \sum_n \langle S_z^n \rangle\, \delta(\underline{r} - \underline{R}_n) \qquad A.19$$

we obtain:

$$H_{sd} = -\frac{J_{sd}\, V}{2\mu_B^2 N} \int M_d(\underline{r})\, M_s(\underline{r})\, d\underline{r} \qquad A.20$$

and comparing this with equation A.7 we obtain:

$$A = -\frac{J_{sd}\, V}{2\mu_B^2 N} \qquad A.21$$

The first term of equation A. 15 is to be interpreted as the moment due to the uniform susceptibility of the metal, and the second and third as the magnetic moments induced by the

local spin coupling into the s and d bands by means of an interaction of the form given by equations A.16 and A.17. If $A\chi_d > 1$, a spin coupled by direct exchange to the s band will indue a negative moment - this might correspond to Gd in Pd, while if $A\chi_s < 1$ a spin coupled by a positive J_d to the d band would induce a postive moment. This is, in fact, how Doniach and Wohlfarth (R 1.31) interpreted the FePd giant moment. They derived equation A.15 for the special case of $\chi_s = 0$, and were able to fit the ferromagnetic and paramagnetic moments of Fe with the parameter $J_d = +0.15$ eV. Shimizu (R 1.44, R 1.78) developed a uniform two band model of Pd, and derived the first term of equation A.15. He obtained the constant A in the same way as we did here, but used for J_{sd} the direct exchange constant, which he estimated from spectroscopic data to be +0.25 eV, and found it to be too small to give any substantial enhancement of the static susceptibility. However, as we will note shortly, a negative J_{sd} up to 1 eV or more can arise from admixture effects, and is capable of giving a considerable enhancement.

A certain amount of progress can be made in estimating the magnitudes of the parameters in equation A.15. Vuillemin and Priestly (R 1.45), from Fermi Surface studies, have suggested that the Pd s band contains 0.36 electrons. Using

a free electron model, a Fermi energy of 3.1 eV is obtained and hence $\chi_s = 0.64 \times 10^{-6}$ emu/cm^3. Doniach (R 1.50), from an examination of the resistance minimum and paramagnetic Curie temperature data for CuMn, a typical d virtual bound state in an s matrix material, has concluded the J_{sd} is roughly -1 eV. By equation A.21 this gives $A = 0.14 \times 10^6$ and $A\chi_s = .09$. Therefore, $(1 - A\chi_s)$ is very close to unity, and the calculation of Doniach and Wohlfarth (R 1.31) proceeds unaltered except that their uniform Pd susceptibility is now approximately our $\chi_d(1 - A^2 \chi_s \chi_d)^{-1}$, neglecting χ_s.

The moment induced in Pd by one Gd atom is $-1.5\,\mu_B$ (R 1.46), and this quantity will be given by the second term of equation A.15. If it is assumed that $A\chi_d \gg 1$, then:

$$\frac{-A\chi_s \chi_d H_s^*}{1 - \chi_s \chi_d A^2} = -1.5\,\mu_B \qquad \text{A.22}$$

and taking the value of $A\chi_s$ given above and the value of the uniform Pd susceptibility as 90×10^{-6} emu/cm^3 (R 1.47), V/N for Pd as 14.7×10^{-24} cm^3 and $\langle S_z \rangle = 7/2$, a figure of $J_s = +0.2$ eV is obtained.

The implication of the model of Pd which we have used, is that the susceptibility is enhanced first by intra-d band interactions, as in equation 1.38, to give χ_d, and then by

the hybridisation mechanism to give χ_{pd} where:

$$\chi_{pd} = \chi_d(1 - \chi_s A)^2/(1 - \chi_s \chi_d A^2) \qquad \text{A.23}$$

In the above equation, all the quantities except χ_d have been estimated (χ_s being ignored as it is much less than χ_d) and it may be solved to give $\chi_{pd}/\chi_d = 1.91$. This shows that, in the context of this model, the d band, which has already been enhanced by intra band interactions to give χ_d, is further enhanced by a factor of 1.91 to give the measured susceptibility χ_{pd}.

The value of $J_s = +0.2$ eV which is obtained is rather larger than that which might be expected from the direct exchange mechanism, which could be of the order of +.05 eV, from data from the spectroscopy of the free ion. However, if J_{sd} is taken to be 3 eV, rather than 1 eV, J_s is correspondingly decreased to +.066 eV, although because $A\chi_d$ is not very much greater than unity, being 3.7, this value of J_s is rather an underestimate. With the value of $J_{sd} = 3$ eV, χ_{pd}/χ_d is found to be about 10 from equation A.23. We see then, that taking $J_{sd} = 3$ eV gives a reasonable value for the Gd exchange constant, and gives a susceptibility enhancement of Pd which is <u>entirely</u> due to the hybridisation mechanism and does not need to take account of

intra d band interactions. If this is indeed so, then the possibility would appear that this band analogue of the virtual bound state admixture antiferromagnetic exchange might even be a driving force for the ferromagnetism (or rather ferrimagnetism) of the 3d metals. This possibility has been suggested qualitatively by Brooks (R 1.103).

For GdPd we have so far assumed that the negative conduction electron polarisation is due to a positive exchange between the f shell and the s band. However, a negative coupling J_d between the f shell and the d band (possibly an admixture effect due to f-d mixing) could also give the same result, and comparing the second and third terms of equation A.15 (taking $J_{sd} = 1$ eV) a figure of $J_d = -.017$ eV is obtained.

For the FePd system Doniach and Wohlfarth (R 1.31) obtained $J_d = +.15$ eV, but they did not specify by what mechanism the iron atom coupled into the d band of the Pd. A model such as that proposed by Lederer and Mills (R 1.97) for NiPd would be expected to produce a positive coupling. They considered a d band enhanced by interactions of the form $U \sum_i n_{i\uparrow} n_{i\downarrow}$, the n's being number operators for electrons on Wannier sites i. An extra interaction in the Ni impurity cell is taken as $\Delta U\, n_{0\uparrow} n_{0\downarrow}$, and this enhances the susceptibility further. For one atom of Ni the susceptibility does

not diverge, but it might do so for Fe to give an effective $-J_d \underline{S}.\underline{s}$ interaction with a positive J_d(R 1.101).

An alternative interpretation of the behaviour of FePd is that the Fe virtual bound state couples to the Pd s band by the usual antiferromagnetic admixture exchange constant J_s (B. R. Coles, 1970 private communication). Comparing the J_s and J_d necessary to do this from equation A.15, $J_d = -J_s A \chi_s$ and taking J_d to be +.15 eV (R 1.31) and J_{sd} to be 1 eV, the antiferromagnetic exchange constant J_s is found to be -1.7 eV, a not unreasonable figure. This coupling hypothesis is, therefore, feasible.

The results of this rough preliminary calculation are encouraging. Further work of calculating the wave vector dependent susceptibility for the case where intra d band interactions are explicitly included, is in progress. In the spirit of the above phenomenological model, the interaction Hamiltonian will be taken to be of the form:

$$\frac{I}{2}\int M_d^2 (\underline{r})\, d\underline{r} \qquad \text{A.24}$$

to give a molecular field component acting on the d band of:

$$- I M_d (\underline{r}) \qquad \text{A.25}$$

One result of the calculation is that, if only the d band is considered, Wolff's equation (1.38) follows directly from A.24.

APPENDIX B

STABILITY CONDITION FOR A TWO-LINK SUSPENSION

If F_M is at its critical value F_M^c, the suspension will be stationary under the influence of the magnetic forces and static reactions. The forces on each link are shown in Fig. B.1., and taking moments about the top end of each link two equations are obtained.

$$x_1(M_1gf_1/l_1 + F_M^c + m_2g - l_1F_M^c/G) - x_2l_1F_M^c/G = 0$$

$$-x_1F_M^cl_2/G + x_2(m_2gf_2/l_2 + F_M^c - F_M^c\, l_2/G) = 0$$

When these two equations are solved to eliminate x_1 and x_2, equation (3c) of R 3.25 results. The expression may be checked by noting that it becomes equation 3.14 when the parameters of either of the links are set to zero. Experimental confirmation of the correctness is given by the fact that when the parameters of thelower link were changed to $l_2 = 32.3$ cm, $f_2 = 27.1$ cm, $m_2 = 2.66$ gram (so that $P = 250 \times 10^3$, $Q = 6200$, $R = 8.79 \times 10^6$) in order to increase F_M^c, the same C resulted from measurements with both suspensions. With the new heavier suspension F_M^c was increased from 30 dynes to 63 dynes, a valuable gain.

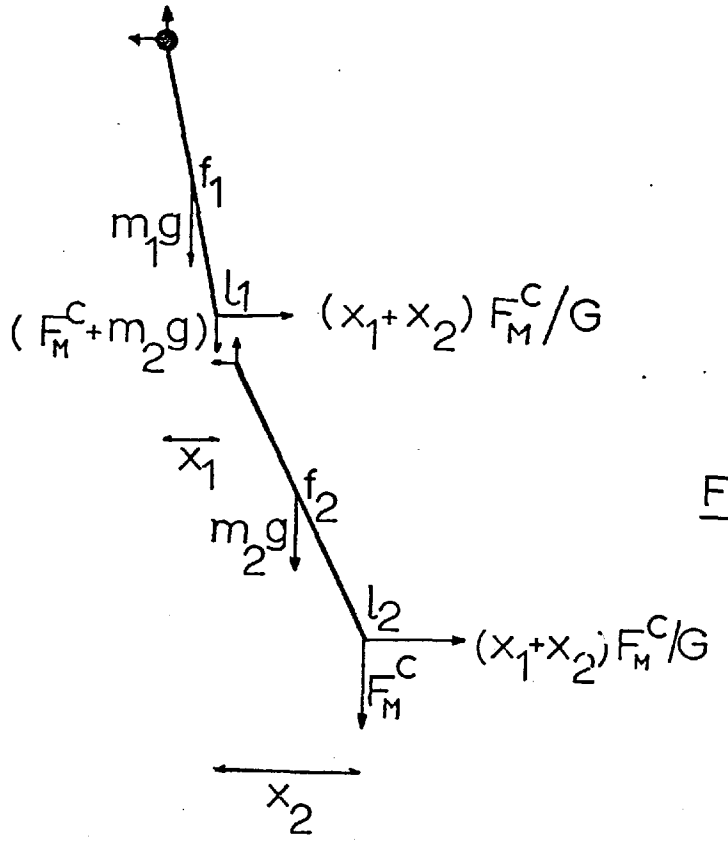


Fig. B.1

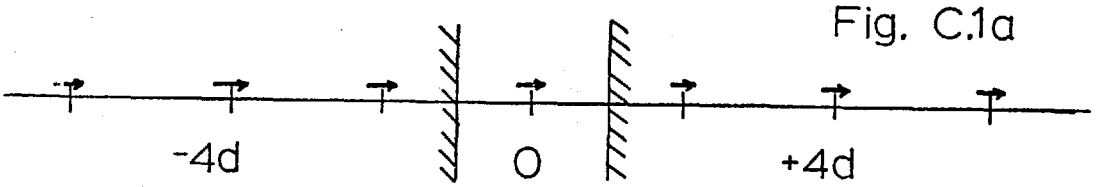


Fig. C.1a

2d

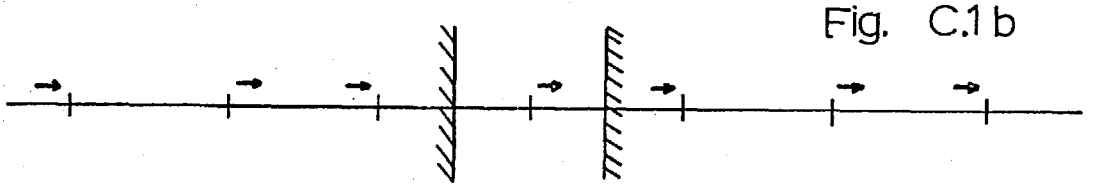


Fig. C.1 b

APPENDIX C

THE LATERAL FORCE DUE TO AN INFINITE SERIES OF IMAGES

The series of images is shown in Fig. C.1a for the situation when the moment is situated centrally between the pole pieces. The images lie at $x = 2nd, -\infty < n < +\infty$ .. When the moment is deflected a small amount x to the right the images will take up the positions shown in Fig. C.1b. The movement of each image is $\pm$ x. However, the distances between the moment and the images at n = an even integer are unchanged, so they make no contribution to the force acting on the moment. Thus, only the change in distance, 2x, between the moment and the images at 2nd, n = an odd integer, need to be taken into account.

If the force between the moment and its image a distance y away is F(y), and y is changed by δy, then the new force due to one image is:

$$F(y + \delta y) = F(y) + \frac{\partial F}{\partial y}\delta y + \tfrac{1}{2}\frac{\partial^2 F}{\partial y^2}\delta y^2 + 1/6\,\frac{\partial^3 F}{\partial y^3}\delta y^3 + \ldots\ldots\ldots$$

and similarly for the other image with δy negative. The force

F' acting on the moment is the difference between the two:

$$F' = \frac{2\partial F}{\partial y}\delta y + \frac{1}{3}\frac{\partial^3 F}{\partial y^3}\delta y^3 + \cdots\cdots$$

and as $\delta y = 2x$, and there are contributions from an infinite series, then:

$$F' = \sum_n \left(4\frac{\partial F(y)}{\partial y}x + \frac{8}{3}\frac{\partial^3 F(y)x^3}{\partial y^3} + \cdots\cdots\right)$$

where the sum is over $n = 0,1,\ldots\infty$, $y = 2d(2n + 1)$. F(y) may easily be calculated to be $6\, m_x^2/y^4$ where m_x is the x component of the magnetic moment of the specimen (the expression given previously for F(y) is too large by a factor of two) and one obtains from substituting F(y) in the above equation:

$$F' = x\frac{3m_x^2}{d^5}\sum_{n=0}^{\infty}\frac{1}{(2n+1)^5} + x^3\frac{15m_x^2}{d^7}\sum_{n=0}^{\infty}\frac{1}{(2n+1)^7}$$

The two infinite series are related (R 3.31) to the Riemann Zeta function, which is tabulated (R 3.32). One finds, from putting in the num erical values, that the term in x is increased by 0.4% and the term in x^3 is increased by 0.1% of their values

when only one image is considered (taking the n=0 term only). The additional contribution from the infinite series of images is therefore negligible. (See also R 3.39).

APPENDIX D

THE MAGNETIC PROPERTIES OF SOME MANGANESE-SILICON COMPOUNDS

At the request of Professor Anderson, measurements were made of the magnetic properties of some Mn-Si alloys in the temperature region $4.5^{\circ}K$ to $77^{\circ}K$, while the improvements to the Susceptibility Balance, which are discussed in Chapter 3, were being incorporated. The measurements are recorded here for future reference.

The properties of the four compounds $MnSi_2$, MnSi, Mn_5Si_3, Mn_3Si have been previously investigated in this laboratory by C. G. Harrison who discussed his results in an internal Report (RE1; the references of this Appendix are placed at the end of it, preceding the Figures). The compounds were formed by vacuum melting, with no subsequent heat treatment, and presented to Harrison in the form of polycrystalline ingots. He found that their X-ray powder diffraction photographs showed the presence of pure Mn, Si and other unidentified materials. As X-ray diffraction is the least sensitive of those means of detecting impurities which were mentioned in Chapter 2, it is apparent that the compounds were of extremely poor metallurgical quality. This is serious, because from the high resistivities of most of the materials (in the region of a few 1000 $\mu\Omega$cm) which Harrison found, it seems probable that they are degenerate semiconductors whose properties, particularly RKKY exchange couplings, will be very sensitive to impurity content.

$MnSi_2$

Harrison found that this compound possessed no magnetic moment in the range 300°K - 77°K, the modulus of its susceptibility being less than 10^{-7} emu/g. Its resistivity at room temperature was about 0.5 $\mu\Omega$ cm, much higher than those of the others, indicating superior purity. NiSi and CoSi have also been reported to have zero moment (RE2) and B. R. Coles has informed the writer (1969 private communication) that $CoSi_2$ has been found to have no localised moment and to be a superconductor.

Because of its lack of magnetic behaviour, no measurements were made on $MnSi_2$ below 77°K.

MnSi

Williams et al (RE2), found that MnSi has an effective paramagnetic moment of 1.4 μ_B, shows ferromagnetic behaviour below 30°K, and at 1.4°K its M-H curve is linear up to 6.2 kOe where it saturates at 0.4 μ_B per Mn atom. Our results, which are shown at the end of this Appendix, are consistent with Williams et al's measurements, except that we obtain a paramagnetic moment of 2.1 μ_B. Brown et al (RE3) have done neutron diffraction experiments on the compound, and have found no antiferromagnetic moment in zero field below the ordering temperature.

Mn_5Si_3

Susceptibility measurements on the compound have been made by

Yasukochi et al (see RE4), Watanabe (RE4), Van Con (RE5) and Narasimhan et al (RE6). The latter measurements, which extend from 660°K to 50°K show that the compound obeys the Curie Weiss Law down to 62°K where it orders anti-ferromagnetically. Neutron diffraction experiments have been done on the compound (RE7) and interpreted in detail by Lander and Brown (RE8). It is found that the Neel point is 68°K and the ordering which takes place is of great complexity.

In the results which we have obtained, we see the characteristic peak in susceptibility near the ordering temperature, but as the temperature is lowered, the magnetisation increases below 30°K. We attribute this effect to contamination of the specimen by ferromagnetic MnSi; 5% would be enough to give it. Further evidence for this is that the M-H curve at 4.5°K tends to saturate above 6 kOe, while the M-H curve of an antiferromagnet would not. The M-H curve of the compound at 77°K is linear.

Mn_3Si

This is the only one of the Manganese-Silicon compounds apart from $MnSi_2$ whose magnetic properties (to the writer's knowledge) have not been examined previously. In the Figure we show the results obtained by Harrison (RE1) above 77°K, and by the writer below that temperature.

Harrison found that the M-H curve at room temperature was linear, but at 77°K it showed signs of saturation. From his results we have

deduced a paramagnetic moment of $2.4\mu_B$. An M-H curve at $64^{\circ}K$ showed that the moment per Mn atom saturated to $0.009\mu_B$ in a field of around 5 kOe, but no M-H curves were taken at lower temperatures.

REFERENCES

RD1 HARRISON, C. G., 1968. Materials Section Internal Report, Department of Electrical Engineering, Imperial College.

RD2 WILLIAMS, H. J., WERNICK, J. H., SHERWOOD, R. C., WERTHEIM, G. K., 1966. J. App. Phys., 37, 1256.

RD3 BROWN, P. J., FORSYTH, J. B., LANDER, G. H., 1968. J. Appl. Phys., 39, 1331.

RD4 KANEMATSU, K., 1962. J. Phys. Soc. Jap., 17, 85.

RD5 VAN CON, 1965. Comptes Rendues. Acad. Sci. Paris, 262, 11.

RD6 NARASIMHAN, K.U.S.L., REIFF, W. M., STEINFINK, H., COLLINS, R. L., 1970. J. Phys. Chem. Solids, 31, 1511.

RD7 LANDER, G. H., BROWN, P. J., FORSYTH, J. B., 1967. Proc. Phys. Soc., 91, 332.

RD8 LANDER, G. H., BROWN, P. J., 1967. Phil Mag. 16, 521.

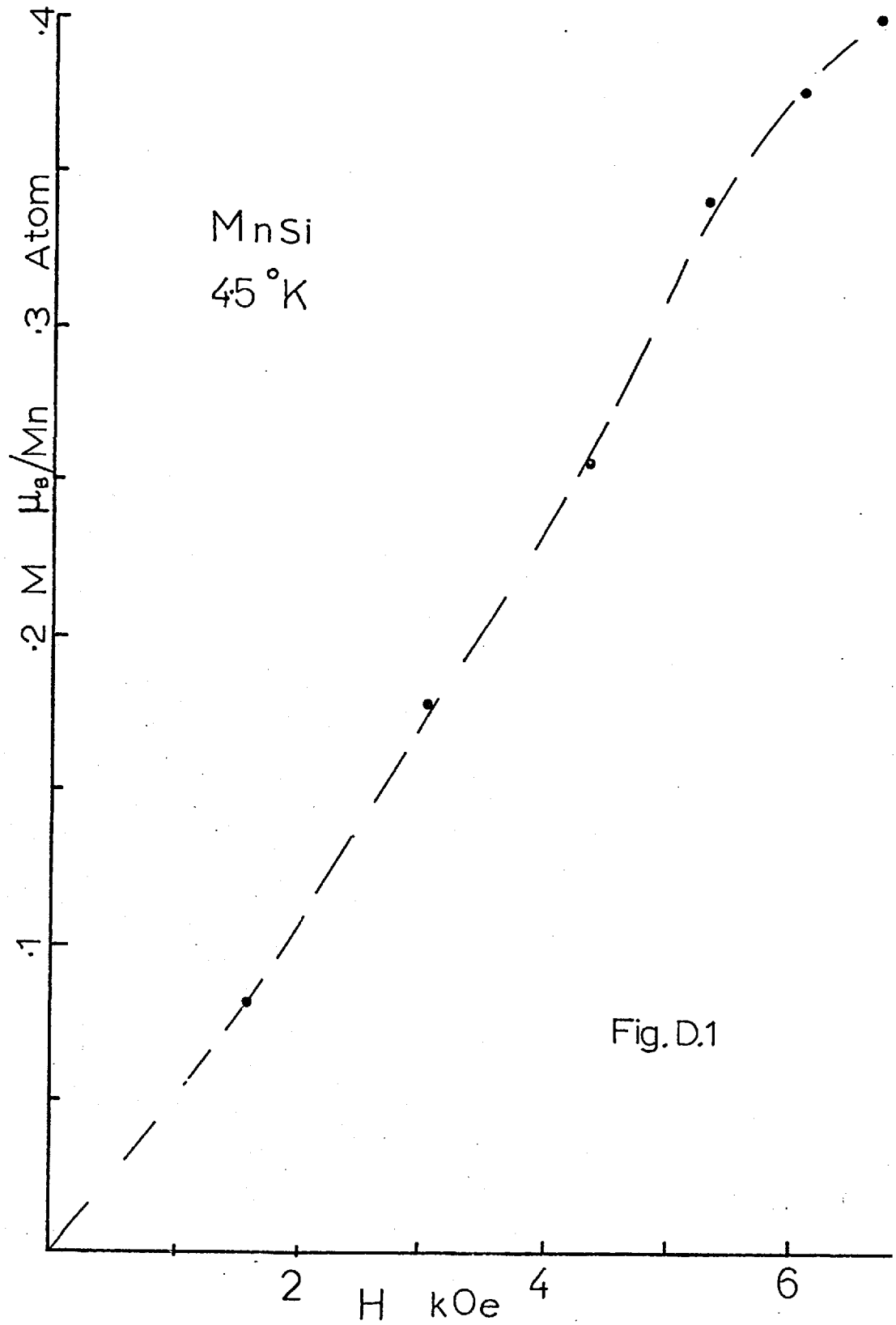


Fig. D.1

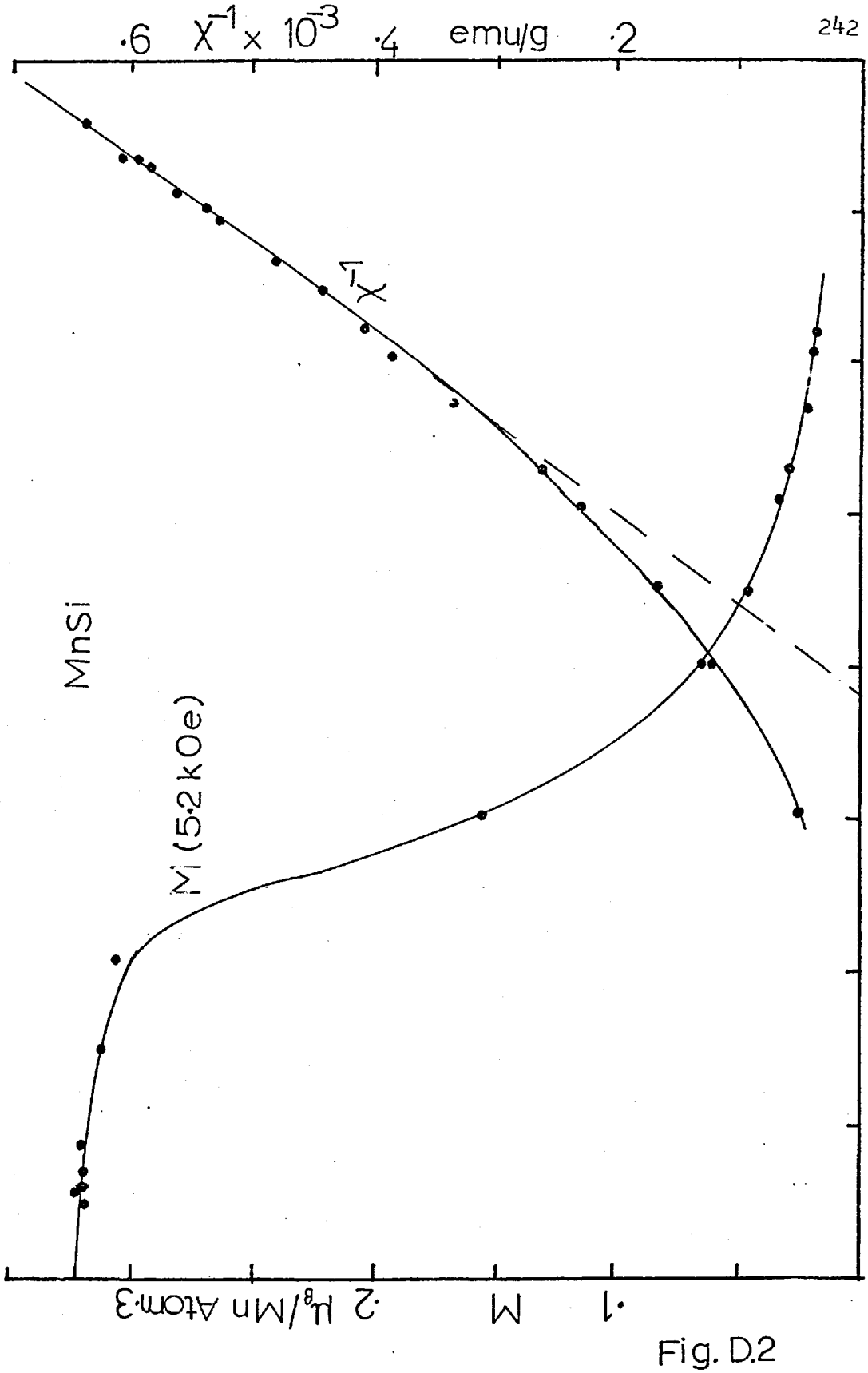

·6 $\chi^{-1} \times 10^{-3}$ ·4 emu/g ·2
χ^{-1}
MnSi
M (5·2 kOe)
20 40 60 T °K
·1 M ·2 μ_B/Mn Atom·3

Fig. D.2

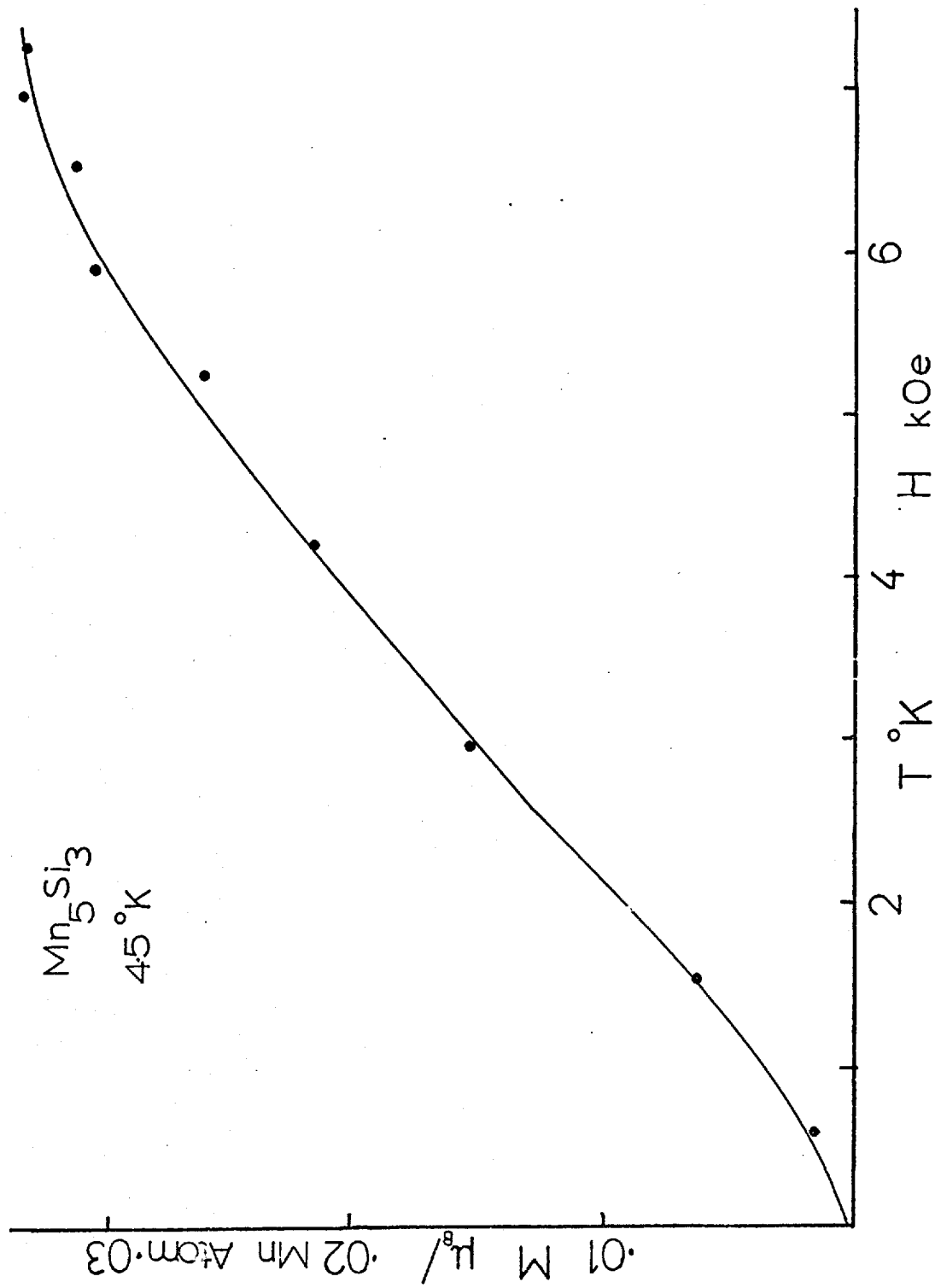


Fig.D.3

Fig. D.4

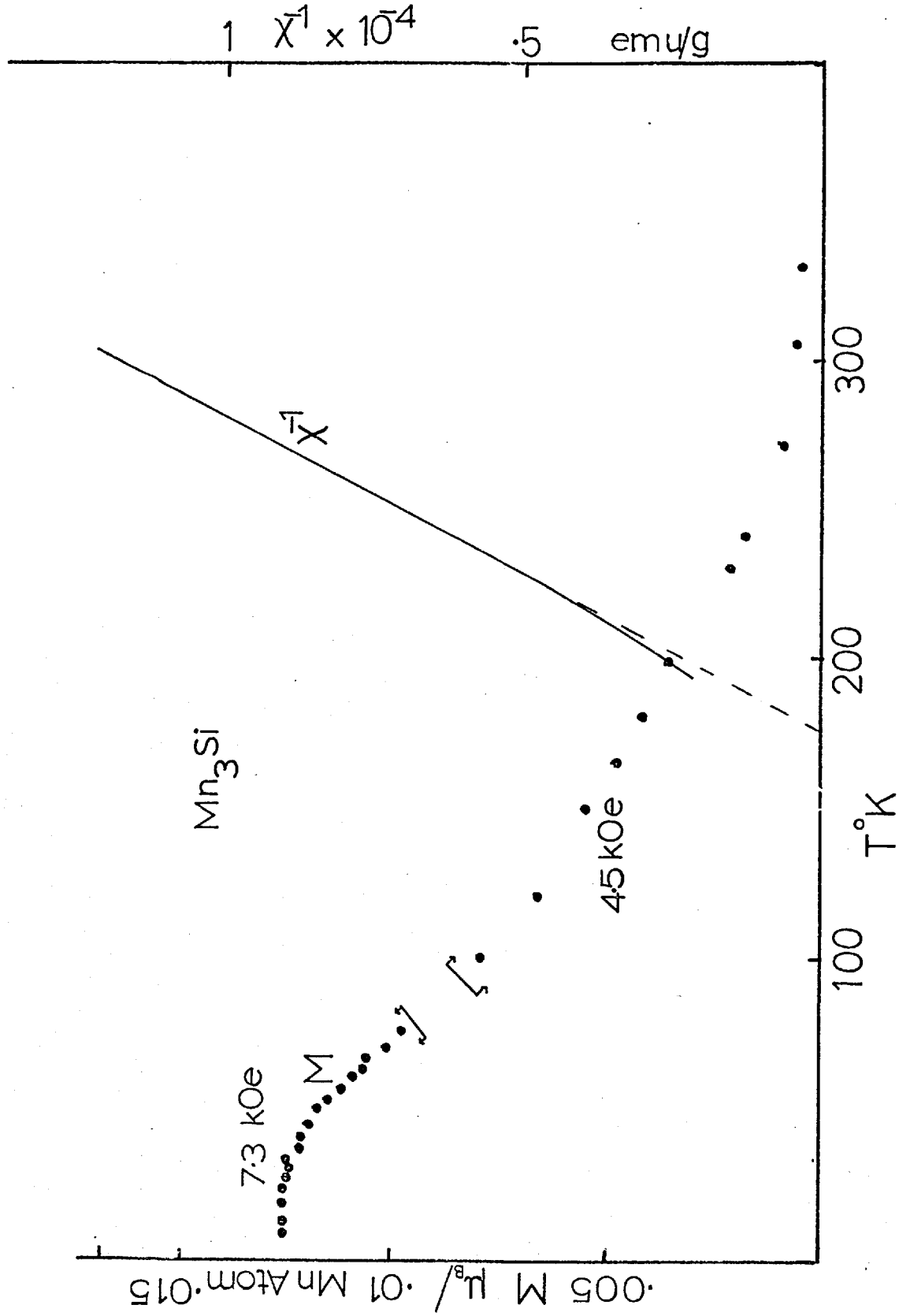

1 $\chi^{-1} \times 10^{-4}$
·5 emu/g
χ^{-1}
Mn_3Si
4.5 kOe
7.3 kOe
M
100
200
300
T°K
·005 M μ_B/ ·01 Mn Atom ·015

Fig. D.5

APPENDIX E

INTERACTIONS IN THE ANDERSON MODEL

It would seem probable, within the context of the Anderson Model (R 1.32), that as the concentration of potentially magnetic impurities is increased, the tendency for a moment to form will become stronger. (An apparent experimental refutation of this suggestion, the behaviour of the Au V system (R 1.149) and references therein , will be discussed later.) The reason for this is that the molecular field at one site, caused by the moments at all the others, will help to polarise the moment at the first site. A mechanism for inter-impurity interactions exists in the many impurity Anderson Model, as, for instance, the mixing operator $V_{kd1} c^{+}_{k\sigma} c_{d1\sigma}$ will transfer an electron from the orbital at site 1 into a conduction state k and thence, with another mixing interaction on to site 2. In the magnetic limit, Schrieffer and Wolff (R 1.63) have showed that this mechanism may be transformed into an equivalent RKKY interaction.

Alexander and Anderson (R 1.148) and Moriya (R 1.150) have considered the special case of two neighbouring impurities coupled by a transfer Hamiltonian:

$$\sum_{\sigma} V_{12} \left(c^{+}_{1\sigma} c_{2\sigma} + c^{+}_{2\sigma} c_{1\sigma} \right) \qquad \text{E1}$$

and have examined the conditions for the formation of moments. Lederer and Blandin (R 1.147) have discussed the effect of interactions on the

formation of moments on impurities which are of the same symmetry type as the matrix in which they are situated, but which have a different intra-atomic Coulomb interaction. Tournier and co-workers (R 1.152 and references therein) have discussed how the presence of neighbouring impurities may lead to reduction of the characteristic spin fluctuation temperature of the cluster and so give a tendency towards magnetic behaviour.

It is suggested that the many-impurity Anderson Model might be, in a mean field approximation, reduced to a one-impurity problem by incorporating in the Anderson equations (1.15) an extra term,

$$-cA\,(n_{d\uparrow} - n_{d\downarrow})^2 \qquad \text{E2}$$

where c is the fractional concentration of impurities and A is a positive constant, which for a given metallurgical system will be somewhat dependent on the state of magnetisation of the impurity, but independent of concentration (see Doniach R 1.50 for a discussion of the concentration dependence of a related quantity, the Paramagnetic Curie Temperature).

A molecular field justification of E2 in the ordered state follows from the expression for the energy of a spin acted upon by a molecular field caused by all the other spins (equation 1.46), in for example, a ferromagnetic state:

$$H_i = -S_i^z \langle S^z \rangle \sum_{j \neq i} 2\, J_{ij} \qquad \text{E3}$$

where the sum is over moment sites. If S^z is replaced by $(n_{d\uparrow} - n_{d\downarrow})/2$, equation E3 becomes:

$$-cA\,(n_{d\uparrow} - n_{d\downarrow})(\langle n_{d\uparrow}\rangle - \langle n_{d\downarrow}\rangle) \qquad E4$$

where $A = \sum_{j\neq i} J_{ij}/2$ and the sum is now over all possible impurity sites (Doniach R 1.50). As the spin will always lie in the direction of the molecular field at its own site, the interaction will tend to magnetise the impurity, although A will not necessarily be given by the same expression as that above for other types of magnetically ordered states.

A rough attempt to estimate the size of A may be made by using the expression for the Paramagnetic Curie Temperature θ of an alloy in which the moment has formed. This is given by (R 1.50):

$$\theta = c \sum_{j\neq i} J_{ij}\, 2S(S+1)/3k \qquad E5$$

Hence

$$A = 3k\theta/cS(S+1) \qquad E6$$

For a typical magnetic dilute alloy CuMn, $\theta/c = 800^{\circ}K$ (R 1.50) which produces a value of A = .006 eV (taking S = 5/2). This appears, at first sight, to be too small to compete with the other energies in the Anderson model, which are typically of the order of 1 eV. However, A might tend to be larger than the value estimated above, for two reasons.

First, the five-fold degeneracy of the d level may increase the magnitude of the interaction of type E2 by, perhaps, a factor S(S + 1), wh ere S is the final spin value. Second, we have estimated A from data on a material i which the moment is well defined. For a moment which is just forming, the interaction of the conduction electrons with the local state could be greater, because in this situation the density of states of the impurity virtual bound state will be large in the vicinity of the Fermi level.

The modified Anderson Model which contains E2 may be solved in a straightforward manner. If E2 is multiplied out we obtain:

$$-cA\ (n_{d\uparrow} + n_{d\downarrow} - 2n_{d\uparrow} n_{d\downarrow}) \qquad \text{E7}$$

because $n_a^2 = n_a$. (For a discussion of the validity of this kind of relation in a molecular field approximation see Sherrington R 1.150).

It is seen, then, that the effect of E2 is to modify the parameters of the single impurity Anderson Model to:

$$\begin{aligned} E_d &\rightarrow E_d - cA \\ U &\rightarrow U + 2cA \end{aligned} \qquad \text{E8}$$

and so, within this scheme, the many-impurity model can be solved just as easily as the single-impurity model. The increase of U will always tend to help the formation of the moment, but the change of E_d will help or hinder it according to the position of E_d with respect to the Fermi

level (Anderson R 1.32).

The latter effect notwithstanding, we see, according to the expressions E8, that if a solitary impurity is just on the verge of magnetism at $0^{\circ}K$, it should gradually become polarised as the concentration is increased. It is less clear how the system will behave in the paramagnetic state, but the following qualitative argument suggests that in that situation U might also be enhanced by concentration effects.

The quantity which is important in the paramagnetic state is the expectation value of the square of the impurity moment. Since the impurity moment lies along the direction of the instantaneous molecular field at its site, it will be an odd function of that field, and so the expectation value of the square of the moment will have in it a component proportional to the expectation value of the square of the molecular field. We identify the molecular field as being proportional to the conduction electron spin density $\underline{S}(\underline{r})$ at the impurity site, caused by all the other moments in the metal. This is given, in general, by:

$$\underline{S}(\underline{r}) = \sum_{j} J'(\underline{r},\underline{R}_j)\underline{S}_j \qquad \text{E9}$$

where the sum is over all the moment sites j except that of the impurity.

In the paramagnetic state, in which to a first approximation $\langle \underline{S}_j \circ \underline{S}_k \rangle = \delta_{j,k} S(S+1)$, we obtain:

$$\langle \underline{S}^2(\underline{r}) \rangle = \overline{\sum_j} \; J'^2(\underline{r},\underline{R}_j)\; S_j(S_j + 1) \qquad \text{E10}$$

a quantity which is non-zero, and so may act to polarise the impurity. If the other spins are potentially magnetic impurities, then $S_j(S_j + 1)$ will be replaced by $\frac{3}{4}(n_{j\uparrow} - n_{j\downarrow})^2$, and the problem must be solved self-consistently. In a dilute alloy, $\langle \underline{S}^2(\underline{r}) \rangle$ will be proportional to concentration.

In this situation, the derivation of E4 will not be valid, and it may be necessary to go beyond the Hartree Fock approximation and see how dynamical effects influence the Localised Spin Fluctuati (R 1.35, R 1.51) rate of the impurity.

Disordered solid solutions of V in Au show two distinct types of variation of the V moment with concentration (R 1.149). At concentrations below about 0.3%, V appears to bear no local moment. Just above that concentration, a concentration independent moment of about $1.6\mu_B$ comes into existence. This could be a consequence of the mechanism which we have discussed in this Appendi However, as the concentration of V is increased, it is found that the average V moment decreases, and approaches zero at around 30%. Crevelling and Luc (R 1.149) have calculated that the effect is consistent with the hypothesis that no V atom bears a moment if one of its nearest or next nearest neighbours is another V atom. The interaction relevant to this situation is possibly the direct

transfer between impurities (expression E1), which acts so as to prevent magnetism, as in pure V metal itself.

REFERENCES

Chapter 1 and Introduction

R 1.1 WYBOURNE, B. G., 1965. Spectroscopic Properties of Rare Earths, (Interscience, New York).

R 1.2 Magnetism. Eds RADO, G. T. and SUHL, H., 1963 (Academic Press, New York).

R 1.3 BLEANEY, B., STEVENS, K. W. H., 1953. Reports on Progress in Physics, 16. (Phys. Soc. Lond).

R 1.4 HEINE, V., 1960. Group Theory in Quantum Mechanics, (Pergamon, Oxford).

R 1.5 BETHE, H., 1929. Ann. der Physik, 3, 133.

R 1.6 JUDD, B. R., 1963. Operator Techniques in Atomic Spectroscopy, (McGraw Hill, New York).

R 1.7 JAHN, H. A., TELLER, E., 1937. Proc. Roy. Soc. A 161, 220.

R 1.8 KRAMERS, H. A., 1930. Proc. Amsterdam Acad. Sci. 33, 959.

R 1.9 STEVENS, K. W. H., 1952. Proc. Phys. Soc. A 65, 209.

R 1.10 HUTCHINS, M. T., 1964. 16 Solid State Physics (Academic Press, New York).

R 1.11 BOWERS, K. D., OWEN, J., 1955. Reports of Prog. in Physics, 13, (Phys. Soc. Lond).

R 1.12 WHITE, J. A., WILLIAMS, H. J., WERNICK, J. H., SHERWOOD, R., 1963. Phys. Rev. 131, 1039

R 1.13 MAPLE, B. M., FISK, Z., 1968. Eleventh International Conference on Low Temperature Physics (St Andrews).

R 1.14 MADER, K. W., SWIFT, W. M., 1968. J. Phys. Chem. Solids, 29, 1759.

R 1.15 WILLIAMS, G., HIRST, L. L., 1969. Phys. Rev. 185, 407

R 1.16 MURANI, A. P., 1970. Proc. Phys. Soc., J. Phys.C.3.

R 1.17 HIRST, L. L., 1967. Solid State Comm. 5, 751.

R 1.18 VAN VLECK, J. H., PENNEY, W. G., 1934. Phil. Mag., 17, 961.

R 1.19 BLUME, M., 1966. Phys. Rev., 141, 517.

R 1.20 FREEMAN, A. J., WATSON, R. E., 1965. Phys. Rev. 139A, 1606.

R 1.21 STERNHEIMER, R. M., BLUME, M., PEIERLS, R. F., 1968. Phys. Rev., 173, 376.

R 1.22 SENGUPTA, D., ARTMAN, J. O., 1970. Phys. Rev. B, 1, 2986.

R 1.23 SUGANO, S., SHULMAN, R. G., 1963. Phys. Rev., 130, 517.

R 1.24 WATSON, R. E., FREEMAN, A. J., 1964. Phys. Rev., 134, 1526.

R 1.25 GLADNEY, H. M., VEILLARD, A., 1969. Phys. Rev., 180, 385.

R 1.26 OWEN, J., STEVENS, K. W. H., 1953. Nature, 171, 836.

R 1.27 SHULMAN, R. G., JACCARINO, V., 1956. Phys. Rev. 103, 1126.

R 1.28 WATSON, R. E., FREEMAN, A. J., 1967. Phys. Rev., 156, 251.

R 1.29 FRIE DEL, J., 1954. Adv. Phys., 12, 446, 1958, Nuovo Cimento, Supp. 7, 287.

R 1.30 KITTEL, C., 1968. Solid State Physics 22 (Academic Press, New York).

R 1.31 DONIACH, S., WOHLFARTH, E. P., 1967. Proc. Roy. Soc., 296, 442.

R 1.32 ANDERSON, P. W., 1961. Phys. Rev., 124, 41.

R 1.33 ABRIKOSOV, A. A., GORKOV, L. P., DZYALOSHINSKI, I. E., 1963. Methods of Quantum Field Theory in Statistical Physics, (Prentice-Hall, New Jersey).

R 1.34 WOLFF, P. A., 1961. Phys. Rev., 124, 1030.

R 1.35 RIVIER, N., SUNJIC, M., ZUCKERMANN, 1968. Phys. Rev. Letters 21, 904

R 1.36 CAPLIN, A. D., RIZZUTO, C., 1968. Phys. Rev. Letters, 21, 746.

R 1.37 DIMMOCK, J. O., FREEMAN, A. J., WATSON, R. E., 1966. Proc. Inst. Conf. on Optical Props. of Metals (Ed. F. Abeles, Amsterdam).

R 1.38 SUGAWARA, T., NAGASAWA, H., YOSIDA, S., 1969. 11th Inst. Conf. on Low Temp. Physics (St Andrews).

R 1.39 FISK, Z., 1969. Thesis, University of California (San Diego).

R 1.40 GAINON, D, DONZE, P., SIERRO, J., 1967. Solid State Comm., 5, 151.

R 1.41 BOES, J., VAN DAM, A. J., BIJVOET, J., 1968. Phys. Letters 28A, 101.

R 1.42 KONDO, J., 1969. Solid State Phys. 23, (Academic Press, New York).

R 1.43 BAILYN, 1966. Adv. in Phys., 58.

R 1.44 SHIMIZU, M., 1961. J. Phys. Soc. Japan, 16, 1114.

R 1.45 VUILLEMIN, J. J., PRIESTLY, M. G., 1965. Phys. Rev. Letters, 14, 307.

R 1.46 CRANGLE, J., 1964. Phys. Rev. Letters, 13, 569.

R 1.47 SHALTIEL, D., WERNICK, J. H., WILLIAMS, H. J., PETER, M., 1964. Phys. Rev., 135A, 1347.

R 1.48 KAPLAN, T. A., LYONS, D. H., 1963. Phys. Rev., 129, 2072.

R 1.49 WATSON, R. E., FREEMAN, A. J., 1966. Phys. Rev., 152, 566, 1969, Phys. Rev., 178, 725.

R 1.50 DONIACH, S., 1967. In "Theory of Magnetism in Transition Metals" Varenna Summer School, (Academic Press, New York).

R 1.51 KASUYA, T., 1956. Prog. Theor. Phys., 16, 45,

R 1.52 YOSIDA, K., 1957. Phys. Rev., 106, 893.

R 1.53 KONDO, J., 1964. Prog. Theor. Phys., 32, 37.

R 1.54 DE GENNES, P. G., 1962. J. Phys. Rad., 23, 511.

R 1.55 ROCHER, Y. A., 1962. Adv. in Phys., 43, 233.

R 1.56 PETER, M., DUPRAZ, J., COTTET, H., 1967. Helv. Phys. Acta, 40, 301.

R 1.57 BUSHOW, K. H. J., FAST, J. F., VAN DIEPEN, A. M., DE WIJN, H. W., 1967. Phys. Stat. Sol., 24, 715.

R 1.58 RUDERMAN, M. A., KITTEL, C., 1954. Phys. Rev., 96, 99.

R 1.59 OWEN, J., BROWNE, M. E., ARP, V., KIP, A. F., 1957. J. Phys. Chem. Solids, 2, 85.

R 1.60 KONDO, J., 1962. Prog. Theor. Phys., 28, 846.

R 1.61 FREEMAN, A. J., WATSON, R. E., KOIDE, S., PETER, M. 1965. Phys. Rev., 139A, 167.

R 1.62 COTTET, H., DONZE, P., DUPRAZ, J., GIOVANNINI, B., PETER, M., 1968. Zeit fur Ange. Physik, 24, 249.

R 1.63 SCHRIEFFER, J. R., WOLFF, P. A., 1966. Phys. Rev., 149, 491.

R 1.64 NAGAOKA, Y., 1965. Phys. Rev., 138, A 1112.

R 1.65 YAFET, Y., KITTEL, C., 1952. Phys. Rev., 87, 290.

R 1.66 COQUBLIN, B., SCHRIEFFER, J. R., 1969. Phys. Rev., 185, 847.

R 1.67 CAROLI, B., Thesis, 1966. See Blandin, A., 1967 Theory of Magnetism in Transition Metals. (Academic Press, New York), 1967. J. Phys. Chem. Solids, 28, 1427.

R 1.68 DE GENNES, P. G., 1958. Compt. Rend., 247, 1836.

R 1.69 LIU, S., 1960. Phys. Rev., 121, 451.

R 1.70 HASEGAWA, H., 1959. Prog. Theor. Phys. 21, 483.

R 1.71 WOLFF, P. A., 1960. Phys. Rev., 120, 814.

R 1.72 MAPLE, M. B., 1968. Phys. Letters, 26A, 513, 1969. Thesis, University of California, (San Diego).

R 1.73 ABRIKOSOV, A. A., GORKOV, L. P., 1961. Soviet Phys. J.E.P.T., 12, 1243.

R 1.74 MATTHIAS, B. T., SUHL, H., CORENZWIT, E., 1958. Phys. Rev. Letters, 1, 92.

R 1.75 SHALTIEL, D., WERNICK, J. H., WILLIAMS, H. J., PETER, M., 1964. Phys. Rev., 135A, 1346.

R 1.76 COTTET, H., PETER, M., 1970. To be published.

R 1.77 GIOVANNINI, B., PETER, M., SCHRIEFFER, J. R., 1964. Phys. Rev. Letters, 12, 201.

R 1.78 SHIMIZU, M., TAKAHASHI, T., KATSUKI, A., 1963. J. Phys. Soc. Jap. 20, 26.

R 1.79 DE BOER, F. R., SCHINKEL, C. J., BIESTERBOS, J., 1967. Phys. Letters, 25A, 606.

R 1.80 ELLIOT, R. J., 1965. Magnetism, Vol IIA (Academic Press, New York).

R 1.81 KASUYA, T., 1966. Magnetism Vol IIB, (Academic Press, New York).

R 1.82 ARROTT, A., 1966. Magnetism Vol IIB, (Academic Press, New York).

R 1.83 WALLACE, W. E., 1968. "Electronic Structure of Alloys and Intermetallic Compounds". Rare Earth Research, Vol 3, (Pergamon, Oxford).

R 1.83a 1961, Rare Earth Research, (Ed. Kleber, E. V.), Macmillan, New York).
1962, Rare Earth Research, (Ed. Nachma, J. F., Lundin, C. E.), (Gordon and Breach, New York).

R 1.84 Progress in the Science and Technology of the Rare Earths. (Ed. Eyring, L.), (Pergamon, Oxford).
1964 Vol. 1
1966 Vol. 2
1968 Vol. 3

R 1.85 LYONS, D. H., KAPLAN, T. A., 1960. Phys. Rev. 120, 1580.

R 1.86 LOWIN, R. J., 1970. Thesis, University of London.

R 1.87 COLES, B. R., GRIFFITHS, D., LOWIN, R. J., TAYLOR, R. H., 1970. J. Phys. C., 6, L121.

R 1.88 FINNEMORE, D. K., WILLIAMS, L. J., SPEDDING, F. H., HOPKINS, D. C., 1968. Phys. Rev., 176, 712.

R 1.89 KANEMATSU, K., ALFIERI, G. T., BANKS, E., 1969. J. Phys. Soc. Jap., 26, 244.

R 1.90 DEBRAY, D. K., WALLACE, W. E., RYBA, E., 1970. To be published.

R 1.91 DEBRAY, D. K., RYBA, E., 1970. J. Appl. Phys. To be published.

R 1.92 BUSHOW, K. H. J., DE WIJN, H. W., DIEPEN, A. M., 1969. Colloque Ampere, 15, (North Holland, Amsterdam).

R 1.93 DEBRAY, D. K., RYBA, E., MULAY, L. N., 1967. J. Appl. Phys., 38, 3459.

R 1.94 PETER, M., 1961. J. App. Phys., 32, 3385.

R 1.95 NIGH, H. E., LEGVOLD, S., SPEDDING, F. H., 1963. Phys. Rev., 132, 1092.

R 1.96 SHULL, C. G., YAMADA, Y., 1962. J. Phys. Soc. Japan, 17, Suppl. BIII, 1.

R 1.97 LEDERER, P., MILLS, D. L., 1968. Phys. Rev., 165, 837

R 1.98 GRIFFITHS, D., COLES, B. R., 1966. Phys. Rev. Letters, 16, 1093.

R 1.99 HIRST, L. L., WILLIAMS, G., GRIFFITHS, D., COLES, B. R., 1968. J. App. Phys. 39, 844.

R 1.100 BURR, C. R., ORBACH, R., 1967. Phys. Rev. Letters, 19, 1133.

R 1.101 KIM, D. J., 1970. Phys. Rev., 9, 3725.

R 1.102 YOSIDA, K., 1957. Phys. Rev., 107, 396.

R 1.103 BROOKS, H., Theoretical Models for Transition Metals and Their Alloys, 1963.

R 1.104 MOOK, H. A., SHULL, C. G., 1966. J. Appl. Phys., 37, 1034.

R 1.105 MOON, R., 1964. Phys. Rev., 136, A195.

R 1.106 VAN den BERG, G. J., 1964. Proc. Low Temp. Conf. L29

R 1.107 SUGAWARA, T., 1965. J. Phys. Soc. Jap., 20, 2252.

R 1.108 YOSIDA, K., OKIJI, A., 1965. Prog. Theor. Phys., 34, 505

R 1.109 SPENSER, J. J., DONIACH, S., 1967. Phys. Rev. Letters 18, 994

R 1.110 FULLENBAUM, M. S., FAIK, D. S., 1967. Phys. Rev., 157, 452

R 1.111 HEEGER, A. J., 1969. Solid State Phys., 23 (Academic Press, New York)

R 1.112 SUGAWARA, T., EGUCHI, H, 1966. J. Phys. Soc. Jap., 21, 725

R 1.113 De WIJN, H. W., BUSHOW, K. H. J., VAN DIEPEN, A. M., 1968. Phys. Stat. Sol., 30, 759

R 1.114 VAN DIEPEN, A. M., De WIJN, H. W., BUSHOW, K. H. J., 1968. Phys. Stat. Sol., 29, 189

R 1.115 COOPER, B. R., 1962. Proc. Phys. Soc., 80, 1225

R 1.116 WHITE, J. A., VAN VLECK, J. H., 1961. Phys. Rev. Letters 6, 412

R 1.117 DE WIJN, H. W., VAN DIEPEN, A. M., BUSHOW, K. H. J., 1967. Phys. Rev., 161, 253

R 1.118 VILLAIN, J., 1959. J. Phys. Chem. Solids, 11, 303

R 1.119 SMART, S. J., 1966. Effective Field Theories of Magnetism, (Saunders, Philadelphia)

R 1.120 NAGAMIYA, T., 1967. Solid State Physics, 20, (Academic Press, New York).

R 1.121 COOPER, B. R., 1968. Solid State Physics, 21, (Academic Press, New York)

R 1.122 ELLIOT, R. J., 1961. Phys. Rev., 124, 346

R 1.123 ELLIOT, R. J., WEDGEWOOD, F. A., Proc. Phys. Soc., 1963 81, 846. 1964, 84, 63

R 1.124 FEDRO, A. J., ARAI, T., 1968. Phys. Rev., 170, 583

R 1.125 MATTIS, D. C., DONATH, W. E., 1962. Phys. Rev., 128 ,1618

R 1.126 YOSIDA, K., 1964. Prog. Low Temp. Phys., 4, (North Holland, Amsterdam)

R 1.127 JACKSON, C., DONIACH, S., 1969. Phys. Letts, 30A, 328

R 1.127a BAKER, J. M., 1967. Can. J. Phys., 45, 403

R 1.128 BLEANEY, B., 1963. Proc. Roy. Soc., A276, 19, 28

R 1.129 TRAMMEL, G. T., 1963. Phys. Rev., 131, 932

R 1.130 WANG, Y. L., COOPER, B. R., Phys. Rev., 1968. 172, 539, 1969, 185, 696.

R 1.131 COOPER, B. R., 1966. Physics Letters, 22, 244

R 1.132 COOPER, B. R., VOGT, O, 1970. Phys. Rev. B, 1, 1211, 1218

R 1.133 VAN VLECK, J. H., 1932. The Theory of Electric and Magnetic Susceptibilities

R 1.134 MANNARI, I, 1959. Prog. Theor. Phys., 22, 335

R 1.135 LIU, S. H., 1964. J. Appl. Phys., 35, 1087

R 1.136 ELLIOT, R. J., 1954. Phys. Rev., 94, 564

R 1.137 HIRST, L. L., 1967. Solid State Comm., 5, 751

R 1.138 DE GENNES, P. G., FRIEDEL, J., 1958. Phys. Chem. Solids 4, 71

R 1.139 MACKINTOSH, A. R., 1963. Phys. Letters, 4, 140

R 1.140 COLES, B. R., 1958. Adv. Phys., 7, 40

R 1.141 VAN DAAL, H. J., BUSHOW, K. H. J., 1969. Solid State Comm., 7, 217

R 1.142 COLES, B. R., COLE, T., LAMBE, J., LAURANCE, N., 1962. Proc. Phys. Soc., Lond., 79, 84

R 1.143 BUSHOW, K. H. J., DE WIJN, H. W., VAN DIEPEN, A. M., 1969. J. Chem. Phys., 50, 137

R 1.144 BUSHOW, K. H. J., FAST, J. F., 1966. Z. Phys. Chem. Neve. Falge., 50, 51

R 1.145 FISHER, M. E., 1962. Phil. Mag., 7, 1731

R 1.146 CAPLIN, A. D., DUNLOP, J. B., TAYLOR, R. H., 1970. Grenoble Conference on Magnetism

R 1.147 LEDERER, P., BLANDIN, A., 1966. Phil. Mag., 14, 363

R 1.148 ALEXANDER, S., ANDERSON, P. W., 1964. Phys. Rev., 133, A1594

R 1.149 CREVELLING, J., LUO, H. L., 1968. Phys. Rev., 176, 614.

R 1.150 SHERRINGTON, D., 1970. To be published.

R 1.151 RIVIER, N., ZUCKERMAN, M. J., 1968. Phys. Rev. Letters, 21,904

R 1.152 TOURNIER, R., BLANDIN, A., 1970. Phys. Rev. Letters, 24, 397

CHAPTER 2

R 2.1 HANSEN M, 1958. Constitution of Binary Alloys 2nd Edn. (McGraw Hill, New York).

R 2.2 ELLIOT, R. P., 1965. Constitution of Binary Alloys, First Supplement (McGraw Hill, New York).

R 2.3 SHUNK, F. A., 1969. Constitution of Binary Alloys, Second Supplement (McGraw Hill, New York).

R 2.4 GSCHNEIDNER, K. A., 1961. Rare Earth Alloys, (Van Nostrand, New York).

R 2.5 SCHRAMM, J, 1941. Z. Metal, 33, 358.

R 2.6 CHAO, C. C.; LUO, H. L, DUWEY, P., 1964. J. App. Phys., 35, 257.

R 2.7 JOHNSON, L, ANDERSON, K. E., 1963. U.S.A.E.C., ANL-6687, 77.

R 2.8 ROLLA, L., IANDELLI, A., 1941. Ricera Sci., 20, 1216.

R 2.9 CHIOTTI, P., MASON, J. T., 1965. Trans. TMS-AIME, 233, 786.

R 2.10 MASON, J. T., to be published.

R 2.11 CHIOTTI, P., MASON, J. T., 1967. TMS-AIME, 239, 547.

R 2.12 MASON, J. T., CHIOTTI, P., 1968. TMS-AIME, 242, 1167.

R 2.13 CHIOTTI, P., MASON, J. T., GILL, K. J., 1963. TMS-AIME 227, 910.

R 2.14 IANDELLI, A., PALENZONA, A., 1967. J. Less. Comm. Metals, 12, 333.

R 2.15 MASON, J. T., SREE HARSHA, K. S., CHIOTTI, P., 1970. Acta Cryst. To be published.

R 2.16 GLORIO, J. V., RUNDLE, R. E., SNOW, A. I., 1952. Acta Cryst. 5, 449.

R 2.17 MICHEL, D. J., RYBA, E., 1969. Scripta Met. 3, 683.

R 2.18 KUZMA, Y. B., KRIPYAKEVICH, P. I., FRENKEVICH, D. P., 1965. Izvest. Akad. Nauk, SSSR, Neorg. Mat., 1, 9, 1547.

R 2.19 KUZMA, Y. B., KRIPYAKEVICH, P. I., UGRIN, 1966. Izvest. Akad. Nauk, SSSR, Neorg. Mat., 2, 4, 630.

R 2.20 MAKAROV, E. S., VINOGRADOV, S. I., 1956. Kristallografiya, 1, 643.

R 2.21 FLORIO, I. V., BAENZIGER, N. C., RUNDLE, R. E., 1956. Acta Cryst., 9, 367.

R 2.22 MASON, J. T., 1969. Private communication.

R 2.23 SANDERSON, M. J., BAENZIGER, N. C., 1953. ActaCryst., 6, 627.

R 2.24 International Table for X-Ray Crystallography, 1962. (Kynoch Press, Birmingham).

R 2.25 LAVES, F., 1967. Factors Governing Crystal Structure. In "Intermetallic Compounds." (Ed. Westbrook) (Wiley, New York).

R 2.26 EDMONDS, A. R., 1960. Angular Momentum in Quantum Mechanics, 2nd Edition (Princeton).

R 2.27 KOSTER, G. F., 1957. Space Groups and Their Representations, Solid State Physics 5 (Academic Press, New York).

R 2.28 BIRSS, R. R., 1964. Symmetry and Magnetism. (North Holland, Amsterdam).

R 2.29 JOHNSON Q., SMITH, G. S., 1967. Acta Cryst., 23, 327.

R.2.30 WANG, F. E., 1967. Acta Cryst., 22, 579.

CHAPTER 3

R 3.1 LANDAU, L. D., LIFSHITZ, E. M., 1960. Electrodynamics of Continuous Media (London, Pergamon).

R 3.2 BOAST, W. B., 1964. Vector Fields (New York, Harper and Row).

R 3.3 DEY, S. K., 1966. Thesis. University of London.

R 3.4 SUCKSMITH, W., 1929. Phil. Mag., 8, 158.

R 3.5 GRIFFITHS, D., 1961. Thesis, University of London.

R 3.6 WHITE, G. K., 1968. Experimental Techniques in Low Temperature Physics (2nd Edition) (Oxford).

R 3.7 ROSE-INNES, A. C., 1964. Low Temperature Techniques (London, English Universities Press).

R 3.8 SACHSE, H. B., 1961. Electronic Industries, Jan.

R 3.9 WARREN, W. H., BADER, W. G., 1969. Rev. Sci., I Instrum, 40. 180.

R 3.10 BERMAN, R., BROCK, J. C. F., HUNTLEY, D. J., 1965. Advances in Cryogenic Engineering, Vol. 10., (Plenum Press).

R 3.11 BERMAN, R., HUNTLEY, D. J., 1963. Cryogenics, 3, 70.

R 3.12 BERMAN, R., 1964. Cryogenics, 4, 233.

R 3.13 ROSENBAUM, R. L., 1968. Rev. Sci. Instrum 39, 6, 890.

R 3.14 HANSEN, M., 1958. Constitution of Binary Alloys, (2nd edition), (McGraw-Hill, New York).

R 3.15 BERRY, R. J., 1962. Can. J. Phys., 40, 359.

R 3.16 MURANI, A. P., 1969. Thesis, University of London.

R 3.17 DUNLOP, J. B., 1969. Private communication.

R 3.18 McGUIRE, T. R., 1959. Methods of Experimental Physics, (Academic Press, New York).

R 3.19 GERRITSEN, A. M., DAMON, D. H., 1962. Rev. Sci. Instrum., 33, 301.

R 2.20 KRUPP, H., ROBENS, E., SANDSTEDE, G., WALTER, G., 1963. Vacuum, 13, 297.

R 3.21 POULIS, J. A., THOMAS, J. M., 1963. J. Sci. Instrum, 40, 95

R 3.22 POULIS, J. A., MASON, C. H., THOMAS, J. M., 1966. J. Sci. Instrum., 43, 234.

R 3.23 HENRY, W. G., ROGERS, J. L. 1956. Phil. Mag. 1, 223.

R 3.24 GARBER, M., HENRY W. G., HOEVE, H. G., 1960. Can. J. Phys., 38, 1595.

R 3.25 STEWART, A. M., 1969. J. Sci. Instrum, 2, 2, 851.

R 3.26 STEWART, A. M., 1970. J. Sci. Instrum, 3, 251.

R 3.27 SUCKSMITH, W., 1929. Phil. Mag., 8, 158.

R 3.28 HILL, G. J., 1968. J. Sci. Instrum, 1, 2, 52.

R 3.29 PARKER, D. W., 1969. Private communication.

R 3.30 MORRIS, B. L., WOLD, A., 1968. Rev. Sci. Instrum., 39, 1937.

R 3.31 BATEMAN, H., 1953. Higher Transcendental Functions, Vol. 1, p32, (McGraw Hill, New York).

R 3.32 DWIGHT, H, B., 1961. Tables of Integrals, (Macmillan, New York).

R 3.33 GRIFFITHS, D., 1961. J. Sci. Instrum., 38, 463.

R 3.34 GERRITSEN, A. N., 1956. Hand. der Physik., 19, (Springer-Verlag, Berlin).

R 3.35 MacDONALD, D. K. C., 1956. Hand. der Physik, 14, (Springer-Verlag, Berlin).

R 3.36 MEADEN, G. T., 1966. Electrical Resistance of Metals, (Heywood, London).

R 3.37 WIPF, S., 1961. Thesis, University of London.

R 3.38 GILMONT, R., 1951. Anal. Chem., 23, 1957.

R 3.39 STONAR, R. E., HERBERT, R. H., SILL, L. R., 1970. J. App. Phys., 41, 3706.

Journal of Scientific Instruments (Journal of Physics E) 1969 Series 2 Volume 2

Prediction of lateral instabilities in the Faraday magnetometer

A M Stewart
Department of Electrical Engineering, Imperial College, London

MS *received 18 April 1969, in revised form 9 July 1969*

Abstract When the Faraday method is used for magnetic measurement, errors are sometimes caused by the specimen holder being attracted towards one of the poles and swinging out of the vertical. An analysis of the reasons for these instabilities shows that they will only occur when the downwards force on the suspension due to magnetic effects exceeds a critical value which is the same for paramagnetic and ferromagnetic specimens and may be substantially independent of electromagnet current.

1 Introduction

When the Faraday method is used for magnetic measurement, errors are sometimes caused by the specimen holder being attracted towards one of the pole pieces and rubbing against the surrounding down-tube. Means experimenters have used to prevent these lateral movements have included attaching to the suspension rod silk fibres (Sucksmith 1929) and phosphor bronze spirals (Sucksmith and Pearce 1938), and fastening a heavy weight to the rod near the bottom (Griffiths 1961 Ph.D. Thesis, University of London). The suspension, which usually consists of one or more freely hung light rigid links is often required to be easily demountable and to hang inside a narrow tube, so in this case the above constraining methods may not be easy to apply.

Since the suspension may not be visible while measurements are being made and as the only way of detecting lateral movements in these circumstances is from discontinuities in the (M, H) curve, it is desirable to be able to predict the conditions under which these movements occur and so avoid them. The following analysis discusses the reasons for the lateral movements and gives a criterion for predicting them which is particularly simple to apply experimentally.

2 Theory

2.1 *Field gradient forces*

The physical system considered is shown in figure 1. The origin of the coordinates is centred between the magnet pole pieces so that the magnetic field has reflection symmetry in the xz and yz planes. The specimen is contained in a bucket at (x, y, z), and the suspension system considered here is a freely hung simple pendulum of length l and mass M (equal to the sum of the masses of the bucket and specimen). When the suspension is vertical the specimen is misaligned a small distance h along the x axis. The specimen and its bucket are considered to be of negligibly small size, and deflections in the y direction are ignored; they will be found to give only second order effects.

The force on a moment μ in the magnetostatic field is $(\mu.\nabla)\boldsymbol{H}$, and as only the x component of the moment will be significant and the field variation in the y direction will not contribute to instability, this force reduces to

$$\hat{z}\mu_x\partial H_x/\partial z + x\mu_x\partial H_x/\partial x$$

where $\hat{r}$ denotes the unit vector. If μ' is the moment of the sample and μ'' the diamagnetic moment induced in the bucket, then the total force F_1 acting on the suspension due to field gradients will be

$$F_1 = \hat{z}(\mu'-\mu'')\frac{\partial H_x}{\partial z} + x(\mu'-\mu'')\frac{\partial H_x}{\partial x}.$$

Now because of the reflection symmetry in the yz plane the variation of H_x with x may be expanded (extending the suggestion of Henry and Rogers (1956)) as

$$H_x(x) = H_x(0) + \frac{1}{2}\frac{\partial^2 H_x}{\partial x^2}x^2 + \frac{1}{24}\frac{\partial^4 H_x}{\partial x^4}x^4 + \text{etc.} \qquad (1)$$

where the differentials are evaluated at $x=0$. Therefore

$$\frac{\partial H_x(x)}{\partial x} = \frac{\partial^2 H_x}{\partial x^2}x + \frac{1}{6}\frac{\partial^4 H_x}{\partial x^4}x^3 + \text{etc.}$$

and substituting we get a final expression

$$F_1 = \hat{z}F_M + \hat{x}F_M\left(\frac{\partial^2 H_x}{\partial x^2}x + \frac{1}{6}\frac{\partial^4 H_x}{\partial x^4}x^3 + \text{etc.}\right)\Big/\frac{\partial H_x}{\partial z}$$

where $F_M = (\mu'-\mu'')\,\partial H_x/\partial z$ is the vertical magnetic force which is measured directly by the pull on the suspension. The proportionality of the lateral magnetic force to the lateral deflection has been pointed out by Garber *et al.* (1960) but the coefficient of proportionality they give is incorrect.

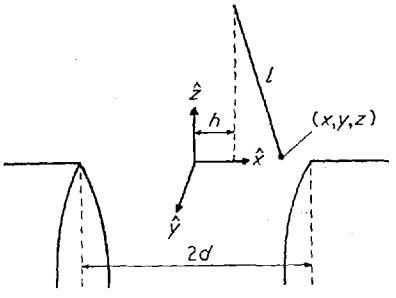


Figure 1 Suspension system and coordinate axes

2.2 *Image forces*

The other force of magnetic origin is that due to the interaction between the moment and its images in the pole pieces. A complete magnetostatic calculation is needed to estimate it

correctly, but an upper limit may be obtained by assuming that the pole faces are planes of infinite extent and of infinite permeability. In this case the force on the specimen will be the same as if there were images of the moment situated a distance d (where $2d$ is the separation of the pole pieces) behind the planes, having the same magnitude and direction as the moment. From the formula for the interaction energy between two dipoles it is straightforward to show that the force on a dipole $\mu=\hat{x}\mu$ placed at a distance d from one infinite plane is $F(d)=3/4\mu^2/d^4$ so that the force on a moment displaced a distance x from the central position between the two planes is

$$F_2(x)=2\frac{\partial F}{\partial d}x+\frac{1}{3}\frac{\partial^3 F}{\partial d^3}x^3+\text{etc.}$$

and if α is a factor less than unity which takes account of the non-infinite condition of the pole pieces, the total force in the x direction due to image effects is

$$F_2=\alpha(\mu'-\mu'')^2\left(\frac{6x}{d^5}+30\frac{x^3}{d^7}+\text{etc.}\right).$$

Now the total downwards force on the suspension is F_M+F_W where $F_W=M_g$ and this will give an equivalent restoring force in the x direction of

$$F_3=-\frac{(x-h)}{l}(F_M+F_W)\left\{1+\frac{(x-h)^2}{2l^2}+\text{etc.}\right\}$$

l being the length of the suspension and h the initial misalignment.

2.3 *Equation of motion*

Thus the equation for the motion of the bottom of the sample holder in the x direction is

$$M\frac{\partial^2 x}{\partial t^2}=\frac{h}{l}(F_M+F_W)-Ax+Bx^3 \qquad (2)$$

where

$$A=\frac{F_M}{l}\left\{1+\frac{F_W}{F_M}-l/G-6\alpha l(\mu'-\mu'')^2/F_M d^5\right\}$$

$$B=F_M\left\{\frac{\partial^4 H_x}{\partial x^4}\Big/6\frac{\partial H_x}{\partial z}+30(\mu'-\mu'')^2\,\alpha/d^7F_M-\frac{(x-h)^3}{2x^3l^3}\left(1+\frac{F_W}{F_M}\right)\right\}$$

and the field gradient ratio

$$G=\frac{\partial H_x}{\partial z}\Big/\frac{\partial^2 H_x}{\partial x^2}. \qquad (2a)$$

To gain further knowledge of the behaviour of the system it is necessary to consider the magnitudes and signs of the coefficients of the various powers of x. The ratio l/G may be determined by measurement of the field. If H_x and $H_x\partial H_x/\partial z$ are known then $\partial H_x/\partial z$ may be deduced, and if $H_x(x)$ is assumed to have the form of expression (1) then $\partial^2 H_x/\partial x^2$ may be found by traversing a fluxmeter Hall probe along the x axis.

The apparatus used in this laboratory to measure susceptibility consists of a Sucksmith ring balance (Sucksmith 1929) whose specimen is suspended between the poles of a Newport type E electromagnet with 7 in cylindrical pole pieces and a 5 cm gap. The specimen is placed in line with the top edge of the poles. A Hall probe of area 3 mm × 7 mm was scanned along the x axis at a magnet current of 20 A and the field profile was found to be parabolic to within experimental error inside the area of interest. The second derivative of the field could then be found by measuring H_x at $x=0$ and $x=1$ cm. The ratio l/G is plotted against magnet current in figure 2 for the parameter $l=87{\cdot}5$ cm. It can be seen from the graph that it is a reasonable approximation to regard this ratio as being constant. It would be exactly constant if varying the magnet current altered the magnitude of the field but left its 'shape' unchanged. This might be expected to be true up to high fields when the pole tips would start to saturate and change the field shape; there is some evidence for this in figure 2.

In the expression for the coefficient A it can be shown that the forces due to image effects are negligibly small compared with those due to field gradients. The ratio of the two is $6\alpha(\mu'-\mu'')/d^5(\partial^2 H_x/\partial x^3)$, and if it is assumed that the largest vertical force F_M ever used is 30 dyn (for reasons which will emerge later), this ratio will become

$$180\alpha\Big/d^5\frac{\partial^2 H_x}{\partial x^2}\frac{\partial H_x}{\partial z}.$$

Now at the smallest magnet current which is used $\partial H_x/\partial z=323$ Oe cm^{-1} and $\partial^2 H_x/\partial x^2=177$ Oe cm^{-2} and putting $d=2{\cdot}5$ cm gives a ratio of $\alpha 31\times10^{-6}$, which shows that the first order image forces may be ignored. This is the most unfavourable condition; for higher magnet currents the ratio will be even smaller.

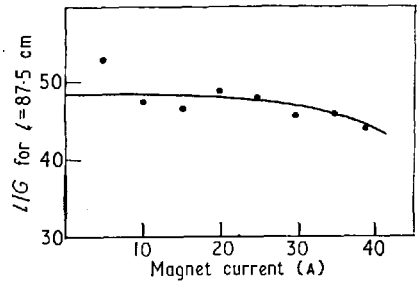


Figure 2 Variation of l/G with magnet current for $l=87{\cdot}5$ cm

With respect to the coefficient B it may be seen from figure 4(*c*) of Hill (1968), on a substantially similar magnet system, that the term in x^3 becomes important for x greater than about 2 mm and also that B is negative. From the measurements of H_x on the magnet used here, described previously, the part of B due to field gradients was found to be very small and probably positive.

2.4 *System behaviour*

To understand the behaviour of the suspension system, which is governed by equation (2), it is best to examine several simple cases separately. If the initial deflection $h=0$, and only small deflections, are considered so that the x^3 term is neglected, the differential equation (2) reduces to the one for simple harmonic motion so long as A is positive. If A becomes negative, which it will when

$$1+F_W/F_M<l/G$$

the system will be unstable. As the ratio on the right-hand side has been shown to be roughly constant in figure 2 the instability will occur when F_M reaches a critical value, say $F_M{}^c$. The motion of the specimen holder will then be as follows. If $F_M<F_M{}^c$ the holder, given a small deflection, will oscillate with simple harmonic motion about $x=0$. The oscillations will be damped by any damping mechanism attached to the force detector and their frequency will vary from the frequency of free oscillation at $F_M=0$ to zero

frequency at $F_M = F_M{}^c$. However, if $F_M > F_M{}^c$, any small deflection will produce a force which acts in a direction so as to increase that deflection and instability results. In figure 3(*a*) the equilibrium deflection x (for $\partial x/\partial t = 0$) is plotted against F_M.

The next situation to be considered is when $h \neq 0$. For small deflections the term in x^3 is ignored and the equation for the equilibrium value of x is

$$x \simeq \frac{hF_W}{Al} = \frac{h}{1 - F_M/F_M{}^c}$$

and so the graph of x against F_M will be of the form of figure 3(*b*) for small deflections.

The cubic term will be important when x is large and in this case h is neglected to give

$$x^2 = \frac{A}{B} = \frac{l^2(1 - F_M/F_M{}^c)}{\left\{\frac{F_M}{F_W}\frac{l^3}{6}\frac{\partial^4 H_x}{\partial x^4}\Big/\frac{\partial H_x}{\partial z} - \frac{1}{2}(1 + F_M/F_W)\right\}}$$

and if the field ratios are taken to be constant the behaviour will be as in figure 3(*c*), provided that B is negative as in figure 4(*c*) given by Hill (1968). If B is positive there will be no equilibrium position, the instability will be even more violent than in the first case examined and $F_M{}^c$ will depend to a small extent upon the amplitude of the initial oscillation.

Thus when all the terms of equation (2) are taken into account the equilibrium behaviour may be expected to be somewhat like that illustrated in figure 3(*d*). If h is minimized by suitably adjusting the position of the magnet the behaviour will tend towards that shown in figure 3(*c*). The important

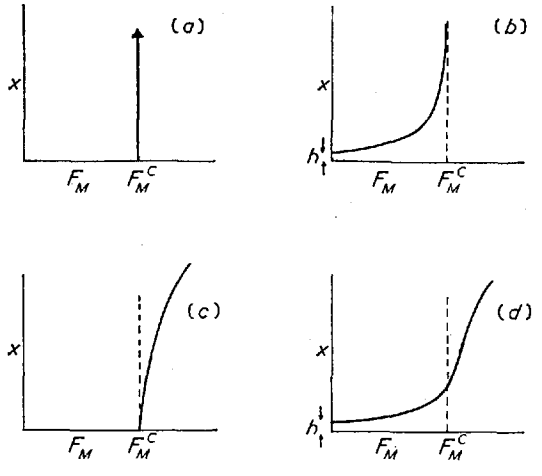


Figure 3 Variation of displacement x with magnetic force F_M

principle which emerges from the analysis is that if $F_M < F_M{}^c$ the x deflection will be very small provided that time is allowed for transient oscillations, which may occur when the magnet is switched on, to die away. However, if $F_M{}^c$ is exceeded then a very large deflection will occur for a small increase in F_M. Therefore, if $F_M{}^c$ is measured once on a particular apparatus and never subsequently exceeded, one can be sure that large lateral displacements of this sort will not take place.

2.5 *Stability conditions*

The stability condition given by the analysis is

$$1 + \frac{F_W}{F_M} \geqslant \frac{l}{G}. \qquad (3a)$$

If the centre of gravity of the suspension link is f below its topmost end then expression (3*a*) is replaced by

$$1 + \frac{F_W f}{F_M l} \geqslant \frac{l}{G} \qquad (3b)$$

and if the suspension is in the form of two hinged links, the upper (1) and the lower (2), it is straightforward though tedious to show that the stability conditions becomes

$$\frac{F_M + R/F_M + Q}{F_M + P/(l_1 + l_2)} \geqslant \frac{l_1 + l_2}{G} \qquad (3c)$$

where

$$P = gm_2l_2 + gm_1f_1l_2/l_1 + gm_2f_2l_1/l_2$$
$$Q = gm_2 + gm_1f_1/l_1 + gm_2f_2/l_2$$
$$R = (m_2 + m_1f_1/l_1)\, g^2 m_2 f_2/l_2$$

Expression (3*a*) may be reduced to a form similar to an equation given by Hill (1968) and Martin and Hill (1968) except that $\partial^2 H_x/\partial x^2$ in our expression is replaced by $(\partial H_x/\partial x)/r$ in theirs, where r is the inside radius of the down-tube. Hill does not state where $\partial H_x/\partial x$ is to be evaluated, but if it is evaluated at $x = r$ his equation will give an overestimate of the magnetic force which may be safely used, as may be seen from figure 4(*c*) of his paper. Obviously, the critical force $F_M{}^c$ must be independent of r. The analysis given in this paper applies also, of course, to specimens which do not have a constant susceptibility. It should be mentioned also that $f(x)$ in equation (2) given by Hill (1968) should be replaced by $f(z)$ as he used a coordinate system which is different from the one used by Garber *et al.* (1960).

Because $\partial^2 H_x/\partial y^2$ may be expected to be negative, specimens with positive moments will be stable against movements in the y direction but specimens with negative moments, such as superconductors, will be stable against movements in the x direction but unstable against them in y direction. A similar formula for the critical force will hold for samples with negative moments except that $\partial^2 H_x/\partial x^2$ will be replaced by $\partial^2 H_x/\partial y^2$ whose negative sign will be manifested in an upwards $F_M{}^c$.

3 Experimental

Measurements were made on the Sucksmith ring magnetometer used in this laboratory to see whether the suspension system, which consists of two hinged quartz rods, behaved in the way predicted by the above analysis and equation (3*c*).

The specimens used were irregularly shaped polycrystalline lumps of nickel and gadolinium which are ferromagnetic and paramagnetic (Elliot *et al.* 1953), respectively, at the temperature of measurement 24°c. With a field strength which gave an F_M of about 80% of its critical value, h was minimized by moving the magnet in the xy plane.

As the magnet current and thus F_M was increased, the transient oscillations were observed to become larger in magnitude and less well damped so that the transition to instability was not completely clear cut. Because of this $F_M{}^c$ could only be estimated to ±2%.

The values of $F_M{}^c$ (in dynes) for various weights of Ni and Gd are tabulated in table 1. The magnet current at which the instability occurred is also given to show that the instability arises at roughly the same value of F_M for a wide range of magnet currents. These figures may be compared with the theoretical value of $F_M{}^c = 31{\cdot}2$ dyn obtained from (3*c*) by putting in the measured parameters, $l_1 = 55{\cdot}3$ cm, $f_1 = 27{\cdot}1$ cm, $m_1 = 2{\cdot}918$ g; $l_2 = 32{\cdot}2$ cm, $f_2 = 26{\cdot}6$ cm, $m_2 = 1{\cdot}094$ g and a value of 48 from figure 2 for $(l_1 + l_2)/G$. In view of the difficulty of measuring high order field gradients the agreement of theory and experiment to within 5–15% is considered satisfactory.

Table 1 Theoretical and experimental values of critical force $F_M{}^c$

Specimen	Gd	Gd	Ni	Ni
Mass (mg)	3·07	0·71	1·08	0·53
Magnet current (A)	6·2	18·0	8·2	22·0
$F_M{}^c$ dyn (experimental)	29·85	29·8	27·9	27·4
$F_M{}^c$ dyn (theoretical)	31·2	31·2	31·2	31·2

4 Conclusion

The horizontal motion of the Faraday magnetometer has been analysed and it has been found that lateral instabilities will occur when the vertical magnetic force exerted on the suspension exceeds a critical value. If the suspension is correctly centred in the magnetic field and the critical value of magnetic force at which these large deflections take place is measured once, then so long as this force is never subsequently exceeded no errors will occur from this cause.

This particularly simple criterion applies to magnets whose field gradient ratio is substantially constant; where it is not, $F_M{}^c$ will have to be considered a function of magnet current. Experimenters would in any case be advised to keep the force well below $F_M{}^c$ in order to avoid transient oscillations and the magnification of inevitable magnet misalignments.

The tendency for the instabilities to take place may be reduced by increasing the weight of the diamagnetic suspension, reducing its length, and by making the field gradient ratio G, equation (2*a*), as large as possible by suitable magnet design.

Acknowledgments

This work was done as part of a Materials Science programme directed by Professor J C Anderson, while the author was in receipt of a SRC Studentship. Valuable discussions on the subject of the paper with Dr D Griffiths and Mr J B Dunlop of the Physics Department, Imperial College are gratefully acknowledged.

References

Elliot J F Legvold S and Spedding F H 1953 *Phys. Rev.* **91** 28–30

Garber M Henry W G and Hoeve H G 1960 *Can. J. Phys.* **38** 1595–613

Henry W G and Rogers J L 1956 *Phil. Mag.* **1** 223–36

Hill G J 1968 *J. Sci. Instrum. (J. Phys.* E) **1** (Ser. 2) 52–4

Martin R H and Hill G J 1968 *J. Sci. Instrum. (J. Phys.* E) **1** (Ser. 2) 1257–9

Sucksmith W 1929 *Phil. Mag.* **8** 158–65

Sucksmith W and Pearce R R 1938 *Proc. R. Soc.* A 167 189–204

Prediction of lateral instabilities in the Faraday magnetometer

The expression derived in the paper by Stewart (1969) for the quantity defined as the field gradient ratio will be modified when the contribution to the horizontal force from the term $\mu_z \partial H_z/\partial x$ is taken into account. If the field component H_z is expanded about $x=0$ the expression for the force in the x direction becomes

$$F_x = x\mu_x \left\{ \frac{\partial^2 H_x}{\partial x^2} + \frac{1}{H_x}\left(\frac{\partial H_x}{\partial z}\right)^2 \right\}.$$

This equation has been correctly derived by Garber *et al.* (1960) in an equivalent form and should replace the expression given previously which contained only the first term. The equation is valid for ferromagnetic specimens of low anisotropy as well as paramagnetic ones and leads to the modified expression for the field gradient ratio G:

$$G^{-1} = \frac{\partial^2 H_x}{\partial x^2} \Big/ \frac{\partial H_x}{\partial z} + \frac{1}{H_x}\frac{\partial H_x}{\partial z}.$$

Because both terms in this equation have the same sign at the specimen position of the magnet on which the measurements described in the paper were carried out, the presence of the second term indicates that lateral instability will occur at a lower value of vertical magnetic force than suggested by the previous expression for G. The value of $(\partial H_x/\partial z)/H_x$ at the specimen position is known to be $-0{\cdot}19\ \mathrm{cm}^{-1}$ which shows that in this case the second term of G^{-1} contributes roughly 30% of the total. The difference between the value of $(\partial^2 H_x/\partial x^2)/(\partial H_x/\partial z)$ measured with a fluxmeter and the values deduced from the critical forces and the expression given here for G is attributed to experimental difficulties in measuring the small difference between two field strengths in a region where field gradients are high.

The dynamical behaviour of the suspension system will be substantially similar to that described before and the stability conditions will be valid when the expression for G given here is used. It should be noted that the magnitudes of the quantities G, F_W and F_M are used in the stability conditions so that each term in them is a positive quantity.

The author is grateful to D W Parker of Newport Instruments Ltd for drawing his attention to the additional term in the field gradient ratio and for valuable discussions concerning it.

Department of Electrical Engineering A M Stewart
Imperial College
London SW7
12 December 1969

References

Garber M Henry W G and Hoeve H G 1960 *Can. J. Phys.* **38** 1595–613

Stewart A M 1969 *J. Phys.* E: *Sci. Instrum.* **2** 851–4, 1140

Journal of Physics E: Scientific Instruments 1970 Volume 3
Printed in Great Britain